University of Cyprus

Department of Mechanical
and Manufacturing Engineering

Synthesis, Characterization and Applications of Novel Magneto-responsive and pH-Responsive Polymer-based Materials

Ph.D. Thesis

Petri C. Papaphilippou

2010

Petri Papaphilippou

Department of Mechanical
and Manufacturing Engineering

Synthesis, Characterization and Applications of Novel Magneto-responsive and pH-Responsive Polymer-based Materials

Petri C. Papaphilippou

A dissertation submitted in partial fulfillment of the requirements for the degree of Doctor of Philosophy at the University of Cyprus

September, 2010

Petri Papaphilippou

Petri Papaphilippou

© Petri C. Papaphilippou

Petri C. Papaphilippou

Synthesis, Characterization and Applications of Novel Magneto-responsive and pH-Responsive Polymer-based Materials

This Ph.D. Thesis has been carried out in partial fulfillment of the requirements for the degree of Doctor of Philosophy at the Department of Mechanical and Manufacturing Engineering and approved on the 10th of September 2010 by the Doctoral Committee.

Doctoral Committee

Research Advisor: Theodora Krasia-Christoforou ……..

Other Members:

Georges Hadziioannou

Apostolos Avgeropoulos

Ioannis Giapintzakis

Charalabos Doumanidis

Petri Papaphilippou

Petri Papaphilippou

Dedicated with love to my father & mother…

Contents

Abstract **i**

Acknowledgements **iii**

List of Figures **vi**

List of Tables **xv**

Abbreviations **xvii**

Research goals **xx**

1 Introduction **1**

1.1 General characteristics of polymers……..... 1

1.1.1 Polymerization methods…….. 2

1.2 Amphiphilic block copolymers and micellization……..... 7

1.3 Magneto-responsive polymer-based hybrid materials…… 9

1.3.1 Magnetic nanoparticles……... 9

1.3.2 Stability of magnetite nanoparticles…… 11

1.3.3 Polymer-stabilized magnetite nanoparticles…… 13

1.3.4 Block copolymer micelles as nanocarriers for magnetic nanoparticles.. 14

1.3.5 Magnetic properties of polymer-coated Fe_xO_y nanoparticles……. 18

1.4 Polymeric micelles in drug delivery applications……. 20

1.4.1 Stability of polymeric micelles used in drug delivery……. 21

1.4.2 Hydrophilic and hydrophobic blocks in amphiphilic block copolymer micelles used as drug delivery systems…… 24

1.4.3 Targeted polymeric drug-nanovehicles……... 26

1.4.4 Drug-loading in polymeric micelles…… 27

1.4.5 Drug-loaded micellar nanocarriers……. 27

1.4.6 Drug-release studies in drug-loaded polymeric micelles…… 29

1.4.7 pH-triggered drug delivery systems…… 30

1.4.8 Temperature-triggered drug delivery systems……. 34

2 Characterization Methods **36**

Petri Papaphilippou

2.1 Microscopy techniques…….. 36
2.1.1 Atomic Force Microscope (AFM)…….. 36
Operating principles in AFM……... 36
Modes of operation in AFM…… 37
2.1.2 Transmission Electron Microscope (TEM). …….. 38
Operation of TEM…… 39
2.2 Thermal analysis methods…… 39
2.2.1 Differential scanning calorimetry (DSC)…… 39
2.2.2 Thermal gravimetric analysis (TGA)…….. 41
2.3 Spectroscopy techniques……... 41
2.3.1 Nuclear Magnetic Resonance Spectroscopy (NMR)…….. 41
2.3.2 X-ray diffraction spectroscopy (XRD). ……. 43
Operating principles in XRD……... 43
2.3.3 Ultraviolet-visible spectroscopy (UV-vis)……. 44
2.4 Scattering methods……..... 46
2.4.1 Dynamic light scattering (DLS)…….. 46
2.5 Chromatography methods…….. 48
2.5.1 Size exclusion chromatography (SEC)…… 48
2.6 Magnetization analysis……... 50
Magnetism - Preface…….. 50
2.6.1 Vibrating Sample Magnetometry (VSM)…… 56
VSM measurements……..… 56
2.6.2 Physical Property Measurement System (PPMS)…… 57
3 Experimental Section 58
3.1 Methods…….. 58
3.2 Reagents..... 59
3.3 Synthesis……. 61
3.3.1 Synthesis of cumyl dithiobenzoate, CDTB (Chain Transfer Agent CTA) 61
3.3.2 Synthesis of $PEGMA_x$ homopolymers…… 61

Petri Papaphilippou

3.3.3 Synthesis of $AEMA_x$ homopolymers…….. 62
3.3.4 Synthesis of $DEAEMA_x$ homopolymers…… 63
3.3.5 Synthesis of $PEGMA_x$-b-$AEMA_y$ diblock copolymers……. 63
3.3.6 Synthesis of $PEGMA_x$-b-$DEAEMA_y$ diblock copolymers……. 65
3.3.7 Synthesis of HEGMA-co-AEMA/EGDMA random co-networks…… 66
3.4 Synthesis of magneto-responsive polymeric materials……. 67
3.4.1 Synthesis of stabilized in aqueous media iron oxide nanoparticles, in the presence of the $PEGMA_x$-b-$AEMA_y$ diblock copolymers…….. 67
3.4.2 Synthesis of single-wall carbon nanotubes decorated with iron oxide nanoparticles, stabilized in aqueous media in the presence of the $PEGMA_x$-b-$AEMA_y$ diblock copolymers……. 70
3.4.3 Synthesis of iron oxide-containing composite co-networks…… 70
3.4.4 Synthesis of OA.Fe_3O_4-containing nanocomposite co-networks…… 71
3.4.5 Determination of the Degree of Swelling…… 72
3.4.6 Deswelling Measurements…… 74
3.5 Synthesis of polymeric drug delivery carriers……..……. 74
3.5.1 Preparation of DOX-loaded $HEGMA_x$-b-$DEAEMA_y$ micelles…….. 74
3.5.2 Determination of DOX Release Kinetics at different pHs…….. 74
3.6 Biological assays…… 75
4 Results and Discussion 77
4.1 Magneto-responsive polymeric materials……... 77
4.1.1 Magneto-responsive polymer-based micelles……. 77
4.1.1.1 Synthesis and molecular characterization of the $PEGMA_x$-b-$AEMA_y$.. 77
Thermal Properties…… 81
Thermoresponsive behavior of the $PEGMA_x$-b-$AEMA_y$ diblock copolymers. 81
Self-assembly behavior of the $PEGMA_x$-b-$AEMA_y$ diblock copolymers in aqueous media…….……. 82
4.1.1.2 Preparation and characterization of stabilized, $PEGMA_x$-b-$AEMA_y$ -coated magnetic nanoparticles in aqueous media……. 84
4.1.1.3 Biological assays of $PEGMA_x$-b-$AEMA_y$/Fe_xO_y……. 93

Petri Papaphilippou

In vitro biocompatibility…… 93
In vitro macrophage uptake…… 94
4.1.2Magneto-responsive polymer/SWCNT nanocomposites…….. 96
4.1.2.1 Preface……. 96
4.1.2.2 Synthesis……... 99
4.1.2.3 Characterization of SWCNT/Fe_xO_y/$PEGMA_x$-b-$AEMA_y$ nanohybrids 101
4.1.3 Synthesis and characterization of magneto-responsive polymer co-networks……. 106
4.1.3.1 Preface……... 106
4.1.3.2 Synthesis…… 108
4.1.3.3 Characterization of the magneto-responsive co-networks…… 111
4.2 $PEGMA_x$-b-$AEMA_y$ diblock copolymers: Biomineralization applications……..……... 119
4.2.1 Preface…… 119
4.2.2 Crystallization of malachite $Cu_2(OH)_2CO_3$ in the presence of the $PEGMA_x$-b-$AEMA_y$ in aqueous media…….…….. 121
4.3 Stimuli-responsive amphiphilic diblock copolymers containing pH and temperature-responsive functionalities: Synthesis, characterization and evaluation as drug release systems…… 123
4.3.1 Preface…….. 123
4.3.1.1 Synthesis…… 123
4.3.1.2 Characterization…… 125
4.3.1.3 Fabrication of DOX-loaded $HEGMA_x$-b-$DEAEMA_y$ micelles…… 128
Synthesis…….. 128
pH-dependent DOX release from the $HEGMA_x$-b-$DEAEMA_y$ micelles …… 129
4.3.1.4 *In-vitro* cytotoxicity studies of the DOX-loaded HEGMA-b-DEAEMA micelles…… 133
Summary and Outlook **136**
Bibliography **142**

Petri Papaphilippou

Abstract

The present work mainly focuses on the synthesis and characterization of novel polymer-based ***magneto-responsive materials*** and ***pH-responsive drug nanocarriers.*** A novel series of well-defined $PEGMA_x$-*b*-$AEMA_y$ diblock copolymers was prepared by RAFT and characterized by several methods including SEC, ^{1}H NMR (molecular characterization), DSC and TGA (thermal characterization) and AFM and DLS (self-assembly behavior). For the first time the $PEGMA_x$-*b*-$AEMA_y$ micelles were used as nanocontainers for the encapsulation and stabilization of magnetic iron oxide nanoparticles in aqueous media, leading to the generation of novel *magneto-responsive micelles*. Magnetic measurements demonstrated the superparamagnetic behavior of these systems. Moreover, *in vitro* cell viability studies provided strong evidence for their *in vitro* biocompatibility. The $PEGMA_x$-*b*-$AEMA_y$ diblock copolymers were also used for stabilizing SWCNT/Fe_xO_y nanoparticles in water. As revealed by TEM, spherical iron oxide nanoparticles were located onto the SWCNT surfaces. VSM measurements showed that the *magneto-responsive SWCNTs* exhibited superparamagnetic behavior. Further to the above-mentioned applicability of the $PEGMA_x$-*b*-$AEMA_y$ towards the fabrication of magneto-responsive materials, preliminary studies demonstrated that the $PEGMA_x$-*b*-$AEMA_y$ may act as potential candidates in biomineralization applications. A new approach for the fabrication of *magneto-responsive polymer networks* presented in this work, involved the random copolymerization of HEGMA and AEMA in the presence of either preformed oleic-acid coated magnetite nanoparticles (OA.Fe_3O_4) or non-coated magnetic iron oxide (nano)particles (Fe_xO_y). Further to the compositional and thermal characterization and the investigation of the swelling behavior in organic and aqueous media, assessment of the magnetic characteristics of these materials by VSM or PPMS, disclosed superparamagnetic behavior for the OA.Fe_3O_4-containing systems, whereas ferrimagnetic behavior was observed in the case of the Fe_xO_y-containing co-networks. pH-responsive diblock copolymers of the type $HEGMA_x$-*b*-$DEAEMA_y$ were prepared by RAFT and tested towards their ability to act as *pH-triggered drug delivery systems*. Kinetic drug release measurements (DOX), clearly demonstrated that in acidic pHs the $HEGMA_x$-*b*-$DEAEMA_y$ micelles collapse (due to the protonation of the DEAEMA ionisable block), resulting to the release of the drug. Cell viability studies were carried out on a breast cancer cell line, in the presence of unloaded and DOX-loaded $HEGMA_x$-*b*-$DEAEMA_y$ micelles and assessed against DPBS (control) and "free" DOX.

Petri Papaphilippou

Περίληψη

Η παρούσα εργασία στοχεύει κυρίως στην σύνθεση και χαρακτηρισμό καινοτόμων ***μαγνητο-αποκρινόμενων υλικών*** και ***νανομεταφορέων φαρμάκων με ικανότητα απόκρισης σε μεταβολές στο pH.*** Μία νέα σειρά αδρομερών συμπολυμερών του τύπου $PEGMA_x$-*b*-$AEMA_y$ έχει παρασκευαστεί με τη μέθοδο RAFT και χαρακτηριστεί με διάφορες μεθόδους συμπεριλαμβανομένων των SEC, ^{1}H NMR (μοριακός χαρακτηρισμός), DSC και TGA (θερμικός χαρακτηρισμός) και AFM και DLS (μελέτη συμπεριφοράς συσσωμάτωσης). Για πρώτη φορά μικύλια των $PEGMA_x$-*b*-$AEMA_y$ έχουν χρησιμοποιηθεί ως νανοσυστήματα για δέσμευση και σταθεροποίηση μαγνητικών νανοσωματιδίων οξειδίου του σιδήρου σε υδατικά διαλύματα, προς δημιουργία καινοτόμων *μαγνητο-αποκρινόμενων μικυλίων*. Μαγνητικές μετρήσεις, επέδειξαν υπερπαραμαγνητική συμπεριφορά των συγκεκριμένων συστημάτων. Επιπλέον, μελέτες κυτταροτοξικότητας που διεξήχθησαν *in vitro* παρείχαν ισχυρά στοιχεία για την *in vitro* βιοσυμβατότητα των υλικών αυτών. Τα $PEGMA_x$-*b*-$AEMA_y$ χρησιμοποιήθηκαν επίσης προς σταθεροποίηση των SWCNT/Fe_xO_y σε νερό. Η μικροσκοπία TEM, απεκάλυψε την παρουσία σφαιρικών νανοσωματιδίων οξειδίου του σιδήρου πάνω στις επιφάνειες των SWCNT. Μετρήσεις VSM έδειξαν ότι τα *μαγνητο-αποκρινόμενα SWCNTs επιδεικνύουν* υπερπαραμαγνητική συμπεριφορά. Πέρα από την εφαρμογή των $PEGMA_x$-*b*-$AEMA_y$ προς παρασκευή μαγνητο-αποκρινόμενων πολυμερικών υλικών, προκαταρκτικές μελέτες έδειξαν ότι τα $PEGMA_x$-*b*-$AEMA_y$ μπορεί να δράσουν ως πιθανά συστήματα σε εφαρμογές *biomineralization*. Μια καινούργια προσέγγιση προς παρασκευή μαγνητο-αποκρινόμενων πολυμερικών πλεγμάτων που περιγράφεται στην παρούσα εργασία, συμπεριλαμβάνει τον τυχαίο συμπολυμερισμό των HEGMA και AEMA στην παρουσία είτε προ-παρασκευασμένων νανοσωματιδίων μαγνητίτη, επικαλυπτόμενων με ολεϊκό οξύ (OA.Fe_3O_4) ή μη-επικαλυπτόμενων μαγνητικών (νανο)σωματιδίων οξειδίου του σιδήρου (Fe_xO_y). Πέρα από τον χαρακτηρισμό των υλικών αυτών ως προς την σύσταση, την συμπεριφορά διόγκωσης σε οργανικούς και υδατικούς διαλύτες και τον θερμικό χαρακτηρισμό, ο προσδιορισμός των μαγνητικών χαρακτηριστικών των συστημάτων αυτών με VSM ή PPMS, απεκάλυψε υπερπαραμαγνητική συμπεριφορά στα πλέγματα που περιείχαν τα OA.Fe_3O_4, ενώ τα πλέγματα στα οποία εμπερικλείονταν τα μη-επικαλυπτόμενα Fe_xO_y παρουσίασαν σιδηριμαγνητική συμπεριφορά. Αδρομερή συμπολυμερή με ικανότητα απόκρισης σε μεταβολή στο pH του τύπου $HEGMA_x$-*b*-$DEAEMA_y$ συντέθηκαν με τη μέθοδο RAFT και εξετάστηκαν ως προς την ικανότητα δράσης τους ως *συστήματα μεταφοράς φαρμάκων*. Μετρήσεις κινητικής απελευθέρωσης φαρμάκου (DOX) επέδειξαν ότι σε όξινα pH, η μυκιλιακή δομή των $HEGMA_x$-*b*-$DEAEMA_y$ καταρρέει (εξαιτίας της πρωτονίωσης του DEAEMA), οδηγώντας σε απελευθέρωση του φαρμάκου. Μελέτες κυτταροτοξικότητας έχουν διεξαχθεί σε σειρά καρκινικών κυττάρων μαστού, στην παρουσία μικυλίων $HEGMA_x$-*b*-$DEAEMA_y$ (με ή χωρίς το DOX) και έχουν συσχετιστεί με τα αποτελέσματα που λήφθηκαν στην παρουσία ελεύθερου DOX και του DPBS (*control*).

Petri Papaphilippou

Acknowledgements

Reaching the end of my Ph.D, it could not be possible to forget everyone who helped and supported me throughout these years. First and foremost, I owe my deepest gratitude to my supervisor, Dr. Theodora Krasia-Christoforou. It has been an honor to be her first Ph.D. student. She has supported me in a number of ways during the experimental work and the hard writing-up period. I have learned a lot of things from her. I appreciate all her efforts towards making my Ph.D. work productive and inspiring. Her enthusiasm, that was highly motivational, prompted me to try harder for the best even during tough periods.

Moving on, it is time to say many thanks to our *beautiful* lab group. Especially, I would like to thank Maria Demetriou who has been very supportive ever since I joined the group. She has been always very helpful and a good advisor in many situations. Besides the perfect collaboration and understanding between us, a nice friendship was also developed and I really hope that this friendship will last for many years. Of course, I could not forget to thank the "youngest" member of our group, Ioanna Savva who has been very supportive, helpful and a good friend in the bad and the good times. At last, I would like to thank the "newest" member of the group Dr. Mariliz Achilleos for her valuable inputs during writing-up.

I would also like to thank all the people whose contribution in this work was valuable:

Prof. Costas Patrickios and his research group (Department of Chemistry, University of Cyprus), for providing access to the DLS, DSC and the UV-vis apparatus used in turbidimetry measurements and for all the valuable discussions.

Prof. Panayiotis Koutentis (Department of Chemistry, University of Cyprus) and especially Sophie Michaelidou-Papadoppoulou for their help with the TGA experiments.

Dr. Theodora Kyratsi (Department of Mechanical and Manufacturing Engineering, University of Cyprus) and my good friends Maria Ioannou and Chrysi Papageorgiou, for helping me with the XRD measurements; I deeply appreciate their true friendship and support.

Petri Papaphilippou

Prof. Ioannis Giapintzakis and Dr. George Athanasopoulos (Department of Mechanical and Manufacturing Engineering, University of Cyprus) for the magnetic measurements carried out by PPMS.

Prof. Charalabos Doumanidis, the Coordinator of the NANOMA project at the University of Cyprus (NANOMA-FP7-ICT-2007-2) funded by the European Commission, for the opportunity to work in this project as a researcher during the period June 2008 – May 2010.

Dr. Andreani Odysseos, Dr. Louiza Loizou and Dr. Yiota Christou, Biomedical Tissue Engineering/Nanobiotechnology Lab, EPOS-Iasis R&D, for their valuable help with the biological assays.

Prof. Helmut Cölfen and Dr. Ruiqi Song (Max-Planck Institute of Colloids and Interfaces, Potsdam, Germany) for carrying out the biomineralization experiments.

Prof. Etelka Tombacz and Angéla Hajdu (University of Szeged, Hungary) for the stability measurements with DLS.

Prof. Ladislau Vekas and his group (University Politechnica Timisoara, Romania), for the VSM magnetic experiments and for their kind hospitality during my visits in Timisoara.

Dr. Rodica Turcu (National Institute R&D for Isotopic and Molecular Technologies, Cluj-Napoca, Romania) for TEM and VSM measurements performed on the magneto-responsive SWCNTs.

Prof. Bradley Nelson and Shou Kaiyu (Institute of Robotics and Intelligent Systems, ETH Zurich, Switzerland), for the TEM characterization of the magneto-responsive SWCNTs.

Ms. Anne Heilig (Max-Planck Institute of Colloids and Interfaces, Potsdam, Germany), for the AFM measurements of the $PEGMA_x$-*b*-$AEMA_y/Fe_xO_y$ micelles.

Petri Papaphilippou

I would also like to acknowledge the project NANOMA-FP7-ICT-2007-2, the Cyprus and Romania Research Promotion Foundations (KY-POY/0407/09) and the University of Cyprus for financial support.

Last but not least, I would like to thank my family for their love and encouragement. My parents, who raised me with a love for science and supported me in all my decisions and efforts. My brother Zenon and my grandmother Petroula, who have been there for me, whenever I needed them. I want them to know how much I appreciate their patience and their understanding throughout these years. Finally, I would like to send a special "Thank you" to my friends, who have always been there for me during the Ph.D, for their support and their love: Maria Constantinou, Athina Demetriou, Eri Kozakou, Elena Maltezou, Eleni Moushi, Maria Spanou, Fani Theocharous and Nectaria Varnava.

"Σα βγεις στον πηγαιμό για την Ιθάκη, να εύχεσαι να `ναι μακρύς ο δρόμος,
γεμάτος περιπέτειες, γεμάτος γνώσεις. Τους Λαιστρυγόνας και τους Κύκλωπας,
τον θυμωμένο Ποσειδώνα μη φοβάσαι, τέτοια στον δρόμο σου ποτέ σου δεν θα βρεις,
αν μεν' η σκέψις σου υψηλή, αν εκλεκτή συγκίνησις το πνεύμα και το σώμα σου αγγίζει"

Κωνσταντίνος. Π. Καβάφης

Petri C. Papaphilippou
University of Cyprus
September 2010

Petri Papaphilippou

List of Figures

Fig. 1.1	Schematic illustration of (a) linear, (b) branched, (c) crosslinked, and (d) network (three-dimensional) molecular structures. The circle configures the individual "mer" units……..	1
Fig. 1.2	Four different types of copolymers: (i) Block, (ii) Random (iii) Alternating and (v) Graft copolymers, consisting of two different monomer units……..	2
Fig. 1.3	General chemical structure of a RAFT chain transfer agents……..	4
Fig. 1.4	The RAFT polymerization mechanism, as proposed by Rizzardo et al...	5
Fig. 1.5	Micellization of an amphiphilic diblock copolymer in water……..	7
Fig. 1.6	Variety of morphologies adopted by block copolymer in solution such as spherical and cylindrical micelles and vesicles……...	8
Fig. 1.7	Various structures of polymer-coated magnetic nanoparticles. (a) End-grafted polymer coated, (b) Fully encapsulated in polymer coating, (c) Liposomes, (d) Polymeric micelle and (e) Heterodimer coating…….	13
Fig. 1.8	Micellization of amphiphilic diblock copolymers in aqueous solution and magnetite nanoparticle incorporation inside the hydrophobic core..	14
Fig. 1.9	Representation of the interparticle magnetic field interactions. The effective magnetic coupling (image (a)) is decreased upon assembly with the polymer (image (b))……...	15
Fig. 1.10	**(a)** Hysteresis loop of particles assembled with zero external magnetic field measured at 300 K, **(b)** Hysteresis loop of oriented chains at 100 K and **(c)** at 5 K……	19
Fig. 1.11	Zero-field-cooling (ZFC) and field cooling (FC) curves of self-assembled magnetite spherical aggregates measured with a field of 100 Oe…….	19
Fig. 1.12	Drug encapsulated into the core of a polymer micelle…….	21
Fig. 1.13	Enhance Permeability Retention (EPR) effect……	23

Petri Papaphilippou

Fig. 1.14 Structural formula of doxorubicin (DOX)……... 28

Fig. 1.15 Release behavior of (a) DOX from PEG-b-PBLA micelles at pHs and (b) ADR from Poly(His)-b-PEG, PLLA-b-PEG mixed micelles at various pHs…….. 31

Fig. 1.16 Preparation of multifunctional polymeric micelles with tumour selectivity for active drug targeting and pH-sensitivity for intracellular site-specific transport. Folate group with high-tumour affinity due to overexpression of its receptors was conjugated onto the surface of the micelle……. 33

Fig. 1.17 Drug release (Adriamycin) from the thermo-sensitive PNIPAAm-b-PBMA block copolymers……. 35

Fig. 1.18 Increasing the temperature above the LCST enhances the release rate of the drug from the polymeric micelles…….. 35

Fig. 2.1 Schematic diagram of the Atomic Force Microscope……... 36

Fig. 2.2 Repulsive and attractive forces acting between the sample and the tip the AFM…… 37

Fig. 2.3 Schematic diagram of the Differential scanning calorimetry (DSC)…... 41

Fig. 2.4 Crystalline and amorphous regions in a semi-crystalline polymer…… 43

Fig. 2.5 Diagram of ground and excitation electron states in a molecule. Bonding (σ, π), non-bonding (n) and anti-bonding (σ^*, π^*) molecular orbitals. 46

Fig. 2.6 Schematic diagram of SEC illlustrating the penetration of particles through the column and the separation according to hydrodynamic size differences……. 49

Fig. 2.7 Magnetic moments of paramagnetic, ferromagnetic, ferrimagnetic and antiferromagnetic materials…….. 53

Fig. 2.8 (a) Magnetization (M) versus applied magnetic field strength (H) plots for ferromagnetic and superparamagnetic materials. (b) Change of coercivity (H_C) of magnetic particles with size……... 54

Fig. 2.9 Temperature-dependence of the magnetic properties of materials exhibiting different magnetic behavior…… 55

Petri Papaphilippou

Fig. 2.10 Virgin Curve, Magnetization (B) of the material related to the applied magnetic field (H)…… 57

Fig. 3.1 Structures of homopolymers and block copolymers synthesized by RAFT controlled radical polymerization……. 66

Fig. 4.1 Synthetic scheme followed for the preparation of the $PEGMA_x$-b-$AEMA_y$ diblock copolymers by RAFT…… 77

Fig. 4.2 SEC traces of the $PEGMA_{97}$ homopolymer and the corresponding $PEGMA_{97}$-b-$AEMA_{35}$ diblock copolymer……... 80

Fig. 4.3 ^1H NMR spectrum of the $PEGMA_{97}$-b-$AEMA_{35}$ diblock copolymer recorded in $CHCl_3$…… 80

Fig. 4.4 DSC thermograms of the $PEGMA_{97}$ homopolymer (solid line), the $PEGMA_{97}$-b-$AEMA_{46}$ diblock copolymer (dashed line) and that of an AEMA homopolymer (dotted line)…….. 81

Fig. 4.5 Plot of transmittance as a function of temperature measured for an aqueous solution of $AEMA_{36}$-b-$PEGMA_{292}$ diblock copolymer (concentration 4 g L^{-1})……. 82

Fig. 4.6 ^1H NMR spectrum of the $PEGMA_{97}$-b-$AEMA_{18}$ diblock copolymer in $CDCl_3$ (black) in D_2O (grey)…… 84

Fig. 4.7 Preparation steps towards the generation of polymer-coated magnetic iron oxide nanoparticles stabilized in aqueous media: (a) micelle formation of $PEGMA_x$-b-$AEMA_y$ diblock copolymers in water (b) addition of the Fe^{3+}/Fe^{2+} mixture in the micellar solution. Complexation of the iron salts with the β-ketoester ligating units found inside the micellar core. (c) Transformation of the iron salt "precursors" into iron oxide nanoparticles inside the micellar core upon addition of ammonium hydroxide aqueous solution……... 86

Fig. 4.8 Coagulation kinetics measurements by DLS performed on the $PEGMA_x$-b-$AEMA_y/Fe_xO_y$ micellar systems (at concentrations of (a) 5 mg/L and (b) 50 mg/L magnetite) in the presence of various NaCl concentrations, demonstrating the salt tolerance of these systems……. 87

Petri Papaphilippou

Fig. 4.9 AFM images of the block copolymer micelles formed in water, loaded with iron oxide nanoparticles: (a) Height image, (b) Amplitude Image, (c) Phase image……. 88

Fig. 4.10 UV-vis spectra of the unloaded (black, solid line) and loaded with iron oxide nanoparticles (grey, dashed line) $PEGMA_{97}$-b-$AEMA_{18}$ micelles... 89

Fig. 4.11 X-Ray Diffraction patterns of the iron oxide nanoparticles coated with the $PEGMA_{292}$-b-$AEMA_{36}$/ Fe_xO_y hybrid system. (a) unpurified sample (b) XRD spectrum of NH_4Cl. (c) after purification by dialysis against water……. 90

Fig. 4.12 TGA thermograms of the $PEGMA_{97}$-b-$AEMA_{46}$ block copolymer and the corresponding hybrid material $PEGMA_{97}$-b-$AEMA_{46}$……... 92

Fig. 4.13 Magnetization curves of the $PEGMA_{70}$-b-$AEMA_{16}$–coated iron oxide nanoparticles corresponding to different magnetic loading (1:1, 1:2 and 1:3 corresponds to [AEMA]/[Fe^{3+}] molar ratio)…….. 93

Fig. 4.14 The MTT colorimetric assay was used to assess the biocompatibility of the hybrid micelles. PC3 cancer cells were exposed for 72 hours to varying concentrations of the micelles ranging from 20 to 100 μg Fe /ml. Resovist® and untreated cells (H_2O) served as controls. Untreated cells (H_2O, indicated by a dotted line) served as controls at each Fe concentration. Untreated cells (0 μg Fe/ml) were considered to have 100% viability and the results were normalized accordingly. Results are given as the means of six values resulting from triplicate measurements of two representative experiments, ±SD. Variability of the error bars principally corresponds to the experimental uncertainty in each measurement……..... 94

Fig. 4.15 In vitro uptake of hybrid micelles by macrophages determined by Prussian Blue staining after incubation for 2 hours with the indicated agent at a concentration equivalent of 0.15mg Fe/mL in complete media: (A) Resovist® , (B) hybrid micelle M1, (C) hybrid micelle M2, (D) untreated control. The presence of Prussian Blue precipitate arising from the formation of potassium ferrous ferricyanide reveals the 95

Petri Papadopoulou

accumulation of the Fe-based agent into the cells……

Fig. 4.16 Functionalization of SWCNTs. (A) defect functionalization, (B) functionalization with surfactants in sidewall by covalent bonds, (C) non-covalent exohedral functionalization, (D) functionalization with polymers by non-covalent bonds and (E) encapsulation of compounds inside the tube……... 97

Fig. 4.17 Synthetic methodology followed for the preparation of SWCNT/Fe_xO_y/PEGMA$_{75}$-b-AEMA$_{23}$ magnetic nanohybrids stabilized in aqueous media…… 99

Fig. 4.18 (a) Unstable solution of SWCNT/Fe_xO_y system in the absence of the diblock copolymer, (b) Stable aqeuous solution of the SWCNT/Fe_xO_y/PEGMA$_{75}$-b-AEMA$_{23}$..... 100

Fig. 4.19 TEM images of SWCNTs decorated with iron oxide nanoparticles and stabilized in aqueous solution in the presence of the PEGMA$_x$-b-AEMA$_y$ diblock copolymers……. 101

Fig. 4.20 TGA traces of (a) SWCNT-COOH (grey-line), (b) SWCNT/PEGMA$_{75}$-b-AEMA$_{23}$/ Fe_xO_y (brown-line) and (c) PEGMA$_{75}$-b-AEMA$_{23}$ block copolymer (black-line)…….. 102

Fig. 4.21 XRD pattern of the SWCNT/Fe_xO_y/PEGMA$_{75}$-b-AEMA$_{23}$ nanocomposite…….. 103

Fig. 4.22 FTIR spectra of (a) carboxylated SWCNT and (b) SWCNT/Fe_xO_y/PEGMA$_{75}$-b-AEMA$_{23}$ composite…….. 104

Fig. 4.23 Magnetization curve of the SWCNT/Fe_xO_y/PEGMA$_{75}$-b-AEMA$_{23}$ nanocomposite recorded at 300 K, demonstrating the superparamagnetic behavior of this system……..... 105

Fig. 4.24 Amphiphilic polymer network consisting of hydrophilic and hydrophobic units……. 106

Fig. 4.25 Chemical structures and names of the main reagents used for the co-network synthesis……. 108

Fig. 4.26 Schematic presentation of the synthetic methodology followed for the fabrication of (a) random HEGMA-co-AEMA/EGDMA co-networks; 109

Petri Papaphilippou

(b) HEGMA-co-AEMA/EGDMA co-networks with embedded OA.Fe_3O_4 nanoparticles and (c) HEGMA-co-AEMA/EGDMA co-networks with embedded Fe_xO_y (nano)particles……..

Fig. 4.27 TEM images and related size histogram corresponding to the OA.Fe_3O_4 nanoparticles prepared in this study…… 110

Fig. 4.28 Deswelling kinetics of sample Gel 1c (23% wt. OA.Fe_3O_4) measured in water at ~ 60 ^oC…… 113

Fig. 4.29 TGA thermograms of Gel 1 (no OA.Fe_3O_4) and Gel 1b (OA.Fe_3O_4, 11% wt.) prepared in EA……. 114

Fig. 4.30 X-ray diffraction patterns of (i) as prepared OA.Fe_3O_4 nanoparticles (ii) Gel 1c and (iii) Gel 2c both containing 23 % wt OA.Fe_3O_4…….. 115

Fig. 4.31 Magnetization curves of (a) Series A (Gel 1b – red curve and 1c – blue curve) and (b) Series B (Gel 2b~~xii~~ red curve and 2c– blue curve) measured at 300K……. 116

Fig. 4.32 Magnetization curves of the PEGMA-co-AEMA/EGDMA-Fe_xO_y corresponding to different magnetic loading (2- blue line, 4-green line and 7-red line % wt), measured at 300K…….. 117

Fig. 4.33 Magnetization curves of the PEGMA-co-AEMA/EGDMA-Fe_xO_y corresponding to different magnetic loading (2- blue line, 4-green line and 7-red line wt%), measured at 5K……... 118

Fig. 4.34 SEM images of $CaCO_3$ crystals achieved in (a) in agarose gel and H_4hpdta ligand after 12 h (b)…… 119

Fig. 4.35 TEM images of malachite nanobiscuits obtained in the absence of additives…… 121

Fig. 4.36 TEM images of malachite "nanofibers" which are further grown into net-like superstructures, generated in the presence of a $PEGMA_x$-b-$AEMA_y$ diblock copolymer in aqueous solution…….. 122

Fig. 4.37 Synthetic methodology followed for the preparation of the $HEGMA_x$-b-$DEAEMA_y$ diblock copolymers by RAFT…… 124

Fig. 4.38 SEC traces of the $HEGMA_{128}$ homopolymer and the corresponding $HEGMA_{128}$-b-$DEAEMA_{34}$ diblock copolymer……. 126

Petri Papadopoulou

Fig. 4.39 ^{1}H NMR spectrum of the $DEAEMA_{30}$-b-$HEGMA_{210}$ diblock copolymer in $CDCl_3$…… 126

Fig. 4.40 TGA thermograms of $DEAEMA_{30}$ homopolymer (black line) and the $DEAEMA_{30}$-b-$HEGMA_{210}$ diblock copolymer (grey line)…… 127

Fig. 4.41 Calibration curve of DOX.HCl in different concentrations in DPBS…… 128

Fig. 4.42 (a) Protonation of the DEAEMA units upon lowering the pH, resulting in a hydrophilic character (b) Titration curve of the $HEGMA_x$-b-$DEAEMA_y$ diblock copolymer…….. 129

Fig. 4.43 Self-assembly of $PEGMA_x$-b-$DEAEMA_y$ block copolymers in micelle form in aqueous solution at pH > 6.8. Hydrophobic drug such as DOX can be loaded inside the core of the micelles. At acidic pHs, DEAEMA are protonated and become hydrophilic resulting the dissociation of the micelles and eventually the drug is released……. 130

Fig. 4.44 UV-Vis spectra of the DOX-loaded $PEGMA_{128}$-b-$DEAEMA_{34}$ micelles recorded at several time intervals (pH 6.0)…… 131

Fig. 4.45 DOX release kinetics from (a) $PEGMA_{128}$-b-$DEAEMA_{34}$ and (b) $DEAEMA_{30}$-b-$PEGMA_{210}$ micelles at different pHs at room temperature: pH 4.6 (green), pH 6.0 (black)……. 132

Fig. 4.46 (a)The MTT colorimetric assay was used to assess the cell viability of the loaded and unloaded micelles on MB231 breast cancer cells. For comparison, cell viability was also determined in the presence of free DOX. Untreated cells in the presence of only DPBS (control) were considered to have 100% viability and the results were normalized accordingly. Results are given as the means of six values resulting from triplicate measurements of two representative experiments, ±SD. Variability of the error bars principally corresponds to the experimental uncertainty in each measurement. (b) Cell viability studies carried out on three different systems: $HEGMA_{120}$-b-$DEAEMA_{34}$/DOX (MD1), $HEGMA_{121}$-b-$DEAEMA_{18}$/DOX (MD2), $DEAEMA_{30}$-b-$HEGMA_{210}$ (MD3)……... 134

Petri Papaphilippou

Fig. 4.47 Brightfield microscopy images of MB231 cells following treatment with (a) unloaded micelles, (b) free DOX and (c) DOX loaded micelles. Cells appear dark and rounded (dead) in the presence of DOX- loaded micelles and especially in the presence of free DOX, whereas cells treated with unloaded micelles appear healthier…… 135

Petri Papaphilippou

List of Tables

Table 1.1 Parameters which control the stability of polymeric micelles……. 23

Table 1.2 Literature examples of block copolymers used in the preparation of drug-loaded micelles…… 27

Table 3.1 Molar quantities of the monomer, the initiator and the CTA used for the preparation of $PEGMA_x$ homopolymers……. 62

Table 3.2 Molar quantities of the monomer, the initiator and the CTA used for the preparation of $AEMA_x$ homopolymers…… 62

Table 3.3 Molar quantities of the monomer, the initiator and the macroCTA used for the preparation of the block copolymers $PEGMA_x$-b-$AEMA_y$ and $AEMA_x$-b-$PEGMA_y$…….. 64

Table 3.4 Molar quantities of the monomer, the initiator and the macroCTA used for the preparation of the block copolymers $PEGMA_x$-b-$DEAEMA_y$ and $DEAEMA_x$-b-$PEGMA_y$..... 65

Table 3.5 Molar quantities of the monomers HEGMA and AEMA, the initiator AIBN and the cross-linker EGDMA that were used for the preparation of the HEGMA-co-AEMA/EGDMA hydrogels……. 67

Table 3.6 Molar quantities of the $PEGMA_x$-b-$AEMA_y$ diblock copolymers, the iron salts $FeCl_3.6H_2O/FeCl_2.4H_2O$ and the NH_4OH used to prepare polymer-coated magnetic nanoparticles in aqueous media……. 68

Table 3.7 Molar quantities of the $PEGMA_x$-b-$AEMA_y$ diblock copolymers, the iron salts $FeCl_3.6H_2O/FeCl_2.4H_2O$ and the NH_4OH used to prepare polymer-coated magnetic nanoparticles in the presence of NaCl (0.1 M)…… 69

Table 3.8 Molar quantities of the monomers HEGMA and AEMA, the initiator AIBN, the cross-linker EGDMA, OA. Fe_3O_4 and $FexO_y$ that were used for the preparation of magneto-responsive co-networks……. 73

Petri Papaphilippou

Table 4.1 Characteristics of the Polymers based on PEGMA and AEMA obtained by RAFT (Polymerization Yields, Molecular Weights and polydispersities)…… 79

Table 4.2 Hydrodynamic diameters obtained by DLS for a series of $PEGMA_x$-b-$AEMA_y$ block copolymer micelles formed in water…… 83

Table 4.3 Diffraction angles and d-spacing values corresponding to the signals observed in the XRD diffraction pattern of the $PEGMA_{97}$-b-$AEMA_{46}$/iron oxide composite material……. 91

Table 4.4 Sol fraction and magnetic loading percentages of the composite co-networks prepared in this study…… 111

Table 4.5 Degrees of swelling of the (composite) co-networks prepared in EA (series A and C) and in THF (series B)……... 112

Table 4.6 Characteristics of the polymers based on HEGMA and DEAEMA obtained by RAFT (MWs, MWDs and Compositions)…….. 125

Petri Papaphilippou

Abbreviations

ABC	Amphiphilic block copolymer
AEMA	(2-acetoacetoxy) ethyl methacrylate
AFM	Atomic Force Microscopy
AIBN	2,2`-azobis(isobutyl nitrile)
ANOVA	Analysis of variance
ATRP	Atom transfer radical polymerization
CDTB	Cumyl dithiobenzoate
CMC	Critical micellar concentration
CNT	Carbon nanotubes
CNT-COOH	Carboxylated carbon nanotubes
CTA	Chain transfer agent
DEAEMA	(2-diethylamino) ethyl methacrylate
D_H	Hydrodynamic diameter
DLS	Dynamic light scattering
DMSO	Dimethyl sulfoxide
DOX	Doxorubicin
DOX.HCl	Doxorubicin hydrochloride
DP	Degree of polymerization
DPBS	Dulbecco's phosphate buffer solution
DRI	Differential refractive index
DS	Degree of swelling
DSC	Differential Scanning Calorimetry
EA	Ethyl acetate
EGDMA	Ethylene glycol dimethacrylate
EO	Ethylene oxide
EPR	Enhance Permeability Retention
FBS	Fetal bovine serum
FTIR	Fourier-Transform Infrared

Petri Papaphilippou

GPC	Gel permeation chromatography
H	magnetic field strength
H NMR	Proton Nuclear Magnetic Resonance
H_C	coercive field
LCST	Lower critical solution temperature
M	Magnetization
MMA	Methyl methacrylate
Mn	Number average molecular weight
Mr	Remanence
MRI	Magnetic resonance imaging
Ms	Saturation magnetization
MTT	[3-(4,5-dimethylthiazol-2-yl)- 2,5-diphenyltetrazolium bromide]
Mw	Weight average molecular weight
Mw/Mn	Polydispersity index
MWCNT	Multi-wall carbon nanotubes
MWD	Molecular weight distribution
NMP	Nitrogen mediated controlled radical polymerization
OA	Oleic acid
PBS	Phosphate-buffered saline
PDI	Polydispersity index
PEG	Poly(ethylene glycol)
PEGMA	Poly(ethylene glycol) methyl ether methacrylate
PEI	Poly(ethylene imine)
PEO	Poly(ethylene oxide)
PLLA	Poly (L-lactic acid)
PMMA	Poly(methyl methacrylate)
PNIPAAm	Poly(N-isopropyl acrylamide)
PPMS	Physical Property Measurement System
PS	Polystyrene
RAFT	Reversible addition-fragmentation chain transfer

Petri Papaphilippou

RES	Reticuloendothelial systems
RI	Refractive index
SD	Standard deviations
SEC	Size exclusion chromatography
SEM	Scanning electron microscopy
SPIONs	Superparamangetic iron oxide nanoparticles
SWCNT	Single wall carbon nanotube
T_B	Blocking temperature
TEM	Transmittion electron microscopy
Tg	Glass transition temperature
TGA	Thermogravimetrical analysis
THF	Tetrahydrofuran
Tm	Melting temperature
UV-vis	Ultraviolet-visible
VSM	Vibrating sample magnetometer
XRD	X-ray diffraction

Petri Papaphilippou

Research goals

The goal of this Ph.D. Thesis was to develop stimuli-responsive (i.e. magneto-responsive, thermo-responsive and pH-responsive) polymer-based materials of various architectures with potential applications in the biomedical field. In general, stimuli-responsive polymers possess functional groups rendering them capable of changing their properties by altering a parameter of the environment, such as the temperature, the pH, the magnetic and the electric field. In the biomedical field there is a great interest in the development of new polymer-based systems that are responsive to changes in (a) the temperature, (b) the presence of an external magnetic field and (c) the pH.

Regarding the first Thesis target was the synthesis of innovative polymer-based magnetoresponsive/thermoresponsive materials were synthesized and characterized. In particular the preparation and characterization of (i) superparamagnetic polymeric micelles and (ii) superparamagnetic single-wall carbon nanotubes stabilized in aqueous media by the use of novel, well-defined amphiphilic block copolymers having hydrophilic/thermoresponsive (polyPEGMA) and metal-binding functionalities (polyAEMA) has been accomplished.

In the field of Materials Science, magneto-responsive polymer-based materials have attracted increasing attention during the last years due to their extremely interesting properties. The combination of the inherent magnetic properties of magnetic nanoparticles with the advantages of a functional polymer matrix, renders these materials promising in various applications in the biomedicine and nanotechnology field. For example such magneto-responsive materials have potential uses in the biomedical area as contrast enhancement agents in MRI, in hyperthermia treatment and as magneto-thermally-triggered drug delivery systems. AEMA (containing a β-ketoester functionality) was chosen to be the hydrophobic unit incorporated within the PEGMA-b-AEMA amphiphilic block copolymers due to its capability to develop strong interactions with inorganic matter. The β-ketoester group is well-known for its ability to act as a strong bidentate ligand and complex various metal ions of different geometries and oxidation states via its keto- or its enolate tautomeric form. For the first time in the present Thesis, novel amphiphilic diblock copolymer micelles comprising of a PEGMA hydrophilic/ thermoresponsive corona and an AEMA hydrophobic/ligating core have been employed as nanosystems for the stabilization of magnetic iron oxide nanoparticles in aqueous solutions.

Petri Papaphilippou

The nanosized micellar containers demonstrated high ability of retaining the magnetic nanoparticles stabilized in aqueous media for a long period of time, not only in neutral water but also under high salt concentrations. Hence, the PEGMA hydrophilic block provided efficient steric stabilization and at the same time, its ability to respond to temperature changes offered the system an additional functionality i.e. to be able to act as a temperature – responsive nanohybrid system in solution. On the other hand, strong interactions developed between the β-ketoester groups and the surfaces of the magnetic nanoparticles encapsulated within the micellar core, provided an improved mechanism for the stabilization of the nanoparticles.

The above-mentioned diblock copolymers were also employed for the stabilization of single-wall carbon nanotubes (SWCNTs) in aqueous media. SWCNT present unique electrical, physical, chemical and mechanical properties. New materials consisting of CNTs combined with iron oxides may find potential applications in biology and biomedicine. A significant obstacle is the difficulty for preparing stable aqueous solutions of these materials attributed to the strong tendency of CNTs for aggregation due to the intrinsic Van der Waals attractive forces and the high aspect ratio of nanotubes as well as the nanoscale dimensions and the large surface to volume ratios of the magnetic nanoparticles characterized by large surface energies combined with the strong attractive magnetic dipole-dipole forces existing between the particles. In the present work, the ability of well-defined diblock copolymers of the type PEGMA-b-AEMA to act as effective stabilizers for SWCNTs/iron oxide nanoparticles in aqueous solutions has been demonstrated for the first time.

Furthermore, in the present Thesis, magnetoresponsive/thermoresponsive polymer random *co*-networks were fabricated and characterized. In these systems either preformed oleic-acid coated or non-coated magnetic (nano)particles were incorporated inside polymeric random co-networks based on PEGMA and AEMA. These novel composite co-networks have shown different magnetic behaviour (either superparamagnetic or ferrimagnetic). Superparamagnetic properties were only observed in the cases where oleic acid-coated magnetite nanoparticles were incorporated inside the polymer matrix. Moreover, it has been demonstrated that these composite conetworks are able to respond to external temperature changes, in a similar way as that observed in the case of the PEGMA-b-AEMA diblock copolymers. Such systems could be useful in environmental applications, for example for the extraction of heavy metals from the

Petri Papaphilippou

water wastes or in the biomedical field e.g. as a potential magneto-thermally triggered drug-delivery system.

The second Thesis target was the synthesis and characterization of well-defined multi-responsive block copolymers possessing hydrophilic/thermoresponsive (polyPEGMA) and pH-responsive moieties (polyDEAEMA) and their evaluation toward their ability to act as pH-triggered drug release systems. The polyDEAEMA block consists of pH-responsive units capable of changing their character from hydrophobic into hydrophilic and vice versa by altering the pH. At pH values lower than the pKa of DEAEMA (6.8), the protonation of the tertiary amino groups in DEAEMA results in distortion of the micellar nanostructure in aqueous media, which are retained at higher pH values (above 6.8) due to the hydrophobic nature of the DEAEMA block which is found in its neutral form. Kinetic drug release studies (involving the anti-cancer drug Doxorubicin) have been carried out at different pHs, demonstrating for the first time the pH-triggered release ability of these systems.

Petri Papaphilippou

1. Introduction.

1.1. General characteristics of Polymers.

Polymers are materials that have attracted a considerable interest in the last decades due to their unique properties and potential applications in many areas. The word "*polymers"* is derived from the Greek word «*πολυ*» which means "*many"* and «μέρος» which means "*part*". A polymer molecule consists of many *"mers"* which are usually bound to each other covalently, constructing high-molecular-weight substances.

The polymer structure plays a crucial role to its properties, and is related to the arrangement of monomers along the backbone of the chain, the type of "*mers"* and the length of the polymer chain. Polymer nomenclature is based upon the type of monomers which constitute the polymer. A polymeric chain comprising of only a single type of monomer is known as homopolymer. As shown in Fig. 1.1 a homopolymer can be classified into four different categories: (a) linear, (b) branched, (c) crosslinked, and (d) network structure depending on the way the monomer units are connected to each other as a consequence of the synthetic methodology followed. Although the "*mers"* are joined together *via* covalent bonds, also secondary forces (intramolecular or intermolecular) usually exist between the polymer chains including Van der Waals forces or hydrogen bonding interactions. [1, 2]

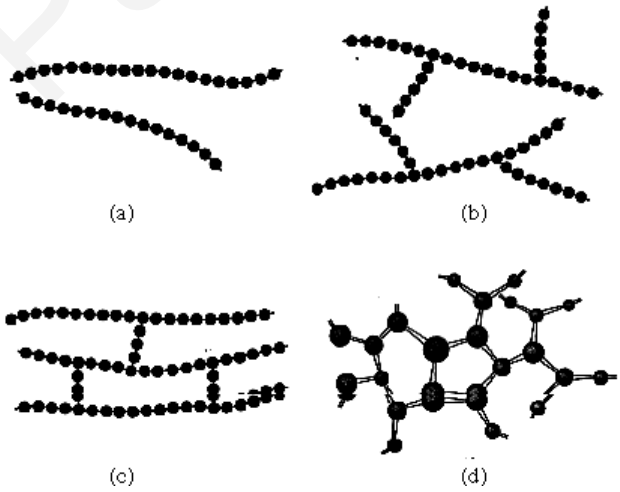

Figure 1.1. *Schematic illustration of (a) linear, (b) branched, (c) crosslinked, and (d) network (three-dimensional) molecular structures. The circle configures the individual "mer" units.*

Petri Papaphilippou

Another category of polymers which are constituted of two or more different monomer units is called *co*polymers. For example DNA molecules are composed of a variety of different *mers* namely nucleotides. Copolymers are classified into various types, depending on the monomer placement along the chain: random, alternating, graft and block copolymers. [1, 2, 3] The structural design of these four polymer types is demonstrated using two monomer units, in Fig. 1.2.

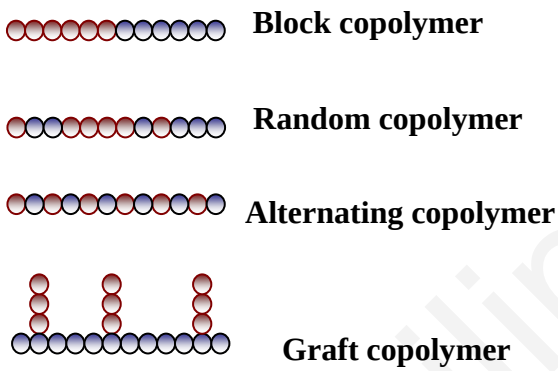

Figure 1.2. *Four different types of copolymers: (i) Block, (ii) Random (iii) Alternating and (v) Graft copolymers, consisting of two different monomer units.*

1.1.1. Polymerization methods.

Synthetic polymers may be prepared by a number of different polymerization techniques including living cationic and anionic polymerizations, the ring opening metathesis polymerization, the group transfer polymerization (GTP), the free radical polymerization and the Ziegler-Natta polymerization.

Free-radical polymerization belongs to the so-called chain-growth polymerization techniques. The mechanism of this method involves three principal steps: the *initiation*, the *propagation* and the *termination*.[4] In the first step, an initiating molecule attacks a monomer molecule thus developing an active monomer. During the next phase of the polymerization, propagation or growth of the active (free radical) chain is achieved by sequential addition of monomers. The propagating chain that loses the active site is transformed to non-active namely as “dead” chain. Finally the termination step involves the destruction of all the active centers.[2, 5] Free radical polymerization has attracted much attention especially in industry because it is a method that does not require extreme conditions to be performed. Nevertheless, it shows an important disadvantage which is the lack of control over the

Petri Papaphilippou

molecular characteristics of the synthesized polymers in particular the polymer molecular weight, molecular weight distribution and the chain end groups.[6]

Controlled radical polymerization is one of the most widely used processes for the commercial production of high molecular weight polymers. This type of polymerization has earned significant development over the last decade due to its possibility to produce polymers characterized by predetermined molecular weights with narrow polydispersity indices (PDI) and well-defined architectures.

The Nitroxide Mediated Polymerization (NMP) and the Atom Transfer Radical Polymerization (ATRP) methods that have been developed in recent years belong to this category and are based on a *reversible activation – deactivation* mechanism, resulting to a uniform growth of all polymer chains. Moreover, in 1998, Rizzardo's group in CSIRO laboratories developed a new controlled radical polymerization methodology namely ***Reversible Addition-Fragmentation Chain Transfer (RAFT)*** polymerization. In RAFT polymerization, a chain transfer agent is employed (usually a thiocarbonylthio compound) that reacts with propagating radicals via a *reversible chain-transfer* process.[7, 39]

RAFT is an extremely versatile polymerization method. This polymerization technique allows the synthesis of functional polymers with controlled molecular weight and low polydispersity indices. It can be used in the fabrication of complex architectures such as block,[8, 9] star,[10, 11] graft polymers,[12] polymer networks,[13] microgels and hyperbranched structures. Moreover, RAFT is applicable to a vast range of monomer types such as styrene, (meth)acrylates, (meth)acrylamides, acrylonitrile, vinyl acetates, vinyl formamide, or monomers bearing protonated acidic groups that cannot be polymerized by other polymerization methods. This polymerization process can be also carried out in different solvents including aqueous media and over a wide temperature range (20-150 ^{o}C) as well as in homogeneous and heterogeneous media such as bulk, solution, emulsion, miniemulsion, and suspension.[14, 42]

An important parameter in RAFT polymerization is the right choice of the chain transfer agent (CTA), depending on the type of monomers and the reaction conditions used. The general structure of a RAFT agent is displayed in Fig. 1.3. The CTAs possess a reactive C=S bond and a weak S-R single bond. The selection of the Z and R groups is important for the

Petri Papaphilippou

determination of both addition and fragmentation rates and hence the effectiveness of the RAFT agent.

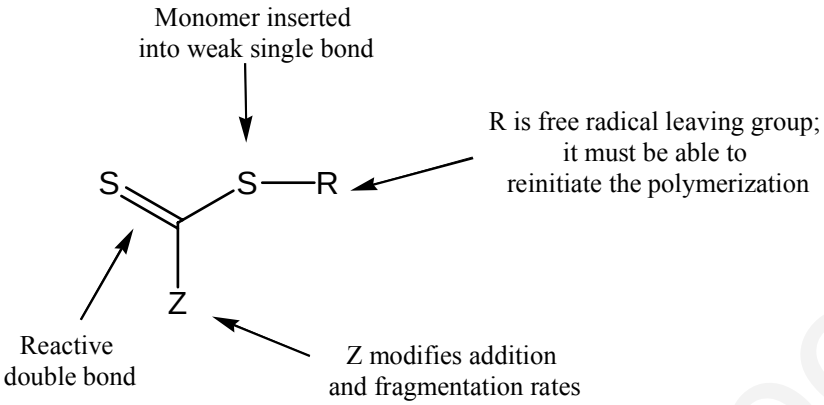

Figure 1.3. *General chemical structure of a RAFT chain transfer agent.*[7]

The Z group must be capable of activating the C=S double bond and it may be an aryl or an alkyl group. The R segment must be a good free-radical leaving group such as cumyl and cyanoisopropyl, with the ability to reinitiate the polymerization.[15]

In RAFT polymerization, peroxy or azo compounds such as 2,2'-azobis(isobutyronitrile) (AIBN), benzoyl peroxide (BPO) and potassium persulfate (KPS) are usually employed as initiators. RAFT can be also performed with the use of UV irradiation, γ-source and plasma initiation. [16] The RAFT mechanism proposed by *Rizzardo et. al.* involves a rapid exchange of the radical between all the growing polymer chains *via* an addition-fragmentation reaction with the chain transfer agent. This causes the uniform growth of all polymer chains and the equal probability to add monomers units.[18] As illustrated in Fig. 1.4, at first (*initiation*) the homolytic cleavage of the initiator occurs thus generating an active free radical. This in turn may react with a monomer molecule creating an active center to which other monomers are added hence developing a polymer chain $P_n\cdot$. Subsequently, the $P_n\cdot$ radical chain is added to the chain transfer molecule forming an intermediate radical. The fragmentation of the intermediate radical in the *reversible chain transfer* step gives either the polymer chain $P_n\cdot$ or a new radical R· which reinitiates the polymerization. The new free radical can react with a monomer molecule and develop a new active centre and finally a new propagation chain $P_m\cdot$. Then the actively growing $P_m\cdot$ radical chain is added on the dormant compound and the $P_n\cdot$ chain is released in the next step namely as *chain equilibration*. The adding cycle to the double bond C=S is ended when all monomer molecules and the initiator are totally

Petri Papaphilippou

consumed. In the final *termination* step the radical polymer chains $P_n\cdot$ and $P_m\cdot$ may connect together resulting to the formation of a "dead" polymer chain.[17]

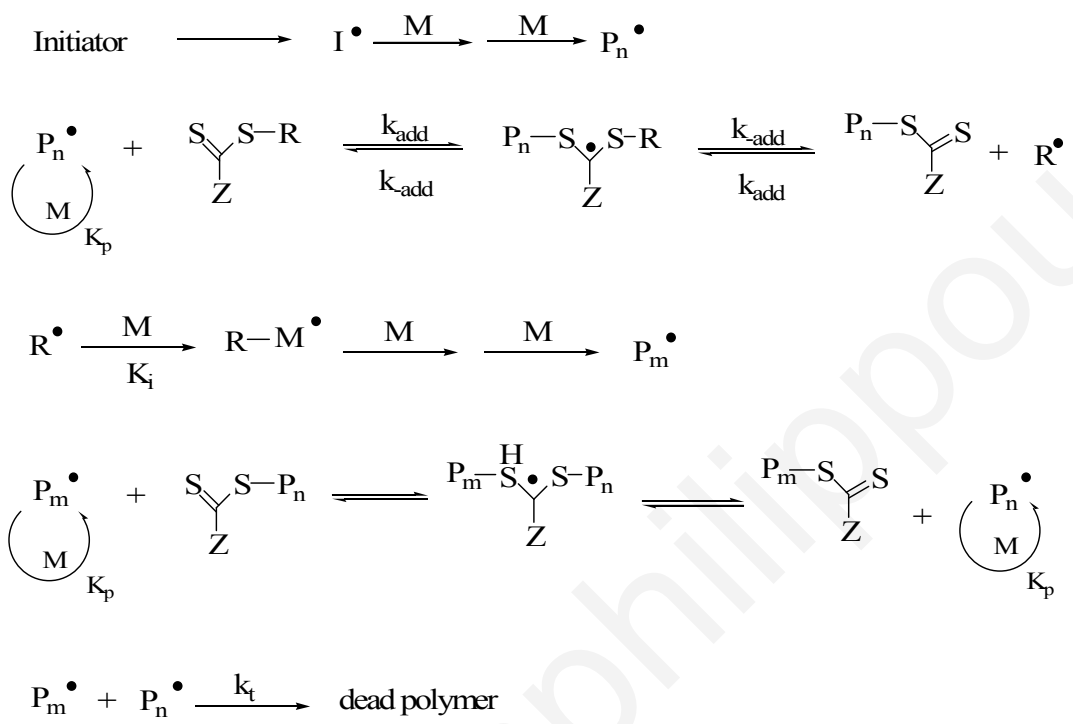

Figure 1.4. *The RAFT polymerization mechanism, as proposed by Rizzardo et. al.* [18]

There are three main points that need to be taken into account in RAFT polymerization. The chain transfer agent used should have a high transfer constant in the monomers to be polymerized. The intermediates should fragment rapidly and give no side reactions and the radicals R· should efficiently reinitiate the polymerization process.

RAFT polymerization is recognized as one of the foremost method for block copolymer synthesis and numerous examples already appear in the literature. This method proceeds with the retention of the thiocarbonylthio group at the chain-end of a homopolymer "precursor", thus assisting the synthesis of AB diblock copolymers *via* the addition of a second monomer. In block copolymer synthesis, it is important to keep a very high fraction of living ends throughout the polymerization process.[19]

Atom transfer radical polymerization (ATRP) is a simple and inexpensive polymerization method which can be used for polymerizing a wide range of monomers including styrenes,

Petri Papaphilippou

acrylates, methacrylates, dienes and acrylonitriles. By ATRP, polymers with controlled molar masses and low PDI can be obtained. It is a versatile method for the preparation of polymers with different chemical compositions and architectures such as a linear, star, dendritic or a hyperbranched structures.

In ATRP the polymerization takes place through "redox" reactions. As initiator molecules alkyl halides (R-Cl), such as the alpha substituted alkyl halides with aryl, allyl, carbonyl and sulfonyl groups as substituents (haloesters and haloacetons) are used. The catalyst used is a transition metal that is complexed by one or more ligands. Transition metals that are commonly used are Fe, Cu, Rh, Ni and Pd. Ligands that are complexed with these metals are pyridines containing nitrogen donor atoms. [20]

According to the ATRP mechanism the control of this polymerization is afforded by the activation of a dormant species or the deactivation of the active radical chain when it reacts with the metal catalyst respectively. Such a process results in a polymer chain that slowly but steadily grows and has a well-defined end group. The "redox" process results to an equilibrium existing between the polymer-halide (P_n-X) and the reactive polymer-radical (Pn-R·) chains.

Nitrogen mediated controlled radical polymerization (NMP) involves the use of a "nitroxide or otherwise alkoxyamine" as a stable radical such as the TEMPO (2,2,6,6-tetramethylpiperidinyl-1-oxy), the SG1 (N-tertphosphono-2,2-dimethylpropyl nitroxide) or the TIPNO.[21, 22, 23, 24] The first step is the *initiation* where the initiator molecule decomposes thus giving a free radical which adds to monomer molecules. Subsequently, in the *propagation* step, a propagation or growth of the active (free-radical) chain takes place by sequential addition of monomers. The *reversible* reaction occurring between the nitroxide stable radical and the propagating chain results in the reduction of the rate of termination reactions. As a consequence all chains present an equal chance to grow resulting in uniformity in chain length and low PDI.[25]

Petri Papaphilippou

1.2. Amphiphilic Block Copolymers and Micellization.

Amphiphilic block copolymers (ABCs) are macromolecules consisting of two or more different blocks of constitutionally and or configurationally different monomeric units, i.e. A_x-B_y, A_x-B_y-A_z etc. In the last decades amphiphilic block copolymers have attracted increasing attention owing to their unique solution and associative properties as a result of their molecular structure.[26] Particularly a diblock copolymer consisting of two different types of blocks has the tendency to self-assemble into micellar nanostructures in selective solvents.

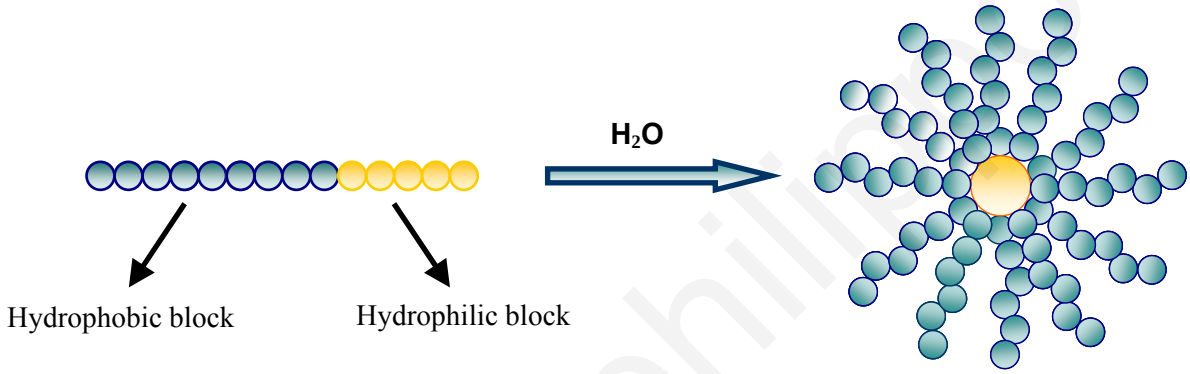

Figure 1.5. *Micellization of an amphiphilic diblock copolymer in water.*

Micellization of an amphiphilic block copolymer in an aqueous solution occurs when one of the blocks is hydrophilic whilst the other is hydrophobic. In an aqueous environment block copolymers form core-shell structures through the isolation of insoluble blocks into the core which is surrounded by the hydrophilic shell.[27] The hydrophobic core has the ability to solubilize non water-soluble compounds while the hydrophilic shell serves as the stabilizing interface between the hydrophobic core and the external aqueous medium.

The major driving force behind self-assembly of ABCs in aqueous media is the decrease of the free energy of the system, due to the removal of the hydrophobic segments from the aqueous environment *via* the formation of the hydrophobic micellar core stabilized by the hydrophilic blocks that are exposed to water.[28]

There are two principle methods for the preparation of block copolymer micelles in aqueous media: (i) the direct dissolution method and (ii) the dialysis method. The choice of which method to use depends on the solubility of the block copolymer in water. If the copolymer is

Petri Papaphilippou

soluble in water the direct dissolution is employed whereas if the copolymer is poorly soluble in water the dialysis method is usually the method of choice.[29] The latter involves the dissolution of the polymer in a good solvent for both block segments followed by the slow addition of a selective solvent for one of the blocks.[30]

Functionalized ABC micelles generated in aqueous media can be used in the biomedical field as drug carriers,[31] targeted drug delivery systems,[32] bioreactors, diagnostic tools and non-viral gene vectors.[33] A block copolymer controls the amphiphilic character of the polymeric micelle by changing the hydrophilic/hydrophobic blocks ratio and can adopt various well-organized architectures including spherical, rod, lamellar, vesicles structures, tubules, hexagonally packed hollow hoops and many more.[34, 35, 36, 37]

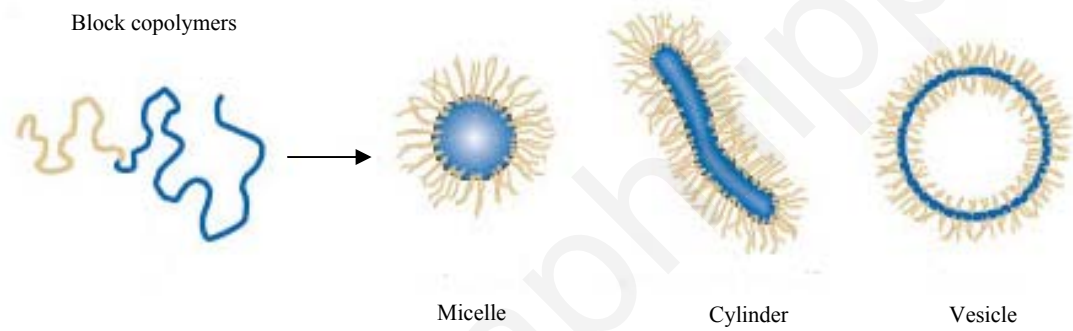

Figure 1.6. *Variety of morphologies adopted by block copolymers in solution such as spherical and cylindrical micelles and vesicles.*

The formation of micelles by ABCs is determined by two main parameters:

(i) The respective block lengths N_A and N_B of the two segments

(ii) The Flory-Huggins interaction parameter, which considers both, polymer-polymer and polymer-solvent interactions.

The molecular weights of both, the core- and the corona-forming blocks influence strongly the micellar morphology. For obtaining spherical micellar structures, the length and hence the molecular weight of the corona-forming hydrophilic segment should be higher than that of the core-forming hydrophobic block.[4] However, if the length of the hydrophilic block is too high, copolymers exist in water as individual molecules (random coils).

Besides self-assembly in solution, ABCs have the ability to self-aggregate in the solid state creating well-defined nanomorphologies such as lamellar, hexagonal packed cylinders and bcc-cubic structures. In this case, the basic parameters which determine the size (usually 10-100 nm) and morphology of the nanodomains formed by an ABC in the solid state are:

Petri Papaphilippou

(i) The total degree of polymerization (DP), N, which equals to the sum of the DPs of the two blocks

(ii) The molar fraction of each block i.e. $f_A = N_A/N$ and $f_B = N_B/N$

(iii) The Flory-Huggins interaction parameter which in this case characterizes only polymer-polymer interactions.

1.3. Magneto-responsive polymer-based hybrid materials.

1.3.1. Magnetic Nanoparticles.

In the last years nanotechonology has become even more regarded due to the possibility of synthesizing, characterizing and altering the properties of nanoparticles designed for biomedical applications. Nanoparticles are of great scientific interest because of their extremely small dimensions. A nanocrystalline material has grains in the order of 1 to 100 nm. It is well known that the average size of an atom is about 1-2 Å and hence within a nm there may be 3-5 atoms.[38]

The properties of materials change as their size approaches the nanoscale and as the percentage of atoms at the surface of a material becomes significant. For this reason the physical, chemical and biological properties of nanoparticles are significantly changed or completely differ from those of the corresponding bulk materials. For the design and synthesis of nanoparticles / nanomaterials with specific properties their chemical and structural characteristics have to be considered. Such characteristics include the chemical composition, the nature of the interactions taking place between the particles, the surface charge, the crystalline or amorphous phase, the size and the morphology. Due to their nanoscale dimensions and the large surface-to-volume ratios, nanocrystalline materials are exceptionally strong, hard, ductile at high temperatures, wear-resistant, erosion-resistant, corrosion-resistant, chemically reactive and present low toxicity effects.[39, 40]

Magnetic nanoparticles, for instance iron oxides such as magnetite and maghemite, have shown potential applicability as MRI contrast agents, as vehicles in magnetic field-directed drug delivery applications and as agents in hyperthermia treatment because of their special chemical, physical and magnetic properties.[41, 42] When these nanoparticles are placed in an

Petri Papaphilippou

external magnetic field, their magnetic moments align rapidly in the direction of the field and the materials display a net magnetization. Depending on their magnetic properties the removal of the magnetic field results in either loss of the net magnetization (superparamagnetic properties) or remanent magnetization (e.g. ferri- or ferromagnetic properties).

Magnetic resonance imaging (MRI) is a non-invasive clinical imaging modality that produces high quality images of the inside of the body. It is widely used in diagnosis and therapy of various human diseases. This technique measures the change in the signal emitted from the hydrogen nuclei inside the body in the presence of an applied magnetic field. For the MRI examinations contrast agents are employed to improve the contrast. MRI contrast agents have the ability to enhance the image contrast between normal and diseased tissue and also indicate the status of organ function or blood flow. Ferromagnetic and mainly superparamagnetic materials are used as contrast agents because they show high magnetization in the presence of a magnetic field. Such compounds are low molecular weight based chelates of metal ions like Mn^{2+}, Gd^{3+} and iron oxide particles. Usually as bioimaging probes in MRI, superparamagnetic iron oxide nanoparticles are used the so called SPIONs. Examples of Market products include the Feridex®, the Endorem® and the Resovist®.[43, 44, 45]

Besides their above-mentioned application, magnetic nanoparticles have been used in several areas such as *in vivo* targeting drug delivery,[16, 46] *in vitro* cell separation,[47] magnetic storage and recording, tumor hyperthermia as a heating source,[48] radioactive therapies, tissue repair, enzyme immobilization, protein purification, magnetic separation, magnetic ink printing,[49] catalysis and as tags for biomolecular sensors.[50] Another application of magnetic particles is the isolation of environmentally hazardous materials like the metal ions from industrial water wastes.[51, 52]

Due to their nanoscale dimensions and their large surface to volume ratios, magnetic nanoparticles present large surface energies (>100 dyn/cm), resulting in strong surface stresses. This, combined with the strong attractive magnetic dipole-dipole forces existing between the particles, favor aggregation/sedimentation in magnetic dispersions so as to reduce their large surface energy.[53] If the particles are too large, magnetic interactions are dominated leading to particles` agglomeration. However, the particles must be larger than 1-2 nm so as to retain their magnetic properties.[54, 55]

Petri Papaphilippou

Iron oxide nanoparticles are considered to be one of the most popular categories of magnetic materials.[56] Magnetite (Fe_3O_4) and maghemite (Fe_2O_3) nanoparticles display strong ferrimagnetic behavior and are more stable against oxidation compared to other magnetic transition metal nanoparticles such as Co, Fe and Ni. Transition metals have high magnetization but are sensitive to oxidation. This results in loss of the magnetic response due to the formation of antiferromagnetic oxides. The iron oxides are intensively used in biomedical applications due to their superior biocompatibility, non-toxicity and biodegradability.

The magnetic properties of Fe_3O_4 and γ-Fe_2O_3 depend on their size. For example magnetite nanoparticles smaller than 30 nm show superparamagnetic behavior at room temperature. As already mentioned, these nanoparticles are called SPIONs (Superparamagnetic Iron Oxide Nanoparticles). SPIONs can be used *in vivo* applications as drug delivery systems and as contrast agents in MRI, enhancing signal intensity. When the size of the iron oxide is larger than 25-30 nm, it displays ferrimagnetic behavior and their use is limited mainly to *in vitro* magnetic separation procedures.[57]

1.3.2. Stability of magnetite nanoparticles.

The technological and medical applications of magnetic nanoparticles require that the particles are superparamagnetic with sizes smaller than 30 nm and with narrow size distribution in order to present uniform chemical and physical properties. Furthermore, the stability of magnetic nanoparticles in magnetic dispersions becomes very important because of the agglomeration and fluctuation phenomena occurring in solution. The nanoparticle surface can influence the material durability in biological environments and also biocompatibility. Due to their small size and large surface, magnetic nanoparticles will tend to aggregate to reduce their surface energy. Magnetic interactions and Van der Waals forces generated between the nanoparticles from residual magnetic moments may cause the observed clustering-aggregation. The magnetic coupling between adjacent particles alters the magnetic properties of a material through magneto static interactions.[58, 59]

Agglomeration of the magnetite particles is initiated from collisions between the particles during nucleus formation. Growth of the agglomeration occurs *via* attraction forces taking place between clusters and particles until equilibrium is reached. As already mentioned, the

Petri Papaphilippou

nanosize of these particles results in large surface energy which accelerates the aggregation process in order to decrease the free energy (ΔG) of the system.

Magnetic particles must remain non-aggregated to prevent them from losing the specific properties associated with their nanometer dimensions. One method to stabilize the "ferrofluid" (*fluid dispersions of small magnetic nanoparticles*) is through electrostatic stabilization that can be achieved by introducing charged layers on the nanoparticles` surfaces developing in this way repulsive forces between them. Moreover, steric stabilization can be used by introducing polymeric materials that can bind onto the surface of the nanoparticles. The presence of polymer chains, prevent the magnetic cores from coming close to each other hence providing stabilization in solution. Coatings can improve colloidal stability, oxidation resistance, the ability for functionalization, phagocyte resistance and mechanical stability. In aqueous solutions of magnetic nanoparticles, electrostatic layers,[60] bilayer surfactants[61] and polymers have been used as stabilizers.[62, 63, 64, 65] These surface coatings have been developed in order to prevent the aggregation, enhance compatibility of the nanoparticles or improve their stability in suspension and provide chemical handles for further conjugation.

Several *natural polymers* for instance polysaccharides such as dextran and starch, chitosan, polypeptides, pullulan and BSA have been used as stabilizing agents for SPIONs because of their strong interactions with the iron oxide surface, their biocompatibility and their hydrophilic properties.[66] Polysaccharide coatings though, present a structural weakness since they may be dissolved in highly acidic environments. The silicon coatings are used to protect the magnetic nanoparticles from lysomal enzymatic digestion and improve chemical stability.[67] Furthermore, oleic or mystiric acids were coated as double layers onto the surface of magnetite nanoparticles preventing the aggregation of the particles due to the combination of steric and electrostatic stabilization.[68] Another alternative is the use of biocompatible *synthetic polymers* which present some advantages over the natural polymers. Depending on the polymerization method the chemical structure, molecular weight and molecular weight distribution may be altered, surfaces can be tailor-engineered and functional groups may be introduced.[25] The polymer interacts with the magnetic nanoparticles *via* its specific functional groups to form a tightly bonded monomolecular layer around the particles. Particularly, the iron oxide exhibits chemical affinity with polymers has -OH and $-NH_2$ groups *via* a coordination reaction and also with those having $-COO^-$ groups *via* the development of Coulomb forces with the iron ions.

Petri Papaphilippou

1.3.3. Polymer-stabilized magnetite nanoparticles.

Polymer coatings can enhance the compatibility with organic ingredients and protect particle surfaces from oxidation. Consequently encapsulation improves good dispersibility, chemical stability and reduces toxicity.[69] Fig. 1.7 presents the structures of polymer nanomorphologies in which magnetic nanoparticles are encapsulated.

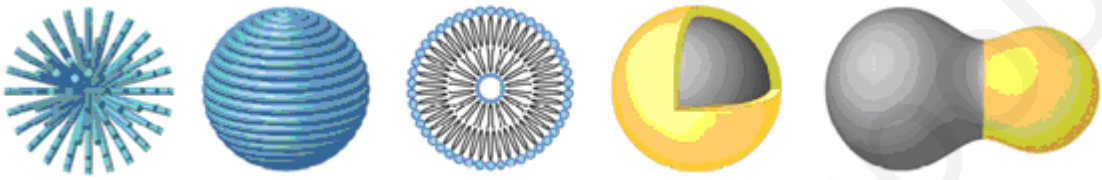

(a) ***(b)*** ***(c)*** ***(d)*** ***(e)***

Figure 1.7. *Various structures of polymer-coated magnetic nanoparticles: (a) End-grafted polymer coated, (b) Fully encapsulated in polymer coating, (c) Liposomes, (d) Polymeric micelle and (e) Heterodimer coating.*[70]

Previous studies have suggested that certain macromolecules such as amphiphilic diblock and triblock copolymers consisting of two or three different polymeric segments in which hydrophilic and hydrophobic moieties are incorporated can be used as effective coatings. The hydrophobic magnetite/maghemite nanoparticles in the absence of the block polymer flocculate and eventually precipitate in aqueous media. However, in the presence of an amphiphilic block copolymer the magnetite dispersions are stabilized, *via* the adsorption of the hydrophobic block onto the hydrophobic surface of magnetite whereas the hydrophilic block segments ensure stability of the whole aggregate in aqueous solution.

Block copolymers having functional groups such as *carboxylic acids*, *phosphates*, *thiols* and *sulfates* can bind to magnetite surfaces by forming chemical bonds with the iron metal.[71, 72] Moreover, small chain alcohols have been used; in that case chemical bonding takes place between the metal and the OH groups. It has been also reported that iron oxide nanoparticles (Fe_3O_4 and γ-Fe_2O_3) of different sizes have been physically encapsulated in the core of block copolymer micelles.[73] Surfactants with head-to-tail structure having a strongly binding head group may be able to bind more securely and densely onto the metal surface.[74] As already mentioned, in addition to the synthetic polymers, there are some natural

Petri Papaphilippou

polymers which can decorate the surfaces of iron oxides particles and prevent the agglomeration. Examples include polysaccharides such as dextran and chitosan.[75, 76]

1.3.4. Block copolymer micelles as nanocarriers for magnetic nanoparticles.

Block copolymers are macromolecules with linear or radial arrangement of two or more different blocks of varying monomer composition. In the last decades block copolymers have attracted increasing attention owing to their unique solution and associative properties as a result of their molecular structure.[26]

The micellization of an amphiphilic block copolymer takes place in aqueous media when one of the blocks is hydrophilic and the other one is hydrophobic, as shown in Fig. 1.8. As mentioned in 1.2, in an aqueous environment block copolymers form a core-shell structure (micelle) through the isolation of insoluble blocks into the core which is surrounded by a hydrophilic shell composed of hydrophilic blocks.[27].

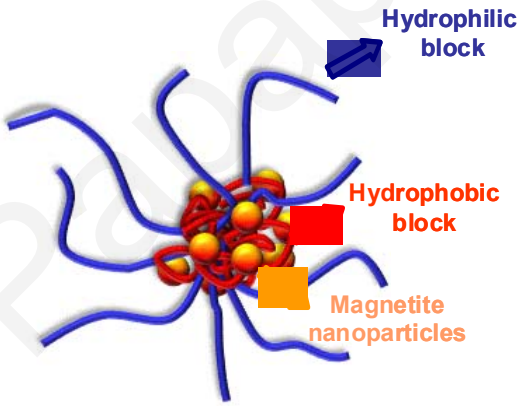

Figure 1.8. *Micellization of amphiphilic diblock copolymers in aqueous solution and magnetite nanoparticle incorporation inside the hydrophobic core.*

The major driving force behind self-association is the decrease of the free energy of the system, due to removal of the hydrophobic segments from the aqueous environment upon the formation of the micellar core, stabilized with hydrophilic blocks exposed to water.[77]

Petri Papaphilippou

The hydrophobic core has the ability to solubilize hydrophobic materials such as magnetic nanoparticles while the hydrophilic corona serves as a stabilizing interface between the hydrophobic core and the external medium.

One important parameter affecting the stabilization process is the block length. The length of the stabilizing polymer chain must be sufficient to balance the magnetic attractions and the Van der Waals attractive forces. When the polymer molecular weight is small (i.e. small chain length), large aggregates are formed, whereas as the molecular weight increases, the enhanced steric stabilization leads to individual dispersion of the particles preventing the formation of aggregates (clusters).[40] This means that polymer self-assembly causes an increase in the average interparticle spacing and a qualitative increase in the overall system ordering. Upon encapsulation of the magnetic nanoparticles by a polymer chain, the effective magnetic coupling is decreased as illustrated in Fig. 1.9.

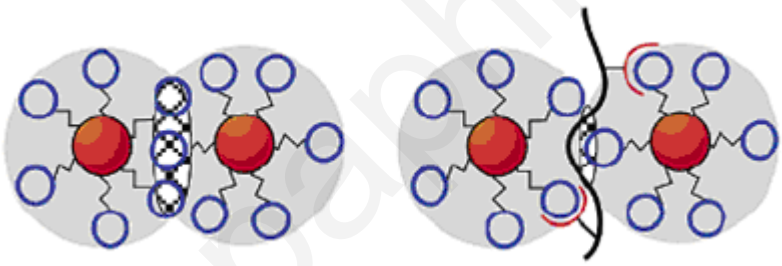

(a) ***(b)***

Figure 1.9. *Representation of the interparticle magnetic field interactions. The effective magnetic coupling (image (a)) is decreased upon assembly with the polymer(image (b)).*[40]

With further increase in molecular weight, the polymer begins to bridge between the particles and the clusters once again begin to form (bridging coagulation). According to the Rosensweig's modified Hamaker equation, the stabilizer sheaths must be greater than 1-2 nm in a good solvent for the tail blocks to sterically stabilize a magnetite nanoparticle with a diameter of 10 nm. A sufficient stabilizer chain creates a potential energy barrier (~ 25 $k\ T$) that is of an order of magnitude greater than the thermal energy associated with each nanoparticle, hence particle coalescence is minimized.

Petri Papaphilippou

The average number of encapsulated nanoparticles per micelle could be controlled by varying the relative starting concentrations of nanoparticles and polymer. By retaining unchanged the polymer concentration and simultaneously increasing particle concentration, the number of particles incorporated into each micelle is increased, affecting in this way the diameter of the magneto-responsive micelle. A fixed concentration of magnetic nanoparticles and a higher concentration of polymer coating may lead to the formation of finer oxide particles with narrower size distribution. The solvent-polymer interaction plays a key role in determining the particle size and structure of the magnetic nanoparticle-polymer composite.

Many researchers tried to fabricate polymer-based magnetoresponsive core-shell nanostructures. The polymer shell may protect the magnetic core against degradation or allow the formation of close-packed particle arrays with a fixed interparticle spacing. For example polymers of methoxy poly (ethylene glycol) (MPEG),[78] poly(ethylene glycol) (PEG),[63] dodecylamine (DDA),[79] poly(methacrylic acid) (PMAA)[80, 81] poly(oligo(ethylene glycol) methacrylate-*co*-methacrylic acid P(OEGMA-*co*-MAA),[82] poly(styrene-*b*-acrylic acid) (PS-*b*-PAA),[83] poly(acrylic acid)-*b*-poly(ethylene oxide) (PAA-*b*-PEO)[84] poly(acrylic acid)-*b*-poly(acrylate methoxy poly(ethylene oxide) (PAA-*b*-PAMPEO),[85] poly(ethyl methacrylate)-*b*-poly(2-hydroxyethyl methacylate) (PEMA-*b*-PHEMA)[85] poly(ethylene glycol) methyl ether-*b*-poly(ε-caprolactone) (mPEG-*b*-PCL),[86,87] poly(styrene-*b*-tetraethylenepentamine) (PS-*b*-TEPA), (PS-*g*-TEPA), (PE-*g*-TEPA),[88] poly(TMSMA-*r*-PEGMA),[89] poly(styrene)-*b*-poly(butyl methacrylate) (PS-*b*-PBMA), a PEG comb-like polymer constituted of poly(2-hydroxyethyl methacrylate)-*co*-hydroxy-poly(oxyethylene) methacrylate (HEMA-*co*-HPOEM)[90] and poly(vinyl pyrrolidone) (PVP) have been used as stabilizers for magnetite Fe_3O_4 or maghemite Fe_2O_3 nanoparticles. Moreover, thermo-responsive polymers that present a lower critical solution temperature (LCST) have been introduced as stabilizers for magnetite nanoparticles. An example of this category of polymers is the poly (N-isopropylacrylamide) (PNIPAAm) which has a LCST around the 32 ˚C and can interact with Fe_3O_4 *via* the amide group. Below the LCST temperature the polymer presents a hydrophilic character and above this temperature it becomes hydrophobic. *Wakamatsu et al*. successfully synthesized poly(N-isopropylacrylamide)-*co*-poly(2-carboxyisopropylacrylamide) (PNIPAAm-*co*-CIPAAm) copolymers and used them to stabilize magnetite nanoparticles. [91]

Petri Papaphilippou

The use of biocompatible polymers as stabilizers for magnetic nanoparticles improves significantly the colloidal stability in physiological media and at the same time reduces toxicity. For example magnetite nanoparticles coated with thin layers of poly(ethylene oxide) may be sufficiently small to be eliminated through the human renal glomerular filtration system.[63] Thus the size range may prove to be important for minimizing any toxicity considerations in biomedical applications. According to *Shourong Wan et al*. the poly(glycerol monoacrylate) (PGA) and poly(glycerol monomethylacrylate) (PGMA) homopolymers and their diblock copolymers employed as magnetite coaters, formed very stable aqueous dispersions. These polymers contain two hydroxyl groups which are coordinated to the magnetite surface. [92] Poly(ethylene glycol)-*b*-poly(glycerol monoacrylate) (PEG-*b*-PGA) and (PEG-*g*-PGA) may also act as stabilizers for Fe_3O_4 particles in aqueous media, upon strong chemisorption of the hydroxyl groups of the PGA onto the Fe atoms found on the particles surfaces.[93]

PGMA can be easily converted into various functional groups such as amine and aldehyde. Upon modification of the poly(glycerol monomethylacrylate) in the presence of ethylenediamine (EDA) more hydrophilic PGMA particles consisting of -NH- and NH_2-amino groups were produced which were used as the metal binding groups. A stable Fe_3O_4 nanoparticle dispersion was also obtained in the presence of poly(ethyl methacrylate)-*b*-poly(2-hydroxyethyl methacrylate) (PEMA-*b*-PHEMA) because of the inherent strong interaction occurring between the magnetite particles and the carboxyl groups and not the hydroxyl group of the PHEMA.[85]

Polymeric micelles constituted of methoxy poly(ethylene glycol)-*b*-oligo(aspartic acid) (MPEG-*b*-Asp) chains were used as stabilizers for magnetite nanoparticles. The latter were incorporated into the inner micellar core *via* the interactions of the oxygen atoms of the oligo(aspartic acid) carboxylate groups with the iron oxide surface, while the MPEG block was extended into water constituting the micellar corona.[94]

Finally, *Qian Zhang et al.* synthesized block copolymer dispersants having either poly(ethylene oxide), poly(ethylene oxide-*co*-propylene oxide), or poly(ethylene oxide-*b*-propylene oxide) outer blocks and a polyurethane center block that contained pendent carboxylate groups. The stability of magnetite particles in aqueous media was provided by the interactions existing between the magnetite nanoparticles and the carboxylate groups.[94]

Petri Papaphilippou

1.3.5. Magnetic properties of polymer-coated Fe_xO_y nanoparticles.

The magnetic properties of polymer coated iron oxides nanoparticles are influenced by various parameters such as the particle size, the morphology, the surface coating as well as the temperature. Regarding the former, it has been demonstrated that samples consisting of larger particles showed higher magnetizations.[92] Samples comprising of very small particles proved to be superparamagnetic but their saturation magnetizations were lower compared to those corresponding to larger particles which indicated ferro- or ferrimagnetic behavior and higher magnetization. This result is probably attributed to the fact that the magnetic order of the small particles has a single magnetic domain and it is easier to randomize, hence the observed saturation magnetization is smaller.

Ningning Guan et al. successfully functionalized the surface of magnetite nanoparticles with the poly(propylene glycol)-*bis*-(2-aminopropyl ether) copolymer resulting in a variety of morphologies. They have reported small differences in saturation magnetization recorded at room temperature for solid or hollow spherical particles and polyhedral-like particles. [95]

Temperature is another parameter which plays a significant role to the magnetic behavior of a sample. At room temperature (300 K) a sample might be superparamagnetic with high magnetic susceptibility by the absence of a hysteresis loop, with almost immeasurable coercivity (H_c) and remanence ratio ($M_r = \sigma_r / \sigma_s$) parameters.[96] The superparamagnetic characteristics at high temperatures indicate that the thermal energy ($\kappa_B T$) is large enough to overcome the low anisotropy energy barrier of a single particle. The magnetization reversal and the production of rapid fluctuations can lead to a time-averaged magnetization of zero-termed superparamagnetic relaxation whereas the net magnetization of the particle assemblies in the absence of an external magnetic field is zero.[97, 98] At lower temperatures (for example 5K) the sample may become ferri- or ferromagnetic because of the small thermal energy ($\kappa_B T$) and high anisotropy energy barrier so it does not improve the magnetization reversal.[57, 98, 99] Hysteresis measurements reported by *Y. Sahoo et al.* demonstrated that the coersivity and remanence ratio was much higher at 5K compared to that recorded at room temperature and the magnetization *vs* applied magnetic field plots exhibited hysteresis, as shown in Fig. 1.10. [96]

Petri Papaphilippou

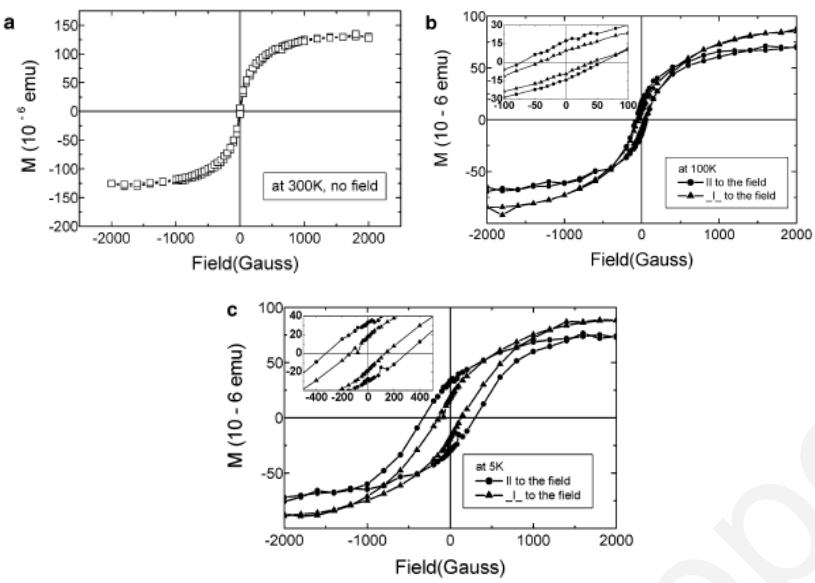

***Figure 1.10**. (a) Hysteresis loop of particles assembled with zero external magnetic field measured at 300 K, (b) Hysteresis loop of oriented chains at 100 K and (c) at 5 K.*[96]

At low temperatures and in the presence of an external magnetic field the reorientation of the moments of the individual particles along the applied field is favored. As the temperature increases much more magnetic nanoparticles reorient their magnetization with the external field and the total magnetization increases and reaches the maximum at the blocking temperature T_B = 70 K as shown in Fig. 1.11. At this specific temperature a transition from the ferromagnetic to superparamagnetic behavior occurs. Above the T_B, the magnetization decreases following the Curie-Weiss law corresponding to the superparamagnetic behavior, suggesting the absence of strong dipole-dipole interactions.[100]

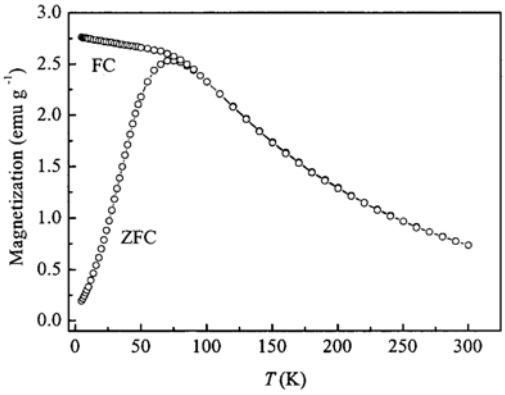

***Figure 1.11.** Zero-field-cooling (ZFC) and field cooling (FC) curves of self-assembled magnetite spherical aggregates measured with a field of 100 Oe.*[100]

Petri Papaphilippou

Yanglong et al. developed composite magnetite nanoparticles coated with 2-caroxyterthiophene (TTP-COOH) *via* π-π interactions, resulting in spherical aggregates of a hydrodynamic diameter ~ 100 nm. At 300 K the saturation magnetization of the assembled magnetite nanoparticles was 83 emu/g at 30 KOe while that of the commercial magnetic liquid was 123 emu/g (Fe) and that of the bulk Fe_3O_4, 92 emu/g. The decrease of the Ms is affected by the presence of surfactants on the surface of the Fe_3O_4 nanoparticles.[100] Moreover, the magnetic measurements studies of PGMA-NH_2 and MPEG-*b*-PGA-coated magnetite nanoparticles indicated that the nanoparticles show superparamagnetic behavior. Also in this case, Ms was found to be 16.3 emu/g and ~20 emu/g respectively which were lower compared to the value corresponding to the bulk material.[101, 102]
Such phenomena, (i.e. reduction of magnetization upon coating) may be attributed among others to the electron exchange between the coating and the surface atoms that could quench the magnetic moment.[96] Generally the lower saturation magnetization of nanoparticles compared to bulk materials is due to other factors besides the presence of a coating onto their surfaces. Some studies suggested that the magnetite molecules on the surface require complete coordination and the spins are likewise disordered, therefore the large surface to volume ratio may be a parameter that leads to a decrease in Ms. Furthermore, the incomplete crystallization of magnetite nanoparticles which lead to undetectable amorphous impurities may be another reason for lower magnetization values.

1.4. Polymeric micelles in drug delivery applications.

Natural and synthetic polymers, liposomes and polymeric micelles are being extensively investigated as nanocarriers in drug delivery applications. Liposomes are artificial phospholipid vesicles with sizes varying from 50 to 1000 nm. They can be loaded with a variety of water-soluble drugs (into the aqueous compartment) and water-insoluble drugs (into the hydrophobic compartment of the phospholipid layer). Binding of targeting moieties onto the liposome surfaces may provide selective accumulation inside an affected organ or tissue, causing an increase in the efficacy of the liposome-incorporated drug.[103]

Polymeric micelles consisting of amphiphilic blocks (hydrophilic/hydrophobic) are characterized by smaller size range -at about 5-100 nm- compared to liposomes and they can adopt different morphologies. Their smaller sizes allow them to spontaneously penetrate into

Petri Papaphilippou

the interstitium in the body compartments *via* the so-called Enhanced Permeability and Retention (EPR) effect. Moreover, the hydrophilic PEG block that is usually employed as the exterior compartment of the micelles provides an improved blood circulation time and biocompatibility.[103, 104]

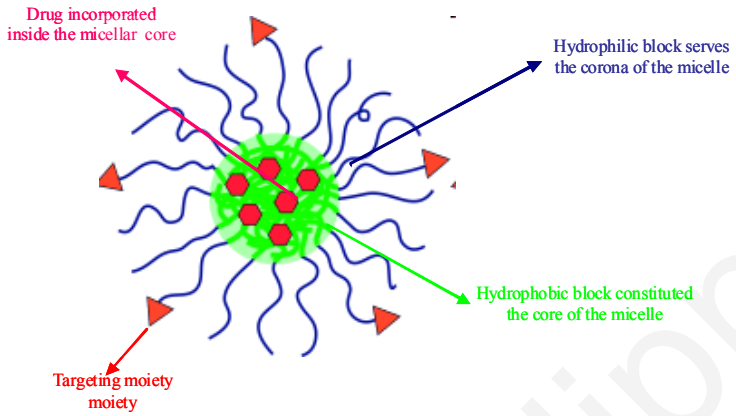

Figure 1.12. *Drug encapsulated into the core of a polymer micelle.*

However, contrary to liposomes that have been shown to incorporate water-soluble drugs into their aqueous interior, polymeric micelles can be carriers for hydrophobic and sparingly soluble pharmaceuticals.[104]

Compared to conventional surfactant micelles, polymer micelles present a superior thermodynamic stability under physiological solutions due to their lower critical micellar concentrations (CMC).[105]

1.4.1. Stability of polymeric micelles used in drug delivery.

The size and surface properties of polymeric micelles are crucial parameters in achieving modulated drug delivery with remarkable efficacy. For successful drug targeting the achievement of a prolonged blood circulation of polymeric nanocarriers might be of primary importance in cases where the polymeric carriers are delivered to the target tissue through the bloodstream.

There are several obstacles to the long circulation of drug nanocarriers in the bloodstream including the recognition and the non-specific uptake by reticuloendothelial systems (RES) located in the liver, spleen and lung and also the glomerular excretion by the kidney.[106, 107]

Petri Papaphilippou

The elements of RES in the liver are regulated by the presence and balance between two groups of blood components: opsonins that promote the phagocytosis and dysopsonins that suppress the process. *Opsonization* is a process where plasma proteins can be adsorbed on the particle's surface leading to its recognition by the body's major defense system, the reticuloendothelial system (RES). The RES is consisted of a diffuse system of phagocytic cells that are linked with the connective tissues in the liver, spleen and lymph nodes. Macrophage cells in the liver and the spleen are important in removing the particles identified by opsonization.

Micelles belong to the large family of the colloidal dispersed systems in which the particle size vary from <1 nm for molecular dispersions to >0.5μm for coarse dispersions. More precisely, micelles are characterized by particle sizes in the range of 10-100 nm.[104] Due to their sizes, polymeric micelles are large enough to avoid renal excretion (MW > 50 kDa) and yet small enough (hydrodynamic radii < 200 nm) to bypass filtration by interendothelial cell slits in the spleen.[108]

Nanocarriers such as polymeric drug-loaded micelles achieving prolonged circulation times, can accumulate in tumor tissues characterized by a 'leaky' endothelia cell layer *via* the EPR effect. According to this, larger particles such as polymer micelles used as drug carriers are only diffused through the "leaky" endothelial cell layers in solid tumors in contrast to low molecular weight substances that are capable of permeating the cell layers of normal tissues as well. This effect is also called "passive drug targeting". In disease states such as tumors, the permeability of blood vessels increases though the loss of junction integrity between endothelial cells and loss of cell-cell and cell-matrix interactions, in contrast to the normal endothelium of blood vessels which presents a physical barrier for extravasations of drug delivery systems to the surrounding tissues. Micelles with hydrodynamic radii at about 50 nm are capable of passing only through the pores between the "leaky" endothelial cell layers that are generated by inflammation or unusual vasculogenesis in tumors and aided by impaired lymphatic drainage they then accumulate in the interstitial fluid.[109, 110, 111]

Petri Papaphilippou

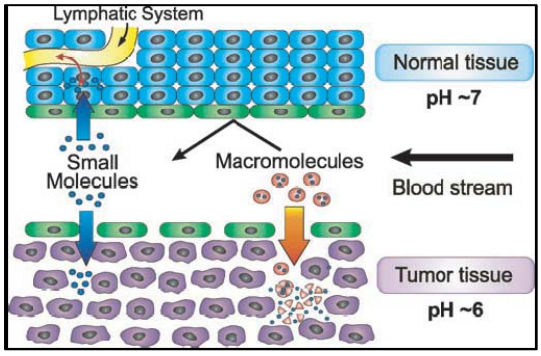

***Figure 1.13**. Enhance Permeability Retention (EPR) effect.*[112]

The kinetic and thermodynamic stability of amphiphilic block copolymer micelles destined to be used in biomedical applications are very important parameters. The Critical Micellar Concentration (CMC), the Glass Transition Temperature (Tg) of the copolymer, the hydrophilic-hydrophobic block ratio and the conjugated drug content are only a few of the factors which can affect the stability of polymeric micelles used as drug delivery vehicles.[34]

***Table 1.1.** Parameters which control the stability of polymeric micelles.*

Parameters		**Micelle stability**
Low CMC	→	High Stability
High Tg	→	High Stability
Low hydrophilic-hydrophobic blocks ratio	→	High Stability
High conjugated drug content	→	High Stability

Critical Micellar Concentration is defined as the copolymer concentration below which only single chains (unimers) exist in solution whereas above CMC usually both, micelles and unimers are found in equilibrium. As shown in Table 1.1, the stabilization of the micelles is improved in systems presenting lower CMC values. Amphiphilic block copolymers, consisting of a highly hydrophobic block exhibit smaller CMC values in water than those possessing a less hydrophobic block. Consequently, the nature and length of the polymer chains constructing the micellar core have significant effect on the CMC.

The higher the Glass Transition Temperature (T*g*) of the hydrophobic block is, the lower the release rate of single polymer chains from the micelles will be. In addition, the physical or chemical conjugation of a hydrophobic drug enhances the stability of the micelle because

Petri Papaphilippou

there is an increase in the hydrophobic interactions developed between the hydrophobic chains and the drug within the core.

1.4.2. Hydrophilic and hydrophobic blocks in amphiphilic block copolymer micelles used as drug delivery systems.

It is well known that the stability of polymeric micelles used as nano-vehicles for drug delivery depends strongly on the nature and the length of the hydrophilic and the hydrophobic blocks. The use of certain amphiphilic molecules as micellar building blocks, introduce the property of micelle-extended blood half-life upon intravenous administration and control the release rate of drugs from the polymeric micelles.

As already described in 1.2, the self-assembly of amphiphilic block copolymers in an aqueous solution leads to a core-shell nanostructure. According to the literature, this kind of micellar structures usually employ a poly(ethylene glycol) (PEG) or poly(ethylene oxide) (PEO) segment as the outer shell-corona to protect the inner core (drug reservoir) from the outer environment. The specific role of the hydrophilic PEG block *in vivo* is the steric stabilization of the micelle preventing the recognition by the reticuloendothelial (RES). This in turn leads to an increased blood circulation time, thus allowing drugs to be administrated over a prolonged period of time. It has been demonstrated that the presence of PEO on the micellar surface reduces the extent phagocytosis by mouse peritoneal macrophage cells *in vitro*.[113] PEO is known to be non-toxic and presents high flexibility as well as high degree of hydration. These properties make a PEG-containing micellar surface protein-resistant, demonstrating minimized protein adsorption and cellular adhesion, probably through a steric exclusion mechanism. Proteins adsorb on to the surface of a foreign material within a few seconds of exposure to the blood especially if the surface is charged or hydrophobic. Protein adsorption may cause damage or lysis of the vehicle and release of the drug. Hence in the presence of a PEGylated micellar corona the contents of the hydrophobic core are effectively protected against hydrolysis and enzymatic degradation. However, the strong hydrogen bonding character of the PEG chains may provoke considerable interaction with biological components possessing strong hydrogen-bonding functionalities affecting the stability of the polymeric micelle. This mode of interaction might become important at the interface of PEGylated micelles with target cells.[34, 113, 114, 115]

Petri Papaphilippou

As previously mentioned, stabilizing moieties which are present on the exterior of polymeric micelles such as PEG, generate steric repulsive forces which compete with the interparticle Van der Waals attractive forces. Coagulation is prevented if the repulsive forces overwhelm the attractive forces existing between the particles. The efficacy of protection of polymeric micelles from destabilization depends on both, the surface density of the PEG blocks and the thickness of the protective layer, which is controlled by the length of the PEG segment.

Inoue et al., reported on the preparation of polymeric micelles generated by an amphiphilic copolymer consisting of a poly(acrylic acid) (PAAc) hydrophilic shell and a oligo(methyl methacrylate) hydrophobic core. In contrast to the micelles where PEG is employed as a neutral hydrophilic corona, the PAAc produced micelles having a negative charge on their surface, at certain pH values.[105] Charged systems may be most useful for delivery to mucosal surfaces and may afford the development of effective oral and aerosol block copolymer micellar formulations.[34] Poly (N-Vinyl-2-pyrrolidone) (PVP), poly (vinyl alcohol) (PVA), or poly(2-ethyl-2-oxazoline) (PEOz) may be also introduced as the hydrophilic blocks in amphiphilic block copolymer micelles used as drug nanocarriers.[116, 117, 118] Poly(N-isopropylacrylamide) (PNIPAAm) is another hydrophilic polymer presenting a thermoresponsive behavior. As previously mentioned, PNIPAAm has LCST i.e. it presents hydrophilicity below a certain temperature whereas at higher temperatures it becomes hydrophobic. Due to this inherent property, PNIPAAm has been extensively investigated as one of the compartments in polymeric micelles used as drug carriers.[119]

In contrast to the universal use of poly (ethylene glycol) as the hydrophilic block in micellar systems destined for use in the biomedical field, a variety of hydrophobic blocks has been explored. Thus the uniqueness associated with the different copolymer systems largely originates from the choice of the hydrophobic block.

Most amphiphilic copolymers employed for drug delivery purposes contain either polyester, poly(amino acid) or poly (ether) derivatives as the hydrophobic component. Poly(lactic acid),[120, 121, 122] poly(ε-caprolactone),[123, 124, 125] poly(glycolic acid), poly(β-benzyl-L-aspartate),[126, 127] poly(γ-benzyl-L-glutamate),[128] poly(D,L-lactide),[129, 130, 131] poly(methacrylic acid)[132] and oligo(methyl methacrylate)[105] are all biocompatible polyesters. Poly(L-amino acids) (PAA) commonly used in drug delivery include poly(aspartic acid),[133, 134] poly(L-lysine),[135, 136] poly(Histidine)[137], poly(spermine)[138] and Pluronic-PLGA (PEO-PPO-PEO-

Petri Papaphilippou

PLGA)[139]. Polyethers constitute another class of hydrophobic polymers that can be employed to prepare amphiphilic micelles such as poly(propylene oxide).[140, 141]

1.4.3. Targeted polymeric drug-nanovehicles.

The specific targeting of drugs to their pathological site of action should increase the therapeutic selectivity and effectiveness as well as reduce side effects. Sometimes the drug travels freely through the body and acts on the desired target tissues but also causes undesirable effects on the normal tissues. The problem of target specificity is affected by the barriers that the body presents toward the successful delivery of the drug to the active site such as enzymes, cells, membranes and organs. As previously mentioned, with the careful design of polymer-based micellar drug-delivery systems all these obstacles may be avoided.

The success of drug loaded-micelles towards targeting lies on their capability to accumulate in desired body compartments. There are several approaches to achieve specific accumulation of the incorporated drug nanocarriers into pathological sites in the body. The first one is based on the EPR effect where the drug-loaded micelles accumulate in areas with 'leaky' vasculature such as tumors, the so-called "passive targeting".[109, 110]

The second targeting mechanism is relied on the incidence that the pathological tissues and organs are attended by a local increase of the temperature or a local change at the pH. Therefore, the micelles which consist of thermo- or pH- responsive components can be destructed, releasing the incorporated drug only at the pathogenic site.[142, 143]

Moreover, the selective drug delivery capability of polymeric micelles may be further enhanced by attaching specific targeting ligands such as antibodies,[144] transferrin, folate,[137, 145] or certain sugar moieties to the termini of the shell forming hydrophilic blocks. These ligands can bind selectively onto the surface of many target cells (such as cancer cells) by forming complexes with the corresponding receptor moieties which are present onto those surfaces ("active" targeting). The targeting moiety has to be chemically bonded to an activated water-exposed free end of a hydrophilic block to avoid the steric hindrances.[146]

Petri Papaphilippou

1.4.4. Drug-loading in polymeric micelles.

The hydrophobic micellar core serves as a cargo to enhance solubility and stability of non-water soluble drugs. The drug can be incorporated into the micelle by simple physical entrapment based on hydrophobic interactions and *via* chemical attachment -covalent/ionic bonding- with the hydrophobic block of the amphiphilic micelle. The loading efficiency and capacity of block copolymer micelles can be influenced by the nature of the hydrophobic core, the length of the core-forming block segment, the solute concentration and the drug-drug and drug-solvent interactions.[147] An increase in the hydrophobic/hydrophilic block length ratio has been found to decrease the CMC, resulting in an increased loading capacity.

The loading efficiency of the drugs into the micellar core can be determined by using the following equation:

Loading (%) =

[(the amount of drug in micelles) / (the amount of drug added initially)] * 100% (1.1)

1.4.5. Drug-loaded micellar nanocarriers.

The high toxicity of the "free" drugs travelling in the body and their non-specific accumulation in certain pathological tissues/cells, created the necessity to entrap them into micellar entities. Literature examples on polymeric micelles that have been investigated as drug-vehicles and for which a high stability and low toxicity have been reported are summarized in Table 1.2.

Table 1.2. *Literature examples of block copolymers used in the preparation of drug-loaded micelles.*

Block copolymers	**Drugs-loaded**	**Ref.**
PEG-*b*-P(Asp) *(poly(aspartic acid)*	ADR CPT CDDP	148 149 150, 151
PEG-*b*-PBLA *(poly(β-benzyl L-aspartate)*	CPT DOX Idomethacine	152 153 126
PEG-*b*-PHPMAmDL *(poly(N-(2-hydroxypropyl) methacrylamide lactate)*	Taxol	154
PEG-*b*-PLLA *(poly(L-lactic acid)*	ADR	137
PEG-*b*-PolyHis	ADR	137, 155

Petri Papaphilippou

PIPAAm-*b*-PBMA *(poly(N-isopropylacrylamide-b-butylmethacrylate)*	ADR	[143]
PHEMA-*b*-AAm *(poly(2-hydroxyethyl-methacrylate)-b-acrylamide*	Diclofenac	[156]
PEG-*b*-P(Glu) *(poly(glutamic acid))*	CDDP	[157]
MePEG-*b*-PCL *(methoxyPEG-b-poly(caprolactone))*	Idomethacine	[125]
oMMA-*b*-PAAc *(oligo (methyl methacrylate)-b-poly (acrylic acid))*	DOX	[105]
PEO-PPO-PEO (*pluronics)-triblock copolymer*	DOX CDDP	[158]
MPEG-*b*-PVL *(methoxy poly(ethylene glycol)-b-poly (valerolactone)*	CPT	[159]
Poly (N, N-diethylamide-co-acrylamide)-*b*-poly (γ-benzyl L-glutamate)	Taxol	[160]
MethoxyPEG-*b*-PLA-methacryloyl acid	Taxol	[161]
PLLA-*b*-PEGmal-TAT *(poly (L-lactic acid -b- poly(ethylene glycol) maleimide ether-TAT[FITC-Gly-Cys-Cys-(Gly)$_3$-Tyr-Gly-Arg-(Lys)$_2$-(Arg)$_2$-Gln-(Arg)$_3$] peptide*	DOX	[162]
PCBS-*b*-PEG *(poly (L-cystine bisamide-g-sulfadiazine) -b-poly (ethylene glycol)*	DOX	[117]
PLL-*b*-PEG-*b*-PLL *poly(L-leucine)-b-poly (ethylene glycol) -b-poly (L-leucine)*	Taxol	[163]
PAA-*b*-(PEG-*b*-PPO-*b*-PEG)-*b*-PAA	DOX	[164]

Doxorubicin (trade name Adriamycin) is an antracyclin drug which is commonly used in the treatment of cancer. This drug has the ability to interact with the DNA by intercalation of cancer tumor cells and therefore it has been widely used in chemotherapy.[165]

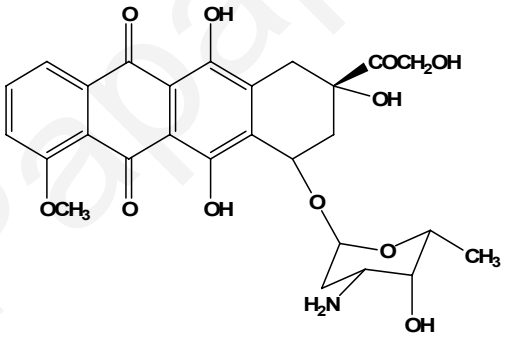

Figure 1.14. *Structural formula of doxorubicin (DOX).*[153]

Doxorubicin has been physically and chemically entrapped into the core of a polymeric micelle consisting of PEG-*b*-PBLA diblock copolymers. [153] Micelles with both chemically-bound and physically-entrapped DOX seem to become more stable resulting in longer circulation time in blood before their disintegration. In this example, it has been demonstrated that the chemically conjugated DOX did not play a role in the expression of anticancer activity, whereas the physically entrapped DOX expressed anticancer activity. Moreover, the DOX-loaded micelles showed a considerably higher antitumor activity against mouse C26 tumor compared to free DOX.

Petri Papaphilippou

Camptothecin (CPT) is a potent cytotoxic quinoline alkaloid which inhibits the enzyme DNA topoisomerase I (topo I). CPT showed remarkable anticancer activity in preliminary clinical trials but also low solubility and adverse drug reaction. CPT was successfully incorporated into polymeric micelles formed by poly(ethylene glycol)-b-poly(aspartic acid) (PEG-*b*-P(Asp)) block copolymers. The solubility and stability of the CPT were improved *via* physical entrapment into the micellar core.[152] The stability of CPT- incorporated micelles *in vivo* strongly depended on the hydrophobic block (i.e. the amount of benzyl ester moieties on the hydrophobic chain), the length of the PEG block and the drug content.[149, 152]

Cisplatin or ***cis*-diaminedichloroplatinum(II)**, **(CDDP)** is a platinum-based chemotherapy drug used to treat various types of cancers, including sarcomas, some carcinomas, lymphomas and germ cell tumors. The anticancer drug of cisplatin was bound to the aspartic residues of the PEG-*b*-P(Asp) block copolymer *via* a ligand substitution (anion Cl^-) reaction. The polymer-metal complexes containing Pt(II) formed a stable micellar structure at room temperature in aqueous media. [150, 151]

Paclitaxel (taxol) is a mitotic inhibitor used in cancer chemotherapy.[166] Paclitaxel is now used in clinical practice and exhibits strong cytotoxic activity against a variety of cancer types, especially lung, ovarian, breast cancer, head and neck cancer, and advanced forms of Kaposi's sarcoma. The PTX has been successfully incorporated in the micellar core of the amphiphilic poly(*N*-(2-hydroxypropyl) methacrylamide lactate)-*b*-poly(ethylene glycol (PEG-*b*-PHPMAmDL) block copolymers *via* hydrophobic interactions.[154] 70% of PTX was released from the PTX-loaded micelles within 20 h at 37 °C and at pH 7.4. Moreover, the PTX-loaded pHPMAmDL-*b*-PEG micelles showed comparable *in vitro* cytotoxicity against B16F10 cells compared to the Taxol standard formulation containing Cremophor EL.

1.4.6. Drug-release studies in drug-loaded polymeric micelles.

Recently the use of polymeric nanocarrier systems with activated mechanisms for drug release as a new strategy for cancer treatment has attracted much attention. Since the ordinary delivery of drugs to target sites of cells/tissues induces undesired side-effects and non-specific accumulation, novel systems have utilized triggered release to provide a high-dose at drug action sites and minimize the toxicity effects on normal cells.

Petri Papaphilippou

Parameters influencing the Release Kinetics

The release of drugs from block copolymer micelles depends on many factors such as the micellar stability, the rate of diffusion of the drug from the micelles and the rate of biodegradation of the copolymer. The rate of drug release from the amphiphilic block copolymer micelle is affected by the following:[34]

(a) The presence of strong interactions between the drug and the hydrophobic core will increases the loading and at the same time will decrease the release rate of the drug from the micelles.
(b) If the drug localizes at the interface between the micellar core and the corona, the release rate would be faster. In contrast, if the drug lies into the core the release rate will decrease.
(c) The diffusion process of a drug entrapped inside a hydrophobic core characterized by a high glass transition temperature (Tg) will be slower.
(d) The longer the core-forming block is, the larger the core and the slower the release of the drug from the micelle will be.

For improving the drug therapeutic effects at the target cells and also reducing the toxicity on physiological tissues, the rate of release from the micelle must be decreased during the circulation of the drug-loaded micelle in the bloodstream. Therefore, all the above statements should be taken into consideration for the design of ultimate polymeric micelles as drug-nanocarriers.

Furthermore, such problems may be overcome by novel-infiltrating polymeric drug-carrier micelles that are sensitive to intracellular environmental changes such as pH and temperature. In particular, an intracellular environment-sensitive polymeric micelle can stably preserve drugs under physiological conditions (pH 7.4) and selectively release the loaded drug by sensing the intracellular pH decreases in the acidic tumour -endocytic-compartments such as endosomes (pH 5-6) and lysosomes (pH 4-5). [142, 146, 167]

1.4.7. pH-triggered drug delivery systems.

A decrease in pH results in structural changes and destabilization of polymeric drug-loaded micelles because of the presence of ionizable groups within the polymer structures.

Petri Papaphilippou

Moreover, by reducing the intracellular pH the cleavage of pH-labile chemical bonds existing between the drug and the constituent polymers is provoked, leading to drug release at specific sites.[142] Many pathological processes present a decrease in pH. For example in contrast to the normal blood having a pH of 7.4, extracellular pH_e in tumorous tissues were determined to be around 6.8-7.0. The acidity of tumour cells is primarily attributed to the tumor's histology and volume and more precisely to the high accumulation of lactic acid at the non-physiological tissues which is produced during glycolysis in tumour cells under either aerobic or anaerobic conditions compared to normal cells. Intracellular compartments such as endosomes and lysosomes exhibit even lower pH_i levels of around 4-6.[108, 142, 168, 169, 170] The acidic environment gives benefit to cancer cells and promotes the invasiveness by destroying the extracellular matrix of the surrounding normal tissues giving them in this way a competitive advantage over normal cells for growth.[171] *Kataoka et al.* utilized the block copolymer PEG-*b*-PBLA to prepare a pH-sensitive drug nanocarrier system. The anticancer drug Doxorubicin (or Adriamysin) was physically loaded into the micelles of the amphiphilic molecules by dialysis or by an oil-in-water (o/w) emulsion method. The physical entrapment of the drug was accomplished *via* π-π stacking interactions developed between the benzyl residues of the PBLA hydrophobic core and DOX.[153] The release of DOX from the polymeric micelles proceeded in two stages: An initial rapid release, followed by a long lasting release of the drug, as observed in Fig. 1.15. As the pH decreased from 7.4 to 5.0, the release rate was accelerated, presumably due to a protonation of the NH_2 group on DOX structure.

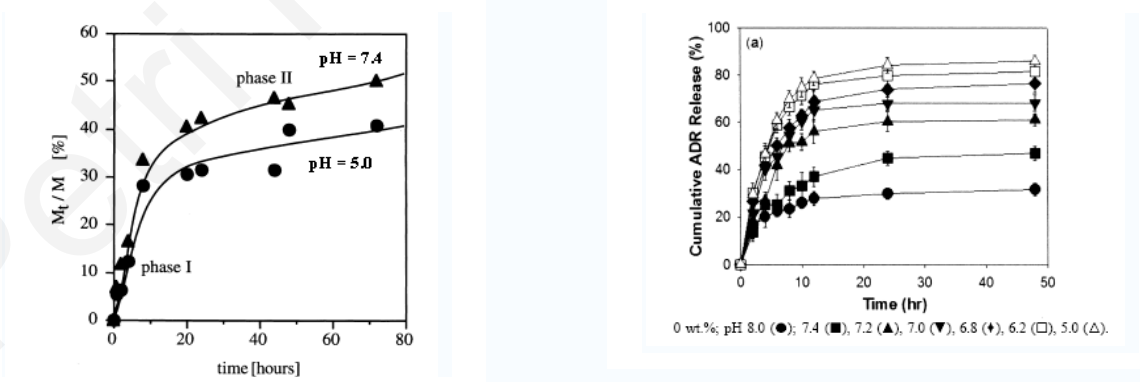

(a) **(b)**

Figure 1.15. *Release behavior of DOX from (a) PEG-b-PBLA micelles at pHs 5.0 and 7.4*[156] *and (b) Poly(His)-b-PEG/PLLA-b-PEG mixed micelles at various pHs.*[137]

The amount of doxorubicin released from the micelles at pH 5.0 was significantly higher than the amount released at pH 7.4.[153] In contrast, the release rate of Indomethacin -anticancer drug- from the PEG-*b*-PBLA micelles, was slower at low pH and faster at higher pH. This is attributed to the ionization of the drug and the enhanced solubility at higher pH values.[171]

Poly(His)-*b*-PEG (or Poly(His)-*b*-PEG-folate) and PLLA-*b*-PEG (or PLLA-*b*-PEG-folate) were used to prepare novel pH-sensitive polymeric mixed micelles. The mixed micelles showed accelerated Adriamycin (or DOX) release as the pH decreased from 7.4 to 5.0. Enhancement of the pH above the pKb ~ 6.5 of the poly(His) block, led to deprotonation of the imidazole group of poly(His) which became hydrophobic. At a pH lower than the pKb of poly(His), protonation of Poly(His) occured and the copolymer became more hydrophilic. This resulted to the destabilization of the micelles and a higher release rate of the drug from the micellar core.

The acidic pH inside the tumour cells and more specific in endosomes and lysosomes is attributed to the high metabolic rate of tumor cells which leads to the production of excess lactic acid and hydrolysis of Adenosine-5'-triphosphate (ATP) under hypoxic conditions. This difference in pH between the tumor and normal cells has been utilized to create “smart” cytosolic anticancer drug delivery systems.[117] Such drug-nanocarrier systems consist of a pH-labile chemical bond existing between the micellar hydrophobic core and the drug, which responds to endosomal/lysosome acidic pH. The cleavable bonds that link the polymer and the drug together may be hydrazone,[146, 167, 172] acetal, sulfonamide pendal groups and N-ethoxy-benzymidazole. The cleavage of such chemical bonds by acidic pH can accelerate antitumor drug release from the nanovehicles. *Kataoka et al.* reported the preparation of a drug-nanocarrier polymeric micelle of poly(ethylene glycol)-*b*-poly(aspartate hydrazone adriamycin) or Poly(Asp-Hyd-ADR)-PEG-folate.[146, 167]

Petri Papaphilippou

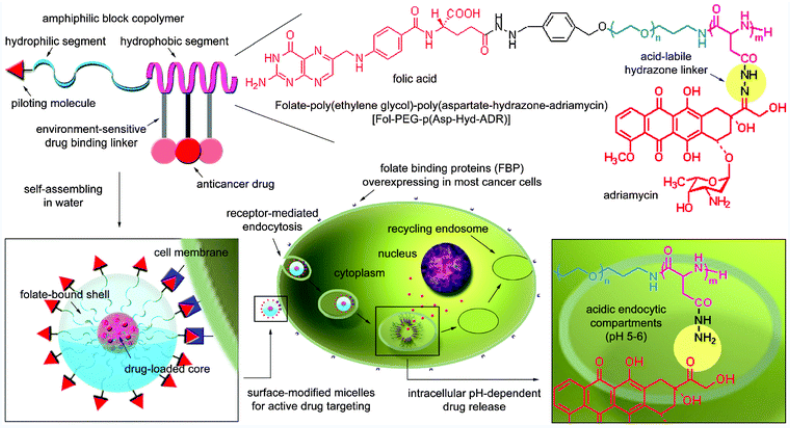

Figure 1.16. *Preparation of multifunctional polymeric micelles with tumour selectivity for active drug targeting and pH-sensitivity for intracellular site-specific transport. Folate group with high-tumour affinity due to overexpression of its receptors was conjugated onto the surface of the micelle.*[146]

The anticancer drug ADR was conjugated to the hydrophobic core of the micelle through hydrazone linkers which are quite stable under physiological conditions (pH 7.4), but hydrolyze at around pH 5-6. The higher release rate of ADR from the block copolymer micelle at pH 5-6 is caused by the catalytic-protonation of the hydrazone linker (Fig.1.28), leading to the cleavage of the polymer-drug bond.

In vivo studies showed that those micelles were stable during blood circulation and had minimal toxicity effects because of the reduced release of the anticancer drug under physiological conditions. Furthermore, the successful access of the polymeric nanovehicle into the tumour cell was accomplished though the folate receptor, *via* an endocytosis mechanism.[146, 167]

Chytil's group developed a novel drug-polymer delivery system for specific-targeting of the antitumor drug Doxorubicin. They have synthesized a water-soluble copolymer based on N-(2-hydroxypropyl)methylacrylamide (HPMA) on which the DOX was covalently attached to the polymer backbone *via* a hydrolytically degradable hydrazone bond. The release rate of the drug was very fast because of the low pH into the endosomes and lysosomes (pH 5-6) and probably due to the presence of the carboxyl groups of the copolymer which may also cause a local decrease in pH at the vicinity of the hydrazone bond. Experiments in mice having EL4 T cell lymphoma showed superior anti-tumor activity to the conjugates in contrast to the free drug.[172]

Petri Papaphilippou

1.4.8. Temperature-triggered drug delivery systems.

Hyperthermia (also called thermotherapy) is a type of cancer treatment in which the body tissue is exposed to high temperatures. A hyperthermic condition usually up to 42˚C damages and kills cancer cells with minimal injury to normal tissues. Hyperthermia is usually combined with other methods of cancer therapy, such as radiation therapy and chemotherapy. Hyperthermia may render cancer cells more sensitive to radiation or harm other cancer cells that radiation cannot damage. In addition, local hyperthermia can also enhance the effects of certain anticancer drugs without causing a biological damage to normal cells.[173]

The combination of a local hyperthermia condition with thermo-responsive polymers at the solid tumour could be a potential cancer treatment. Some block copolymers consisting of a hydrophobic and a thermo-sensinitive hydrophilic segment, upon heating in water undergo conformational charges.

One of the most known temperature-sensitive polymers is poly(*N*-isopropylacrylamide) (PNIPAAm). As already mentioned, this polymer is hydrophobic and hence insoluble in water above the LCST, whereas it becomes hydrophilic and soluble below the LCST. This can be explained by the formation of hydrogen bonding between the amino groups of PNIPAAm and water molecules and the hydration of the *N*-isopropyl groups along the polymer chain making the polymer hydrophilic below the LCST. In contrast, above the LCST PNIPAAm becomes dehydrated resulting in increased hydrophobic interactions between the *N*-isopropyl groups.[142]

Several hydrophobic polymers were used to form the micellar core in PNIPAAm copolymers such as the poly(*N*-butyl methacrylate) (PBMA),[143] the polystyrene (PS), the poly(D, L-lactide-co-glycolide) (PLGA) and the poly(*N*-(2-hydroxypropyl) methacrylamide lactate) (pHPMAmDL).[154] The resulting polymeric micelles showed different temperature-responsitivity depending on the structure of the copolymers. Micelles prepared from PNIPAAm-*b*-PBMA block copolymers exhibited temperature-depended drug (ADR) release. Below 37˚C, the drug release was suppressed and only the 10% of the initial drug was released while above 37˚C the release rate was accelerated, (up to 90% of adriamycin was released) as shown in Fig. 1.29.[143]

Petri Papaphilippou

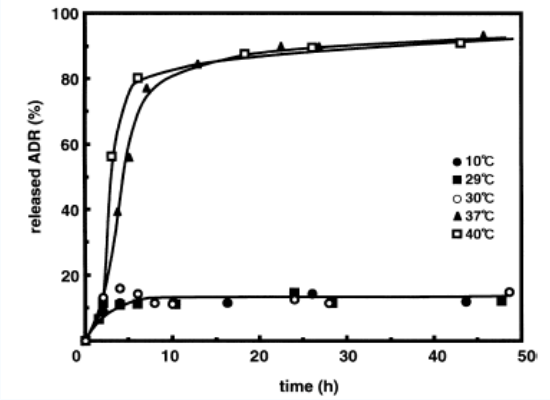

Figure 1.17. *Drug release (Adriamycin) from the thermo-sensitive PNIPAAm-b-PBMA block copolymers.*[143]

Structural deformation of PNIPAAm-*b*-PBMA micelles upon heating probably causes the accelerated drug release. The polymeric micelle of PNIPAAm-*b*-PBMA consists of the outer PNIPAAm shell which provides stabilization and thermoresponsiveness and the hydrophobic inner core of PBMA, containing the drug. Above the LCST, the thermoresponsive shell collapses and becomes hydrophobic hence interacting actively with biocomponents such as cells and proteins, while below the LCST the hydrated flexible PNIPAAm chains do not present this ability. As shown in Fig. 1.18, above the LCST temperature the micellar corona becomes hydrophobic, resulting in the development of intermicellar attractive forces that lead to aggregation and drug release acceleration.

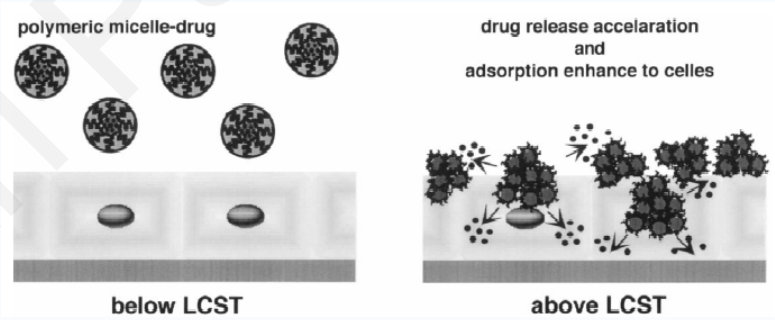

Figure 1.18. *Increasing the temperature above the LCST enhances the release rate of the drug from the polymeric micelles.*[143]

PetriPapaphilippou

Petri Papaphilippou

[1] "*Textbook of Polymer Science"*, F. W. Billmeyer, Wiley-Interscience Publications, 3rd edition, 1984, Wiley.

[2] "*Contemporary Polymer Chemistry",* Third edition, H. R. Allcock, F. W. Lampe, J. E. Mark.

[3] N. Kumar, N. V. Majeti, Ravikumar, A. J. Domb, *Advanced Drug Delivery Reviews*, 53, **2001**, 23.

[4] "*Polymer Science and technology*", J. R. Fried, 1995, Prentice Hall.

[5] R. Savic, Aa. Eisenberg, D. Maysinger, *Journal of drug Targeting*, 14(6), **2006**, 343.

[6] V. Lima, X. Jiang, J. Broken-Sijp, P. J. Schoenmakers, B. Klumperman, R. V. Der Linde, *Journal of Polymer Science: Part A: Polymer Chemistry*, 43, **2005**, 959.

[7] M. F. Cunningham*, Prog. Polym. Sci*., 27(6), **2002**, 1039.

[8] C. E. Lipscomb, M. K. Mahanthappa, *Macromolecules*, 42, **2009**, 4571.

[9] Y. S. Jo, A. J. Van der Vlies, J. Gantz, S. Antonijevic, D. Demurtas, D. Velluto, J. A. Hubbell, *Macromolecules*, 41, **2008**, 1140.

[10] L. A. Connal, Q. Li, J. F. Quinn, E. Tjipto, F. Caruso, G. G. Qiao, *Macromolecules*, 41, **2008**, 2620.

[11] H. Mori, H. Ookuma, T. Endo, *Macromolecules*, 41, **2008**, 6925.

[12] Y. Zhang, Z. Shen, D. Yang, C. Feng, J. Hu, G. Lu, X. Huang, , *Macromolecules*, 43, **2010,** 117.

[13] M. Achilleos, T. Krasia-Christoforou, C. S. Patrickios, , *Macromolecules*, 40, **2007**, 5575.

[14] J. B. Mcleary, M. P. Tonge, D. de Wet Roos, R. D. Sanderson and B. Klumperman, *Journal of Polymer Science: Part A: Polymer Chemistry*, 42, **2004**, 960.

[15] J. Chiefari, Y. K. (Bill)Chong, F. Ercole, J. Krstina, J. Jeffery, T. P. T. Le, R. T. A. Mayadunne, G. F. Meijs, C. L. Moad, G. Moad, E. Rizzardo, S. H. Thang, *Macromolecules*, 31, **1998**, 5559.

[16] Z. Zhang, J. Zhu, Z. Cheng, X. Zhu, *Polymer*, 48, **2007**, 4393.

[17] G. Moad, Y. K. Chong, A. Postma, E. Rizzardo, S. H. Thang, *Polymer*, 46, **2005**, 8458.

[18] B. Y. K. Chong, J. Krstina, T. P. T. Le, G. Moad, A. Postma, E. Rizzardo, S. H. Thang, *Macromolecules,* 36, **2003**, 2256.

[19] G. Moad, R. T.A. Mayadunne, E. Rizzardo, M. Skidmore, S. H. Thang, *Macromol. Symp*. 192, **2003**, 1.

[20] V. Coessens, T. Pintaeur, K. Matyjaszewski, *Prog. Polym. Sci.,* 26, **2001**, 337.

[21] P. V. R. Mesa, J. Belincanta, L. M. F. Lona, *European Symposium on Computer Aided Process Engineering*, **2005**.

[22] M. D. Nur Alam, P. B. Zetterlund, M. Okubo, *Journal of Polymer Science: Part A: Polymer Chemistry*, 45, **2007**, 2007.

[23] P. B. Zetterlund, Y. Saka, R. Mchale, T. Nakamura, F. Aldabbagh. M. Okubo, *Polymer*, **2007**, 47, 7900.

[24] P. M. Kazmaier, K. Daimon, M. K. Georges, G. K. Hamer, R. P. N. Veregin, *Macromolecules*, 30, **1997**, 2228.

Petri Papaphilippou

[25] C. K. Hong, H. S. Jang, S. H. Hong, S. E. Shim, *Macromolecular Research*, 17(1), 14.

[26] G. Riess, *Prog. Polym. Sci*., 28, **2003**, 1107.

[27] H. Otsuka, Y. Nagasaki, K. Kataoka, *Current Opinion in Colloid & Interface Science*, 6, **2001**, 3.

[28] J. Leroux, *Eur. J. Pharm. Biopharm*., 48, **1999**, 101.

[29] V. P. Torchilin, *Journal of Controlled Release*, 73, **2001**, 137.

[30] L. Zhang, A. Eisenberg, *Science*, 268, **1995**, 1728.

[31] S. Svenson, *"Carrier-Based Drug Delivery",* Chapter 1, ACS Symposium Series, Washington, DC, **2004**.

[32] M. Oba, K. Aoyagi, K. Miyata, Y. Matsumoto, K. Itaka, N. Nishiyama, Y. Yamasaki, H. Koyama, K. Kataoka, *Molecular Pharmaceutics*, 5(6), **2008**, 1080.

[33] X. Zhao, F. Pan, Z. Zhang, C. Grant, Y. Ma, S. P. Armes, Y. Tang, A. L. Lewis, T. Waigh, J. R. Lu, *Biomacromolecules*, 8, **2008**, 3493.

[34] C. Allen, D. Maysinger, A. Eisenberg, *Colloids and Surfaces B: Biointerfaces*, 16, **1999**, 3.

[35] A. Harada, K. Kataoka, *Prog. Polym. Sci*., 31, **2006**, 949.

[36] B. Hamdoun, *European Polymer Journal*, 40, **2004**, 1559.

[37] R. C. Hayward, D. J. Pochan, *Macromolecules*, 43, **2010**, 3577.

[38] (a) M. Wilson, K. Kannangara, G. Smith, M. Simmons, B. Raguse, *"Nanotechnology: Basic Science and Emerging Technologies",* (b) MME 461, *"Mechanics and thermodynamics in nanoscale"*, Dr. Andreas Kyprianou.

[39] K. J. Kurzydlowski, *Materials Science*., 42(1), **2006**, 85.

[40] S. Ven, R. V. Kulkami, K. S. Saxena, *Appl. Phys. Lett*., 89, **2006**, 261901.

[41] L. Levy, Y. Sahoo, K. S. Kim, E. J. Bergey, P. N. Prasad, *Chem Mater*., 14, **2002**, 3715.

[42] H. T. Song, J. S. Choi, Y. M. Huh, S. Kim, Y. Jun, J. S. Suh, J. Cheon, *J. Am. Chem. Soc*., 127, **2005**, 12387.

[43] J-H Kim, K. Park, H. Y. Nam, S. Lee, K. Kim, C. Kwon, *Prog. Polym. Sci.,* 32, **2007**, 1031.

[44] G-P Yan, L. Robinson, P. Hogg, *Radiography*, 13, **2007**, e5.

[45] D. Pan, G. M. Lanza, S. A. Wickline, S. D. Caruthers, *European Journal of Radiology*, 70, **2009**, 274.

[46] A. H. Faraji, P. Wipf, *Bioorg. Med. Chem*., 17, **2009**, 2950.

[47] S. J. Rota, *J. Magn. Magn. Mater*., 122, **1993**, 329.

Petri Papaphilippou

[48] (a) K. Raj, B. Moskowitz, R. Casciari, *Magn. Magn. Mater*., 149, **1995**, 174, (b) S. A. Rovers, R. Hoogenboom, M. F. Kemmere, J. T. F. Keurentjes, *J. Phys. Chem. C*, 112(40), **2008**, 15463.

[49] V. T. Peikov, K. S. Jeon, A. M. Lane, J. *Magn. Magn. Mater*., 193, **1999**, 307.

[50] J. M. Perez, F. J. Simeone, Y. Saeki, L. Josephson, R. Weissleder, *J. Am. Chem. Soc*., 125(34), **2003**, 10192.

[51] A. A. Atia, A. M. Donia, A. M. Yousif, *Separation and Purification Technology*, 61, **2008**, 348.

[52] P. I. Girginova, A. L. Daniel-da-Silva, C. B. Lopes, P. Figueira, M. Otero, V. S. Amaral, E. Pereira, T. Trindade, *Journal of Colloid and Interface Science*, 345, **2010**, 234.

[53] W. Shourong, H. Junsheng, G. Miao, Z. Hongkai, C. Youjia, Y. Husheng, L. Keliang, *Journal of Biomedical Materials Research Part A*, **2006**, 946.

[54] H. Daniel, S. Nataliya, L. Frastisek, *Journal of Polymer Science: Part A*, 41, **2003**, 1848.

[55] H. Daniel, B. Nataliya, *Journal of Polymer Science Part A*, 42, **2004**, 5827.

[56] S. Shouheng, H. Zeng, *J. Am. Chem. Soc*., 124, **2002**, 8204.

[57] K. D. Kim, M. Mikhaylova, Y. Zhang, M. Muhammed, *Chem. Mater*., 15, **2003**, 1617.

[58] K. A. Boal, L. B. Frankamp, O. Uzun, T. M. Tuominem, M. V. Rotello, *Chem. Mater.,* 16, **2004**, 3252.

[59] A. Ditsch, E. P. Laibinis, C. L. Wang, A. Hatton, *Langmuir*, 21, **2005**, 6006.

[60] J. K. Bacri, R. Perzynski, D. Salin, V. Cabuil, R. Massart, *J. Magn. Magn. Mater.,* 85(1-3), **1990**, 27.

[61] L. Shen, A. Stachowiak, K. Fateen, E. P. Laibinis, A. Alan Hatton, *Langmuir,* 17, **2001**, 288.

[62] M. Aslam, A. E. Schultz, T. Sun, T. Meade, P. V. Dravid, *Crystal Growth & D, esign*, 7(3)**2007**, 471.

[63] H. Khalil, D. Majan, M. Rafailovich, M. Gelfer, K. Pandya, *Langmuir*, 20, **2004**, 6896.

[64] J-F Berret, N. Schonbeck, F. Gazeau, E. D. Kharrat, O. Sandre, A. Vacher, M. Airiau, *J. Am. Chem. Soc*., 128, **2006**, 1755.

[65] G. Li, J. Fan, R. Jiang, Y. Gao, *Chem. Mater*., 16, **2004**, 1835.

[66] A. Zhu, L. Yuan, W. Jin, S. Dai, Q. Wang, Z. Xue, A. Qin, *Acta Biomaterialia*, 5, **2009**, 1489.

[67] "*Nanobiomagnetics"*, D. L. Leslie-Pelecky, V. Labhasetwar, R. H. Kraus, *Advanced Magnetic Nanostructures*, Springer, **2006**, 461.

Petri Papaphilippou

[68] E. Tombacz, D. Bica, A. Hadju, E. Illes, A. Majsik and L. Vekas, *J. Phys.: Condens. Matter.,* 20, **2008**, 204103.

[69] M. Arruebo, R. Fernandez-Pacheco, M. R. Ibarra and J. Santamaria, *Nanotoday*, 2(3), **2007**, 22.

[70] C. Sun, J. S. H. Lee, M. Zhang, *Advanced Drug Delivery Reviews*, 60, **2008**, 1252.

[71] L. Vekas, D. Bica and M. V. Avdeev, *China Particuology*, 5, **2007**, 43.

[72] T. Gong, D. Yang, J. Hu, W. Yang, C. Wang and J. Q. Lu, *Colloids and Surfaces A: Physicochem. Eng. Aspects*, 339, **2009**, 232.

[73] C. Giacomelli, G. Lafitte and R. Borsali, *Makromol. Symp.,*229, **2005**, 107.

[74] Y. S. Kim, G. I. Shin, M. Y. Lee, G. C. Cho and K. Y. Sung, *Journal of Controlled Release*, 51, **1998**, 13.

[75] C. Lemarchand, R. Gref, P. Couvreur, *Europeran Journal of Pharmaceutics and Biopharmaceutics*, 58, **2004**, 327.

[76] Q. Yuan, R. Venkatasubramanian, S. Hein, R. D. K. Misra, *Acta Biomaterialia*, 4, **2008**, 1024.

[77] J. Leroux, *Eur. J. Pharm. Biopharm*., 48, **1999**, 101.

[78] K. D. Kim, M. Mikhaylova, Y. Zhang, M. Muhammed, *Chem. Mater*., 15(8), **2003**, 1617.

[79] M. Aslam, A. E. Schultz, T. Sun, T. Meade, P. V. Dravid, *Crystal Growth & Design*, 7(3) **2007**, 471.

[80] B. Tural, N. Ozkan, M. Volkan, *Journal of Physics and Chemistry of Solids*, 70, **2009**, 860.

[81] E. Marutani, S. Yamamoto, T. Ninjbadgar, Y. Tsujii, T. Fukuda, M. Takano, *Polymer*, 45, **2004**, 2231.

[82] J-F Lutz, S. Stiller, A. Hon, L. Kaufner, U. Pison, R. Cartier, *Biomacromolecules,* 7, **2006**, 3132.

[83] B-S Kim, J-M Qiu, J-P Wang, T. A. Taton, *Nano Lett.*, 5(10), **2005**, 1987.

[84] A. Aqil, S. Vasseur, E. Duguet, C. Passirani, J.P. Benoit, A. Roch, R. Muller, R. Jerome, C. Jerome, *Europeran Polymer Journal*, 44, **2008**, 3191.

[85] Y. Bai, B. Teng, S. Chen, Y. Chang, Z. Li, *Macromol. Rapid. Commun.,* 27, **2006**, 2107.

[86] M. Rutnakornpituk, S. Meerod, B. Boontha, U. Wichai, *Polymer,* 50, **2009**, 3508.

[87] S. Meerod, G. Tumcharern, U. Wichai, M. Rutnakornpituk, *Polymer*, 49, **2008**, 3950.

[88] A. D. Burke, D. H. Stover, P. F. Dawson, *Chem. Mater*., 14, **2002**, 4752.

[89] H. Lee, E. Lee, Do K. Kim, N. K. Jang, Y. Y. Jeong and S. Jon, *J. Am. Chem. Soc*., 128, **2006**, 7383.

Petri Papaphilippou

[90] M. Kim, J. Jung, J. Lee, K. Na, S. Park, J. Hyun, *Colloids and Surfaces B: Biointerfaces*, 76, **2010**, 236.

[91] H. Wakamatsu, K. Yamamoto, A. Nakao, T. Aoyagi, *Journal of Magnetism and Magnetic Materials*, 302, **2006**, 327.

[92] S. Wan, Y. Zheng, Y. Liu, H. Yan, K. Liu, *J. Mater. Chem.*, 15, **2005**, 3430.

[93] S. Wan, J. Huang, H. Yan, K. Liu, *J. Mater. Chem.*, 16, **2006**, 298.

[94] Q. Zhang, S. M. Thompson, Y. A. Garmichael-Baranauskas, L. B. Caba, A. M. Zalich, Y-N Lin, T. O. Mefford, M. R. Davis, S. J. Riffle, *Langmuir*, 23, **2007**, 6927.

[95] N. Guan, J. Xu, L. Wang, D. Sun, *Colloids snd Surfaces A: Physicochem. Eng. Aspects*, 346, **2009**, 221.

[96] Y. Sahoo, M. Cheon, S. Wang, H. Luo, P. E. Furlani, N. P. Prasad, *J. Phys. Chem B*, 108, **2004**, 3380.

[97] K. A. Boal, L. B. Frankamp, O. Uzun, T. M. Tuominem, M. V. Rotello, *Chem. Mater.*, 16, **2004**, 3252.

[98] Y. Koseoglu, H. Kavas, B. Aktas, *Phys. Stat. Sol.*, 203(7), **2006**, 1595.

[99] R. S. Ahmed, B. S. Ogale, C. G. Papaefthymiou, R. Ramesh, P. Kofinas, *J. Appl. Phys. Lett.*, 80(9), **2002**, 1616.

[100] Y. Hou, S. Gao, T. Ohtra, H. Kondoh, *Eur. J. Inorg. Chem.*, **2004**, 1169.

[101] M. Yamagata, M. Abe, H. Handa, H. Kawaguchi, *Macromol. Symp*, 245, **2006**, 363.

[102] Z. Ma, Y. Guan, H. Liu, *Journal of Polymer Science: Part A*, *43,* **2005**, 3433.

[103] P. V. Torchilin, *Advanced Drug Delivery Reviews*, 57, **2005**, 95.

[104] P. V. Torchilin, *Journal of Controlled Release*, 73, **2001**, 137.

[105] T. Inoue, G. Chen, K. Nakamae, A. S. Hoffman, *Journal of Controlled Release*, 51, **1998**, 221.

[106] K. Kataoka, A. Harada, Y. Nagasaki, *Advanced Drug Delivery Reviews*, 47, **2001**, 113.

[107] N. Nishiyama, K. Kataoka, *Pharmacology & Therapeutics*, 112, **2006**, 630.

[108] G. Gaucher, M-H. Dufrense, V. P. Ant, N. Kang, D. Maysinger, J-C Leroux, *Journal of Controlled Release,* 109, **2005**, 169.

[109] V. P. Torchilin, *Cell. Mol. Life Sci.,* 61, **2004**, 2549.

[110] H. Maeda, J. Wu, T. Sawa, Y. Matsumura, K. Hori, *Journal of Controlled Release*, 65, **2000**, 271.

[111] K. Greish, *Journal of Drug Targeting*, 15(7), **2007**, 457.

Petri Papaphilippou

[112] *"Polymer properties and polymers in medical applications"*, MME 555, Dr. Theodora Krasia-Christoforou, 2008.

[113] H. Lee, E. Lee, K. D. Kim, N. K. Jang, Y. Y. Jeong, S. Jon, *J. Am. Chem. Soc*., 128, **2006**, 7383.

[114] A. Rosler, G. W. M. Vandermeulen, H-A Klok, *Advanced Drug Delivery Reviews*, 53, **2001**, 95.

[115] K. Kataoka, G. S. Kwon, M. Yokoyama, T. Okano, Y. Sakurai, *Journal of Controlled Release*, 24, **1993**, 119.

[116] C. H. Wang, G. H. Hsiue, *Biomacromolecules,* 4(6), **2003**, 1487.

[117] A. N. Lukyanov, V. P. Torchilin, *Adv. Drug Deliv. Rev.,* 56(9), **2004**, 1273.

[118] G. Zuccari, R. Carosio, A. Fini, PG. Montaldo, I. Orienti, *J. Control Release*, 103(2), **2005**, 369.

[119] M. Nakayama, T. Okano, T. Miyazaki, F. Kohori, K. Sakai, M. Yokoyama, *Journal of Controlled Release* 115, **2006**, 46.

[120] T. Riley, T. Govender, S. Stolnik, C. D. Xiong, M. C. Garnett, L. Illum, S. S Davis, *Colloids and Surfaces B: Biointerfaces*, 16, **1999**, 147.

[121] D. Cohn, H. Younes, Journal of Biomedical Materials Research, 22, **1988**, 993.

[122] S. Ben-Shabat, N. Kumar, A. J. Domb, *Macromol. Biosci.,* 6, **2006**, 1019.

[123] Y. S. Kim, G. I. Shin, M. Y. Lee, G. C. Cho, K. Y. Sung, *Journal of Controlled Release*, 51, **1998**, 13.

[124] C. Giacomelli, G. Lafitte, R. Borsali, *Makromol. Symp.,*229, **2005**, 107.

[125] K. Letchford, R. Liggins, H. Burt, *Journal of Pharmaceuticals Sciences*, **2007**, 1.

[126] S. B. La, T. Okano, K. Kataoka, *Journal of Pharmaceuticals Sciences*, 85, **1996**, 85.

[127] G. Kwon, M. Naito, M. Yokohama, T. Okano, Y. Sakurai, K. Kataoka, *Journal of Controlled Release*, 48, **1997**, 195.

[128] Y. I. Jeong, J. B. Cheon, S. H. Kim, J. W. Nah, Y. M. Lee, Y. K. Sung, T. Akaike, C. S. Cho, *Journal of Controlled Release*, 51, **1998**, 169.

[129] S. A. Hagan, A. G. A. Coombes, M. C. Garnett, S. E. Duna, M. C. Davies, L. Illum, S. S. Davis, *Langmuir*, 12, **1996**, 2153.

[130] M. Ramaswamy, X. Zhang, H. M. Burt, K. M.-Wasan, *Journal of Pharmaceuticals Sciences*, 86, **1997**, 460.

[131] K. Yasugi, Y. Nagasaki, M. Kato, K. Kataoka, *Journal of Controlled Release*, 62, **1999**, 89.

Petri Papaphilippou

[132] C. Donini, D. N. Robinson, P. Colombo, F. Giordano, N. A. Peppas, *International Journal of Pharmaceutics*, 245, **2002**, 83.

[133] M. Yokohama, M. Miyauchi, N. Yamada, T. Okano, Y. Sakurai, K. Kataoka, S. Inoue, *Cancer Res.*, 50, **1990**, 1693.

[134] A. Harada, K. Kataoka, *Macromolecules*, 31, **1998**, 288.

[135] S. V. Trubetskoy, S. G. Gazelle, L. G. Wolf, P. V. Torchilin, *Journal of Drug Targeting*, 4, **1997**, 381.

[136] S. Katayose, K. Kataoka, *Journal of Pharmaceuticals Sciences*, 87, **1998**, 160.

[137] Eun S. Lee, K. Na, You H. Bae, *Journal of Controlled Release*, 91, **2003**, 103.

[138] A. V. Kabanov, V. A. Kabanov, *Advanced Drug Delivery Reviews*, 30, **1990**, 49.

[139] Yan Wu, Fu-Bin Che, Jiang-Han Chen, *Journal of Applied Polymer Science*, 110, **2008**, 1118.

[140] D. W. Miller, E. V. Batrakova, O. T. Waltner, V. Y. Alakhov, A. V. Kabanov, *Bioconj. Chem.*, 8, **1997**, 649.

[141] A. Kabanov, E. V. Batrakova, V. Y. Alakhov, *Journal of Controlled Release*, 82, **2002**, 189.

[142] K. T. Oh, H. Yin, Eun S. Lee, You H. Bae, *J. Mater. Chem.*, 17, **2007**, 3987.

[143] J. E. Chung, M. Yokoyama, M. Yamato, T. Aoyagi, Y. Sakurai, T. Okano, *Journal of Controlled Release*, 62, **1999**, 115.

[144] D. R. Friend, S. Pangburn, *Medicinal Research Reviews*, 7, **1987**, 53.

[145] Y. Bae, N. Nishiyama, K. Kataoka, *Bioconj. Chem.*, 18(4), **2007**, 1131.

[146] Y. Bae, W-D Jang, N. Nishiyama, S. Fukushima, K. Kataoka, *Mol. Biosyst.*, 1, **2005**, 242.

[147] Z. Sezgin, N. Yuksel, T. Baykara, *European Journal of Pharmaceutics and Biopharmaceutics*, 64, **2006**, 261.

[148] M. Yokoyama, S. Fukushima, R. Uehara, K. Okamoto, K. Kataoka, Y. Sakurai, T. Okano, *Journal of Controlled Release*, 50, **1998**, 79.

[149] P. Opanasopit, M. Yokoyama, M. Watanabe, K. Kawano, Y. Maitani, T. Okano, *Pharmaceutical Research*, 21(11), **2004**, 2001.

[150] N. Nishiyama, M. Yokoyama, T. Aoyyagi, T. Okano, Y. Sakurai, K. Kataoka, *Langmuir*, 15, **1999**, 377.

[151] N. Nishiyama, K. Kataoka, *Journal of Controlled Release*, 74, **2001**, 83.

[152] M. Watanabe, K. Kawano, M. Yokoyama, P. Opanasopit, T. Okano, Y. Maitani, *International Journal of Pharmaceutics*, 308, **2006**, 183.

Petri Papaphilippou

[153] K. Kataoka, T. Matsumoto, M. Yokoyama, T. Okano, Y. Sakurai, S. Fukushima, K. Okamoto, G. S. Kwon, *Journal of Controlled Release*, 64, **2000**, 143.

[154] O. Soga, C. F. van Nostrum, M. Fens, C. J.F. Rijcken, R. M. Schiffelers, G. Storm, W. H. Hennink, *Journal of Controlled Release*, 103, **2005**, 341.

[155] T. O. Kyung, E. S. Lee, D. Kim, Y. H. Bae, *International Journal of Pharmaceutics,* 358, **2008**, 177.

[156] N. Babazadeh, *Journal of Applied Polymer Science*, 104, **2007**, 2403.

[157] N. Nishiyanna, S. Okazaki, H. Cabral, M. Miyamoto, Y. Kato, Y. Sugiyama, *Cancer Res.*, 63, **2003**, 8977.

[158] V. Y. Alakhov, E. Y. Moskaleva, E. V. Batrakova, A. V. Kabanov, *Bioconj. Chem.*, 7, **1996**, 209.

[159] Y-C Chang, I-M Chu, *European Polymer Journal*, 44, **2008**, 3922.

[160] Y. Li, S. Pan, W. Zhang, Z. Du, *Nanotechnology*, 20, **2005**, 1.

[161] J. Heung, K. Emoto, M. Iigima, Y. Nagasaki, T. Aoyagi, T. Okano, Y. Sakurai, K. Kataoka, *Polym. Adv. Tecnhol.*, 10, **1999**, 647.

[162] V. A. Sethuraman, M. C. Lee, Y. H. Bae, *Pharmaceutical Research*, 25(3), **2008**, 657.

[163] S-H Hua, Y-Y Li, Y. Liu, W. Xiao, C. Li, F-W Huang, X-Z Zhang, R-X Zhuo, *Macromol. Rapid Commun.,* 31, **2010**, 81.

[164] Y. Tian, L. Bromberg, S. N. Lin, T. A. Hatton, K. C. Tam, *Journal of Controlled Release*, 121, **2007**, 137.

[165] H. S. Na, Y. K. Lim, Y-I Jeong, H. S. Lee, Y. J. Lim, M. S. Kang, C-S Cho, H. C. Lee, *International Journal of Pharmaceutics*, 383, **2010**, 192.

[166] http://biotech.icmb.utexas.edu/botany/tax.html

[167] Y. Bae, N. Nishiyama, S. Fukushima, H. Koyama, M. Yasuhiro, K. Kataoka, *Bioconj. Chem.*, 16, **2005**, 122.

[168] M. Stubbs, P. M. J. McSheehy, J. R. Griffiths, C. L.Bashford, *Molecular Medicine Today*, 6(1), **2000**, 15.

[169] K. Newel, A. Franchi, J. Pouyessegur, I. Tannok, *Proc. Natl. Acad. Sci.*, 90, **1993**, 1127.

[170] I. F. Tannock, D. Rotin, *Cancer Res.*, 49, **1989**, 4373.

[171] S. Kwon, T. Okano, K. Kataoka, *Advanced Drug Delivery Reviews*, 21, **1996**, 107.

[172] P. Chytil, T. Etrych, C. Konak, M. Sirova, T. Mrkvan, B. Rihova, K. Ulbrich, *Journal of Controlled Release*, 115, **2006**, 26.

Petri Papaphilippou

[173] "*Hyperthermia in Cancer Treatment: Questions and Answers*", *National Cancer Institute FactSheet*, http://www.cancer.gov/publications

Petri Papaphilippou

2. Characterization Methods.

2.1. Microscopy techniques.

2.1.1. Atomic Force Microscope (AFM).

Atomic Force Microscope (*AFM*) or Scanning Force Microscope (*SFM*) belongs to the "family" of the Scanning Probe Microscopes (*SPMs*). Atomic Force Microscope developed in 1986 is a useful tool for imaging and characterization of a variety of surfaces at the nanoscale.[174, 175] This powerful tool it enables the detection of a wide range of insulating surfaces including ceramic materials, composite glasses, synthetic and biological membranes, polymers but also metals and semiconductors. AFM finds applications in electronics, telecommunications, biological, chemical, automotive, aerospace and energy industries.[176]

Operating principles in AFM.

AFM consists of a cantilever that is made of silicon (Si) or silicon nitride (Si_3N_4) at the micro-scale with a sharp tip (probe) attached at the end of it, which is used to scan the surface of a specimen

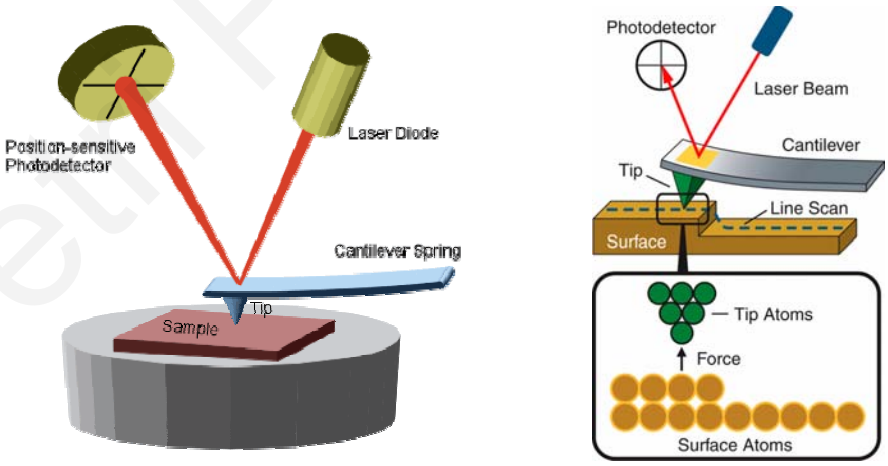

Figure 2.1. *Schematic diagram of the Atomic Force Microscope.*

Petri Papaphilippou

The sample is placed at the top of a piezoelectric driver system which can be moved in the three dimensions x, y and z thus enabling the presentation of 3D images of a sample surface. When the tip approaches to the surface of a material, forces are raised between the tip and the surface. The detector does not measure these forces directly. There is a photodiode that measures the reflections of the laser beam which incidence at the top of the cantilever. These reflections correspond to the deflections of the cantilever due to the tip-sample interactions and consequently the morphology of the surface. The forces between the tip and the sample may be Van der Waals, mechanical contact, electrostatic or magnetic forces.[177, 178]

Depending on the interaction of the tip and the surface of the sample, the AFM can be classified as repulsive or contact mode and attractive or non-contact mode.

Modes of operation in AFM.

Contact and non-contact mode.

The contact mode is the foremost mode of operation used in AFM. The tip scans the surface sample in a very close distance, hence the force developed between the tip and the sample is repulsive in the order of 10^{-9} N. In the non-contact mode, the tip is far enough from the surface sample, i.e. there is no contact between the tip and the sample. Thus the forces among the tip and the surface of the sample are quite low at about 10^{-12} N. The cantilevers in non-contact mode can oscillate.[177, 178]

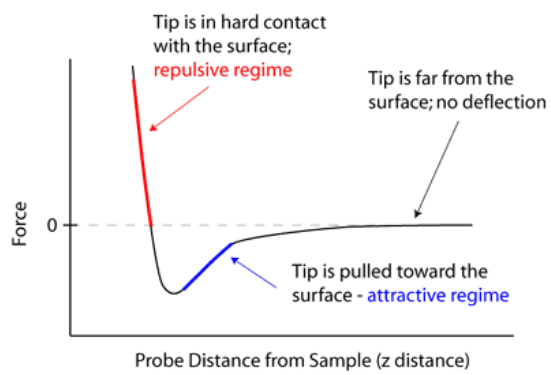

Figure 2.2. *Repulsive and attractive forces acting between the sample and the tip in the AFM.*[179]

Tapping mode.

Tapping mode is the most common AFM mode and the one used in the present work. With it, high resolution topographic imaging of "problematic" sample surfaces can be achieved, surfaces which can be easily damaged and are held weakly to their substrate or are difficult to visualize with other AFM techniques. Additionally, by tapping mode problems associated with friction, adhesion or electrostatic forces are overcome. In this last AFM mode, the tip is alternately placed in contact with a surface and then is lifted off the surface to avoid dragging it across. The piezo-motion causes the oscillation of the cantilever usually with amplitude greater than 20 nm when the tip is not touching the surface. The oscillating tip is then moved slowly towards the surface and begins to tap it lightly. When the cantilever touches the surface, its oscillation amplitude is reduced due to the loss in energy. It is this reduction that is used for measuring the characteristics of a surface. This mode is preferred for the measurement of soft and fragile materials.[178, 180]

2.1.2. Transmission Electron Microscope (TEM).

The physicists discovered that electrons possess a wavelike character. Louis de Broglie being inspired by the Einstein's photon description of electromagnetic radiation proposed that the wavelength of the electrons is given by the following equation:

$$\lambda = h / p = h / (m\nu) \quad (2.1)$$

Where λ = wavelength, h = planck constant, m = mass and ν = speed of the electrons. If the wavelength of the electron is similar to the atomic dimensions, then it can be diffracted from the regular array of atoms at the surface of a crystalline material. *Transmission electron microscope* was the first electron microscope developed and extensively used for the characterization of a sample at a very fine scale. The electron microscope uses a beam of highly energetic electrons instead of photons of visible light used in light microscopes.[181] TEM is an important tool in materials science since information about the morphology, structure and composition of a specimen can be obtained. More specifically, it gives details in relation to the size, shape and arrangement of the particles in the sample. Furthermore, it enables the investigation of the crystal

Petri Papaphilippou

structure including the arrangement of the atoms in an object as well as the quantification of the different compounds comprising the specimen.[181, 182]

Operating principles of TEM.

A beam of monochromatic electrons is produced by an electron gun. This electron beam is focused to a small and thin coherent beam by electromagnetic lenses. Continuously, the beam is restricted by the condenser aperture leaving out high angle electrons. Then the focused electron beam strikes the sample which is on a concrete base namely grid holder and parts of the beam are transmitted. The transmitted radiation is transformed by the objective lens into an image. After the objective lens, optional objective and selected area metal apertures are placed inside the column where they can restrain the beam by blocking out the high angle diffracted electrons and examine the periodic diffraction of electrons by ordered arrangements of atoms in the sample. The beam passes down the column through the projector lenses, being enlarged all the way. Eventually, the beam strikes the phosphor image screen and light is generated allowing the user to observe the image. The darker areas of the image represent those areas of the sample through which fewer electrons were transmitted and the lighter areas of the image represent those areas of the sample through which more electrons were transmitted.[183]

TEM can image and analyze successfully a wide range of solid materials, such as metals, ceramics, minerals, polymers as well as other organic and biological materials. Hence this microscopy technique is extensively used in materials science and technology.

2.2. Thermal analysis methods.

2.2.1. Differential scanning calorimetry (DSC).

Several methods of thermal measurement analysis of polymers exist nowadays. Thermal analysis techniques include among others the traditional calorimetric and differential thermal analysis, the thermogravimetric analysis, the thermomechanical analysis and the electrical thermal analysis.

Petri Papaphilippou

Differential scanning calorimetry (DSC) is a thermoanalytical technique which measures the temperatures and heat flows associated with transitions in materials as a function of time and temperature in a controlled atmosphere. DSC can be used to measure a number of characteristic properties of a sample. This technique is employed to study the physical and chemical changes involving phase transitions upon changing the temperature, such as the melting and boiling points, glass transitions, endothermic or exothermic processes, or changes in heat capacity. Furthermore, it provides information on the crystallization time and temperature, the heat of fusion, the oxidative or thermal stability, any chemical reactions taking place upon heating and the purity of a sample. The DSC method uses a reference material which is heated simultaneously with the sample during the experiment by individual electric heaters. The difference in the amount of heat required to increase the temperature of a sample and a reference material are measured as a function of temperature.[181, 182, 184]

Differential Scanning Calorimetry is a technique that is widely used for examining the thermal transitions of a polymeric material such as the melting temperature (Tm) and the glass transition temperature (Tg). In this experiment it is important to keep the heating rate the same for the two pans. During an exothermic process, the polymer sample needs to take more heat to increase its temperature at the same rate as the reference. This change in absorption of heat by the sample can be monitored electrically promoting a sensitive measure of transition in polymers.[181, 182, 184]

As seen in the heat flow *vs* temperature diagram presented in Fig. 2.3, a glass transition of a polymer (amorphous solid) occurs as the temperature is increased. These transitions appear as a step in the baseline of the DSC signal. Upon further increasing the temperature, a semi-crystalline polymer presents the so-called melting temperature T*m* (fig. 2.3). At this point, crystalline areas existing within the polymer are destroyed and the sample melts. The DSC method may give information related to the percentage of the crystalline and amorphous content in the sample.

Petri Papaphilippou

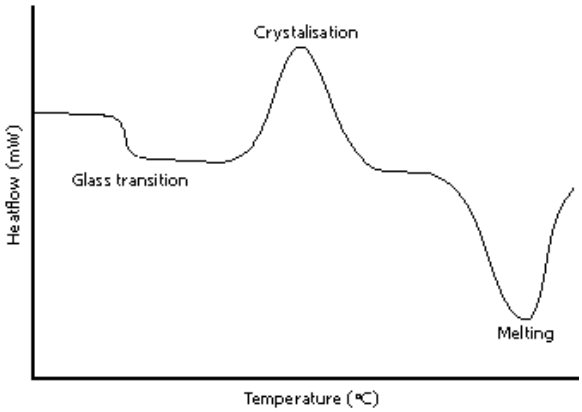

Figure 2.3. *Features of DSC signals.*

2.2.2. Thermal gravimetric analysis (TGA).

Thermogravimetric Analysis (TGA) is a simple thermal analytical technique that measures the weight loss of a sample as a function of temperature. TGA is commonly used to verify polymer degradation temperatures, residual solvent levels, absorbed moisture content and the amount of fillers in composite materials.

A sample of the material is placed into an alumina cup, which is attached to a sensitive microbalance assembly located outside the furnace chamber. Then the sample holder is placed into the high temperature furnace and heated by following a predetermined thermal cycle at a controlled heating rate. The weight loss of the sample is determined by the difference between the initial and the final weight. The TGA curve presents at the Y-axis the change percentage of the sample and at the X-axis the temperature.[181, 182]

2.3. Spectroscopy techniques.

2.3.1. Nuclear Magnetic Resonance Spectroscopy (NMR).

Nuclear Magnetic Resonance spectroscopy commonly known as NMR spectroscopy is one of the most useful techniques for determining the structure of organic compounds. The NMR method is based on the magnetic properties of the nuclei and not of the electrons. The nucleus consisting of protons and neutrons is charged positively and has the ability to spin

Petri Papaphilippou

around its axes. By spinning around itself, a magnetic nucleus generates a magnetic field.[185, 186]

In the absence of an external magnetic field, the spins of a magnetic nucleus are randomly orientated. When a nucleus like ^{1}H and ^{13}C with J = ½, is located between two strong magnets, it will adopt two possible orientations (+ ½ and – ½ presenting different energies). The magnetic moment of the lower energy + ½ state is aligned to the direction of the external field, whereas that of the higher energy – ½ spin state is opposed to the external field. The nucleus prefers to occupy the lower energy level. It is possible to excite the nucleus into the higher energy level with electromagnetic radiation. The frequency of the radiation needed is determined by the difference in energy (ΔE) between the energy levels.[185, 186]

$$\Delta E = \gamma hB / 2\pi \qquad (2.2)$$

$$\gamma = \mu / L \qquad (2.3)$$

γ is the gyromagnetic ratio, μ is the magnetic dipole moment, L the angular momentum, h is the Planck's constant and B is the strength of the magnetic field.

When the populations of the higher and the lower state become equal, then there will be no further absorption of radiation and the spin system is saturated. After saturation, it is possible for the nuclei to return to the lower state through the relaxation processes. There are two major relaxation processes, the spin-lattice (longitudinal) and the spin-spin (transverse) relaxation.[187]

The local chemical environment influences the energy absorption of a nucleus. It is not possible for all the protons in a molecule to resonate at the same frequencies. Hence, the magnetic field at the nucleus is not equal to the applied magnetic field. The difference between the applied magnetic field and the field at the nucleus is termed *nuclear shielding* or *chemical shift*. The chemical shift (δ) is reported as a relative measure from some reference resonance frequency such as the TMS (tetramethylsilane). More specific this difference between the frequency of the signal and the frequency of the reference is divided by the frequency of the reference signal to give the chemical shift.[185]

Petri Papaphilippou

2.3.2. X-ray diffraction spectroscopy (XRD).

X-ray diffraction (XRD) spectroscopy is one of the most useful techniques for the analysis of semi-crystalline polymers in the solid state. XRD is a versatile, non-destructive method that gives important information on the crystallographic structure, chemical composition and physical properties of a material. Such experiments provide information on the degree of crystallinity of a polymer, the extent of orientation of crystallites in a polymer and the way in which chains are organized at the solid state. [2, 181]

Polymer may constitute of both crystalline and amorphous regions as seen in Fig. 2.4. The crystalline region corresponds to the part of the polymer in which the chains are arranged in a regular manner. Among these ordered regions, polymer chains found in random conformation exist, the so-called amorphous regions. The degree of crystallinity of a polymer can be determined by XRD analysis.

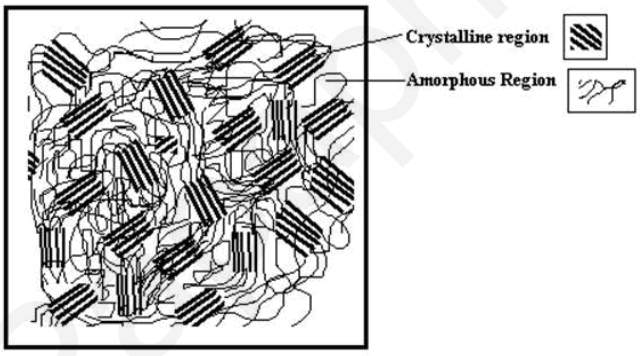

Figure 2.4*. Crystalline and amorphous regions in a semicrystalline polymer.*

Operating principles in XRD.

The X-Ray diffraction technique belongs to the family of the X-Ray scattering methods. The XRD method uses X-Rays of a specific wavelength and thus energy. There are a number of XRD methods that can be used to characterize a material. For instance the single-crystal X-Ray diffraction is a technique employed to solve the complete structure of crystalline materials. The powder XRD is a method that characterizes the crystallographic structure, the grain size and preferred orientation in polycrystalline or powdered solid samples. Powder diffraction is mainly used to identify unknown materials by comparing diffraction data against a database maintained by the International Centre for Diffraction Data.[181, 182, 188]

When the X-Rays hit a 3D crystal lattice, the diffraction beam is geometrically equal to the reflection beam. The diffraction rays which are in phase satisfy the Braggs law: [184, 185]

$$2d_{hkl}\sin\theta = n\lambda \qquad (2.4)$$

n is an integer determined by the order given, λ is the X-Ray wavelength, d_{hkl} is the distance between the parallel planes of the lattice and Θ is the incident angle.

From the X-Ray spectrum and the Scherrer equation (2.4) the crystallite size can be calculated:[189]

$$t_{hkl} = K.\lambda \ / \ fwhm.\cos\Theta_B \qquad (2.5)$$

t is the thickness of the crystallite, *K* is a constant that depends on the crystallite shape (0.89), *λ* is the X-Ray wavelength, *fwhm* is the full width at half max or integral breadth and Θ_B is the Bragg angle.

2.3.3. Ultraviolet-visible spectroscopy (UV-vis).

UV-vis is a spectrophotometric technique that uses photons from the ultraviolet (UV) and the visible (vis) region of the electromagnetic spectrum to cause electron transitions inside a molecule. The electromagnetic spectrum ranges from very short wavelengths such as the gamma and the X-Rays to very long wavelengths including microwaves and radio waves. UV radiation has wavelengths of 200-400 nm and vis light has wavelengths of 400-800 nm. The energy carried by a photon of a given wavelength of light is given by the follow equation:[190]

$$\Delta E = h.\nu \qquad (2.6)$$

Where h is the Planck's constant, and v is the frequency ($\nu = c / \lambda$).

Different molecules absorb radiation at different wavelengths. A UV-vis spectrum may present a number of absorption bands corresponding to structural groups within the molecule. Absorbance of UV-vis light is directly proportional to the path *l* and the concentration *c* of the molecule, according to the Lambert-Beer Law:[190]

Petri Papaphilippou

$$A = \varepsilon . c . l \qquad (2.7)$$

Where A is the absorbance, *l* is the length path of the radiation, *c* is the concentration of the molecule and *ε* is the constant of proportionality called the absorptivity or extinction coefficient.

The absorption of UV or visible radiation causes the excitation of the outer shell (valence) electrons. There are three types of electron transition: (a) transitions involving π, σ and n electrons, (b) transitions involving charge-transfer electrons and (c) transitions involving *d* and *f* electrons. In a molecule where atoms are bonded to each other by covalent bonds, their atomic orbitals such as the s, p_x, p_y and p_z are mixed together and construct new molecular orbitals like the σ and π bonding, the n non-bonding and the anti-bonding $\sigma^*$and π^* orbitals. The shared electron pairs of covalently bonded atoms occupy the new molecular orbitals (MO).

Fig. 2.5 presents the various types of electronic excitation. Usually the electron transitions taking place between $n \rightarrow \pi^*$ and $\pi \rightarrow \pi^*$ orbitals correspond to wavelength in the UV-vis radiation range (200 to 800 nm). Electrons are excited from the highest occupied molecular orbital (HOMO-bonding) to the lowest unoccupied molecular orbital (LUMO). When a molecule is exposed to light, it absorbs the energy that is requested for a specific electron transition. An optical spectrometer records the wavelengths at which absorption occurs and also the degree of absorption at each wavelength. The resulting spectrum is presented as a graph of absorbance (A) *vs* wavelength (λ). The absorbance of a sample is proportional to the number of absorbing molecules in the light beam. Due to this, it is necessary to correct the absorbance value if the spectra of different compounds are to be compared. The corrected absorption value is called *absorptivity ε* (equation 2.7). ε is very useful when comparing the spectra of different compounds and determining the relative strength of light absorbing functions (chromophores).[190]

Petri Papaphilippou

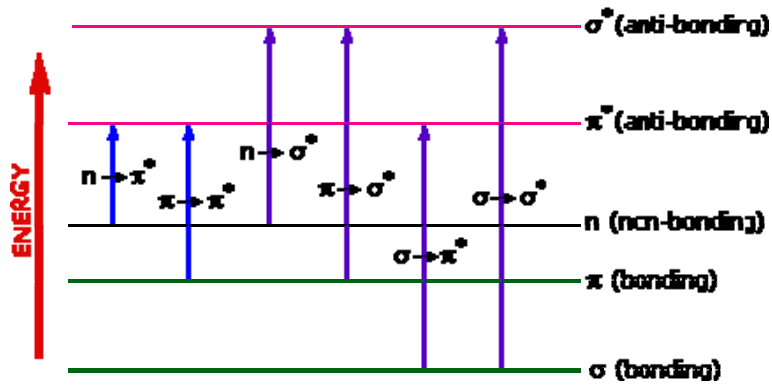

Figure 2.5. *Diagram of ground and excitation electron states in a molecule. Bonding (π, σ), non-bonding (n) and anti-bonding (π*, σ*) molecular orbitals.*

The UV-vis spectrophotometer measures the intensity of light passing through a sample (I). The ratio I / I_o is called the transmittance, where the (I_o) is the intensity of the light beam before it passes through the sample. Eventually the absorbance may be expressed as:[190]

$$\mathbf{A = -\log[(I / I_o)]} \qquad \mathbf{(2.8)}$$

2.4. Scattering methods.

2.4.1. Dynamic light scattering (DLS).

Dynamic light scattering (DLS) also known as photon correlation spectroscopy is one of the most popular techniques used to determine the hydrodynamic radii and polydispersity of colloidal systems. When light passes through a dilute solution of suspended particles it is scattered in all directions relative to the incident beam. The major portion of the scattered light has almost the same λ as that of the incident radiation. The intensity of the scattered light I_Θ is detected at angle θ to the incident beam direction and at distance r from the centre of the system. According to the semi-classical light scattering theory, when light hits a material the electric field of the light induces an oscillating polarization of electrons in the molecules. Therefore the molecules provide a secondary source of light and subsequently scatter light. The frequency shifts, the angular distribution, the polarization and the intensity of the scattered light depend on the size, shape and molecular interactions in the scattering material.[191, 192]

Petri Papaphilippou

DLS measures the time dependence of the light scattered from a very small region in the solution. The intensity of the scattered light varies because of the different diffusion rates of the molecules. This method has the ability to measure the diffusion coefficient of the particles and thus to describe the particles motion. If the light source is a laser, then a monochromatic and coherent beam interacts with the sample particles that undergo a Brownian motion (as they can move freely in the solvent and collide randomly with solvent molecules). This causes a Doppler shift, changing the wavelength of the incoming light. The change of the wavelength of the light is related to the size of the particles. The scattered light generated from each particle may be added or deducted, depending on the relative phase and the amplitude of the moving particles. A faster particle movement causes faster signal changes. The above process is dynamic and therefore the scattering is called Dynamic Light Scattering. In DLS the output from the photomultiplier tube is the unormalised intensity autocorrelation function, $G_2(t)$ which is given as:

$$\mathbf{G_2(t)=A+[Bg_1(t)]^2} \qquad \textbf{(2.9)}$$

A is a constant background intensity to which the correlation function decays after a suitably long delay time t, and B is a constant close to unity.

If the polymer system is monodisperse and only concentration relaxation processes exist, then:

$$\mathbf{g_1(t) = exp(-\Gamma t)} \qquad \textbf{(2.10)}$$

$$\mathbf{\Gamma = Dq^2} \qquad \textbf{(2.11)}$$

Γ^{-1} is the relaxation time of the diffusive process of the polymer, *D* is the translational diffusion coefficient, and q is the scattering vector. The latter is expressed as:

$$\mathbf{q} = \frac{4\pi n \sin(\theta/2)}{\lambda_o} \qquad \textbf{(2.12)}$$

n is the refractive index of the pure solvent, θ the scattering angle and λ_o the laser's wavelength.

Petri Papaphilippou

In polymer solutions, D is concentration dependent as shown in equation 2.13. D_o correspond to the diffusion coefficient value at infinite dilution and c is the polymer concentration. k_D is a term in which thermodynamic as well as frictional parameters of a polymer in a specific solvent are included.

$$\mathbf{D = D_o\,(1 + k_D\,c)} \qquad \mathbf{(2.13)}$$

The relation between the diffusion and particle size is based on theoretical relationships for the Brownian motion of spherical particles, originally derived by Einstein. As seen in equation 2.14 (Stokes-Einstein equation) the R_H which is the hydrodynamic radius of a spherical particle and is inversely proportional to the diffusion coefficient, D.[182]

$$\mathbf{R_H = k\,T / 6\,\pi\,\eta\,D} \qquad \mathbf{(2.14)}$$

T is the temperature, η corresponds to the solvent viscosity, κ is the Boltzmann's constant and D is the diffusion coefficient.

DLS is capable of distinguishing whether a block copolymer in solution exists as a unimer or whether it self-aggregates into micellar or vesicular morphologies. The advantage of using DLS lies on its capability to analyze samples containing broad distributions of species of widely differing molecular masses.

2.5. Chromatography methods.

2.5.1. Size exclusion chromatography (SEC).

Size exclusion chromatography (SEC) or Gel Permeation Chromatography (GPC) is a chromatographic method that is extensively used in the characterization of polymers and biological molecules such as proteins. More precisely, it has the ability to separate macromolecules according to their size and consequently their molecular weight. There are many synthetic routes for the preparation of polymers hence the development of such a technique which is capable of distinguishing polymers based on their size as well as separating the desired product from a mixture was essential.[193, 194]

Petri Papaphilippou

SEC uses porous particles to separate molecules of different sizes, located inside a chromatographic column. More precisely, the column usually consists of a hollow tube, tightly packed with extremely small porous polymer beads (usually polystyrene) constituting the stationary phase. The mobile phase consisting of a solvent containing a broad molecular weight distribution of polymer chains, oligomers and may be unreacted monomer, is allowed to flow through the stationary phase. This results in the separation of particles based on their hydrodynamic volume. The smaller molecules may enter the pores of the column and therefore present a delay in their elution through the column. Larger molecules are unable to penetrate the pores and hence they are eluted faster.[2]

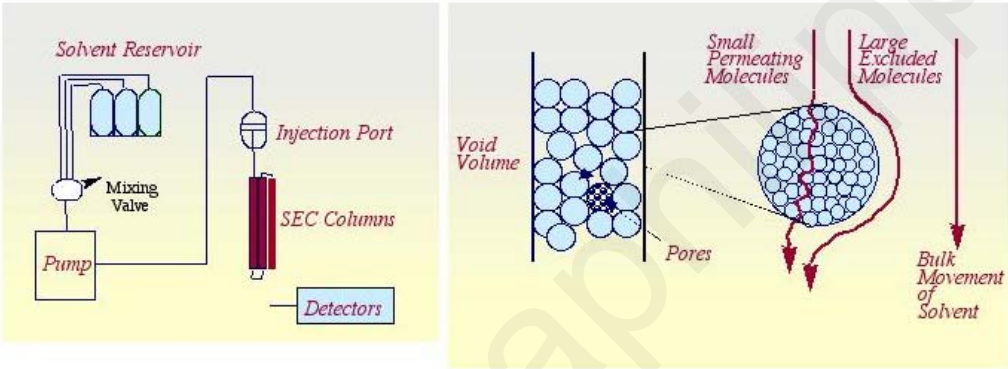

Figure 2.6. *Schematic diagram of SEC illustrating the penetration of particles through the column and the separation according to hydrodynamic size differences.*

Subsequently, the eluent passes through a detector. Usually two kind of detectors are employed: the differential refractometer (DRI) and the ultraviolet spectrophotometer (UV-vis). A differential refractometer measures the difference in the refractive index between the eluted solution and the pure solvent. This difference is proportional to the concentration of the polymer chains. The UV detector is usually set to a particular wavelength (e.g to the aromatic absorption region of a polymer with phenyl rings) and the absorbance is monitored as a function of the elution time.

GPC is a comparative method for determining molecular weights (MWs) of polymers. As in the case of other relative characterization methods, SEC requires calibration, which is carried out by using well-defined polymer samples, the molecular weights of which have been already determined by absolute methods such as osmometry and light scattering.

Petri Papapimpou

These samples are known as polymer "standards". In a SEC calibration curve, the logarithm of the molecular weight [log(M)] is plotted against the elution volume V*e*, for a number of polymer "standards".

From the calibration curve and the obtained chromatogram, the molecular weight of different fractions of the polymer can be calculated. More precisely, the number- and weight-average molecular weights (M_n, M_w respectively) can be obtained among others (equations 2.15 and 2.16) as well as the polydispersity index (PDI = M_w/M_n). M_w/M_n takes values from $1 \rightarrow \infty$.

$$\bar{M}_n \equiv \frac{\sum_i c_i}{\sum_i c_i / M_i} \qquad \textbf{(2.15)}$$

$$\bar{M}_w \equiv \frac{\sum_i c_i M_i}{\sum_i c_i} \qquad \textbf{(2.16)}$$

The molecular weight characteristics of more complex polymer structures, such as block copolymers, cannot be easily determined by SEC. To obtain absolute molecular weights, corrections with respect to the one block-specific detector response must be made, and on-line molar-mass-sensitive detectors are required, such as differential viscosity and multi-angle laser light scattering, which are expensive and require special knowledge for data evaluation.[182]

2.6. Magnetization analysis.

Magnetism - Preface

Magnetization is a phenomenon that describes the behavior of a material in the presence of an applied magnetic field. The wide range of magnetic properties induced by the interaction taking place between a magnetic material and an external magnetic field are of high interest in the areas of biomedicine and nanotechnology. A variety of steels and iron oxides are some well-known magnetic materials.

Petri Papaphilippou

Matter is composed of atoms, and atoms are constituted of protons, neutrons and electrons. The protons and the neutrons are located in the atom's nucleus and the electrons are in constant motion around the nucleus. Electrons have a negative electrical charge and produce a magnetic field as they move through space. A magnetic field is produced whenever an electrical charge is in motion. The strength of this field is called the *magnetic moment*. The magnetic moment of a magnetic material shows its tendency to align with the magnetic field. When a material is placed into an external magnetic field then its magnetic properties will be affected. This effect is known as Faraday's Law of Magnetic Induction. The change of the magnetic forces of matter depends on many factors such as the atomic and molecular structure of the material and the net magnetic field associated with the atoms. The atomic magnetic moments have three origins. These are the electron orbital motion, the change in orbital motion caused by an external magnetic field and the spin of the electrons. Usually in most atoms the electrons are in pair of opposite direction, thus canceling out the magnetic moment field to each other. Some other atoms, in which the electrons are unpaired, retain their magnetic moments and interact with the applied magnetic field.

$$\mathbf{B = \mu . H} \qquad \mathbf{(2.17)}$$

Equation (2.17) describes the intensity of the induced magnetic field B of a material. μ is the magnetic permeability and H indicates the intensity of the applied magnetic field. Another important parameter in magnetism is the related magnetic permeability μ_r which corresponds to the ratio of μ towards μ_o (magnetic permeability *in vacuo* $1.257*10^6$ H/m), (eq. 2.18).

$$\mu_r = \mu / \mu_o \qquad \mathbf{(2.18)}$$

$$\mathbf{M = \chi_m . H} \qquad \mathbf{(2.19)}$$

In eq. 2.19, M is the magnetization of a material per unit volume, χ_m is the magnetic susceptibility and H is the intensity of the external magnetic field. Materials can be classified into four categories according to their magnetization behavior: *diamagnetic*, *ferromagnetic*, *antiferromagnetic* and *paramagnetic*. The magnetic behavior of a material is strongly size-dependent. More precisely, at a particular temperature the magnetic properties of a material can be changed by tuning its size.

Petri Papaphilippou

Diamagnetism is a weak form of magnetism (magnetic susceptibility are negative (-10^{-6} to -10^{-3}). It appears only in the presence of an applied magnetic field and it is not permanently retained after the external field is removed. This phenomenon is caused only by the orbital motion of the electrons under the influence of an applied field. Transition metals like copper, silver and gold are diamagnetic.

Paramagnetic materials also show weak magnetization having small positive magnetic permeability and magnetic susceptibility in the order of 10^{-6} to 10^{-1}. These materials have unpaired electrons that in the absence of the magnetic field are randomly oriented. These electrons in the presence of an external field are aligned parallel to the applied magnetic field. This type of materials have no coercivity nor remanence indicating that after the external field is removed the internal magnetic dipoles randomize again and no extra energy is required to demagnetize the material. Hence the material does not remain magnetized. Examples of paramagnetic materials include magnesium, molybdenum, lithium and tantalum.

Ferromagnetism is a magnetization phenomenon exhibiting strong magnetization. Ferromagnetic materials are characterized by a large and positive susceptibility in the presence of an external magnetic field. They possess unpaired electrons and therefore their atoms show a net magnetic moment. Their strong magnetic properties are attributed to the presence of magnetic domains. In these domains, large numbers of atom's moments (10^{12} to 10^{15}) are aligned parallel so that the magnetic force within the domain is strong even in the absence of an applied magnetic field. There are three main parameters that describe the strength and magnetization of the material. The first one is the maximum magnetization of a material that can be achieved, known as the saturation magnetization M_S. This is due to the parallel orientation of all the magnetic dipoles to the direction of the applied magnetic field. The second one is the remanent magnetization M_R, which indicates the residual magnetization at zero applied field. The final parameter is the coercive field H_C, presenting the external field of opposite sign that is required to reduce the magnetization back to zero. Moreover, this parameter shows the minimum energy that is needed for the reversal of the magnetization of the material and it is strictly related to the magnetic anisotropy constant, K_u, that determines the energy to be overcome in order to invert the direction of the magnetic dipoles of the material. K_u depends on the shape and the morphology of the particles. All the above mentioned parameters result in the presence of a hysteresis loop for

these materials. Therefore, when the field is switched off the magnetization of the material still remains. Iron, nickel, and cobalt are examples of ferromagnetic materials.[195, 196]

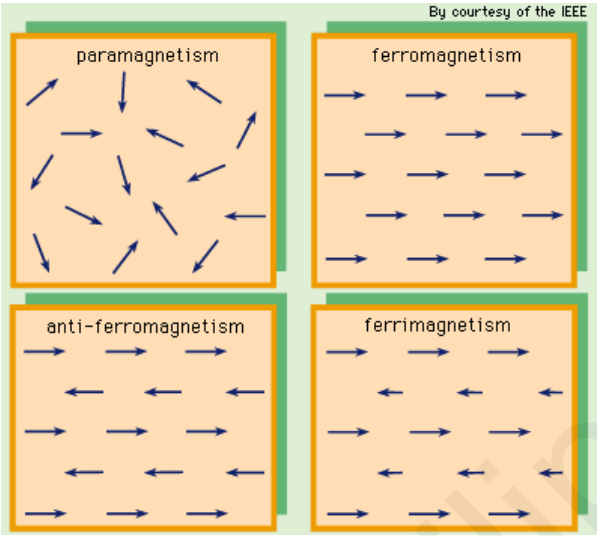

Figure 2.7. *Magnetic moments of paramagnetic, ferromagnetic, ferrimagnetic and antiferromagnetic materials.*

Besides the ferromagnetic materials, there is a different magnetization state at which the magnetic dipoles or interacting spins of a material are aligned antiparallel in the lattice hence showing a net zero magnetism namely as *antiferromagnetism*. The iron oxide particles such as the magnetite and the maghemite also present hysteresis but they belong to a different magnetization category, the so-called *ferrimagnetics*. In this class of materials the magnetic moments of the atoms found at different sublattices are opposed, but since those are unequal, a net magnetization value remains.

The decrease of the size of the magnetic particles renders them even more suitable agents in diagnostic and therapeutic applications compared to their bulk counterparts. In the order of tens of nanometers (< 30 nm), ferri- or ferromagnetic materials become single domain because the formation of domain walls is not energetically favorable and therefore these materials are shifted towards the, so-called *superparamagnetic* behavior. In this state, the coercivity parameter becomes zero and above the blocking temperature (T_B), the thermal energy is sufficient for the moment to freely rotate resulting in a loss of net magnetization in the absence of an external field (remanent magnetization is zero). Due to this a superparamagnetic material does not present a hysteresis loop. Furthermore the coupling

Petri Papaphilippou

interactions within these single domains result in much higher magnetic susceptibilities compared to paramagnetic materials.[197]

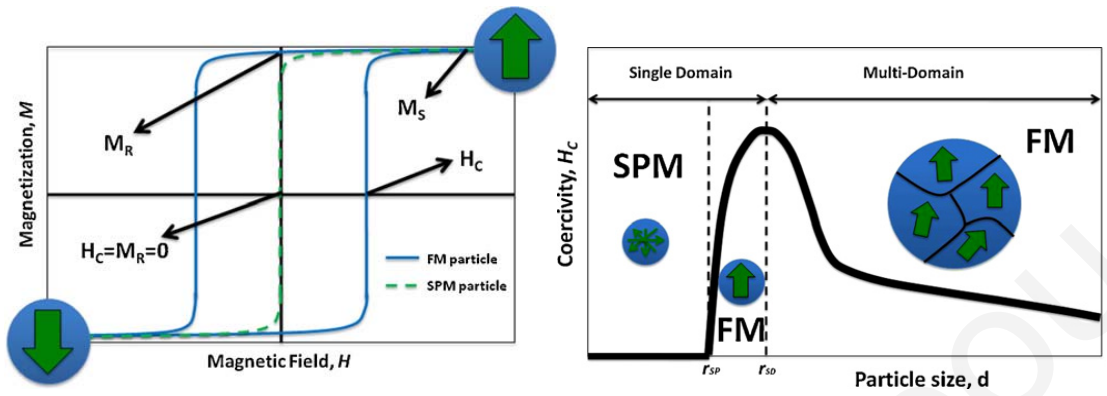

(a) ***(b)***

Figure 2.8. *(a) Magnetization (M) versus applied magnetic field strength (H) plots for ferromagnetic and superparamagnetic materials. (b) Change of coercivity (H_C) of magnetic particles with size.*[197]

The hysteresis loop appears only in ferro- or ferrimagnetic materials. According to their magnetization characteristics, these compounds can be classified as soft and hard magnetic materials. Soft magnets have high magnetization permeability and low coercivity H_C indicating that they can be easily magnetized and demagnetized without any losses of energy hysteresis. Hard magnets in contrast to the soft magnets present high coercivity H_C but low magnetic permeability, providing thus losses of high energies.

Temperature is another parameter that plays a crucial role on the magnetic behavior of a material. As already known, the magnetic dipoles have the tendency to fluctuate randomly and with the raise of the temperature this phenomenon increases, therefore the moments cannot align to each other. This results to the reduction of the saturation magnetization M_S. It was found that at a certain temperature the so-called *Curie* temperature T_C, a ferromagnetic material becomes paramagnetic. *Néel* temperature T_N corresponds to the transition temperature of an antiferromagnetic or ferrimagnetic behavior to paramagnetic.

Petri Papaphilippou

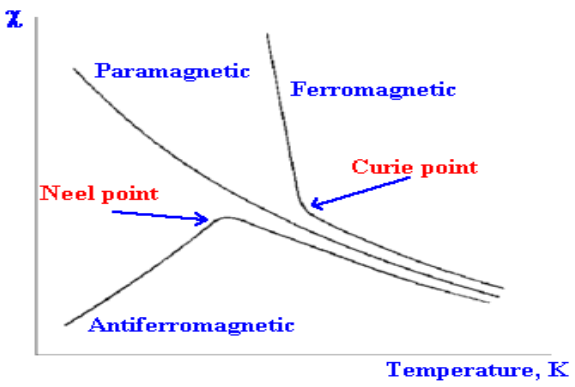

Figure 2.9. *Temperature-dependence of the magnetic properties of materials exhibiting different magnetic behavior.*

Magnetic nanoparticles in solution undergo three types of loss processes, in the presence of alternating magnetic field: hysteresis losses, Néel relaxation and Brownian relaxation. In the Brownian relaxation the entire particle can be rotated (external rotation) whereas Néel relaxation is attributed to internal diffusion of the particles magnetic moments. In nanoparticles characterized by core diameter < 20 nm (single domain particles) magnetization relaxation is only governed by a combination of the Brownian and Néel relaxation mechanisms. The contribution from hysteresis losses is negligible.

$$\tau_B = 3\eta V_H / kT \quad (2.20)$$

$$\tau_N = \tau_o \exp(\Delta E / kT) \quad (2.21)$$

$$1/\tau = 1/\tau_B + 1/\tau_N \quad (2.22)$$

In eq. 2.20, τ_B is defined as the Brownian's relaxation time where V_H is the hydrodynamic volume of the particle, k is the Boltzmann constant, T is the temperature and η is the dynamic viscosity of the carrier liquid. The Néel relaxation time is defined by eq. 2.21 where ΔE is the energy barrier over which the magnetization must reverse and $\tau_o \sim 10^{-9}$ s. This energy is usually is determined by the product of the anisotropy K and the magnetic volume V: $\Delta E = KV$. The combined effect can be expressed as seen in eq. 2.22. Superparamagnetic materials exhibit relaxation times faster than 100 s.

Petri Papaphilippou

2.6.1. Vibrating Sample Magnetometry (VSM).

Vibrating sample magnetometry (VSM) is a powerful method that is generally used to measure the magnetic properties of materials. It provides information on the magnetic properties of a sample. More precisely, the VSM technique allows for the performance of various types of experiments such as the measurement of the virgin curve, the hysteresis loop, the DC demagnetization, the AC Remanence etc. Vibrating sample magnetometer operates on Faraday's Law of induction, which states that by changing the magnetic flux, an electric field is produced and this can be measured by two-detection coils.[198]

Initially, the sample is exposed to a constant magnetic field which can magnetize the magnetic material by aligning its magnetic domains with the field. The magnetic dipole moment of the sample will create a magnetic field around it. As the sample vibrates and is moving up and down, this magnetic field changes relative to time and can be sensed by a set of pick-up coils. As already known, the magnetic field produced causes an electric field in the pick-up coils according to Faraday's Law. This current will be proportional to the magnetization of the material. The higher the magnetization is, the greater the induced current will be. VSM has a transimpedance and a lock-in amplifier which improves the induction current. The instrument is connected to a computer and the software provides data on the change of the magnetization of a sample relative to the strength of the applied magnetic field.

VSM measurements.

The Virgin curve presented in Fig. 2.10 illustrates the magnetization of a sample as a function of the applied field. This experiment occurs by measuring the magnetic moment related to a field that is slowly increased from 0 to a certain maximum field.[199]
The Hysteresis Loop measurement is the most common magnetic experiment. The parameters extracted from this experiment are used to characterize the magnetic properties of a material such as the saturation magnetization Ms, the remanence Mr and the coercivity Hc. By applying an external magnetic field starting from a maximum value (positive or negative) the magnetometer measures the magnetization of the material at each point (Fig. 2.23 (a)).[199] The presence of a hysteresis loop is typical for ferromagnetic and ferrimagnetic materials whereas superparamagnetic materials exhibit no hysteresis.

Petri Papaphilippou

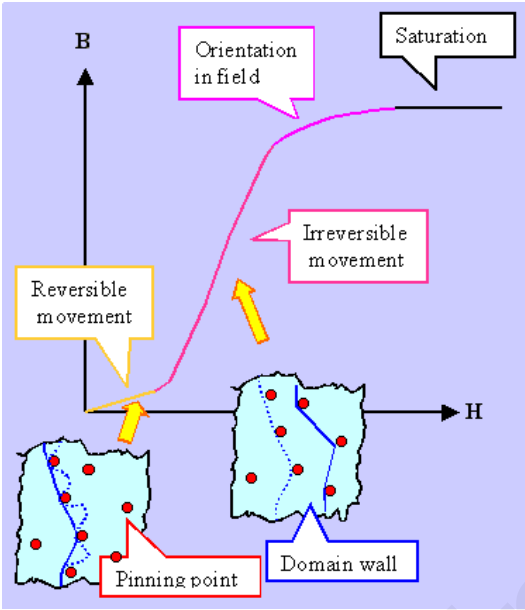

Figure 2.10. *Virgin Curve: Magnetization (B) of the material related to the applied magnetic field (H).*

2.6.2. Physical Property Measurement System (PPMS).

The Quantum Design Physical Property Measurement System (PPMS) has the capability to perform a variety of experiments. This system can be used to obtain information on the heat capacity, the thermal conductivity, the electrical properties and the magnetic behavior of a sample.The PPMS magnetometer has the ability to determine the magnetization and the magnetic susceptibility of a sample through the detection of the magnetic moment of the material. The superconductivity is an important parameter for the PPMS magnetometer, resulting to the production of a very stable and large magnetic field. The advantage of using a superconducting magnet is that, large amount of electrical current can pass through it without any loss of the energy in the form of heat.[200]

The principle of a PPMS experiment is similar to VSM. The sample is located in a chamber at the centre of the magnet and it is surrounded by two detection coils. The sample has the ability to move through the coils and consequently the magnetic moment of the material induces an electric current in the detection coils.

Petri Papaphilippou

Petri Papaphilippou

[174] C. R. Blanchard, "*Atomic Force Microscopy"*, Springer, 1(5), **1996**.

[175] E. Meyer, H. J. Hug, R. Bennewitz, "*Scanning Probe Microscopy: The lab on a Tip*".

[176] History of AFM, Pacific Nanotechnology (Nanotechnological advances), LOT.

[177] B. Ruozi, G.Tosi, E.Leo, M.A. Vandelli, *Talanta,* 73, **2007**, 12.

[178] H. N. Pishkenari, N. Jalili, A. Meghdari, *Mechatronics,* 16, **2006**, 655.

[179] www.nanoscience.com/education/AFM.html.

[180] K. Oikawa, H. Kimb, N. Watanabe, M.Shigeno,Y. Shirakawabe, K. Yasuda, *Ultramicroscopy,* 107, **2007**, 1061.

[181] *"Characterization techniques of materials",* MMK 554, Dr. Theodora Kyratsi, 2008.

[182] *"Characterization methods of polymers and colloids*", MMK 551, Dr. Theodora Krasia-Christoforou.

[183] "*Transmission Electron Microscopy and Diffractometry of Materials*", B. Fultz, J. M. Howe, Springer, **2007**.

[184] *" Differential Scanning Calorimetry"*, H. K. D. H. Bhadeshia, University of Cambridge, Materials Science and Metallurgy.

[185] *«Οργανική Χημεία»,* John McMurry, Τόμος Ι, Πανεπιστημιακές Εκδόσεις Κρήτης.

[186] www.teaching.shu.ac.uk/hwb/chemistry/tutorials/molspec/nmr 1.html

[187] www.cem.msu.edu/reusch/VirtualText/Spectrpy/nmr/nmr 1.html

[188] *"The basics of Crystallography and Diffraction",* C. Hammond, Oxford Science Publications.

[189] B. TH. De Keijser, E. J. Mittemeijer, H. C. F. Rozendaal, *J. Appl. Cryst*. 16, **1983**, 309.

[190] *«Σύγχρονες μέθοδοι στη χημική ανάλυση»,* Pecsok, Shields, Cairns, McWilliam, Δεύτερη έκδοση.

[191] *"Dynamic Light Scattering",* M. Sartor, University of California.

[192] *"Laser Light Scattering: Basic Principles and Practise",* Charles S. Johnson and Don A. Gabriel, Academic Press, **1991**.

[193] "*Contemporary Polymer Chemistry",* Harry R. Allcock, Frederick W. Lampe and James E. Mark Pearson Education, Inc.

Petri Papaphilippou

[194] *"Introduction to Physical Polymer Science",* L. H. Sperling, John Wiley and Sons, Inc.

[195] C. Sun, J. S. H. Lee, M. Zhang, *Advanced Drug Delivery*, 60, **2008**, 1252.

[196] Albert Figuerola, Riccardo Di Corato, Liberato Manna and Teresa Pellegrino, *Pharmacological Research*, xxx, **2010**, xxx.

[197] *"Magnetism: Molecules to Materials III", Nanosized Magnetic Materials*, J. S. Miller, M. Drillon.

[198] DMS Vibrating Sample Magnetometer, AD Tecnhologies.

[199] *HPLC of Polymers*, H. Pasch, B. Trathnigg, Springer: Berlin, **1997**.

[200] *"Fundamentals of Magnetism and Magnetic measurements featuring quantum design's Magnetic Property Measurement System",* M. McElfresh, Purdue University.

Petri Papaphilippou

3. Experimental Section.

3.1. Methods.

For the characterization of the chemical structure of all the compounds prepared in the present study an *Avance Brucker 300 MHz spectrometer* was used equipped with an Ultrashield magnet. ^{1}H NMR spectra were obtained in $CDCl_3$ with tetramethylsilane (TMS) used as an internal standard.

The molecular weights (MWs) and molecular weight distributions (MWDs) of the polymers were determined by *size exclusion chromatography (SEC)* using equipment supplied by Polymer Standards Service (PSS). All measurements were carried out at room temperature using Styragel HR 3 and Styragel HR 4 columns. A calibration curve was performed using poly (methyl methacrylate) (PMMA) standards.

Differential scanning calorimetry (DSC) was used to measure the glass transition temperatures T_gs of the homopolymers and diblock copolymers using the Q100 TA Instrument with a heating rate of 10 ºC min^{-1}. Each sample was scanned twice between –100 ºC and +150 ºC. The second run (heat) was used for data analysis.

Thermal gravimetric analysis (TGA) measurements were performed on a Q 500 TA Instrument under a nitrogen flow at a heating rate of 10 ºC min^{-1} between 25 and 600 ºC.

Dynamic light scattering (DLS) measurements were carried out using a 90Plus Brookhaven DLS spectrometer equipped with a 30 mW laser operating at 633 nm. DLS experiments were performed at a 90° scattering angle. Solution concentrations maintained at 4 g L^{-1}. The high quality of the scattering curves was ensured by repeating the measurements several times. All polymer solutions were filtered through cellulose acetate microfilters (pore size: 0.45 μm) prior to the measurements.

Atomic force microscopy (AFM) measurements were performed on a Multimode-AFM (Veeco-Instruments). The tips used were of the type NC (NANOWORLD). The resonant frequency was approximately 285 KHz and the force constant around 42 N/m. Dilute sample

Petri Papaphilippou

solutions were spin-coated on a mica surface to be visualized by AFM. All measurements were carried out with tapping mode.

Transmittion electron microscopy (TEM) were performed on a 1010 JEOL microscope (200kV).

A Lambda 10 *UV-vis spectrophotometer* from Perkin-Elmer was used for the turbidimetry measurements. A Jasco V-630 UV-vis spectrophotometer was used to carry out the drug release kinetic measurements.

Fourier transform infrared spectroscopy Jasco 460 *(FT-IR)* was used to characterize the materials using powder samples pressed into KBr pellets.

X-ray diffraction spectroscopy measurements were performed on an XRD, Rigaku (30 kV, 25 mA with λ = 1.5405 Å (Cu)) instrument in the range of 5 to 90˚ at a rate of 0.5˚/min.

Magnetization curves were recorded using either a Cryogenics VSM or a *vibrating sample magnetometer (VSM)* (VSM Model 880 ADE Technologies, USA). Due to the low magnetic moment of the highly diluted samples, the data analysis took into account also the diamagnetic moment of the cylindrical sample holder of plexiglas. Magnetization curves corresponding to the magnetoactive polymer conetworks were recorded using the *Physical Property Measurement System, PPMS 6000* at 5K and 300K.

3.2. Reagents.

Benzene (Fluka, ≥ 99.5%) and ethyl acetate (Scharlau) used as the polymerization solvents, were stored over CaH_2 (Merck, 99.9%) and distilled under reduced pressure immediately prior to the polymerization reactions. Methanol (Labscan, 99%), *n*- Hexane (LabScan, 99%), HCl (Merck, 37% solution), NH_4OH (Scharlau, 25 % (v/v) H_2O), chloroform (Scharlau), diethyl ether (LabScan, 99.5%), acetate buffer solution, with pH 4.6 (Fluka analytical), citric acid/sodium hydroxide buffer solution with pH 6.0, Dulbecco's phosphate buffer solution DPBS, pH 7.2 (Sigma) and deuterated chloroform $CDCl_3$ (Merck) were used as received.

Petri Papaphilippou

The following inorganic compounds were used without further purification: Sulfur (Aldrich, powder ~ 100 mesh), silica gel (Aldrich, 60 Ǻ, 70-230 mesh), CaH_2, NaOH pellets (Scharlau) and anhydrous $MgSO_4$ (Scharlau). 2-(acetoacetoxy)ethyl methacrylate (AEMA) (Aldrich, 95%) and Poly(ethylene glycol) methyl ether methacrylate (PEGMA) also abbreviated as HEGMA (Hexa(ethylene glycol) methyl ether methacrylate) (Aldrich) were passed through a basic alumina column prior to the polymerizations and used without further purification. 2-diethylamino ethyl methacrylate (DEAEMA) (Aldrich, 95%) was stored over CaH_2 and distilled under reduced pressure immediately prior to the polymerization reaction. Ethylene glycol dimethacrylate (EGDMA) cross-linker (Merck) was used without further purification. Benzyl chloride (Aldrich, 99%), carbon tetrachloride (Riedel de Haën, ≥ 99.8%), α-methylstyrene (Aldrich, 99%) and sodium methoxide (Aldrich, 30% solution in methanol) were used as received by the manufacturer. Iron chloride (III) hexahydrate (Sigma-Aldrich, 97%) and iron chloride (II) tetrahydrate (Sigma-Aldrich, 99%) were used for the preparation of non-coated magnetic particles, whereas iron sulfate (II) heptahydrate (Sigma-Aldrich ≥ 99.0%), and iron chloride (III) hexahydrate (Sigma-Aldrich, 97%) were used for the fabrication of the oleic acid-coated magnetite nanoparticles. The latter were fabricated at the Center for Fundamental and Advanced Technical Research, Romanian Academy, Timisoara branch, Romania by following an experimental procedure developed by Bica *et al*.[201]

The anticancer drug doxorubicin hydrochloride DOX.HCl (Sigma Life sciences) was used as received. The PC3 (grade IV, androgen unresponsive metastatic prostate cancer) and RAW264.7 (murine macrophage) cell lines were a generous gift from Professor Andreas Evdokiou, Adelaide University, Australia. The tissue culture reagents Dulbecco's modified Eagle's medium (DMEM), fetal bovine serum (FBS), antibiotic/antimycotic, 0.25% trypsin, 0.4% trypan blue, and phosphate-buffered saline (PBS) were obtained from GIBCO, Invitrogen. Resovist® (Schering, AG) was a kind contribution of Dr. Ioannis Seimenis, Medical Diagnostic Center "Ayios Therissos", Nicosia, Cyprus. The biological assays were carried out in collaboration with Dr. A. Odysseos, Dr. L. Loizou and Dr. Y. Christou, EPOS-Iasis R&D, Biomedical Tissue Engineering/Nanobiotechnology Lab.

Petri Papaphilippou

3.3. Synthesis.

3.3.1. Synthesis of cumyl dithiobenzoate, CDTB (Chain Transfer Agent, CTA).

CDTB was synthesized in two steps, following a procedure reported by *Rizzardo et* al.[202] Briefly, the first step involved the preparation of dithiobenzoic acid *via* the reaction of sulfur, sodium methoxide and benzyl chloride in methanol at 60 ^{o}C for 18 hours. Subsequently, dithiobenzoic acid was left to react with α-methylstyrene in carbon tetrachloride at 70 ^{o}C for 18 hours to obtain CDTB in 19.3 % yield after purification by column chromatography (silica gel), using *n*-hexane as an eluent.

^{1}H NMR (300 MHz, $CDCl_3$): δ (ppm) = 7.87 (a, 2H), 7.58-7.22 (b, 8H), 2.01 (c, CH_3).

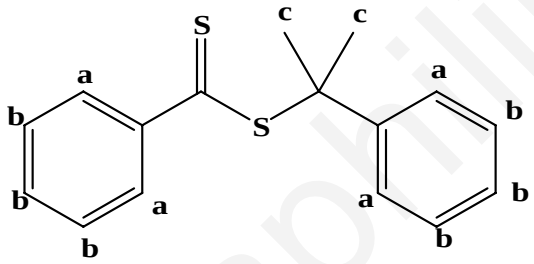

3.3.2. Synthesis of PEGMA$_x$ homopolymers.

The polymerization procedure followed for the preparation of a PEGMA$_x$ homopolymer is described as follows: CDTB was dried under high vacuum for approximately 30 min prior to use. In a round-bottom flask (100 mL) maintained under a dry nitrogen atmosphere, CDTB (48.0 mg, 0.176 mmol) and AIBN (8.9 mg, 0.054 mmol) were dissolved in freshly distilled benzene (45 mL). PEGMA (10 mL, 35 mmol) was transferred into the flask with the aid of a syringe. The resulting solution was degassed by three freeze-evacuate-thaw cycles, placed under a dry nitrogen atmosphere and heated at 65 ^{o}C for 20 hours. The polymerization was terminated by cooling the reaction down to room temperature. The produced homopolymer (7.21 g, 69% polymerization yield, pink color) was retrieved by precipitation in *n*-hexane and was left to dry *in vacuo* for 24 hours.

^{1}H NMR (300 MHz, $CDCl_3$): δ (ppm) = 4.06 (c, 2H, br), 3.64 (d, 2H, br), 3.35 (e, 3H, s), 2.00-1.73 (a, 2H, m, br), 1.22-0.85 (b, 3H, m, br) (Fig. 3.1).

Petri Papaphilippou

Table 3.1. *Molar quantities of the monomer, the initiator and the CTA used for the preparation of PEGMA$_x$ homopolymers.*

HomoPolymers [a]	Sample code	PEGMA (mmol)	CDTB (mmol)	AIBN (mmol)
PEGMA$_{97}$	PPR10	35.00	0.17	0.054
PEGMA$_{70}$	PPR17	33.33	0.33	0.100
PEGMA$_{128}$	PPR18	33.33	0.11	0.034
PEGMA$_{29}$	PPR26	26.67	0.67	0.210
PEGMA$_{132}$	PPR30	16.67	0.11	0.034
PEGMA$_{121}$	PPR37	33.33	0.13	0.041

[a] Experimental polymer molecular weight as determined by SEC, using PMMA calibration standards.

3.3.3. Synthesis of AEMA$_x$ homopolymers.

The polymerization procedure followed for the preparation of an AEMA$_x$ homopolymer is described as follows: CDTB was dried under high vacuum for approximately 30 min prior to use. In a round-bottom flask (100 mL) maintained under a dry nitrogen atmosphere, CDTB (275 mg, 1.00 mmol) and AIBN (49 mg, 0.030 mmol) were dissolved in freshly distilled benzene (45 mL). AEMA (3.8 mL, 20.04 mmol) was transferred into the flask with the aid of a syringe. The resulting solution was then degassed by three freeze-evacuate-thaw cycles, placed under a dry nitrogen atmosphere and heated at 65 ^{o}C for 20 hours. The polymerization was terminated by cooling the reaction down to room temperature. The produced homopolymer (7.21 g, 69% polymerization yield, pink color) was retrieved by precipitation in *n*-hexane and was left to dry *in vacuo* for 24 hours.

^{1}H NMR (300 MHz, $CDCl_3$): δ (ppm) = 4.16 (f, 2H, br), 4.34 (g, 2H, br), 3.56 (h, 2H, s), 2.28 (i, 3H, s), 2.14-1.81 (a, 2H, m, br), 1.23-0.83 (b, 3H, m, br) (Fig. 2.1).

Table 3.2. *Molar quantities of the monomer, the initiator and the CTA used for the preparation of AEMA$_x$ homopolymers.*

Homopolymers [a]	Sample code	AEMA (mmol)	CDTB (mmol)	AIBN (mmol)
AEMA$_{36}$	PPR11	20.04	1.00	0.030
AEMA$_{38}$	PPR40	28.00	0.70	0.22

[a] Experimental polymer molecular weight as determined by SEC, using PMMA calibration standards.

Petri Papaphilippou

3.3.4. Synthesis of DEAEMA$_x$ homopolymers.

The polymerization procedure for the synthesis of DEAEMA$_x$ is described as follows: CDTB was dried under high vacuum for approximately 30 min prior to use. In a round-bottom flask (100 mL) maintained under a dry nitrogen atmosphere, CDTB (148 mg, 0.54 mmol) and AIBN (27.4 mg, 0.167 mmol) were dissolved in freshly distilled ethyl acetate (18 mL). DEAEMA (5.4 mL, 26.98 mmol) was transferred into the flask with the aid of a syringe. The resulting solution was then degassed by three freeze-evacuate-thaw cycles, placed under a dry nitrogen atmosphere and heated at 65 ^{o}C for 20 hours. The polymerization was terminated by cooling the reaction down to room temperature. The produced homopolymer was retrieved upon extraction with water (40 mL x 2). Subsequently, the organic phase was isolated and the solvent was removed under reduced pressure to yield an orange-colored solid, (1.56 g, 30% polymerization yield) that was left to dry *in vacuo* for 24 hours.
^{1}H NMR (300 MHz, $CDCl_3$): δ (ppm) = 4.07 (f, 2H, br), 2.78 (g, 2H, s), 2.64 (h, 4H, s), 2.16-1.79 (a 2H, m), 1.24-0.84 (i 3H, b 3H, m, br) (Fig. 3.1).

3.3.5. Synthesis of PEGMA$_x$-b-AEMA$_y$ diblock copolymers.

Chain-growth of the obtained PEGMA$_x$ homopolymers was accomplished *via* the addition of the second monomer AEMA. The synthetic methodology followed for the preparation of a PEGMA$_x$-*b*-AEMA$_y$ diblock copolymer is exemplarily described as follows: The macro-chain transfer agent (macro-CTA), PEGMA$_{97}$, (M_n^{SEC} = 29200 g.mol^{-1}, 2.00 g, 0.068 mmol) was placed in a round-bottom flask (50 mL) and dissolved in freshly distilled ethyl acetate (12 mL) under a dry nitrogen atmosphere. AIBN (0.0035 g, 0.021 mmol) dissolved in ethyl acetate and AEMA (0.673 g, 3.14 mmol) were then transferred into the flask *via* a syringe. The reaction mixture was degassed by three freeze-evacuate-thaw cycles and placed under nitrogen atmosphere at 65 ^{o}C for 20 hours. The polymerization was terminated by cooling the reaction down to room temperature. The produced diblock copolymer (2.46 g, 69% polymerization yield, pink color) was retrieved by precipitation in *n*-hexane and was left to dry *in vacuo* for 24 hours.
^{1}H NMR (300 MHz, $CDCl_3$): δ (ppm) = 4.36 (g 2H, br), 4.10 (f, 2H, br), 3.64 (h, 2H, br, d, 2H, br), 3.36 (e, 3H, s), 2.25 (i, 3H, br), 2.25-1.78 (a, a' 2H, m, br), 1.22-0.85 (b, b' 3H, m, br) (Fig. 3.1).

Petri Papaphilippou

Table 3.3. *Molar quantities of the monomer, the initiator and the macroCTA used for the preparation of the block copolymers PEGMA$_x$-b-AEMA$_y$ and AEMA$_x$-b-PEGMA$_y$.*

Diblock Copolymers [a]/ Sample Codes	PolyPEGMA (mmol)	PolyAEMA (mmol)	AIBN (mmol)	PEGMA (mmol)	AEMA (mmol)	Yield %
PEGMA$_{97}$-*b*-AEMA$_{18}$ PPR12	0.068	-	0.021	-	1.56	41
PEGMA$_{97}$-*b*-AEMA$_{35}$ PPR13	0.068	-	0.021	-	3.14	69
PEGMA$_{97}$-*b*-AEMA$_{46}$ PPR16	0.031	-	0.0098	-	1.85	97
PEGMA$_{70}$-*b*-AEMA$_{16}$ PPR19	0.094	-	0.029	-	6.58	13
AEMA$_{36}$-*b*- PEGMA$_{292}$ PPR14	-	0.063	0.019	19.70	-	74
PEGMA$_{128}$-b-AEMA$_{19}$ PPR20	0.077	-	0.024	-	1.55	n.d
PEGMA$_{70}$-*b*-AEMA$_{56}$ PPR21	0.094	-	0.029	-	6.58	48
PEGMA$_{57}$-*b*-AEMA$_{21}$ PPR23	0.019	-	0.060	-	0.93	23
PEGMA$_{132}$-*b*-AEMA$_{42}$ PPR31	0.035	-	0.019	-	1.90	n.d
PEGMA$_{121}$-*b*-AEMA$_{44}$ PPR38	0.055	-	0.017	-	2.20	15
AEMA$_{38}$-*b*- PEGMA$_{316}$ PPR42	-	0.060	0.019	19.38	-	82

[a] Experimental polymer molecular weight as determined by SEC and ^{1}H NMR. The degree of polymerization for the 1st block was determined by SEC; this combined with the information obtained by ^{1}H NMR let to the determination of the DP for the 2nd block. n.d: not determined.

Petri Papaphilippou

3.3.6. Synthesis of HEGMA$_x$-b-DEAEMA$_y$ diblock copolymers.

Chain-growth of the obtained HEGMA$_x$ homopolymers was accomplished *via* the addition of the second monomer DEAEMA. An example of the synthetic methodology followed for the preparation of a PEGMA$_x$-*b*-DEAEMA$_y$ diblock copolymer is described as follows: The macro-chain transfer agent (macro-CTA), PEGMA$_{128}$, (M_n^{SEC} = 38668 g.mol^{-1}, 1.70 g, 0.044 mmol) was placed in a round-bottom flask (50 mL) and dissolved in freshly distilled ethyl acetate (9 mL) under a dry nitrogen atmosphere. AIBN (0.0022 g, 0.014 mmol) dissolved in ethyl acetate and DEAEMA (0.41 g, 2.19 mmol) were then transferred into the flask *via* a syringe. The reaction mixture was degassed by three freeze-evacuate-thaw cycles and placed under nitrogen atmosphere at 65 ^oC for 20 hours. The polymerization was terminated by cooling the reaction down to room temperature. The produced diblock copolymer (1.76 g, 15% polymerization yield, pale orange color) was retrieved by precipitation in *n*-hexane and was left to dry *in vacuo* for 24 hours.

^{1}H NMR (300 MHz, $CDCl_3$): δ (ppm) = 4.07 (f, 2H, br), 3.64 (d, 2H, br), 3.36 (e, 3H, br), 2.71 (g, 2H, br), 2.60 (h, 4H, br), 2.16-1.79 (a, a' 2H, m, br), 1.24-0.84 (i ,3H, b, b' 3H, m, br) (Fig. 3.1).

Table 3.4. *Molar quantities of the monomer, the initiator and the macroCTA used for the preparation of the block copolymers PEGMA$_x$-b-DEAEMA$_y$ and DEAEMA$_x$-b-PEGMA$_y$.*

Diblock Copolymers [a]/ Sample codes	Poly PEGMA (mmol)	Poly DEAEMA (mmol)	AIBN (mmol)	PEGMA (mmol)	DEAEMA (mmol)
PEGMA$_{128}$-*b*-DEAEMA$_{34}$ PPR28	0.044	-	0.014	-	2.19
PEGMA$_{121}$-*b*-DEAEMA$_{18}$ PPR39	0.027	-	0.0085	-	2.20
DEAEMA$_{30}$-b-PEGMA$_{210}$ PPR41	-	0.14	0.045	28.80	-

[a] Experimental polymer molecular weight as determined by SEC and ^{1}H NMR. The degree of polymerization for the 1st block was determined by SEC; this combined with the information obtained by ^{1}H NMR let to the determination of the DP for the 2nd block.

Petri Papaphilippou

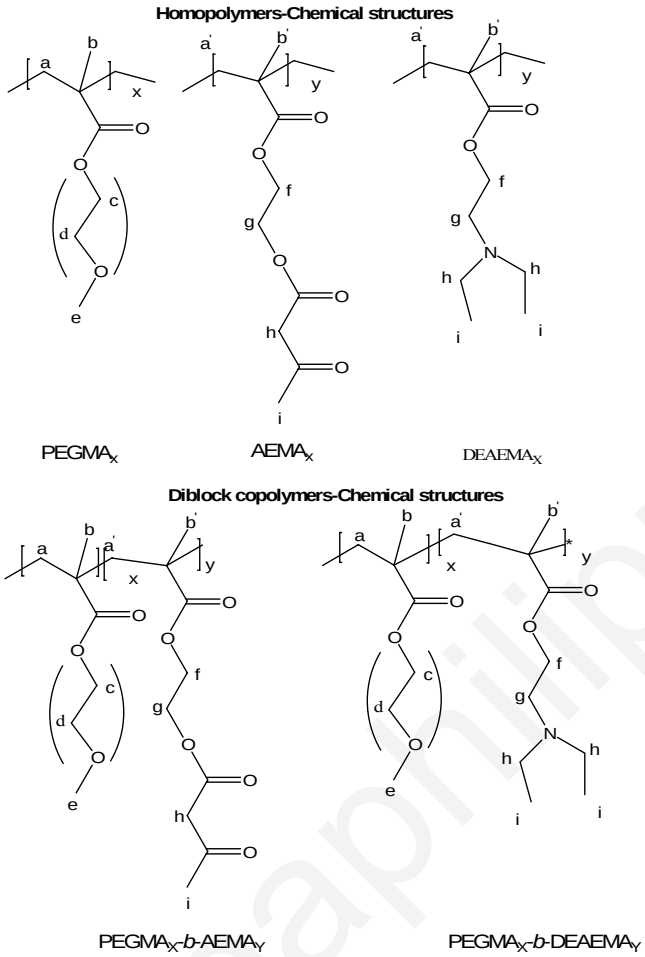

Figure 3.1. *Structures of homopolymers and block copolymers synthesized by RAFT controlled radical polymerization.*

3.3.7. Synthesis of HEGMA-co-AEMA/EGDMA random co-networks.

The polymerizations were carried out in a 50 mL round-bottom flask, fitted with a rubber septum. The monomers HEGMA (2.10 g, 7 mmol) and AEMA (1.5 g, 7 mmol) as well as the cross-linker EGDMA (1.6 mL) (1.68 g, 17.5 mmol) were transferred *via* a syringe to the flask and either EA or THF (10 mL) was subsequently added followed by the addition of the initiator, AIBN (0.023 g, 0.14 mmol) dissolved in the solvent (2 mL). The reaction was carried out at 65 °C for 24 h. After the product was cooled down to room temperature the gel was removed from the flask and placed in a glass container where ethyl acetate or tetrahydrofuran (100ml) was added. It was left there for 1 week to remove the sol fraction (extractables) and filtered. The filtrate was placed under reduced pressure to remove the solvent in order to

Petri Papaphilippou

determine the percentage of the extractables (non-reacted reagents). This was calculated as the ratio of the dried mass of the extractables divided by the theoretical mass of all components in the network (i.e. polymer plus crosslinker).

Table 3.5. *Molar quantities of the monomers HEGMA and AEMA, the initiator AIBN and the cross-linker EGDMA that were used for the preparation of the HEGMA-co-AEMA/EGDMA random co-networks.*

	Sample code	Solvent[a]	PEGMA (mmol)	AEMA (mmol)	EGDMA (mmol)	AIBN (mmol)
No Iron Oxide	Gel 1	Ethyl Acetate	7.0	7.0	8.5	0.14
No Iron Oxide	Gel 2	THF	7.0	7.0	8.5	0.14

[a]EA: ethyl acetate, THF: tetrahydrofuran.

3.4. Synthesis of Magneto-responsive Polymeric Materials.

3.4.1. Synthesis of stabilized in aqueous media iron oxide nanoparticles, in the presence of the PEGMA$_x$-b-AEMA$_y$ diblock copolymers.

The polymer-stabilized magnetic nanoparticles were produced *via* a conventional chemical reaction method that was carried out at room temperature, involving chemical co-precipitation of Fe(III) and Fe(II) cations in a 2:1 molar ratio under weak basic conditions (NH_4OH) in the presence of the PEGMA$_x$-*b*-AEMA$_y$ copolymers.

Prior to the reaction, the water and ammonium hydroxide solutions were carefully deoxygenated by purging with ultra-high-purity N_2 for at least 30 min. The reaction was carried out under continuous nitrogen flow. In a typical procedure, the diblock copolymer PEGMA$_{97}$-*b*-AEMA$_{35}$ (M_n =38500 g mol^{-1} 200 mg, 0.182 mmol of AEMA units) was placed in a round-bottom flask (25 mL) and dissolved in degassed water (4 mL). Aqueous solutions of $FeCl_3.6H_2O$ (49.2 mg, 0.182 mmol) and $FeCl_2.4H_2O$ (18 mg, 0.091 mmol) which were prepared separately in water (2 mL each) were syringed into the copolymer solution under an inert nitrogen atmosphere. The resulting orange-colored solution was left to stir for 15 min before adding the NH_4OH solution. Finally, NH_4OH (25% v/v in H_2O) (0.24 mL) was added under strong stirring conditions and inert atmosphere. The solution immediately turned from orange to dark brown transparent, indicating the formation of stabilized iron oxide

Petri Papaphilippou

nanoparticles. The solution mixture was allowed to stir for 30 min under nitrogen atmosphere at room temperature. Finally, the mixture was dialyzed (dialysis tubing benzoylated with AVG. flat width 32mm) against water to remove any remained side-products or free copolymer.

The polymer-coated iron oxide nanoparticles were also prepared in an aqueous solution of sodium chloride (NaCl, 0.1M). Prior to the reaction, the NaCl and NH_4OH solutions were carefully deoxygenated by purging with ultra-high-purity N_2 for at least 30 min. The reaction was carried out under continuous nitrogen flow. In a typical procedure, the diblock copolymer $AEMA_{36}$-*b*-$PEGMA_{217}$ (M_n =72800 g mol^{-1}, 200 mg, 0.099 mmol of AEMA units) was placed in a round-bottom flask (25 mL) and dissolved in degassed NaCl solution (4 mL). Aqueous solutions of $FeCl_3.6H_2O$ (107 mg, 0.395 mmol) and $FeCl_2.4H_2O$ (39.3 mg, 0.198 mmol) which were prepared separately in water (2 mL each) were syringed into the copolymer solution under an inert nitrogen atmosphere. The resulting orange-colored solution was left to stir for 15 min before adding the NH_4OH solution. Finally, NH_4OH (25% v/v in H_2O) (0.25 mL) was added under strong stirring conditions and inert atmosphere. The solution immediately turned from orange to dark brown transparent, indicating the formation of stabilized iron oxide nanoparticles. The solution mixture was allowed to stir for 30 min under nitrogen atmosphere at room temperature.

Table 3.6. *Molar quantities of the $PEGMA_x$-b-$AEMA_y$ diblock copolymers, the iron salts $FeCl_3.6H_2O/FeCl_2.4H_2O$ and the NH_4OH used to prepare polymer-coated magnetic nanoparticles in aqueous media.*

Diblock copolymers-Iron oxide	**PPR19 (mmol)**	**$FeCl_3.6H_2O$ (mmol)**	**$FeCl_2.4H_2O$ (mmol)**	**NH_4OH (mL)**
$PEGMA_{70}$-*b*-$AEMA_{16}$/ Fe_xO_y	0.131	0.131	0.065	0.16
	0.131	0.262	0.131	0.16
	0.131	0.393	0.196	0.24
	PPR12 (mmol)	**$FeCl_3.6H_2O$ (mmol)**	**$FeCl_2.4H_2O$ (mmol)**	**NH_4OH (mL)**
$PEGMA_{97}$-*b*-$AEMA_{18}$/ Fe_xO_y	0.109	0.109	0.054	0.07
	0.109	0.218	0.109	0.13

	PPR14 (mmol)	$FeCl_3.6H_2O$ (mmol)	$FeCl_2.4H_2O$ (mmol)	NH_4OH (mL)
$PEGMA_{292}$-*b*-$AEMA_{36}$/ Fe_xO_y	0.113	0.113	0.057	0.19
	0.075	0.150	0.075	0.28
	0.075	0.225	0.112	0.28
	PPR13 (mmol)	**$FeCl_3.6H_2O$ (mmol)**	**$FeCl_2.4H_2O$ (mmol)**	**NH_4OH (mL)**
$PEGMA_{97}$-*b*-$AEMA_{35}$/ Fe_xO_y	0.0191	0.191	0.096	0.24
	PPR16 (mmol)	**$FeCl_3.6H_2O$ (mmol)**	**$FeCl_2.4H_2O$ (mmol)**	**NH_4OH (mL)**
$PEGMA_{97}$-*b*-$AEMA_{46}$/ Fe_xO_y	0.236	0.236	0.118	0.074
	PPR23 (mmol)	**$FeCl_3.6H_2O$ (mmol)**	**$FeCl_2.4H_2O$ (mmol)**	**NH_4OH (mL)**
$PEGMA_{57}$-*b*-$AEMA_{29}$/ Fe_xO_y	0.041	0.041	0.021	0.027
	PPR31 (mmol)	**$FeCl_3.6H_2O$ (mmol)**	**$FeCl_2.4H_2O$ (mmol)**	**NH_4OH (mL)**
$PEGMA_{75}$-*b*-$AEMA_{23}$/ Fe_xO_y	0.084	0.084	0.042	0.054
	PPR33 (mmol)	**$FeCl_3.6H_2O$ (mmol)**	**$FeCl_2.4H_2O$ (mmol)**	**NH_4OH (mL)**
$AEMA_{36}$-*b*-$PEGMA_{217}$/ Fe_xO_y	0.099	0.198	0.099	0.12

Table 3.7. *Molar quantities of the $PEGMA_x$-b-$AEMA_y$ diblock copolymers, the iron salts $FeCl_3.6H_2O/FeCl_2.4H_2O$ and the NH_4OH used to prepare polymer-coated magnetic nanoparticles in the presence of NaCl (0.1 M).*

Diblock copolymers-iron oxide	**PPR19 (mmol)**	**$FeCl_3.6H_2O$ (mmol)**	**$FeCl_2.4H_2O$ (mmol)**	**NH_4OH (mL)**
$PEGMA_{70}$-*b*-$AEMA_{16}$/ Fe_xO_y	0.065	0.065	0.033	0.04
	0.131	0.393	0.196	0.24
	0.131	0.524	0.262	0.96
	PPR33 (mmol)	**$FeCl_3.6H_2O$ (mmol)**	**$FeCl_2.4H_2O$ (mmol)**	**NH_4OH (mL)**
$AEMA_{36}$-*b*-$PEGMA_{217}$/ Fe_xO_y	0.099	0.395	0.198	0.25

Petri Papagiannopoulou

3.4.2. Synthesis of single-wall carbon nanotubes decorated with iron oxide nanoparticles, stabilized in aqueous media in the presence of the PEGMA$_x$-b-AEMA$_y$ diblock copolymers.

The water and ammonium hydroxide solutions were carefully deoxygenated by purging with ultra-high-purity N_2 for at least 30 min. CNT-COOH (0.8 mg) was placed in a round-bottom flask (25 mL) and dissolved in degassed water (5 mL). This was followed by ultrasonication for ~ 1h to assist dissolution. Subsequently, the dark grey colored solution was filtered twice to remove any undissolved impurities. 2.5 mL of degassed water were then added into the SWCNTs solution, followed by the addition of an aqueous solution (6 mL) of the diblock copolymer PEGMA$_{132}$-*b*-AEMA$_{42}$ (102 mg, 0.088 mmol) under inert conditions (N_2). The mixture was then stirred at room temperature for 1h and was then placed for 30 min in an ultrasonic bath. Aqueous solutions of $FeCl_3.6H_2O$ (9.1 mg, 0.034 mmol) and $FeCl_2.4H_2O$ (3.4 mg, 0.017 mmol) which were prepared separately in water (0.5 mL each) were syringed into the solution under an inert nitrogen atmosphere. The resulting solution was left to stir for 1h at room temperature in the sonicator for another hour, before adding the NH_4OH solution. Finally, NH_4OH (25% v/v in H_2O) (20 μL) was added under strong stirring conditions and inert atmosphere. The solution mixture was allowed to stir for 30 min under nitrogen atmosphere at room temperature. Finally, the mixture was dialyzed (dialysis tubing benzoylated with AVG. flat width 32mm) against water to remove any remained side-products or free copolymer.

3.4.3. Synthesis of iron oxide-containing composite co-networks.

The synthetic procedure followed for the fabrication of composite PEGMA-co-AEMA/EGDMA co-networks containing iron oxide particles was similar to that reported in 3.3.7. At first, the monomers HEGMA (2.10 g, 7 mmol), AEMA (1.5 g, 7 mmol) and the iron oxide particles (0.105 g, 0.448 mmol) that were in-house synthesized by chemical co-precipitation of $FeCl_3.6H_2O$ and $FeCl_2.4H_2O$ salts under weak basic conditions were placed in a round-bottom flask. The mixture was then placed in a sonicator for 1 h to ensure a homogeneous dispersion. Subsequently ethyl acetate (12 mL), the cross-linker EGDMA (1.6 mL) (1.68 g, 17.5 mmol) and AIBN (0.023 g, 0.14 mmol) were added in the flask. The reaction was carried out at 65 °C. Gelation was reached after 24 h. The prepared composite co-network (black color) was taken out of the polymerization flask and was left to equilibrate in

Petri Papadimitriou

ethyl acetate (100 mL) for 1 week. Subsequently, the solvent was removed by filtration and evaporated off under reduced pressure. The recovered extractables were dried under vacuum for 3 days at room temperature and their mass was determined gravimetrically. Table 3.8 presents the quantities of the chemical reagents that used to prepare the co-networks (solvent, monomers, cross-linker, initiator, Fe_xO_y magnetic particles) and the corresponding sol fraction percentages.(Series C).

3.4.4. Synthesis of OA.Fe_3O_4-containing nanocomposite co-networks.

Oleic acid-coated magnetite nanoparticles

The oleic acid-coated magnetite nanoparticles (OA.Fe_3O_4) were prepared at the Center for Fundamental and Advanced Technical Research, Romanian Academy, Timisoara branch, Romania by following an experimental procedure developed by Bica *et al.*[205] Briefly, magnetite nanoparticles, Fe_3O_4, were obtained by the co-precipitation in aqueous solution of Fe^{2+} and Fe^{3+} ions (salts $FeSO_4.7H_2O$; $FeCl_3.4H_2O$) in the presence of NH_4OH, at 80–82 ^oC. The temperature of 80^oC set for the co-precipitation reaction is essential to obtain magnetite and not other iron oxides; the same temperature range is also favourable for the chemisorption of oleic acid on the surface of magnetite nanoparticles. Additionally, the significant excess amount of NH_4OH ensures the formation of magnetite over other iron oxides. Subsequently, oleic acid was added in a significant excess (about 30 vol %) to the system right after the co-precipitation had started, which resulted in the chemisorption of the acid on the magnetite surface. This was followed by a washing process with distilled water with magnetic decantation and filtration to remove aggregated (non-dispersed) particles. Then, flocculation (acetone) was used to extract magnetite particles coated with a single surfactant layer from the solution of residual salts and free surfactant. The dried powder was redispersed in light hydrocarbon. This flocculation/re-dispersion procedure was performed several times to ensure that the presence of free surfactant in the final solution was negligible.

Petri Papaphilippou

A typical procedure followed for the preparation of OA.Fe_3O_4-containing nanocomposite co-networks in ethyl acetate (EA) is described as follows: At first, the monomers HEGMA (2.10 g, 7 mmol), AEMA (1.5 g, 7 mmol) and the OA.Fe_3O_4 (0.105 g) were placed into a 50 mL round-bottom flask. Subsequently, sonication was applied for 1 h to assist homogeneous mixing. EA (12 mL), EGDMA (1.68 g, 17.5 mmol) and AIBN (0.023 g, 0.14 mmol) were then transferred into the reaction flask with the aid of a syringe. The reaction mixture (dispersion) was placed in an oil bath at 65 °C. Gelation was reached within 24 h. The prepared composite co-network was taken out of the polymerization flask and was left to equilibrate in ethyl acetate (100 mL) for 1 week to remove the sol fraction (extractables). Subsequently, the solvent was recovered by filtration and evaporated off under reduced pressure. The recovered extractables were dried under vacuum at room temperature for 24 h and their mass was determined gravimetrically.

The above-mentioned procedure was also followed for the synthesis of OA.Fe_3O_4-containing nanocomposite co-networks in THF with the only difference that in this solvent dissolution of the OA.Fe_3O_4 was accomplished at a molecular level. Hence polymerization in THF was carried out in solution and not in dispersion. Furthermore, the gelation process was slower in THF – gelation was reached within 48 h. In Table 3.8 the quantities of the chemical reagents used to prepare the co-networks (solvent, monomers, cross-linker, initiator, OA.Fe_3O_4 magnetic nanoparticles) are summarized, together with the corresponding sol fraction percentages.

3.4.5 Determination of the Degree of Swelling.

The washed co-networks were cut into small pieces and their EA (series A and C) or THF (series B)-swollen mass was determined gravimetrically before placing all samples in a vacuum oven for drying for 24 h at room temperature. The dry co-network mass was then determined, followed by the transfer of the co-networks in neutral water. The samples were left to equilibrate in aqueous solutions for 2 weeks and the water swollen co-network masses were measured. It is noteworthy to mention that leakage of the magnetic content from the water-swollen co-network was not observed for long time periods (longer than 3 months). The DSs were calculated as the ratio of the swollen co-network mass divided by the dry co-network mass.

Petri Papaphilippou

Table 3.8. *Molar quantities of the monomers HEGMA and AEMA, the initiator AIBN, the cross-linker EGDMA, OA. Fe_3O_4 and $FexO_y$ that were used for the preparation of magneto-responsive co-networks.*

		Solvent/ 14 mL	PEGMA (mmol)	AEMA (mmol)	EGDMA (mmol)	AIBN (mmol)	OA.Fe_3O_4 (gr)	Sol fraction (%)	% OA.Fe_xO_y
					Series A				
No OA.Fe_3O_4	Gel 1	EA	7.00	7.00	8.50	0.14	-	1.56	-
With OA.Fe_3O_4	Gel 1a	EA	7.00	7.00	8.50	0.14	0.424	3.23	7.0
	Gel 1b	EA	7.00	7.00	8.50	0.14	0.639	4.14	11.0
	Gel 1c	EA	7.00	7.00	8.50	0.14	1.591	5.57	23.0
					Series B				
No OA.Fe_3O_4	Gel 2	THF	7.00	7.00	8.50	0.14	-	8.79	-
With OA.Fe_3O_4	Gel 2a	THF	7.00	7.00	8.50	0.14	0.424	11.06	7.0
	Gel 2b	THF	7.00	7.00	8.50	0.14	0.639	15.87	11.0
	Gel 2c	THF	7.00	7.00	8.50	0.14	1.591	18.19	23.0
					Series C				
							Fe_xO_y (gr)		**% Fe_xO_y**
No Fe_xO_y	Gel 1	EA	7.00	7.00	8.50	0.14	-	1.56	-
with Fe_xO_y	Gel 3a	EA	7.00	7.00	8.50	0.14	0.212	16.6	4.0
	Gel 3b	EA	7.00	7.00	8.50	0.14	0.424	35.8	7.0
	Gel 3c	EA	7.00	7.00	8.50	0.14	0.639	22.3	11.0
	Gel 3d	EA	7.00	7.00	8.50	0.14	1.591	n.a	23.0
	Gel 3e	EA	7.00	7.00	8.50	0.14	0.106	n.a	2.0

Petri Papaphilippou

3.4.6. Deswelling Measurements.

The deswelling kinetics of Gel 1c (nanocomposite co-network containing 23% wt. OA.Fe_3O_4) was measured gravimetrically at ~ 60 ^oC. After allowing the sample to equilibrate for 2 weeks in distilled water at 25 ^oC, the swollen gel was transferred into water at 60 ^oC and its weight was recorded at different time intervals. The water content at each time interval was determined as W_t/W_o, where W_t corresponds to the weight of the co-network at a designated time during deswelling and W_o to the weight of the co-network measured initially at 25 ^oC.

3.5. Synthesis of Polymeric Drug Delivery Carriers.

3.5.1. Preparation of DOX-loaded HEGMA$_x$-b-DEAEMA$_y$ micelles.

The anti-cancer drug doxorubicin (DOX) was loaded into the PEGMA$_x$-*b*-DEAEMA$_y$ diblock copolymer micelles using the oil/water emulsion method.[203] DOX.HCl (1 mg, 0.00172 mmol) was dissolved in 0.20 mL chloroform in the presence of 3 mol. equiv of triethylamine and placed in the ultrasonic bath. This solution was added dropwise to a stirred solution containing PEGMA$_{128}$-*b*-DEAEMA$_{34}$ (3.4 mg, 0.0000756 mmol) in 7 mL of DPBS. The resulting emulsion was stirred overnight in dark at room temperature allowing the chloroform to evaporate. Insoluble free DOX was removed by centrifugation at 2000 g for 10 min. Soluble free DOX was removed from the micelles by ultrafiltration in DPBS (3 mL) using a dialysis tube Slid-A-Lyzer with a molecular cutoff of 10 000 g/mol. This process was carried out for 3 days and the DPBS solution was repeatably changed. DOX loading was quantified by measuring the UV-*vis* spectrum of the micellar solution, at 490 nm (characteristic absorption wavelength of DOX). The concentration of the DOX loaded into the polymer micelles was determined from the absorption *vs* concentration calibration curve constructed by measuring the absorbance of DOX.HCl solutions of known concentrations (0.143, 0114, 0.086, 0.057, 0.029 $g.L^{-1}$) prepared in DPBS.

3.5.2. Determination of DOX Release Kinetics at different pHs.

The solution of DOX-loaded micelles prepared as described in 3.5.1 was placed in a dialysis cassette (Slid-A-Lyzer with a molecular cutoff of 10 000 g/mol). Kinetic drug release

Petri Papaphilippou

measurements were carried out upon immersing the cassette containing the drug-loaded micellar solution into an acetate buffer solution (pH = 4.6) or a citric acid buffer solution (pH = 6.0). The solution was removed periodically from the dialysis cassette and after measuring its absorbance at ~ 490-500 nm, it was returned back.

3.6. Biological assays.

Cell viability assays and assessment of *in vitro* biocompatibility of the PEGMA$_x$-*b*-AEMA$_y$ stabilized magnetic nanoparticles.

The capability of the magneto-responsive hybrid micelles consisting of iron oxide nanoparticles and PEGMA$_{292}$-*b*-AEMA$_{36}$ diblock copolymers to maintain cell viability in cultures was investigated in PC-3 cells. Cells were seeded in flat-bottom 96-well plates (5 X 103/200 μL/well) and allowed to adhere to the plate over 18 h. The cells were then exposed to either the indicated concentrations of hybrid micelles M1 and M2, corresponding to the [AEMA]/[Fe^{3+}] molar ratio of 1:1 and 1:2, respectively, or Resovist (Schering AG) for 72 h. Following 72 h of incubation, cell viability was determined by the MTT [3-(4,5-dimethylthiazol-2-yl)- 2,5-diphenyltetrazolium bromide] assay. This assay is based on the ability of active dehydrogenases in viable cells to reduce MTT from a yellow water-soluble dye to a dark blue insoluble formazan derivative. 50 MTT was dissolved in phosphate-buffered saline (PBS) at a concentration of 5 mg/mL and added to the wells at the final concentration of 0.50 mg/mL. After 1 h, the medium was removed and the formazan crystals were dissolved in 150 μL DMSO. Optical density was assessed using a microplate reader at 570 nm. The experiment was repeated twice with triplicate wells and results were given as means for triplicate measurements (SD). Comparison of the effect of the different micelles on absorbance at the appropriate wavelength was made by analysis of variance (ANOVA). Posthoc comparisons were made with paired student's *t*-test for 95% confidence.

***In vitro* uptake of hybrid micelles by macrophages.**

To assess the potential of magneto-responsive micelles to evade nonspecific macrophage uptake, RAW264.7 murine macrophages were incubated with the micelles followed by Prussian Blue staining, a specific stain for Fe. The uptake of the M1 and M2 hybrid micelles

Petri Papaphilippou

was compared to that of Resovist. Briefly, RAW264.7 cells were grown on sterile glass coverslips placed in six-well plates for 2 days to reach a confluency of 70%. They were then incubated with either the hybrid micelles or Resovist at a concentration equivalent of 0.15 mg Fe/mL, in complete DMEM. Incubation was performed for 2 h in a humidified incubator at 37 ^{o}C and 5% CO_2. Control samples consisted of macrophages incubated in the absence of any agent (double-distilled H_2O). Subsequently, the cells were washed three times with PBS and fixed by incubation with 4% formaldehyde in PBS at room temperature for 15 min. Following three washes with PBS, the cells were stained with Prussian Blue Stain (2:1 mixture of 2% potassium ferrocyanide(II) trihydrate and 2% HCl) for 30 min in a humidified incubator at 37 ^{o}C and 5% CO_2. The coverslips were washed thoroughly with PBS and loaded onto microscope slides to assess.

Cell viability assays and assessment of *in vitro* antiproliferative and pro-apoptotic efficacy of DOX loaded PEGMA$_x$-*b*-DEAEMA$_y$ micelles.

The capability of the DOX-loaded PEGMA$_x$-*b*-DEAEMA$_y$ micelle to maintain cell viability in cultures was investigated in human breast cancer cells (MDAMB231). Cells were seeded in flat-bottom 96-well plates (5 X 103/200 μL/well) and allowed to adhere to the plate over 18 h. The cells were then exposed to the PEGMA$_x$-*b*-DEAEMA$_y$/DOX micelles in various concentrations (0.001-0.1 g/L) corresponding to the block copolymer molar mass, against the unloaded PEGMA-*b*-DEAEMA, the DPBS and the "free" DOX. Following 72 h of incubation, cell viability was determined by the MTT [3-(4,5-dimethylthiazol-2-yl)- 2,5-diphenyltetrazolium bromide] assay. 50 MTT was dissolved in phosphate-buffered saline (PBS) at a concentration of 5 mg/mL and added to the wells at the final concentration of 0.50 mg/mL. After 1 h, the medium was removed and the formazan crystals were dissolved in 150 μL DMSO. Optical density was assessed using a microplate reader at 570 nm. The experiment was repeated twice with triplicate wells and results are given as means for triplicate measurements (SD). Comparison of the effect of the different micelles on absorbance at the appropriate wavelength was made by analysis of variance (ANOVA). Posthoc comparisons were made with paired student's *t*-test for 95% confidence.

Petri Papaphilippou

[201] (a) D. Bica, *Rom.Rep.Phys*., 47, **1995**, 265. (b) L. Vekas, D. Bica, M.V. Avdeev, *China Particuology*, 5, **2007**, 43. (c) L. Vékás, M.V. Avdeev, Doina Bica, *Magnetic Nanofluids: Synthesis and Structure, Chapter 25 in: NanoScience in Biomedicine* (Ed. Donglu Shi) Springer, **2009**, (USA) 645.

[202] T. P. T. Le, G. Moad, E. Rizzardo, S. H. Thang, *PCT. Int. Appl. WO* 9801478 Al 980115.

[203] E. R. Gillies, J. M. Frechet, *Bioconjugate. Chem.,* 16, **2005**, 361.

Petri Papaphilippou

4. Results and Discussion.

4.1. Magneto-responsive polymeric materials.

4.1.1. Magneto-responsive polymer-based micelles.

4.1.1.1. Synthesis and molecular characterization of the PEGMA$_x$-b-AEMA$_y$.

The amphiphilic PEGMA$_x$-*b*-AEMA$_y$ diblock copolymers were obtained *via* RAFT polymerization.[204] The synthetic procedure followed for the preparation of the diblock copolymers is schematically presented in Fig. 4.1. The PEGMA$_x$-*b*-AEMA$_y$ diblock copolymer is a novel type of polymer having on the one hand, a block segment consisting of β-ketoester functionalities (AEMA) capable of binding onto inorganic surfaces and on the other hand, a second block constituted of PEG side chains, providing a hydrophilic and thermoresponsive character to the block copolymer. The PEGMA$_x$-*b*-AEMA$_y$ block copolymers were synthesized by RAFT in a two-step procedure. Primarily, PEGMA$_x$ homopolymers were prepared in benzene and subsequently used as the macro-CTAs for the polymerization of AEMA in ethyl acetate, to prepare well-defined PEGMA$_x$-*b*-AEMA$_y$ diblock copolymers. CDTB was used as the CTA and AIBN served as the radical source as illustrated in the figure below.

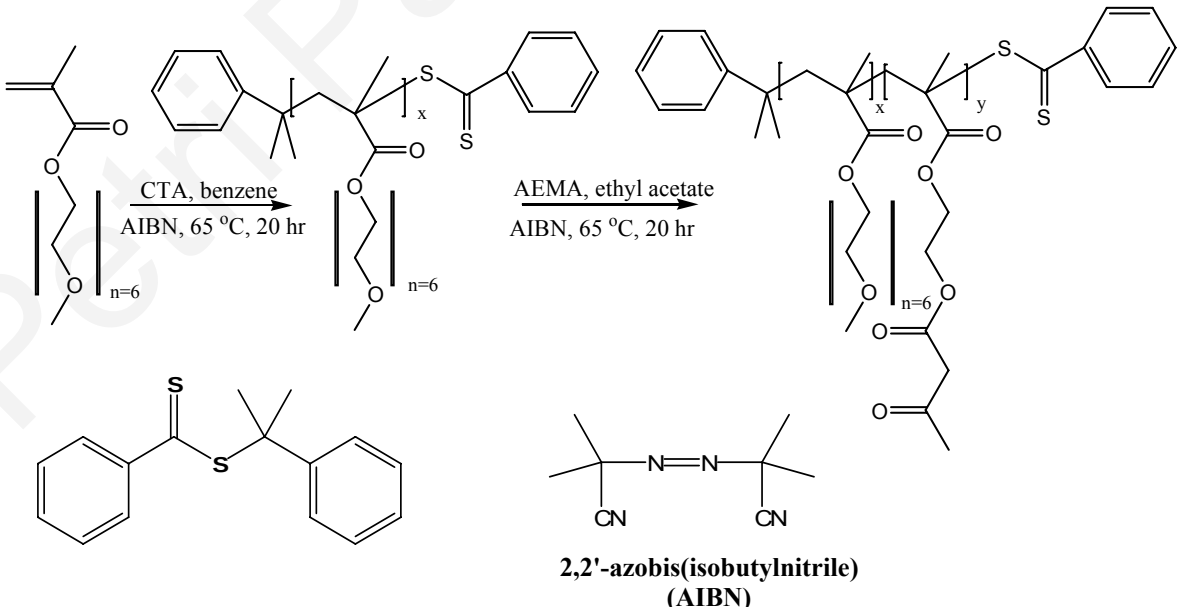

Figure 4.1. *Synthetic scheme followed for the preparation of the PEGMA$_x$-b-AEMA$_y$ diblock copolymers by RAFT.*

PetriPapadopoulou

The polymerization of AEMA was carried out in ethyl acetate due to the insolubility of the $AEMA_y$ homopolymer in benzene.[205] The first attempts to synthesize well-defined PEGMA homopolymers by the RAFT were not successful, leading to either cross-linked polymeric materials or linear chains characterized by broad molecular weight distributions. Optimization of the polymerization experimental conditions (monomer purification process, monomer concentration) led to well-defined $PEGMA_x$-b-$AEMA_y$ diblock copolymers.

Table 4.1 shows the experimental chemical structures, the molecular weights (MW), polydispersity indices (PDI) and polymerization yields for the $PEGMA_x$ and $AEMA_x$ homopolymers and the corresponding $PEGMA_x$-*b*-$AEMA_y$ diblock copolymers prepared in this study.

According to the data presented in Table 4.1, the homopolymers and diblock copolymers show low PDIs (between 1.17-1.32). By comparing the experimental M_n determined by SEC with the theoretical values (by taking into account the polymerization yields), it can be observed that the former are systematically lower. This is probably due to differences in the hydrodynamic volume of the PEGMA and AEMA units compared with that of PMMA calibration standards used in SEC. The same observation (i.e., lower experimental MWs compared to the theoretical values) has been reported by Lutz and co-workers for a block copolymer system containing oligo(ethylene glycol) methacrylate and *tert*-butyl methacrylate functionalities.[206]

Petri Papaphilippou

Table 4.1. *Characteristics of the Polymers based on PEGMA and AEMA obtained by RAFT (Polymerization Yields, Molecular Weights and polydispersities).*

Homopolymers[a]	Sample Code	Theor[b] MW (g / mol)	SEC[c] Mn	PDI	Conversion %
PolyPEGMA$_{97}$	PPR10	41200	29100	1.18	69
PolyPEGMA$_{70}$	PPR17	21300	21300	1.25	71
PolyPEGMA$_{128}$	PPR18	56700	38700	1.25	63
PolyPEGMA$_{29}$	PPR26	5520	8700	1.24	46
PolyPEGMA$_{121}$	PPR37	62400	36300	1.21	59
PolyPEGMA$_{132}$	PPR30	25200	22700	1.22	56
PolyAEMA$_{36}$	PPR11	3855	8000	1.24	90
PolyAEMA$_{38}$	PPR40	7000	8100	1.26	81
Diblock Copolymers[a]					
PEGMA$_{97}$-*b*-AEMA$_{18}$	PPR12	31200	36500	1.26	41
PEGMA$_{97}$-*b*-AEMA$_{35}$	PPR13	35700	38500	1.27	69
PEGMA$_{97}$-*b*-AEMA$_{46}$	PPR16	41600	40600	1.37	97
PEGMA$_{70}$-*b*-AEMA$_{16}$	PPR19	21800	28400	1.27	13
AEMA$_{36}$-*b*- PEGMA$_{292}$	PPR14	77900	49500	1.24	74
PEGMA$_{128}$-b-AEMA$_{19}$	PPR20	n.d	52300	1.30	n.d
PEGMA$_{70}$-*b*-AEMA$_{56}$	PPR21	28400	36300	1.31	48
PEGMA$_{57}$-*b*-AEMA$_{21}$	PPR23	19600	31100	1.25	23
PEGMA$_{29}$-*b*-AEMA$_{16}$	PPR27	9500	12900	1.25	23
AEMA$_{36}$-b-PEGMA$_{217}$	PPR33	54300	35100	1.28	49
PEGMA$_{132}$-*b*-AEMA$_{42}$	PPR31	n.d	13300	1.48	n.d
PEGMA$_{121}$-*b*-AEMA$_{44}$	PPR38	37600	42000	1.31	15
AEMA$_{38}$-b-PEGMA$_{316}$	PPR42	85600	58900	1.42	82

[a] Determined by SEC and ^{1}H NMR. [b] [(g monomer)/(mol RAFT agent)] × (polymerization yield) + MW of CTA (for homopolymers) and [(g monomer)/(mol CTA agent)] × (polymerization yield) + *M*n of macro-CTA (for diblock copolymers), [c] SEC calibrated with PMMA standards; *M*n: number average molecular weight; PDI: polydispersity index; PEGMA: poly(ethylene glycol) methyl ether methacrylate, AEMA: 2-(acetoacetoxy) ethyl methacrylate, n.d.: not determined.

The SEC chromatograms of the PEGMA$_{97}$ homopolymer and the corresponding PEGMA$_{97}$-*b*-AEMA$_{35}$ diblock copolymer are exemplarily illustrated in Fig. 4.2. The molecular weight distribution (MWD) of the PEGMA$_{97}$-*b*-AEMA$_{35}$ diblock copolymer is shifted toward higher MWs compared to that of the PEGMA$_{97}$ homopolymer, demonstrating the block efficiency from homopolymer to block copolymer. However, the high MW shoulder presented in the

Petri Papaphilippou

chromatogram of the diblock copolymer indicates partial recombination of the polymer chains.

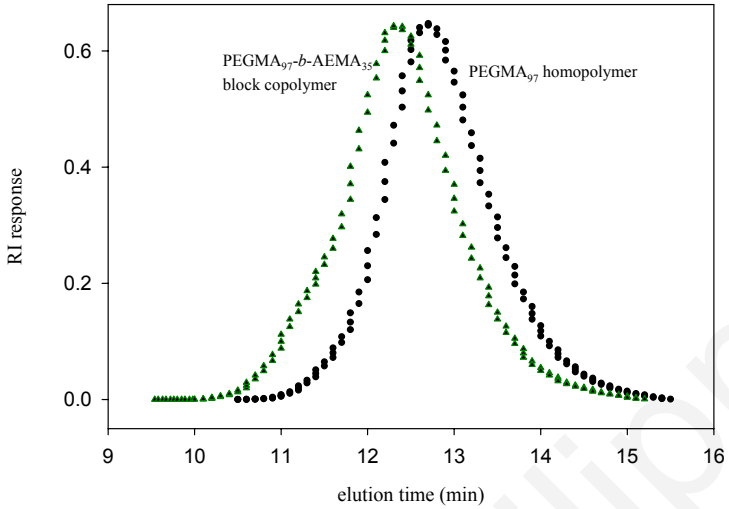

Figure 4.2. *SEC traces of the PEGMA$_{97}$ homopolymer and the corresponding PEGMA$_{97}$-b-AEMA$_{35}$ diblock copolymer.*

The chemical structure of the block copolymers was confirmed by ^{1}H NMR spectroscopy. Fig. 4.3 shows the ^{1}H NMR spectrum of the PEGMA$_{97}$-*b*-AEMA$_{35}$ block copolymer. The peak assignments are shown in the spectrum. The molar ratios of the two blocks were calculated by using the relative intensities between the -CH$_3$ signal corresponding to the AEMA (h) and the PEGMA (d) units, appearing at 2.27 and 3.39 ppm, respectively.

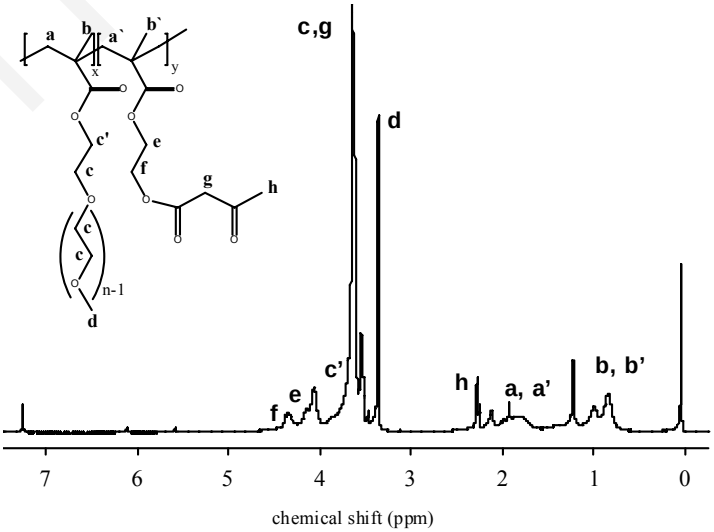

Figure 4.3. *^{1}H NMR spectrum of the PEGMA$_{97}$-b-AEMA$_{35}$ diblock copolymer recorded in CDCl$_3$.*

Thermal Properties.

The glass transition temperatures (Tgs) of the $PEGMA_x$ homopolymers and the $PEGMA_x$-*b*-$AEMA_y$ block copolymers were determined by Differential Scanning Calorimetry (DSC). The Tg of the $PEGMA_{97}$ homopolymer was determined to be – 62 ^oC, which is close to those reported in literature.[207, 208, 209, 210, 211] The Tg of an AEMA homopolymer was determined to be around 1 ^oC which is in close approximation with previously reported values.[205] Block copolymers such as the $PEGMA_{97}$-*b*-$AEMA_{46}$ exhibited two Tgs at ~ –54.5 ^oC and ~ –1.5 ^oC, corresponding to the $PEGMA_x$ block and for the $AEMA_y$ blocks, respectively. These results suggested that the $PEGMA_x$-*b*-$AEMA_y$ diblock copolymers exhibit microphase separation in the bulk. No further investigation was carried out in order to obtain information on whether the two blocks are totally incompatible, therefore totally immiscible.

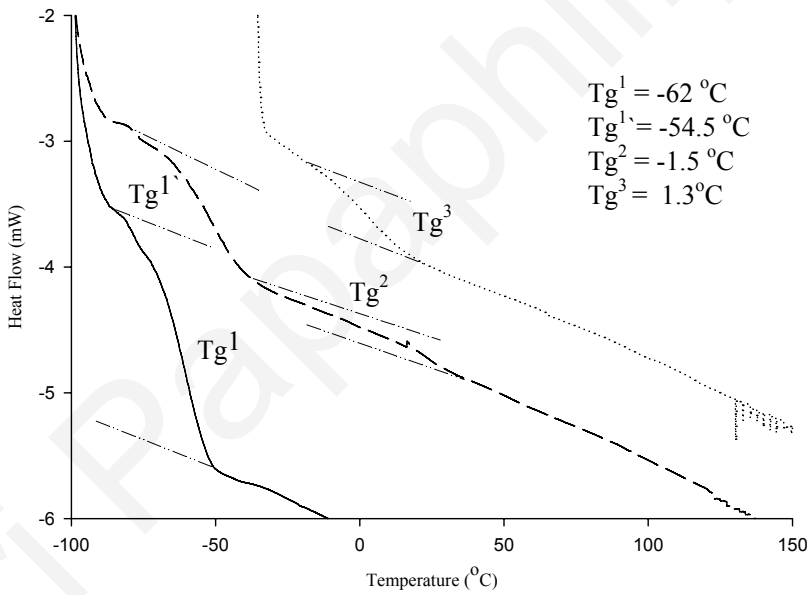

Figure 4.4. *DSC thermograms of the $PEGMA_{97}$ homopolymer (solid line), the $PEGMA_{97}$-b-$AEMA_{46}$ diblock copolymer (dashed line) and that of an AEMA homopolymer (dotted line).*

Thermoresponsive behaviour of the $PEGMA_x$-b-$AEMA_y$ diblock copolymers.

Polymers having an oligo(ethylene glycol) segment in their chain show a LCST (Lower Critical Solution Temperature) in aqueous media.[212, 213, 214] The phase transition of the $AEMA_{36}$-*b*-$PEGMA_{292}$ diblock copolymer in water upon increasing temperature was

measured by turbidimetry. The plot of transmittance as a function of temperature is shown in Fig. 4.5.

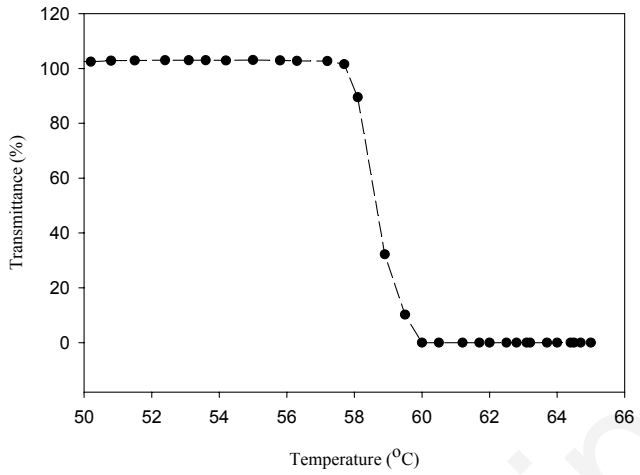

Figure 4.5. *Plot of transmittance as a function of temperature measured for an aqueous solution of $AEMA_{36}$-b-$PEGMA_{292}$ diblock copolymer (concentration 4 g L^{-1}).*

According to the above transmittance *vs* temperature plot, at ~ 60 °C a phase transition occurs, i.e. the hydrophilic PEG side-chains become hydrophobic. This result is in the range of previously reported findings.[210, 215] *Lutz and Hoth* first reported that by randomly copolymerizing PEG_xMAs with different PEG side-chain lengths, it is possible to adjust the (LCST) and hence the thermoresponsive behaviour of these materials.[213] Future experiments may involve the incorporation of an oligo (ethylene glycol) methyl ether methacrylate possessing a lower number of PEG side chains within the poly(PEG_6MA) hydrophilic block segment, aiming to decrease the LCST down to 42-45 °C. Polymers presenting a thermoresponsive character within this temperature range may be potentially used in hyperthermia treatment or as remote-triggered drug delivery systems when combined with magnetic nanoparticles.[216]

Self-assembly behavior of the $PEGMA_x$-b-$AEMA_y$ diblock copolymers in aqueous media.

Due to their amphiphilic nature, the $PEGMA_x$-*b*-$AEMA_y$ diblock copolymers were expected to generate organized morphologies in the nanoscale upon self-organization. More precisely, the presence of the hydrophilic PEGMA block and the water-insoluble AEMA block, resulted to the formation of micellar nanomorphologies in aqueous solutions. The hydrodynamic diameters (D_H) of these macromolecular aggregates were determined by Dynamic Light

Petri Papaphilippou

Scattering (DLS). Table 4.2 summarizes the experimental and theoretical (contour length) D_Hs values for the PEGMA$_x$-*b*-AEMA$_y$ block copolymer micelles formed in water. As seen in the table, the experimental values (ranging between 11-70 nm) were systematically lower compared to the theoretical ones, calculated assuming a spherical morphology for the micelles and fully extended chains (0.252 nm per monomer repeating unit), as expected. The experimental data presented in Table 4.2 suggest that, by varying the block lengths of the two segments within the block copolymer, it is possible to obtain PEGMA$_x$-*b*-AEMA$_y$ micelles of tunable diameters. This is very important in cases where such materials are considered to be used in biomedical applications in combination with SPIONs (Superparamagnetic Iron Oxide Nanoparticles), since the latter characterized by an average diameter below 30 nm exhibit typically a longer half-life time in blood than larger nanoparticles. [205, 206] Furthermore, the sizes of intravenously applied SPIONs range between 20 -150 nm (including coating).[217, 218]

Table 4.2. *Hydrodynamic diameters obtained by DLS for a series of PEGMA$_x$-b-AEMA$_y$ block copolymer micelles formed in water.*

Sample code	DP PEGMA[a]	DP AEMA[b]	D_H exper. (nm)	D_H theor. (nm)
PPR12	97	18	24	58
PPR13	97	35	41	66
PPR14	292	36	70	165
PPR16	97	46	45	72
PPR19	70	16	11	43

[a,b]determined by SEC and ^{1}H NMR, PEGMA = poly(ethylene glycol) ethyl ether methacrylate, AEMA 2-(acetoacetoxy) ethyl methacrylate

Numerous reports appear in the literature where NMR spectroscopy was used to study micellization phenomena in cationic, anionic and amphiphilic systems. For example, *Heald and co-workers*have combined liquid-state ^{1}H NMR together with solid-state ^{13}C NMR to obtain information on the structure of nanoparticles formed by a series of *poly*(lactic acid)-*b*-*poly*(ethylene oxide) block copolymers.[219] Furthermore, *Pan et al.* have reported among others, the synthesis of *poly*(styrene)-*b*-*poly*(p-nitrophenyl methacrylate) (PS-*b*-PNPM) and studied their micellization behavior in selective solvents using NMR.[220] They showed that micelles consisting of a PS corona and a PNPM core were formed in chloroform, whereas in DMSO "reverse" micellar structures were observed.

Petri Papaphilippou

^{1}H NMR spectroscopy was one of the techniques used in the present work, to study the micellization of the PEGMA$_x$-*b*-AEMA$_y$ diblock copolymers in water. As seen in the ^{1}H NMR spectrum of the PEGMA$_{97}$-b-AEMA$_{18}$ diblock copolymer recorded in D_2O (Fig. 4.6), the proton signals of the AEMA$_y$ block almost disappear. This indicates the formation of micelles, with the PEGMA$_x$ chains being located on the outside and the AEMA$_y$ on the inside of the micellar aggregates.

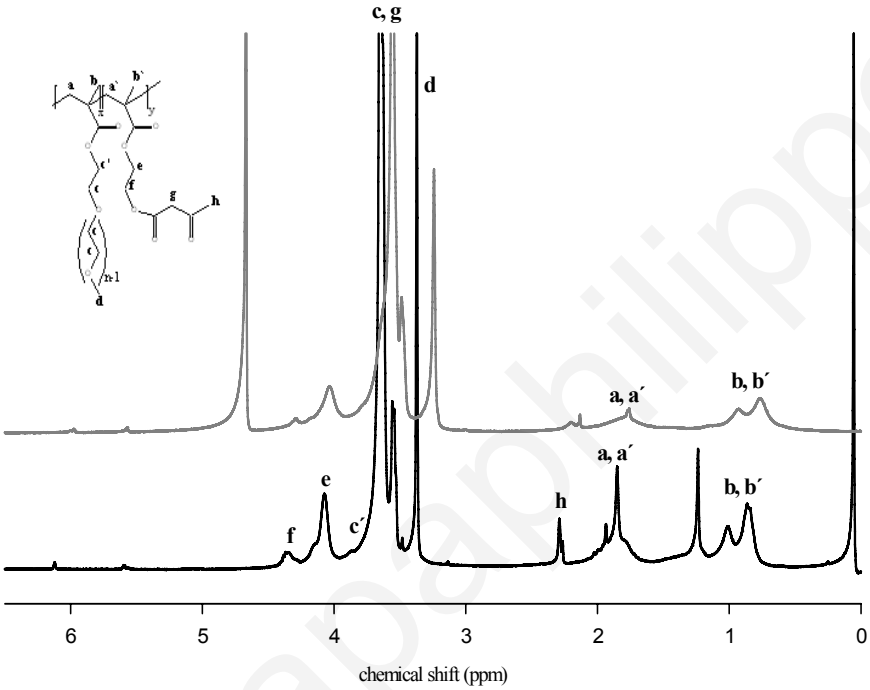

Figure 4.6. *^{1}H NMR spectrum of the PEGMA$_{97}$-b-AEMA$_{18}$ diblock copolymer recorded in $CDCl_3$ (black) and in D_2O (grey).*

4.1.1.2. Preparation and characterization of stabilized, PEGMA$_x$-b-AEMA$_y$ - coated magnetic nanoparticles in aqueous media.

As previously mentioned, magnetic nanoparticles such as the magnetite (Fe_3O_4) or maghemite (Fe_2O_3) require the presence of polymers or other surfactants in order to avoid agglomeration and therefore precipitation in aqueous media. Iron oxide nanoparticles have been synthesized *via* the widely used chemical co-precipitation method, [221] in the presence of the PEGMA$_x$-b-AEMA$_y$ diblock copolymers leading to the formation of magneto-responsive hybrid micelles.

Petri Papaphilippou

The co-precipitation method is one of the most widely used chemical methods enabling the preparation of magnetic nanoparticles. A mixture of aqueous solutions of Fe^{2+} and Fe^{3+} (in a 1:2 molar ratio) was left to react with a base (in this work NH_4OH) as shown in the following chemical reaction:[222, 223]

$$\mathbf{Fe^{2+}(aq) + Fe^{3+}(aq) + 8OH^- \rightarrow Fe_3O_4(s) + 4H_2O \quad (4.1)}$$

This synthetic methodology for preparing magnetite nanoparticles occurs under inert gas atmosphere (N_2) in order to protect the magnetite nanoparticles from being oxidized further into maghemite. Furthermore, the size of the particles produced under these conditions is smaller compared to those prepared in the presence of oxygen. [223]

According to *Tourinho et al.*, the use of ammonium hydroxide (NH_4OH) instead of sodium hydroxide favours the reduction in particle size.[224] Another parameter that significantly affects the size of the magnetic nanoparticles produced during the chemical co-precipitation process is temperature. Vekas and co-workers have demonstrated that upon performing the chemical co-precipitation reaction at higher temperatures (~ 80 ^oC), the formation of Fe_3O_4 over Fe_2O_3 was favoured.[71, 225]

By simply mixing the ferric hexahydrate and ferrous tetrahydrate chloride salts with a $PEGMA_x$-b-$AEMA_y$ micellar solution in water, at room temperature and under an inert atmosphere followed by the addition of NH_4OH, the solution turned from white transparent into dark brown, indicating the formation of magnetic nanoparticles.

Although AEMA has been incorporated in polymers capable of binding onto inorganic matter,[226, 227, 228, 229] to the best of our knowledge there are only two examples where the AEMA units are used to stabilize magnetic nanoparticles in water leading to the formation of hybrid microgels.[230] Hence, for the first time well-defined diblock copolymers possessing *β*-ketoester functionalities have been employed to prepare hybrid micelles used as nanocontainers for the encapsulation and stabilization of magnetic nanoparticles in aqueous media.[204]

Petri Papaphilippou

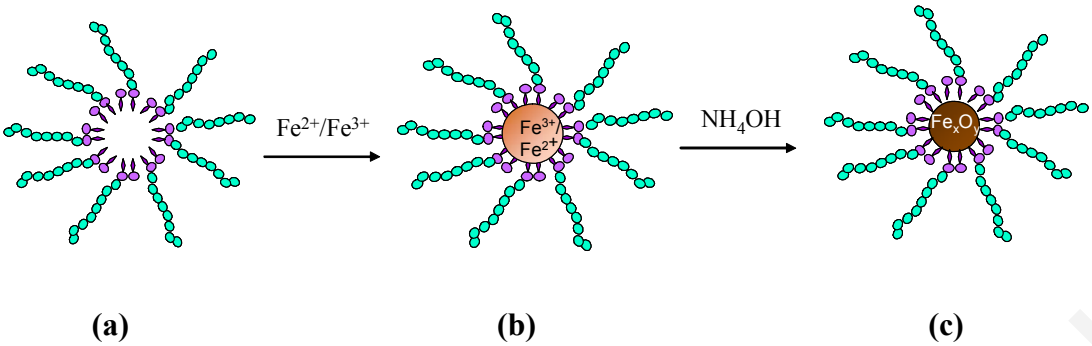

Figure 4.7. *Preparation steps towards the generation of polymer-coated magnetic iron oxide nanoparticles stabilized in aqueous media: (a) micelle formation of PEGMA$_x$-b-AEMA$_y$ diblock copolymers in water (b) addition of the Fe^{3+}/Fe^{2+} mixture in the micellar solution. Complexation of the iron salts with the β-ketoester ligating units found inside the micellar core. (c) Transformation of the iron salt "precursors" into iron oxide nanoparticles inside the micellar core upon addition of ammonium hydroxide aqueous solution.*

The ratio of 1:1 of AEMA/$FeCl_3 \cdot 6H_2O$ (and 1:0.5 of AEMA/ $FeCl_2.4H_2O$ respectively) was selected initially as a starting point, aiming to detect the critical concentration of the precursor salts, above which the system was not stable and precipitated upon transformation of the salts into iron oxide nanoparticles.

Noteworthy, highly stable hybrid micelles were obtained, even when the concentration of the precursor salts was doubled or tripled. However, the maximum quantity of the salts that can be encapsulated in the core of the polymeric micelles without leading to coagulation and precipitation phenomena upon transformation into iron oxide was not determined.

The polymer-coated iron oxide nanoparticles were also prepared in an aqueous solution of 0.1 M NaCl. A stable hybrid micellar solution was obtained even at high molar ratio of AEMA/$FeCl_3 \cdot 6H_2O$ (1:4). Even though this was a first indication of the effectiveness of the diblock copolymers to stabilize magnetic nanoparticles under physiological conditions, systematic coagulation kinetics measurements were carried out in the research group of Prof. E. Tombacz, University of Szeged, Hungary, demonstrating the salt tolerance of these systems. In Fig. 4.8 the average particle size of the PEGMA$_x$-*b*-AEMA$_y$/Fe_xO_y micellar systems determined by DLS against the time is plotted. As it is showed the size of these micellar systems (5 mg/L and 50mg/L according to Fe_xO_y nanoparticles) remained constant

with low PDI indices by increasing the amount of the NaCl salt. No coagulation observed even at very high salt concentrations.

(a)

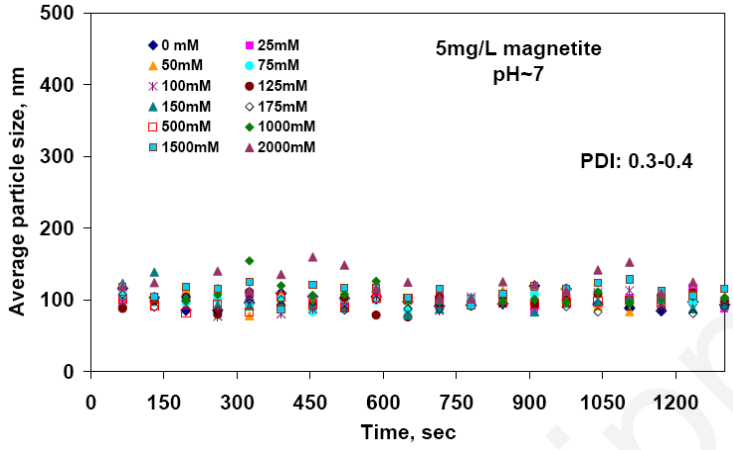

(b)

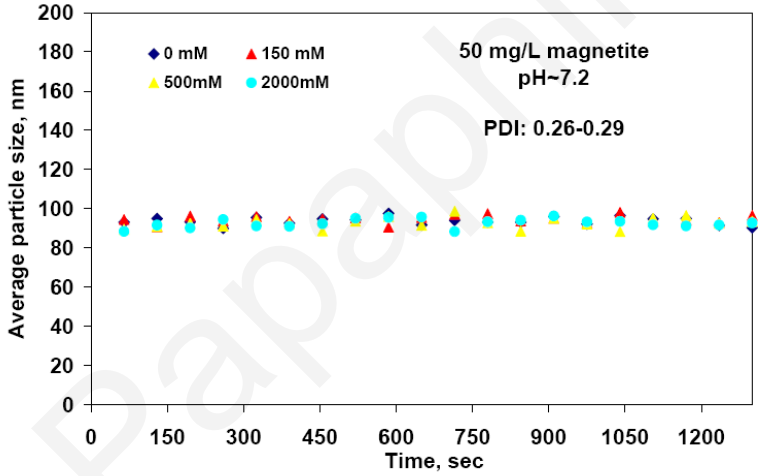

Figure 4.8. *Coagulation kinetics measurements by DLS performed on the PEGMA$_x$-b-AEMA$_y$/Fe$_x$O$_y$ micellar systems (at concentrations of (a) 5 mg/L and (b) 50 mg/L magnetite) in the presence of various NaCl concentrations, demonstrating the salt tolerance of these systems.*

The iron oxide-containing micelles were visualized by Atomic Force Microscopy (AFM). In Fig. 4.9, AFM micrographs of spherical block copolymer micelles loaded with iron oxide nanoparticles in water are presented. The presence of collapsed spherical micelles loaded with iron oxide nanoparticles of ~ 8 nm in diameter is more evident in the phase image. Any aggregates observed might be attributed to the low *Tg* of the poly (ethylene oxide) side chain

Petri Papaphilippou

distributed all along the hydrophilic segment, which might allow the partial interpenetration of the corona.[231]

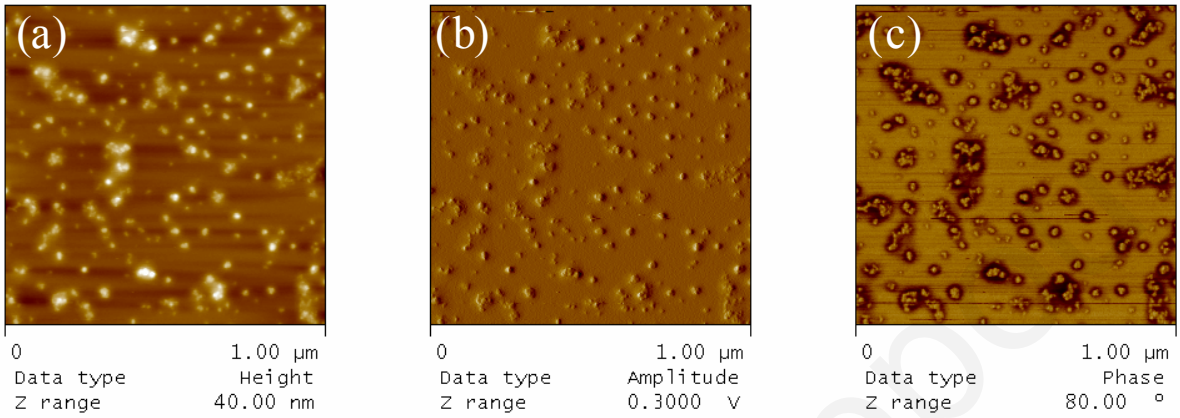

Figure 4.9. *AFM images of the block copolymer micelles formed in water, loaded with iron oxide nanoparticles: (a) Height Image, (b) Amplitude Image, (c) Phase Image.*

The nanoparticle size depends on the type of the stabilizer used as coating. It is expected that the amphiphilic PEGMA$_x$-*b*-AEMA$_y$ controls the growth of the magnetic nanoparticles during the co-precipitation synthesis. The molecular weight and thus the lengths of the two block segments within the copolymer affect the particles size and morphology. The spherical morphology adopted by the block copolymers in aqueous solution seems to lead to the formation of spherical iron oxide nanoparticles as observed in the phase image.[218]

The UV-vis spectra of the PEGMA$_{97}$-*b*-AEMA$_{18}$ in water before and after the incorporation of the magnetic nanoparticles are presented in Fig. 4.10. As shown in the spectra, an absorption signal appears between 300 and 450 nm indicating the generation of iron oxide nanoparticles inside the micellar core. Similar observations were also reported by *Jian and co-workers* for polystyrene-functionalized magnetite nanocomposites and attributed to the embedded iron oxide nanoparticles.[232]

Petri Papaphilippou

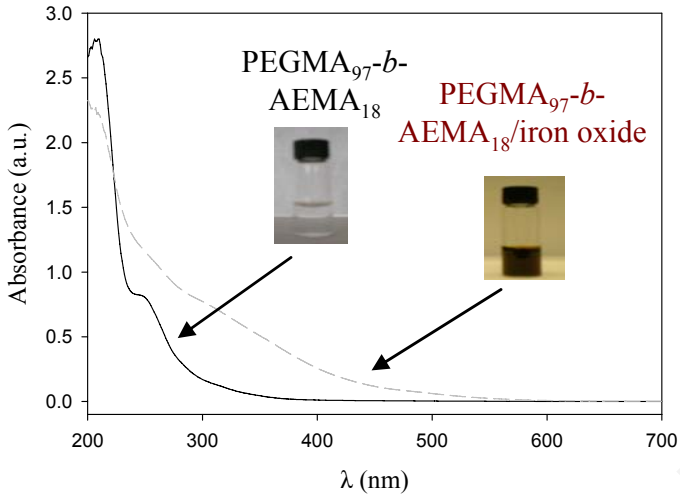

Figure 4.10. *UV-vis spectra of the unloaded (black, solid line) and loaded with iron oxide nanoparticles (grey, dashed line) PEGMA$_{97}$-b-AEMA$_{18}$ micelles.*

X-ray diffraction spectroscopy (XRD) was employed to determine the nanocrystalline phase adopted by the iron oxide nanoparticles embedded inside the polymer matrix. The powder X-ray diffraction pattern of the polymer-nanomagnetite hybrids (purified sample) consisting of iron oxide nanoparticles and the PEGMA$_{97}$-*b*-AEMA$_{46}$ block copolymer is shown in Fig. 4.11*c*. The diffraction pattern displays six broad peaks appearing at 2θ 30, 35.1, 42.5, 52.5, 56.6, and 61.9°. This result agrees with the findings of other groups, indicating the presence of Fe_3O_4.[233]

Furthermore, as shown in Table 4.3, the *d*-spacing values of the hybrid polymer/iron oxide materials were close to standard JCPDS Fe_3O_4 data [JCPDS card number 19-629].

Petri Papaphilippou

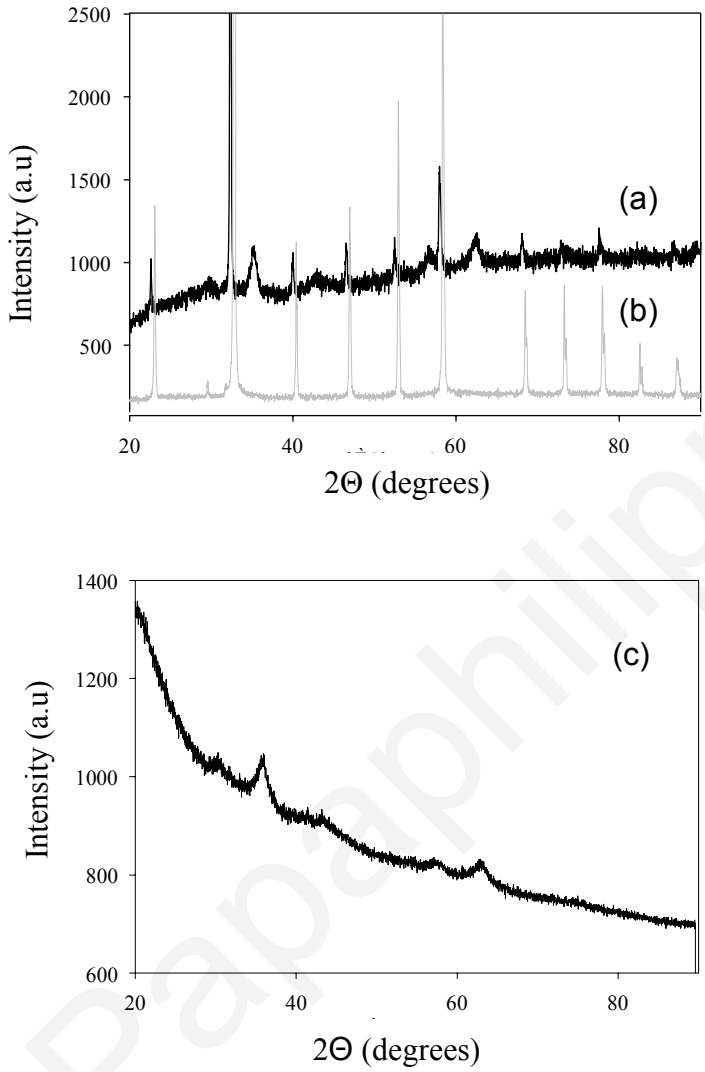

Figure 4.11. *X-Ray Diffraction patterns of the iron oxide nanoparticles coated with the* $PEGMA_{292}$*-b-*$AEMA_{36}$*/* Fe_xO_y *hybrid system. (a) unpurified sample (b) XRD spectrum of* NH_4Cl*. (c) after purification by dialysis against water.*

However, the XRD analysis of the crude material (Fig. 4.11*a*) revealed the presence of a crystalline by-product produced during the magnetite formation. The by-product that was proved to be ammonium chloride (NH_4Cl) (as seen in Fig. 4.11*b) was* successfully removed by dialysis against water.

Petri Papaphilippou

Table 4.3. *Diffraction angles and d-spacing values corresponding to the signals observed in the XRD diffraction pattern of the PEGMA$_{97}$-b-AEMA$_{46}$/iron oxide composite material.*

Peak	Diffraction Angle (2θ)	d experimental data (Å)	d standard JCPDS data Fe_3O_4 (Å)
1	30.0	2.976	2.967
2	35.1	2.554	2.532
3	42.5	2.125	2.099
4	52.5	1.742	1.715
5	56.6	1.625	1.616
6	61.9	1.498	1.485

TGA measurements were also performed to determine the decomposition temperatures of the block copolymers in the absence and presence of iron oxide nanoparticles. The PEGMA$_{96}$-b-AEMA$_{46}$ block copolymer and the corresponding polymer/Fe_3O_4 hybrid system is illustrated in Fig. 4.12. The latter was isolated upon solvent (water) removal under reduced pressure from the corresponding stabilized, polymer-coated nanoparticle solution. As shown in the figure, the PEGMA$_{97}$-*b*-AEMA$_{46}$ block copolymer started losing weight at ~ 200 ^{o}C and decomposed, losing all of its weight at 400 ^{o}C. By comparing the thermal stability of the composite with that of the pure polymer it can be clearly seen that the former starts decomposing at slightly higher temperatures compared to the pristine block copolymer and at around 400 ^{o}C approximately 40% of its mass is still maintained. Similar observations were observed by *Li et al.* who have reported on the increase in the thermal stability of a composite material consisting of polyaniline and ferrite particles,[234] attributed to interactions developed between the polymer chains and the ferrite particles. Furthermore, *Lee et al.* have verified that magnetic hybrid materials based on sulfonated polyaniline and magnetite particles were thermally more stable compared to the pure polymer.[235] Moreover, *Fessi et al.* showed that the magnetite nanoparticles coated with poly(lactide) PLLA, provided higher thermal stability to the polymer system compared to the pure polymer. [236]

Petri Papaphilippou

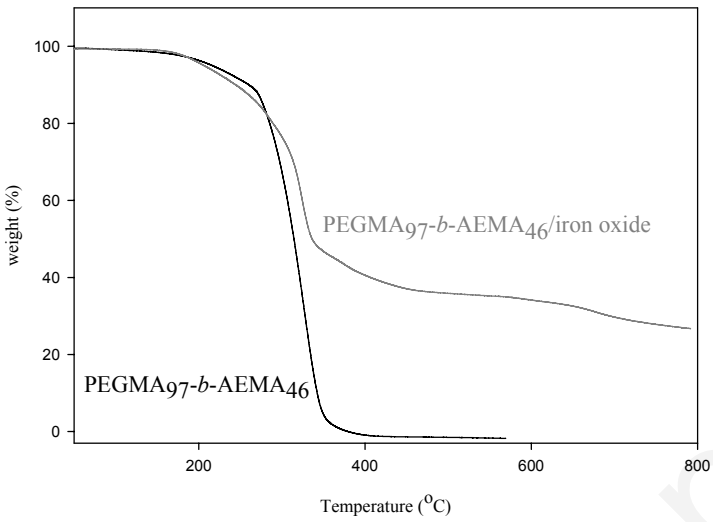

Figure 4.12. *TGA thermograms of the PEGMA$_{97}$-b-AEMA$_{46}$ block copolymer and the corresponding hybrid material PEGMA$_{97}$-b-AEMA$_{46}$.*

The magnetic behavior of these hybrid systems was investigated by Vibrating Sample Magnetometry (VSM). The magnetic measurement studies that were carried out in the research group of Prof. L. Vekas, Romania, indicated that the nanoparticles are superparamagnetic, demonstrated by the symmetrical sigmoidal shape of the magnetization curves exhibiting no hysteresis (absence of remanence ratio and coercivity). This feature, that is, the disappearance of magnetic interaction between the particles after the magnetic field has been removed, is extremely important for their applicability in magnetic resonance imaging.[237] Furthermore, an increase in magnetic loading causes a significant increase in the saturation magnetization (Ms) as shown in Fig. 4.13. The Ms of the PEGMA$_{70}$-*b*-AEMA$_{16}$-coated magnetic nanoparticles was determined to be 3.5, 180, and 300 (A/m) for the 1:1, 2:1 and 3:1 [Fe^{3+}]/[AEMA] molar ratio, respectively. These values were calculated based on the total mass of the micellar hybrids and not on the mass of the magnetic content (iron oxide) incorporated within the micelles. Unfortunately, the magnetization curve for the 1:1 molar ratio is only informative because, in this case the magnetization values are at the limit of sensitivity of the instrumentation used for these magnetic investigations. The magnetization values are reduced due to very low volume concentration of magnetite nanoparticles, well below 0.1%. *Kaiser et al.* have successfully stabilized magnetite nanoparticles by using carboxylated polystyrene.[238] The reported Ms values ranged from 300 to 1000 (A/m) and increased upon increasing the magnetic content. Another group reported the preparation of

stabilized magnetite nanoparticles by using poly(2-methoxyethyl methacrylate) (PMEMA) that is capable of covalently anchoring onto the inorganic surfaces. However, very low Ms values were reported for these systems of about 0.1-2 x 10^{-3} (A/m).[239]

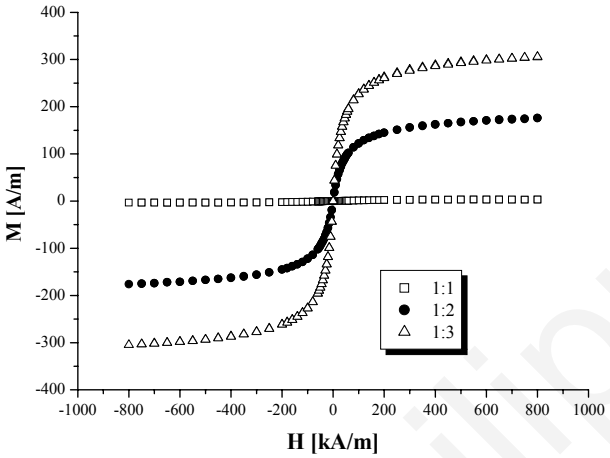

Figure 4.13. *Magnetization curves of the PEGMA$_{70}$-b-AEMA$_{16}$–coated iron oxide nanoparticles corresponding to different magnetic loading (1:1, 1:2 and 1:3 corresponds to [AEMA]/[Fe^{3+}] molar ratio).*

4.1.1.3. Biological assays of PEGMA$_x$-b-AEMA$_y$/Fe_xO_y.

In Vitro Biocompatibility.

The potential toxicity of the novel micelles and their effect on PC3 cell viability in culture was assessed against (a) double distilled H_2O and (b) Resovist® following incubation with various concentrations of the micelles (20-100 μg Fe/mL) over 72 h (Fig. 4.14). This work was carried out in collaboration with Dr. A. Odysseos and Dr. L. Loizou, EPOS-Iasis ltd. Analysis of variance (ANOVA) across the treated groups revealed no statistically significant variances (Fv = 0.98, Pv >0.05), Further comparison of M1 or M2 with H_2O by paired Student's t-test failed to yield any statistically significant differences in cell viability (Pv = 0.22 and 0.26, respectively), providing substantial evidence that these systems are biocompatible in cell cultures and thus safe for further studies. Similar *in vitro* biocompatibility data have been provided by *Lee and coworkers* for a comparable poly-PEGMAbased SPION which has been safely applied in preclinical studies.[240]

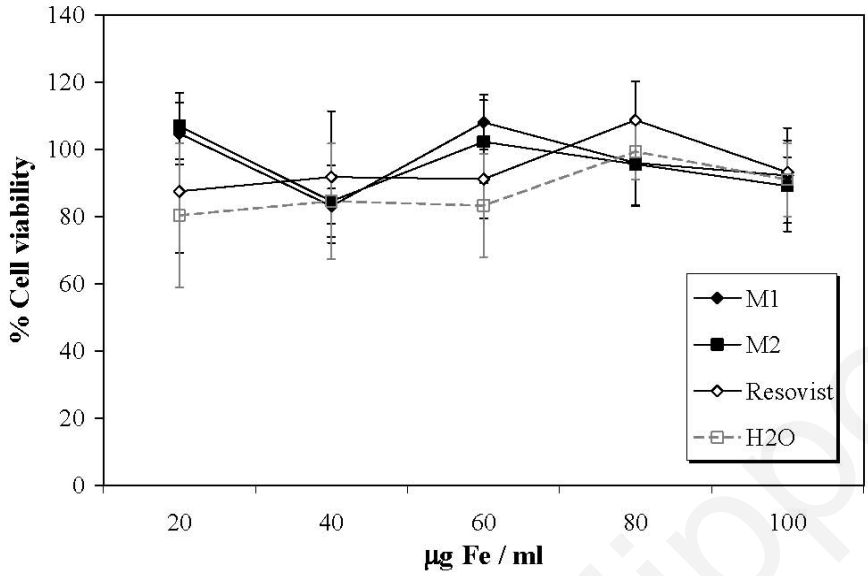

Figure 4.14. *The MTT colorimetric assay was used to assess the biocompatibility of the hybrid micelles. PC3 cancer cells were exposed for 72 hours to varying concentrations of the micelles ranging from 20 to 100 μg Fe /ml. Resovist® and untreated cells (H_2O) served as controls. Untreated cells (H_2O, indicated by a dotted line) served as controls at each Fe concentration. Untreated cells (0 μg Fe/ml) were considered to have 100% viability and the results were normalized accordingly. Results are given as the means of six values resulting from triplicate measurements of two representative experiments, ±SD. Variability of the error bars principally corresponds to the experimental uncertainty in each measurement.*

In Vitro Macrophage Uptake.

Lowering the uptake of SPIONs by RES, such as macrophages, for the magnetic nanoparticles to circulate long enough and be accumulated into the tumor by the enhanced permeability and retention (EPR) effect remains a key consideration for the *in vivo* use of SPIONs in cancer imaging. To assess this property *in vitro*, cell uptake experiments were conducted using the RAW264.7 macrophage cell line. The uptake of both M1 and M2 was compared to that of the clinically approved dextran-based agent Resovist®, which is of comparable size and has well-established uptake by macrophages.[241] The incorporation of M1, M2, and Resovist® into the cells was determined by Prussian Blue staining, following a 2 h incubation with the macrophages (Fig. 4.15). Interestingly, most of the cells retained a blue staining as a result of high uptake in the samples treated with Resovist (Fig. 4.15A),

Petri Papaphilippou

whereas both M1 and M2 showed significantly lower uptake (Figure 4.15B,C). These data strongly suggest that the coating layer ($AEMA_{36}$-*b*-$PEGMA_{292}$) in these systems minimizes pronouncedly the recognition and phagocytosis of the hybrid micelles by macrophages.

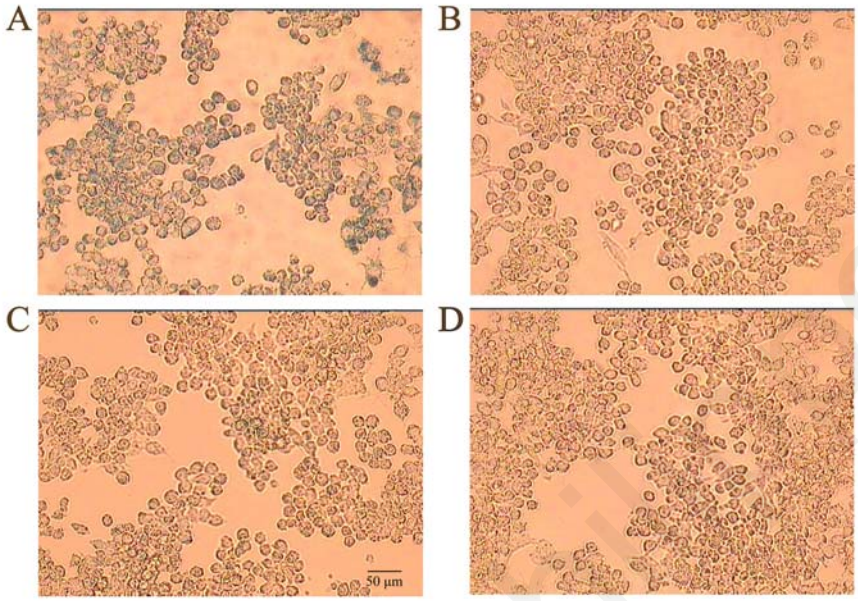

Figure 4.15. *In vitro uptake of hybrid micelles by macrophages determined by Prussian Blue staining after incubation for 2 hours with the indicated agent at a concentration equivalent of 0.15mg Fe/mL in complete media: (A) Resovist®, (B) hybrid micelle M1, (C) hybrid micelle M2, (D) untreated control. The presence of Prussian Blue precipitate arising from the formation of potassium ferrous ferricyanide reveals the accumulation of the Fe-based agent into the cells.*

Petri Papaphilippou

4.1.2 Magneto-responsive polymer/SWCNT nanocomposites.

4.1.2.1 Preface.

Carbon nanotubes (CNTs) have attracted great attention over the past decade due to their potential use in nanotechnology and biomedicine. CNTs, first discovered by Iijima[242] in 1991, are molecular-scale tubes of graphite constructed by rolling up a thin graphene sheet.[38] Due to their enthralling nanoscale dimensions and high aspect ratios (i.e. high length-to-diameter ratios), CNTs present excellent properties rendering them potentially useful in many applications such as in nanotechnology, electronics, optics, mechanics, biomedicine and other fields of material science.[243, 244] They exhibit extraordinary strength and unique electrical properties and are efficient thermal conductors. Carbon nanotubes can be classified into two major categories: single-wall carbon nanotubes (SWNTs) and multi-wall carbon nanotubes (MWNTs). SWCNTs comprised of only one graphene sheet layer, whereas MWCNTs are constituted of nested graphene cylinders which are co-axially arranged around a central hollow core.[38]

Due to their internal hollow space, CNTs can be utilized as containers for small compounds. Moreover, their unique nanostructure and particularly their convex surface make them useful for transferring ions and supporting guest compounds on their exterior. Small organic compounds, surfactants, macromolecules, metal ions and oxides are some of the materials that can be encapsulated in or attached onto the surfaces of CNTs *via* covalent bonding or physical adsorption. Recently, it has been demonstrated that CNTs can act as ideal carriers of inorganic magnetic nanoparticles, such as the iron oxide nanoparticles (Fe_3O_4 [245, 246, 247, 248, 249, 250] or γ-Fe_2O_3 [251, 252]). Due to their physical and chemical properties, these nanoparticles have attracted great interest, especially in the biomedical field, as contrast agents in MRI or as magnetically-triggered drug delivery systems. CNTs combined with iron oxides may find potential applications in biology and biomedicine. Even though there are some publications on magneto-responsive CNTs, it is still difficult to control the location and the amount of magnetic nanoparticles that are loaded on CNTs. Furthermore, an additional obstacle is the stabilization of such hybrid nanosystems in aqueous media in order to be able to find applicability in the biomedical field.

Petri Papaphilippou

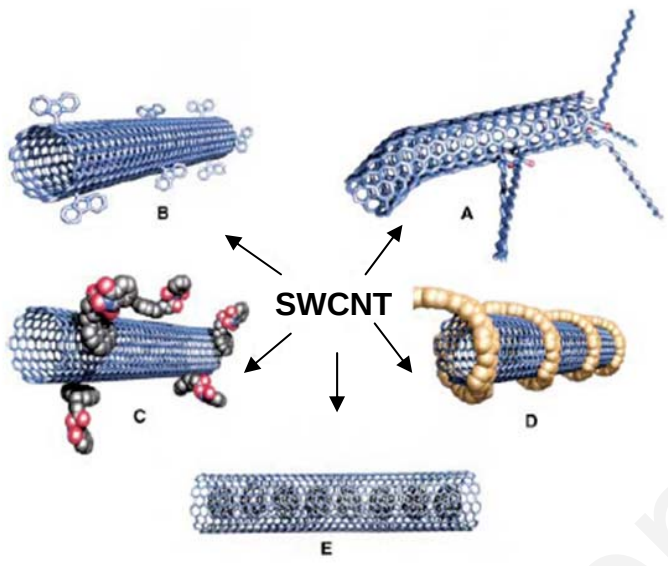

Figure 4.16. *Functionalization of SWCNTs. (A) defect functionalization, (B) functionalization with surfactants in sidewall by covalent bonds, (C) non-covalent exohedral functionalization, (D) functionalization with polymers by non-covalent bonds and (E) encapsulation of compounds inside the tube.*[253]

The latter, i.e. the difficulty for preparing stable solutions of these materials is mainly attributed to the strong tendency of CNTs for aggregation due to the intrinsic Van der Waals attractive forces, combined with the high aspect ratio of nanotubes, leading to coagulation phenomena. Particularly in SWCNTs characterized by an attractive force of ~0.5 eV per nanometer of nanotube-to-nanotube contact[254], such phenomena are more pronounced, resulting in the production of ropes and bundles. To overcome such problems, covalent and non-covalent functionalization of CNTs with polymers has been carried out.

Examples of covalent functionalization include among others click-chemistry functionalization[255, 256] and surface modification with carboxylic groups[257] that are further subjected to chemical modification in order to introduce polymerizable functional sites used in the growth of grafted polymer chains.[258] Moreover, hydroxyl, carboxyl or amide functionalities can be bound onto the surfaces of CNTs *via* esterification or amidation reactions. Non-covalent functionalization is more advantageous in regards to its non-destructive nature, since it does not affect the graphene structure of the nanotube. The latter involves the physical adsorption of the stabilizing agents onto the nanotube surfaces.[259]

Petri Papaphilippou

As previously mentioned, ferrofluids based on CNTs decorated with iron oxides may find potential applications in biology and biomedicine. Lately, several groups have used polymers as well as other organic compounds as coatings to stabilize the surface of magnetite nanoparticles decorating the CNTs.[260, 261, 262] *Zhang et al.* have synthesized composite CNTs containing Fe_3O_4 nanoparticles onto their surfaces, stabilized by carboxylated polyaniline (PANI) chains.[263] *Georgakillas et. al.* have prepared magneto-responsive SWCNTs upon coating the surface of the nanotubes with a carboxylic derivative of pyrene.[264] The physical adsorption of this stabilizing agent was accomplished *via* π-π stacking interactions developed between the CNT and the pyrene moiety. The Fe_3O_4 nanoparticles were attached onto the nanotubes through the carboxylate group of the pyrene derivative. Another example of a small organic compound used as stabilizer in magneto-responsive CNTs is 1-methyl-2-pyrrolidone [265, 266] that was successfully introduced to stabilize the iron oxide nanoparticles onto the surface of MWCNT-COOH. *Gao et al.* synthesized magnetic CNTs employing an electrostatic interaction mechanism. Poly[(2-diethylamino)ethyl methacrylate] (PDEAEMA) was covalently grafted onto the surfaces of the MWCNTs.[267] The tertiary amino functionalities were then quaternized with methyl iodide (CH_3I) resulting in cationic polyelectrolyte-grafted MWCNTs. Magnetic nanotubes were afforded *via* electrostatic self-assembling between the cationic groups of the quaternized polymer chains and the iron oxide nanoparticles. Finally, in the work reported by *Wang et al.* polymer/MWCNTs/Fe_3O_4 composites were prepared in which the pristine MWCNTs (non-oxidized) were functionalized with poly(ethyleneimine) (PEI) based on non-covalent bond interactions.[268] Moreover, polymer/MWCNT/Fe_3O_4 composites have been prepared by using Polypyrole (PPy) homopolymer as the stabilizing agent.[272]

This work aimed towards the synthesis and characterization of novel, magneto-responsive nanocomposites consisting of SWCNT decorated with iron oxide nanoparticles (Fe_xO_y) and $PEGMA_x$-*b*-$AEMA_y$ diblock copolymers, acting as stabilizers of these hybrid nanomaterials in aqueous media.[269]

Petri Papaphilippou

4.1.2.2 Synthesis.

The synthetic route followed for the preparation of the SWCNT (carboxylated)/PEGMA$_{132}$-*b*-AEMA$_{42}$/Fe$_x$O$_y$ nanohybrids is illustrated in Fig. 4.17. The preparation process was achieved in three steps. At first, SWCNTs (-COOH functionalized) were mixed with the PEGMA$_{132}$-*b*-AEMA$_{42}$ diblock copolymer in deoxygenated water. The carboxylate groups which are present onto the SWCNTs surfaces introduce negative charges on the nanotube surfaces thus promoting interactions with the Fe(II) and Fe(III) ions. The second step involved the addition of aqueous solutions of $FeCl_3.6H_2O$ and $FeCl_2.4H_2O$ into the SWCNT/polymer mixture. Finally, NH_4OH aqueous solution was added under strong stirring conditions and inert atmosphere. The resulting systems remained stable in solution for over 2 months when kept in the fridge. However, it is noteworthy to mention that the molar ratio between the AEMA groups of the polymer and the iron salts plays a significant role in the stabilization of the system in aqueous media. By using a [2.5]:[1]:[0.5] [AEMA]:[Fe^{3+}]:[Fe^{2+}] molar ratio stable solutions were obtained whereas a [1]:[1]:[0.5] molar ratio led to destabilization and precipitation.

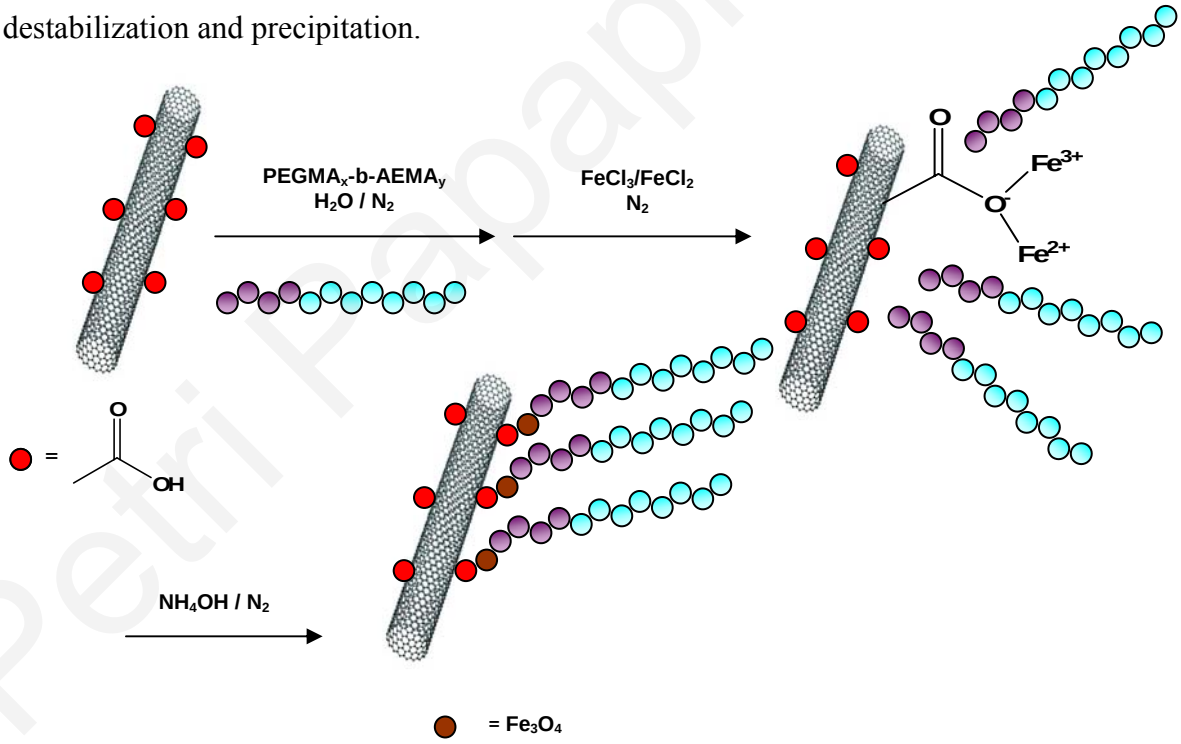

Figure 4.17. *Synthetic methodology followed for the preparation of SWCNT/Fe$_x$O$_y$/PEGMA$_{132}$-b-AEMA$_{42}$ magnetic nanohybrids stabilized in aqueous media.*

Petri Papaphilippou

In a control experiment where the above-mentioned synthetic route was carried out under exactly the same experimental conditions maintaining the [AEMA]:[Fe^{3+}]:[Fe^{2+}] molar ratios to [2.5]:[1]:[0.5] with the only difference being the absence of the diblock copolymer, non-stable dispersions (Fig. 4.18*a*) were obtained. This result clearly demonstrated that the presence of the $PEGMA_x$-b-$AEMA_y$ was crucial for the stabilization of these hybrid materials in aqueous solution.

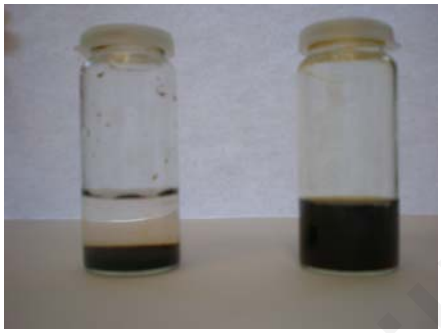

(a) ***(b)***

Figure 4.18. *(a) Unstable solution of SWCNT/Fe_xO_y system in the absence of the diblock copolymer, (b) Stable aqeuous solution of the SWCNT/Fe_xO_y/$PEGMA_{132}$-b-$AEMA_{42}$.*

The sequence of addition of the reactants was also found to affect the success of the whole process. Even though examples appear in the literature where the CNT/Fe_3O_4 composites are prepared first, followed by the addition of the polymer stabilizer, [263] in our case, when this route was followed (i.e. a: preparation of a SWCNT:Fe^{3+}:Fe^{2+} mixture b: addition of the base and c: introduction of the $PEGMA_{132}$-*b*-$AEMA_{42}$ diblock copolymer), non-stable dispersions were obtained.

Another important parameter that could hinder the successful synthesis of these materials is the presence of impurities produced during the fabrication process of CNTs. The first unsuccessful attempts for the preparation of these systems were carried out by using unmodified MWCNTs (i.e. having no –COOH functionalities onto their surfaces) of low purity (~ 50% w/w). Hence, it might be concluded that, besides the use of the $PEGMA_x$-b-$AEMA_y$ diblock copolymers as stabilizing agents, the introduction of CNTs of higher purity having additional functionalities capable of binding onto the iron ions might have been essential for the successful synthesis and stabilization of these systems in aqueous solutions.

Petri Papaphilippou

4.1.2.3. Characterization of SWCNT/Fe_xO_y/PEGMA$_x$-b-AEMA$_y$ nanohybrids.

The resulting dark brown solutions of the *SWCNT/Fe_xO_y/PEGMA$_{132}$-b-AEMA$_{42}$* hybrid materials were characterized by Transmision Electron Microscopy (TEM). These measurements were carried out in the research groups of Dr. Rodica Turcu, Romania and Prof. B. Nelson, Switzerland. As illustrated in Fig. 4.19, the surfaces of the nanotubes are decorated with spherical iron oxide nanoparticles.

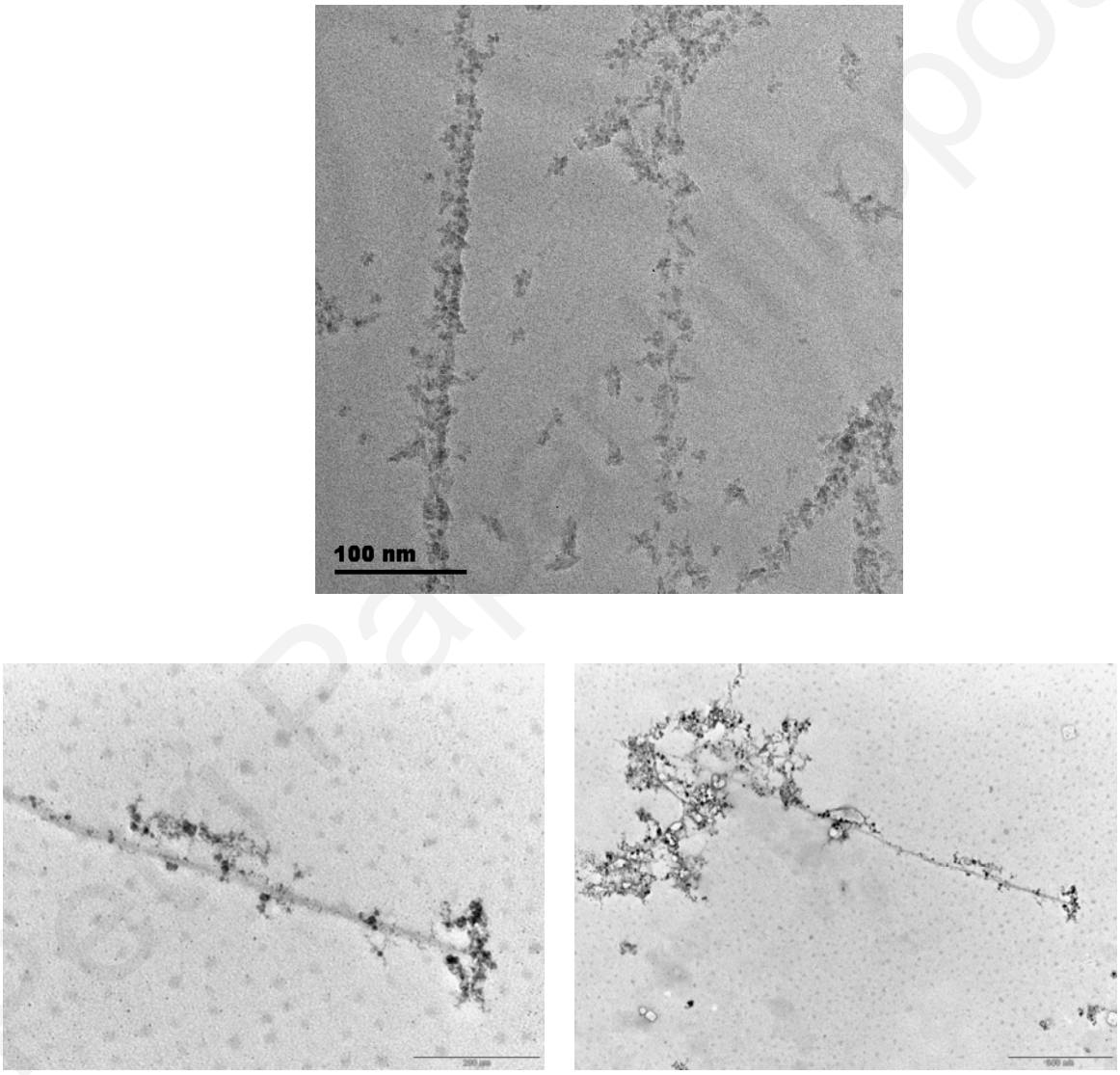

Figure 4.19. *TEM images of SWCNTs decorated with iron oxide nanoparticles and stabilized in aqueous solution in the presence of the PEGMA$_x$-b-AEMA$_y$ diblock copolymers.*

The decomposition temperatures of the *SWCNT/Fe_xO_y/PEGMA$_x$-b-AEMA$_y$* nanocomposites were determined by TGA. Fig. 4.20 depicts the TGA curves of (a) the carboxylated SWCNTs, (b) the PEGMA$_{75}$-*b*-AEMA$_{23}$ and (c) the SWCNT/Fe_xO_y /PEGMA$_{132}$-*b*-AEMA$_{42}$ composite. A weight loss of ~ 20% observed in the case of the carboxylated SWCNTs is probably due to the decomposition of the –COOH organic moieties. As seen in the Fig., the pristine block copolymer begins to loose weight at ~ 300 ^oC and decomposes completely at 400 ^oC. The *SWCNT/Fe_xO_y/PEGMA$_{132}$-b-AEMA$_{42}$* composite begins to decompose at slightly higher temperatures retaining 20% of its weight at T > 400 ^oC. By comparing the TGA curves of the carboxylated SWCNTs and the *SWCNT/Fe_xO_y/PEGMA$_x$-b-AEMA$_y$*, significant differences can be observed. These differences may be attributed to the very small quantity of SWCNTs present in the composite system (less than 1% wt.) Similar observations were reported by *C.Y. Hong and co-workers* who showed that the decomposition of the poly(St-*alt*-MAh)-*g*-PEO/MWCNT composite began at 200 ^oC whereas at 450 ^oC, 80% of its weight was lost, owing to the decomposition of the copolymer.[270]

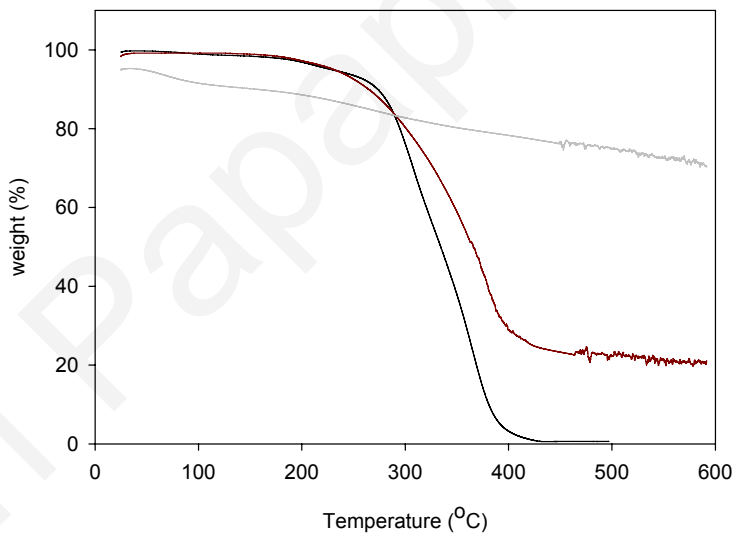

Figure 4.20. *TGA traces of (a) SWCNT-COOH (grey-line), (b) SWCNT/Fe_xO_y/PEGMA$_{75}$-b-AEMA$_{23}$ (brown-line) and (c) PEGMA$_{132}$-b-AEMA$_{42}$ block copolymer (black-line).*

Powder XRD spectroscopy was employed to characterize these systems. The X-ray diffraction pattern of the obtained composite material is illustrated in Fig. 4.21. The diffraction peaks appearing at 2Θ = 28.44° and at 40.66° which are close to literature values are closely associated with graphite's basal plane (002) and pyramidal plane (101)

respectively.[271] The signal appearing at about 2Θ < 20° corresponds to amorphous polymeric material.

The nanocrystalline phase adopted by the magnetic nanoparticles incorporated into the composites could not be determined by XRD since in the diffraction pattern the signals reflected to magnetic nanoparticles were too broadened and thus non-detectable. The presence of a thin layer of amorphous polymeric material onto the surface of the iron oxide nanoparticles decorating the SWCNT surfaces (as schematically presented in Fig. 4.20), combined with the low magnetic content within the composite may be the reasons for the very low intensity of the signals corresponding to the magnetic nanoparticles. Similar observations were reported by *Wu and co-workers* who have prepared a magnetic nanocomposite consisting of MWCNT decorated with Fe_3O_4 and stabilized by a layer of polypyrole.[272]

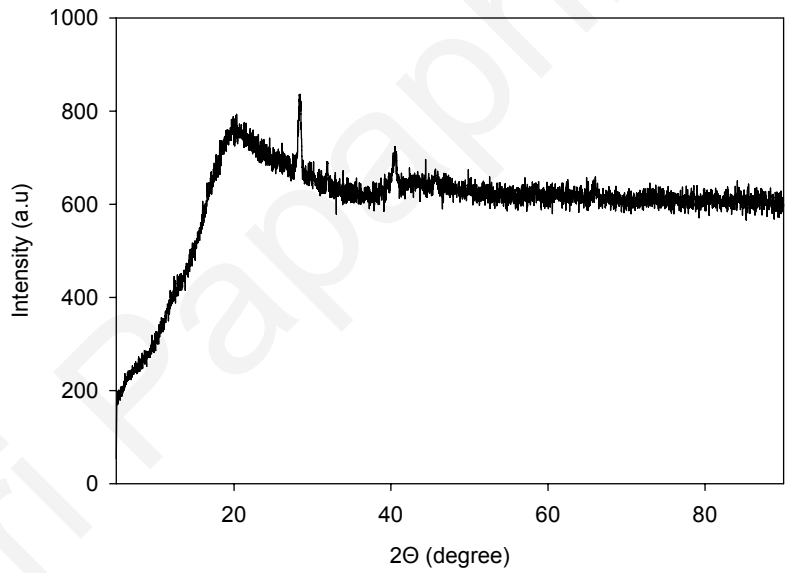

Figure 4.21. *XRD pattern of the SWCNT/Fe_xO_y/PEGMA$_{132}$-b-AEMA$_{42}$ nanocomposite.*

The SWCNT/Fe_xO_y/PEGMA$_{132}$-*b*-AEMA$_{42}$ composite was also characterized by FTIR spectroscopy. Fig. 4.22 presents the FTIR spectra of both, the carboxylated SWCNTs and the composite. In spectrum (a), the signals appearing in the range between 1639-1740 cm^{-1} and at 1267 cm^{-1} correspond to the C=O and C-O vibration frequencies of the –COOH groups respectively. [266] In spectrum (b), the vibration bands appearing at 1736 cm^{-1} and 1655 cm^{-1} correspond to the C=O bond that is present in the PEGMA$_{132}$-b-AEMA$_{42}$ diblock copolymer. [273] The strong signal appearing at 1104 cm^{-1} displayed the vibration frequency

Petri Papaphilippou

of the C-O bond that is present in the ester group of the polymer, a result which is in agreement with previously reported data. [273] Moreover, FTIR signals appearing between 3000-2800 cm^{-1} assigned to the non-symmetrical and symmetrical stretching of the $-CH_2-$ groups are also observed in the spectrum. Finally, the broad band appearing at ~ 513 cm^{-1} in spectrum (b) is due to the vibration frequency of the Fe-O bond,[268] thus indicating the existence of iron oxide particles within the composite.

(a)

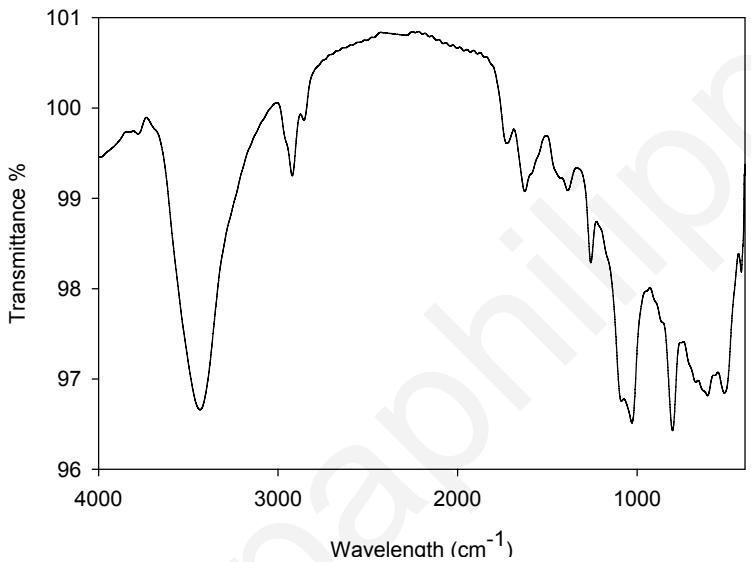

(b)

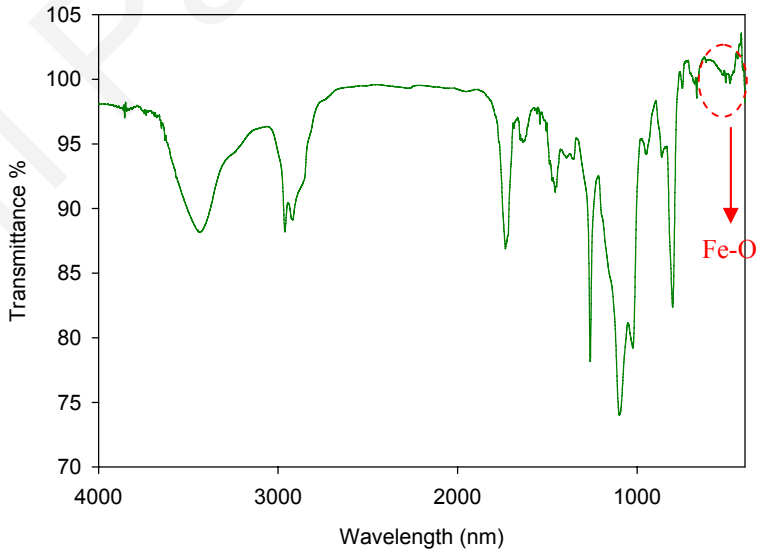

Figure 4.22. *FTIR spectra of (a) carboxylated SWCNT and (b) SWCNT/Fe_xO_y/$PEGMA_{132}$-b-$AEMA_{42}$ composite.*

Petri Papaphilippou

The magnetic properties of the SWCNT/Fe_xO_y/PEGMA$_{132}$-*b*-AEMA$_{42}$ nanocomposites have been investigated by vibrating sample magnetometer (VSM). These measurements were carried out in the research group of Dr. Rodica Turcu, Romania. A typical M= *f* (B) magnetization curve (where M is magnetization and B is the strength of the applied magnetic field) recorded at room temperature (300 K) is presented in Fig. 4.23. As seen in the graph, no pronounced hysteresis loop exists, thus demonstrating that both the remanence (Mr) and the coercivity (Hc) ratio of the composites are zero. This phenomenon indicates a superparamagnetic behavior. The Ms of the SWCNT/Fe_xO_y/PEGMA$_{132}$-*b*-AEMA$_{42}$ nanocomposite is 2.60 emu/g. This value is significantly higher compared to other similar systems appearing in literature. For example the Ms value for a nanocomposite consisting of multi wall carbon nanotubes (MWCNTs), polypyrrole and magnetite, which presented a ferromagnetic behavior.[272] Moreover, *Jiangtao Feng et. al.* who have synthesized magnetoactive MWCNTs having poly (L-lactic acid) (PLLA) covalently attached onto its surface, have reported a very low Ms value for this composite (at about ~ 0.08 emu/g) and superparamagnetic behaviour.[274] It is noteworthy to mention at this point that the above mentioned value (Ms = 2.6 emu/g) was calculated based on the total mass of the SWCNT/Fe_xO_y/PEGMA$_{132}$-*b*-AEMA$_{42}$ and not on the mass of the magnetic content (iron oxide).

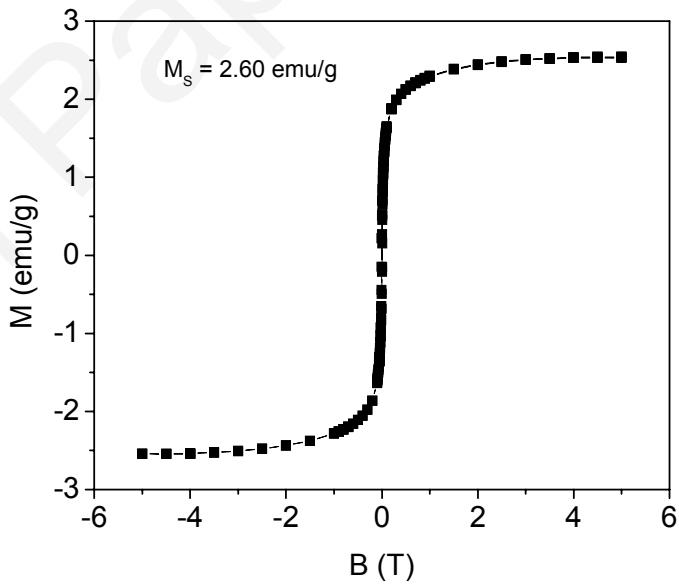

Figure 4.23. *Magnetization curve of the SWCNT/Fe_xO_y/PEGMA$_{132}$-b-AEMA$_{42}$ nanocomposite recorded at 300 K, demonstrating the superparamagnetic behavior of this system.*

Petri Papaphilippou

4.1.3. Synthesis and Characterization of Magneto-responsive Polymer Co-networks.

4.1.3.1. Preface.

Polymer networks are three-dimensional structures comprising of polymer chains which are interconnected *via* chemical cross-links or physical interactions, namely covalent and physical networks, respectively. Amphiphilic polymer networks, consist of both, hydrophilic as well as hydrophobic units. Due to their amphiphilic character, these systems have the ability to absorb or retain large amount of liquids such as organic and aqueous solvents and adsorb hydrophilic as well and hydrophobic solutes.[275]

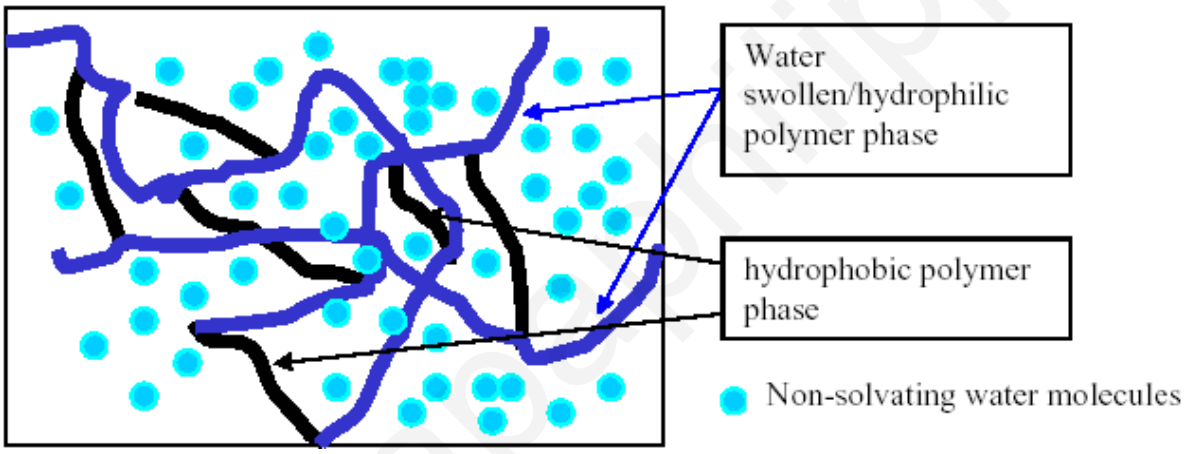

Figure 4.24. *Amphiphilic polymer network consisting of hydrophilic and hydrophobic units.*

During the last years "smart" materials have attracted great attention because of their ability to respond to external stimuli such as temperature,[276, 277, 278] pH,[278] light,[277, 279] magnetic [280] and electric field [281] undergoing conformational changes.[282] Magneto-responsive polymers belong to this broad category of "intelligent" composite materials. Among others, magnetic polymer networks, a new class of soft composite materials, exhibit great interest since they could be potentially used in magnetic drug delivery, cell sorting, catalysis, as sensors and actuators and in bioseparation processes.[283, 284, 285, 286, 287, 288]

Magnetic gels which are frequently termed as "ferrogels" are a new class of materials comprised of swollen polymer networks in which magnetic particles are embedded. Their

properties are influenced by the presence of an external magnetic field. The magnetoelastic properties of these materials can be used to construct sensors and actuators.[289]

This study deals with the synthesis and characterization of novel composite amphiphilic random co-networks consisting of (a) oleic acid-coated iron oxide nanoparticles ($OA.Fe_3O_4$) or non-coated iron oxides (nano)particles (Fe_xO_y), (b) hydrophilic, thermoresponsive and biocompatible (hexa(ethylene glycol) methyl ether methacrylate (HEGMA) units and (c) hydrophobic 2-(acetoacetoxy)ethyl methacrylate (AEMA) units bearing *β*-ketoester metal-chelating functionalities.[290]

HEGMA, belonging to the family of the non-linear poly(ethylene glycol) analogues, was the hydrophilic unit of choice, due to its biocompatibility and thermoresponsive properties.[291] The thermoresponsive behavior of polymers possessing oligo(ethylene glycol) segments as side chains has been already reported in the literature.[292] As previously mentioned, $PEGMA_x$ having a side-PEG chain of intermediate length (2 ethylene oxide units (EO) < 10, in this study 6 EO units) presents a LCST in aqueous media, meaning that it may turn from hydrophilic into hydrophobic as temperature rises above a certain value.[291] Moreover, related to other thermoresponsive materials such as N-isopropylacrylamide, PEGMA*x* presents sharp and reversible phase transitions.[291, 293] PEG-containing hydrogels have been employed among others in enzyme immobilization,[294] drug delivery [295] and regenerative medicine.[296]

AEMA was chosen to be the second monomeric unit within the co-networks, due to its well-known ability to act as strong bidentate ligand and bind effectively onto the inorganic iron oxide surfaces providing an improved stabilization. We have already demonstrated the ability of well-defined diblock copolymers possessing *β*-ketoester functionalities to act as effective stabilizers for iron oxide nanoparticles in aqueous solutions.[204]

Free-radical polymerization was employed for the synthesis of the HEGMA-*co*-AEMA/EGDMA hydrogels in the absence and presence of (i) preformed oleic acid-coated magnetite nanoparticles ($OA.Fe_3O_4$) or (ii) iron oxide (nano)particles (Fe_xO_y). The latter were *in-house* synthesized by following the conventional chemical co-precipitation method. Oleic acid, $C_{18}H_{34}O_2$ is an unsaturated carboxylic acid with a double bond kink in the middle of its tale. The kink plays a crucial role in the organization of the surfactant on the surface of magnetic particles and hence provides steric repulsion between the magnetite

Petri Papaphilippou

nanoparticles.[297] This is confirmed by the fact that the saturated stearic acid (SA) of the same tail length, $C_{18}H_{34}O_2$, but without this kink, is a poor stabilizer. OA is considered to be one of the best organic molecules for stabilizing magnetite nanoparticles in organic solvent *via* chemisorption of its polar head on the surface of magnetic particles, while the hydrophobic tails dissolve in the dispersion medium.[71, 298, 299]

4.1.3.2. Synthesis.

The preparation of the polymer random co-networks in the absence and presence of the magnetic (nano)particles (coated and non-coated) was accomplished *via* free radical polymerization by using EGDMA as the cross-linker and AIBN as the radical initiator. Fig. 4.25 presents the chemical structures and names of monomers, crosslinker and initiator used in the fabrication of the HEGMA-co-AEMA/EGDMA random conetworks.

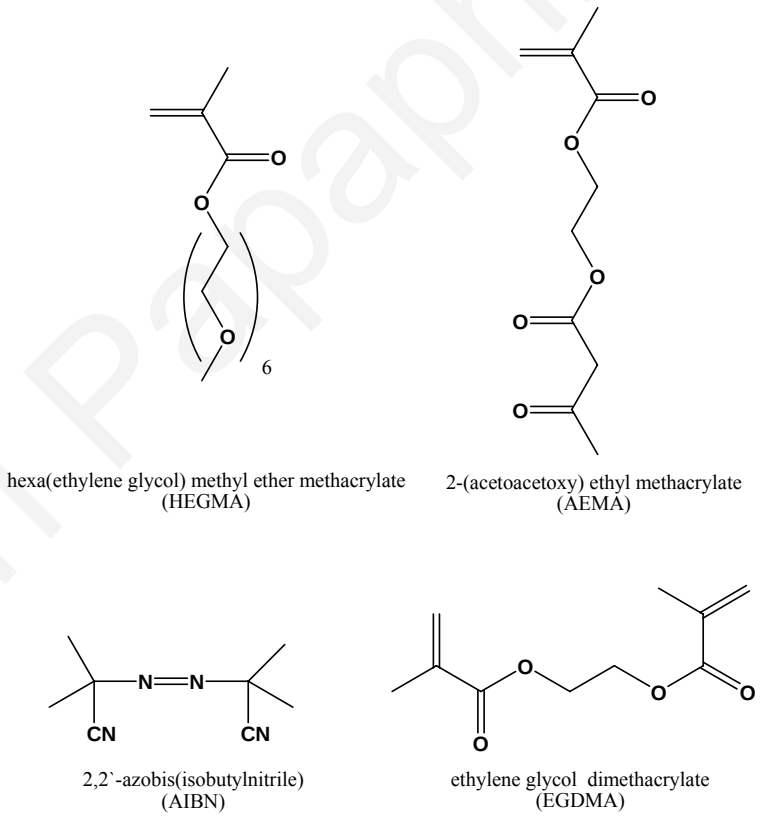

Figure 4.25. *Chemical structures and names of the main reagents used for the co-network synthesis.*

Petri Papaphilippou

The first two series of the magneto-responsive polymer co-networks (Series A and B) were synthesized in the presence of preformed oleic acid-coated magnetite nanoparticles, whereas in the 3rd series (Series C), Fe_xO_y nanoparticles (non-coated) have been incorporated into the networks during the polymerization process.

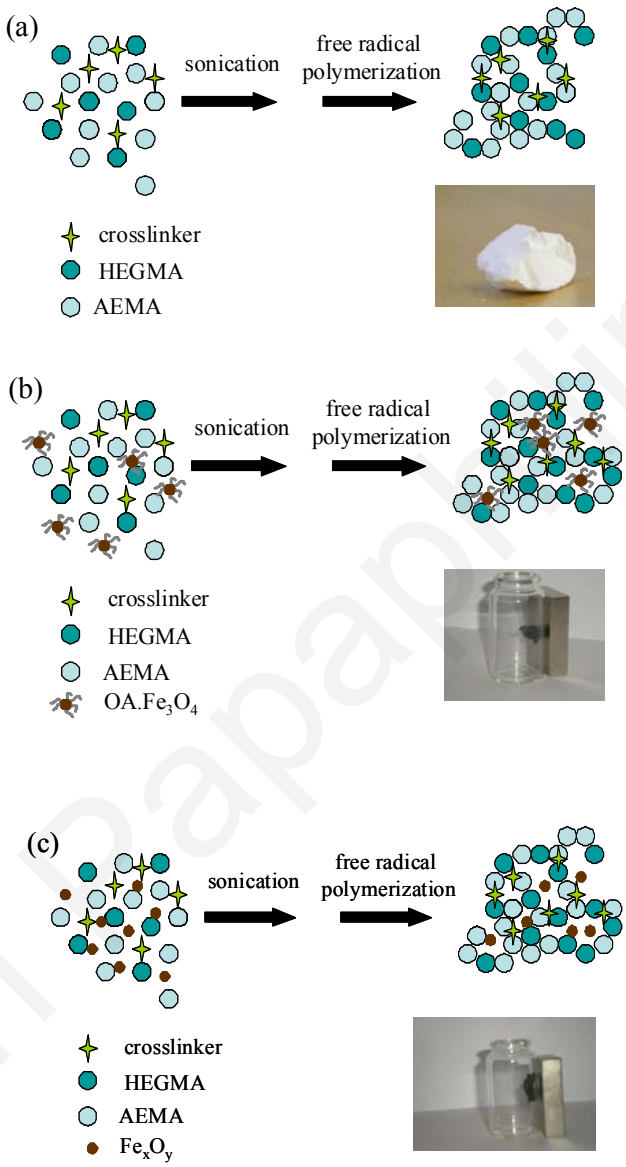

Figure 4.26. *Schematic presentation of the synthetic methodology followed for the fabrication of (a) random HEGMA-co-AEMA/EGDMA co-networks; (b) HEGMA-co-AEMA/EGDMA co-networks with embedded OA.Fe_3O_4 nanoparticles and (c) HEGMA-co-AEMA/EGDMA co-networks with embedded Fe_xO_y (nano)particles.*

Petri Papaphilippou

Fig. 4.26 displays schematically the synthetic methodology followed for the preparation of the (composite) co-networks. The incorporation of the OA.Fe_3O_4 magnetic nanoparticles into the HEGMA-co-AEMA/EGDMA random co-networks has been accomplished in 2 steps: (i) fabrication of OA.Fe_3O_4 following the chemical co-precipitation method and (ii) free radical cross-linking copolymerization of mixtures containing different amounts of the OA.Fe_3O_4, the two monomers, the initiator, the cross-linker and the solvent.

TEM was used to visualize the OA.Fe_3O_4 magnetite nanoparticles. Exemplarily, a TEM image is presented in Figure 4.27, showing many individual and some superimposed OA. Fe_3O_4 nanoparticles. From the related histogram it can be clearly seen that most of the particles are characterized by very small diameters, at around 4-5 nm.

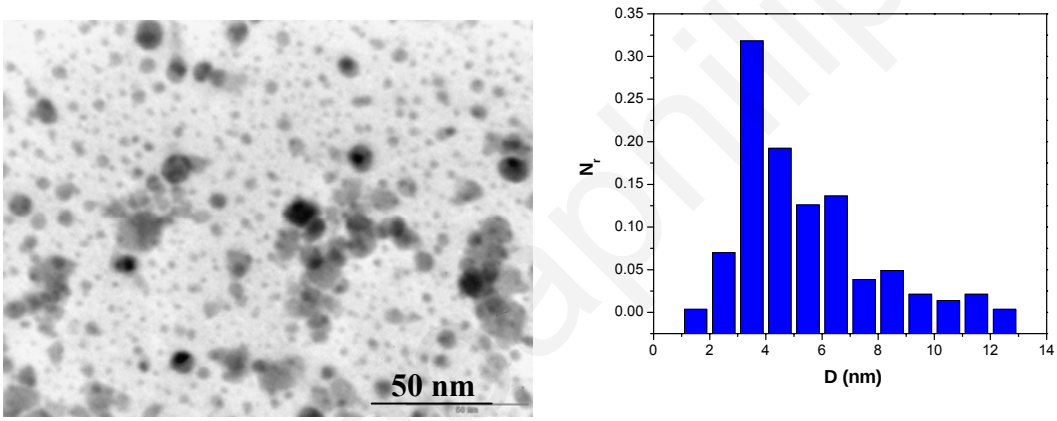

Figure 4.27. *TEM images and related size histogram corresponding to the OA.Fe_3O_4 nanoparticles prepared in this study.*

As already mentioned, three series of composite *co*-networks were prepared, in which the organic content (HEGMA, AEMA, AIBN and EGDMA) was kept constant and only the inorganic content (OA.Fe_3O_4 or Fe_xO_y) varied (*for series A*: OA.Fe_3O_4 % wt 0, 7, 11, 23 corresponding to Gel 1, Gel 1a, Gel 1b, Gel 1c respectively, *for series B*: OA.Fe_3O_4 % wt 0, 7, 11, 23 corresponding to Gel 2, Gel 2a, Gel 2b and Gel 2c respectively and *for series C*: Fe_xO_y % wt 0, 7, 11, 23, 2, 4 corresponding to Gel 1, Gel 3a, Gel 3b, Gel 3c, Gel 3d and Gel 3e respectively).

Petri Papaphilippou

The sol fraction (extractables) of the conetworks varied from ~ 3 to 6% for series A, whereas for series B a higher sol fraction ranging between 9-18% was observed (Table 4.4). The lowest percentage of extractables, corresponded to the cases in which gelation was carried out in the absence of OA. Fe_3O_4.

Table 4.4. *Sol fraction and magnetic loading percentages of the composite co-networks prepared in this study.*

	Sample Code	Solvent	Sol fraction (%)	% OA.Fe_xO_y
		Series A		
No OA.Fe_3O_4	Gel 1	EA	1.56	-
With OA.Fe_3O_4	Gel 1a	EA	3.23	7.0
	Gel 1b	EA	4.14	11.0
	Gel 1c	EA	5.57	23.0
		Series B		
No OA.Fe_3O_4	Gel 2	THF	8.79	-
With OA.Fe_3O_4	Gel 2a	THF	11.06	7.0
	Gel 2b	THF	15.87	11.0
	Gel 2c	THF	18.19	23.0
		Series C		
No Fe_xO_y	Gel 1	EA	1.56	-
With Fe_xO_y	Gel 3a	EA	16.6	4.0
	Gel 3b	EA	35.8	7.0
	Gel 3c	EA	22.3	11.0
	Gel 3d	EA	n.a	23.0
	Gel 3e	EA	n.a	2.0

n.a: not available

4.1.3.3. Characterization of the magneto-responsive co-networks.

The degrees of swelling (DS) of the polymer co-networks were measured in water and EA for the A and C series and in water and THF, for series B. The DS values depend on the nature of the monomeric units that are present in the co-network. The DS of the co-networks measured in EA and water (for series A and C) and in THF and water (for series B) together with the 95% confidence intervals are summarized in Table 4.5. The DS measured for series

Petri Panaphilippou

A and B (containing the OA.Fe_3O_4 nanoparticles) in the organic solvents (either EA or THF) were comparable for both series within the experimental error (in the range ~ 2.5 - 4).

Table 4.5. *Degrees of swelling of the (composite) co-networks prepared in EA (series A and C) and in THF (series B).*

	Sample Code	**Solvent**	**Series A: DS in EA**	**Series A: DS in water**
No OA.Fe_3O_4	Gel 1	EA	3.04 ± 0.05	2.37 ± 0.12
With OA.Fe_3O_4	Gel 1a	EA	3.35 ±0.50	2.74 ±0.55
	Gel 1b	EA	2.98 ±0.49	2.36 ±0.14
	Gel 1c	EA	2.60 ±0.07	2.09 ±0.16
			Series B: DS in THF	**Series B: DS in water**
No OA.Fe_3O_4	Gel 2	THF	2.47 ± 0.34	1.71 ± 0.99
With OA.Fe_3O_4	Gel 2a	THF	2.75 ± 1.22	1.69 ± 0.51
	Gel 2b	THF	2.61 ± 1.49	1.46 ± 0.42
	Gel 2c	THF	2.55 ± 1.66	1.16 ± 0.06
			Series C: DS in EA	**Series C: DS in water**
No Fe_xO_y	Gel 1	EA	3.04 ± 0.05	2.37 ± 0.12
With Fe_xO_y	Gel 3a	EA	4.55±0.80	1.23±0.13
	Gel 3b	EA	5.14±n.d	1.55±n.d
	Gel 3c	EA	5.24±n.d	1.60±0.17
	Gel 3d	EA	2.87±0.40	2.38±1.10

As seen in the Table 4.5, in all cases, the DS measured in water were lower compared to those obtained in the organic media. The lower DSs in aqueous media are due to the fact that EA as well as THF are non-selective (good) solvents for both the HEGMA and the AEMA units while water is only selective for HEGMA. Hence, the insolubility of AEMA units in water leads to a reduction of the DS in aqueous media as expected. Similar observations were reported for amphiphilic polymethacrylate model co-networks comprised of hydrophilic 2-(dimethylamino) ethyl methacrylate (DMAEMA) units and hydrophobic *n*-butyl methacrylate (BuMA) units.[300] These systems exhibited lower DSs in water compared to

Petri Papaphilippou

those recorded in THF due to the fact that water was only selective for the hydrophilic (DMAEMA) groups. The insolubility of the hydrophobic *n*-BuMA units caused a reduction in the DSs of the *n*-BuMA-containing co-networks in water.

As previously mentioned, polymers possessing oligo(ethylene glycol) segments as side chains, display a LCST in aqueous media.[213] In a recent publication[204] we have demonstrated that diblock copolymers based on HEGMA and AEMA units presented a phase transition in water upon temperature increase at ~ 60 ^{o}C, a result which is in the range of previously reported findings.[291, 301]

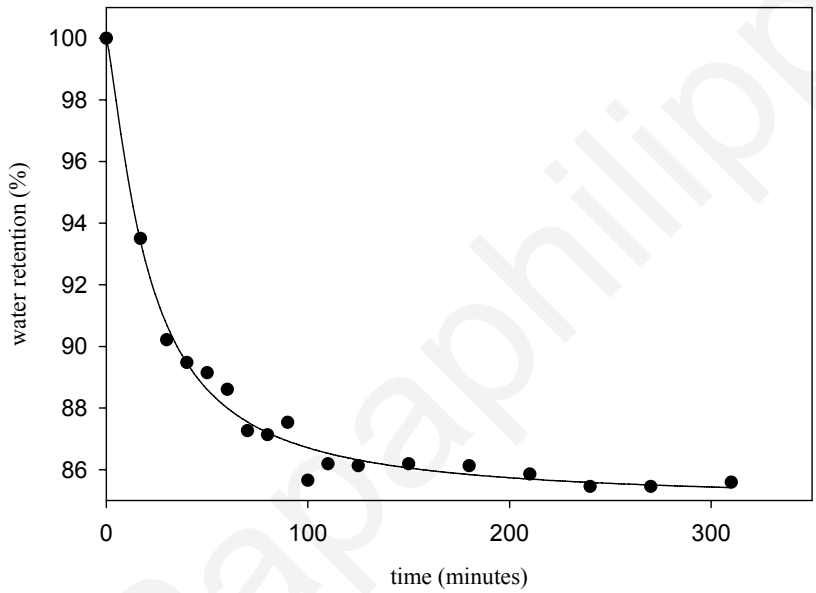

Figure 4.28. *Deswelling kinetics of sample Gel 1c (23% wt. OA.Fe_3O_4) measured in water at ~ 60 ^{o}C.*

The deswelling behavior of the co-networks was monitored upon transferring samples from their swollen state in neutral water at 25 ^{o}C into pre-heated water at 60 ^{o}C and measuring the decrease in their mass at different time intervals. Exemplarily, the deswelling kinetics plot for Gel 1c (23% wt. OA.Fe_3O_4) is presented in Fig. 4.28, demonstrating the thermoresponsive properties of these materials.

The decomposition temperatures of the HEGMA-*co*-AEMA/EGDMA co-networks in the absence and presence of the magnetic (nano)particles were determined by TGA. Fig. 4.29 exemplarily presents the TGA traces of Gel 1 (no OA.Fe_3O_4) and Gel 1b (OA. Fe_3O_4, 11% wt) prepared in EA. The differences appearing between the HEGMA-co-AEMA/EGDMA-

OA.Fe_3O_4 and the HEGMA-co-AEMA/EGDMA in regards to thermal stability are because of the presence of the inorganic magnetite nanoparticles. From the TGA thermograms it can be clearly seen that the magnetic nanoparticles affect positively the thermal stability of the co-networks. The pristine polymer co-network (Gel 1) began to loose weight at ~ 190°C and decomposed completely at ~ 400 °C. The decomposition of Gel 1b began at higher temperatures (~ 230 °C) compared to Gel 1. The residue appearing at higher temperatures (T > 400 ^{o}C) in the TGA thermogram of the composite co-network (~ 10% wt) corresponds to the weight percentage of the magnetic nanoparticles. These results are in line with the observations of *Goiti et. al.* who have demonstrated the improvement of the thermal stability of composite poly(hydroxyl ethyl)methacrylate and poly(vinyl alcohol) hydrogels upon the incorporation of magnetite particles.[302]

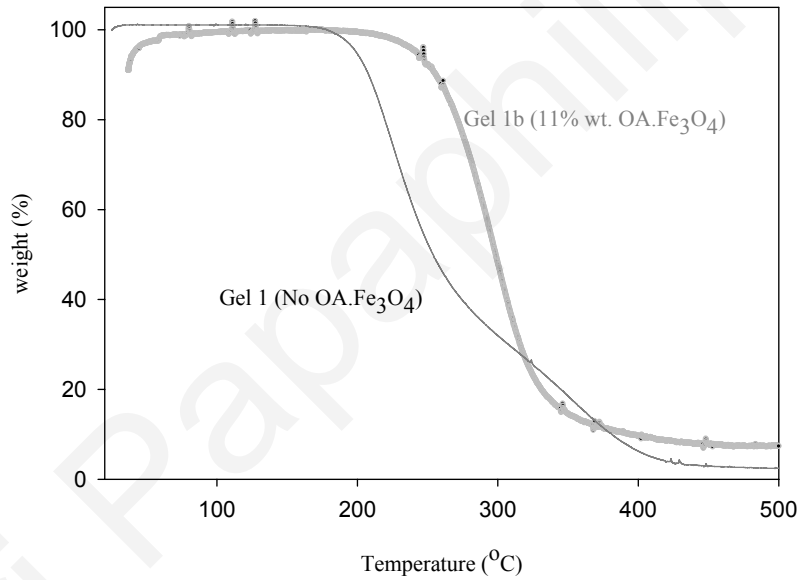

Figure 4.29. *TGA thermograms of Gel 1 (no OA.Fe_3O_4) and Gel 1b (OA.Fe_3O_4, 11% wt.) prepared in EA.*

The nanocrystalline phase adopted by the embedded OA.Fe_3O_4 nanoparticles was investigated by XRD. In Fig. 4.30 the powder XRD patterns of the Gel 1c and Gel 2c composite co-networks, both containing 23% wt. OA.Fe_3O_4 together with the XRD spectrum of the as prepared OA.Fe_3O_4 nanoparticles are presented.

In all cases, the diffraction pattern displays six broad peaks appearing at 2θ ~ 30, 36, 43, 54, 58 and 63°. These data were found to be in agreement with the findings of other groups thus verifying the existence of Fe_3O_4 within the co-networks. [303, 304]

Petri Papaphilippou

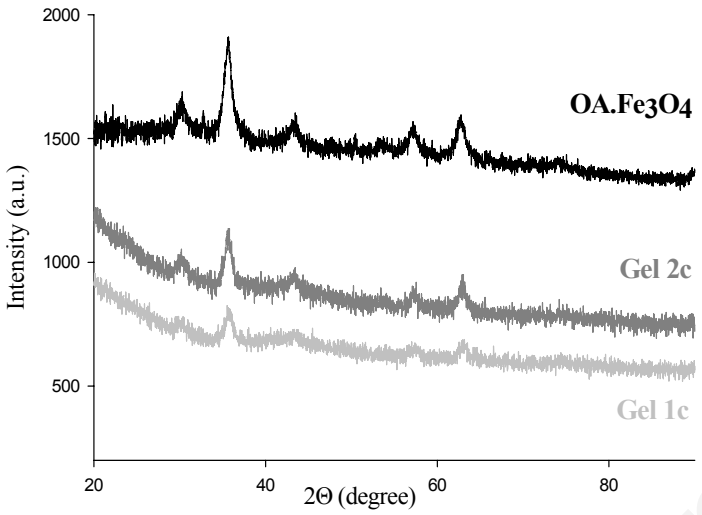

Figure 4.30. *X-ray diffraction patterns of (i) as prepared OA.Fe_3O_4 nanoparticles (ii) Gel 1c and (iii) Gel 2c both containing 23 % wt OA.Fe_3O_4.*

The magnetic properties of the composite co-networks containing the OA.Fe_3O_4 (Series A and B) were determined by VSM at 300K. These measurements were carried out in the research group of Prof. L. Vekas, Romania. Fig. 4.31 presents the magnetization *versus* applied magnetic field strength plots for (a) Series A (11 and 23% wt. OA.Fe_3O_4, Gels 1b and 1c respectively) and (ii) series B (11 and 23% wt. OA.Fe_3O_4, Gels 2b and 2c respectively).

As seen in Fig. 4.31, in all cases the magnetization curves are sigmoidal exhibiting no hysteresis, demonstrating the superparamagnetic behavior of these systems. These results suggest that the OA coating that is present onto the Fe_3O_4 nanoparticles, acts as an effective stabilizer thus preventing agglomeration from occurring during the polymerization process. The latter could have led to the formation of larger particles resulting to deviation from superparamagnetism. Furthermore, as seen in the diagrams, an increase in the magnetic loading causes a significant increase in the saturation magnetization (Ms) in both series. The magnetization values corresponding to the composites fabricated in THF were higher compared to those prepared in EA. More precisely, in series A, Ms varied between 0.7 (Gel 1b) and 2.9 (Gel 1c) emu/g, whereas in series B higher Ms values were observed (3.3 emu/g for Gel 2b and 9.1 emu/g for Gel 2c). This is due to differences in the solubility of the OA.Fe_3O_4 in the two solvents employed during the polymerization process. As already mentioned in the experimental section, the OA.Fe_3O_4 is readily soluble in THF whereas its solubility is limited in EA, hence prior to gelation the OA.Fe_3O_4 is only dispersed in the

Petri Papaphilippou

reaction medium and not completely dissolved. The "poor" solubility of the OA.Fe_3O_4 in EA, may have resulted in the entrapment of less magnetic content within the networks during network formation, resulting in lower magnetization values. The above mentioned magnetization values were calculated based on the total mass of the OA.Fe_3O_4/co-network and not on the mass of the magnetic content (magnetite nanoparticles).

(a)

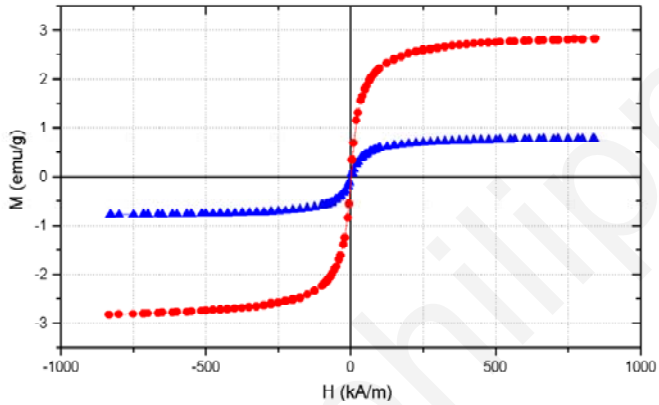

(b)

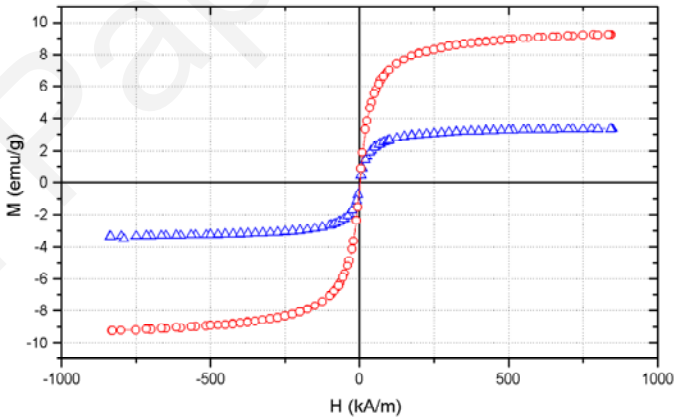

Figure 4.31. *Magnetization curves of (a) Series A (Gel 1b – blue curve and 1c – red curve) and (b) Series B (Gel 2b – blue curve and 2c– red curve) measured at 300K.*

The saturation magnetization of these samples is smaller than that of the bulk Fe_3O_4 (92 emu/g).[305] The low Ms may be attributed to the diamagnetic contribution of the polymer co-network matrix (PEGMA-co-AEMA/EGDMA) surrounding the magnetic nanoparticles.

Petri Papaphilippou

Similarly, *Rhee et al*. has reported on the reduction of the Ms of magnetic nanoparticles encapsulated into a polyacrylamide hydrogel. [306]

The magnetic properties of the PEGMA-co-AEMA/EGDMA-Fe_xO_y systems bearing non-coated iron oxide (nano)particles were determined by using the PPMS system. Measurements were carried out at 5K and 300K. These measurements were carried out in the research laboratory of Prof. I. Giapintzakis at the University of Cyprus, by Dr. G. Athanasopoulos. Fig. 4.32 presents the magnetization *versus* applied magnetic field strength plots for three different composite co-networks in which 2, 4 and 7 wt% of magnetic Fe_xO_y (nano)particles are embedded. (Gel 3c, 3a and 3b, respectively)

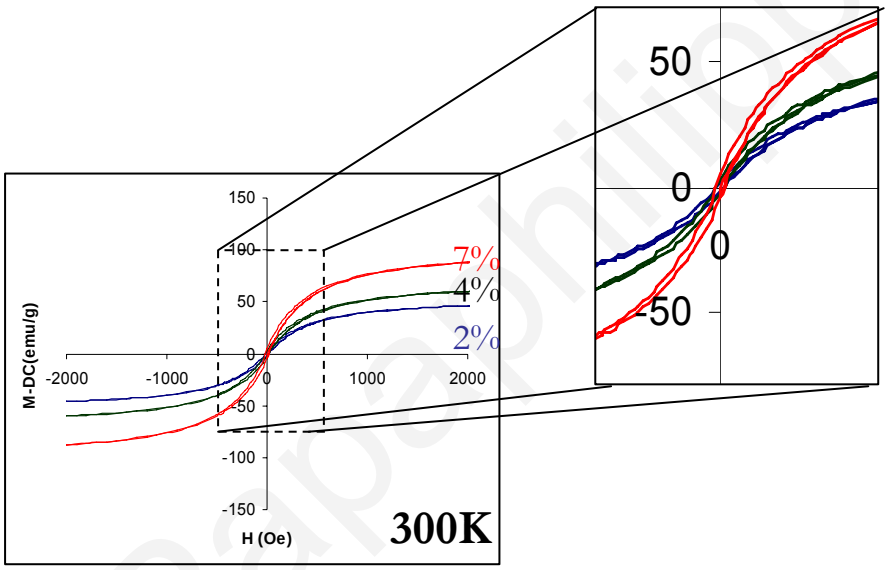

Figure 4.32. *Magnetization curves of the PEGMA-co-AEMA/EGDMA-Fe_xO_y corresponding to different magnetic loading (2- blue line, 4-green line and 7-red line % wt), measured at 300K.*

At 300K, a very small hysteresis loop exists in all cases (which is clearly observed in the magnification image presented in Fig. 4.32), indicating that the incorporation of the non-coated Fe_xO_y results in a ferrimagnetic behavior.

Moreover, the saturation magnetization Ms increases with an increase in the magnetic content within the composites (45, 54, 91 emu/g for the co-networks containing 2, 4 and 7% respectively). In this case the magnetization values were calculated based on the mass of the magnetic content (iron oxide).

Petri Papaphilippou

By comparing the Ms values among the series A, B and C, it can be observed that the magneto-responsive co-networks bearing the non-coated Fe_xO_y show higher values compared to the OA.Fe_3O_4-containing composites. This phenomenon may be attributed to the strong attractive forces developed between the non-coated Fe_xO_y leading to agglomeration thus larger particles exhibiting higher Ms values.[92]

In Fig. 4.33 the magnetization *vs* applied magnetic field strength plots recorded at 5K for the above-mentioned systems are illustrated. Obviously, upon decreasing the temperature from 300K down to 5K the hysteresis loop in all cases is more pronounced, demonstrating the ferrimagnetic behavior of these materials.

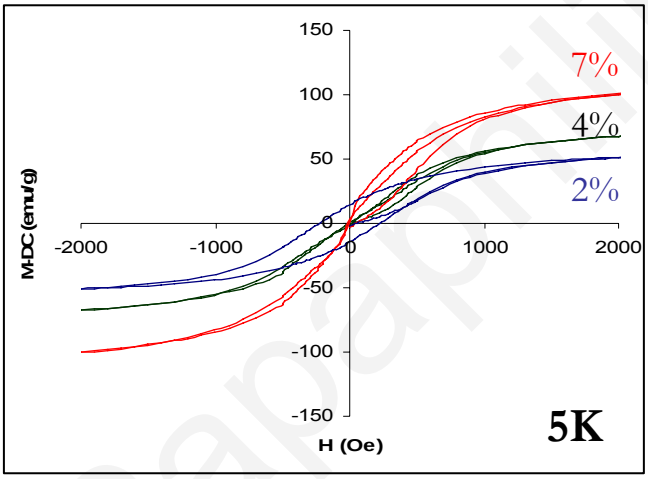

Figure 4.33. *Magnetization curves of the PEGMA-co-AEMA/EGDMA-Fe_xO_y corresponding to different magnetic loading (2- blue line, 4-green line and 7-red line wt%), measured at 5K.*

Petri Papaphilippou

4.2. PEGMA$_x$-b-AEMA$_y$ diblock copolymers: Biomineralization applications.

4.2.1. Preface.

The remarkable synthetic capability of biological organisms to produce intricate materials such as seashells, pearls and corals *by* "sculpturing" simple minerals (e.g $CaCO_3$, $Ca_3(PO_4)_2$) is certainly very impressive for every observer.[307] Biomineralization is a research field that deals with the formation of inorganic solids known as minerals, in the presence of organic materials. The existence of specific molecular interactions at the organic-inorganic interface may define the crystallographic orientation of inorganic particles. Such processes are characterised as "organic matrix-mediated" and the unusual nucleation of an inorganic mineral on the surface of an organic material involves surface and bulk processes[308]. The presence of organic matrices or molecules plays a crucial role in the nucleation and growth process of the minerals. Well-organized structures of various minerals characterized by different sizes and unusual shapes are presented in the literature, including *helical fibers, mesocrystals, complex spherical structures, hollow spheres, stars and sponge-like structures*.[309]

Different kind of organic additives affect the structure of well-known minerals such as the $CaCO_3$ and $BaCO_3$ including biopolymers, synthetic macromolecules, supramolecular assemblies like Langmuir monolayers and low-molecular-weight compounds.[310, 311]

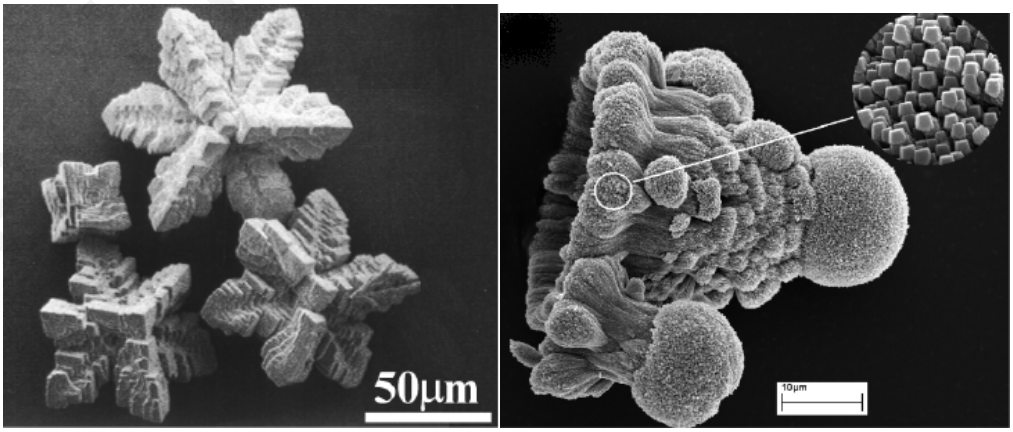

(a) ***(b)***

Figure 4.34. *SEM images of $CaCO_3$ crystals achieved in (a) in agarose gel and H_4hpdta ligand after 12 h (b).*[313, 312]

For example, *Mukkamala et. al.* synthesized calcium carbonate in its calcite form by controlling the crystal growth and thus the orientation and morphology of the crystals with the use of a small organic molecule namely 1,3-diamino-2-hydroxypropane-N, N, N', N'-tetraacetic acid (*H_4hpdta*) (Fig. 4.34*b)*. [313]

Moreover, it has been demonstrated that biomacromolecules such as insoluble collagen, chitin and soluble polymers such as proteins, glycoproteins and polysacharrides may act as effective agents for the crystal growth and morphology of minerals. For instance, agarose which is a linear polysaccharide comprised of the 1,3-linked β-D-galactose and 1,4-linked 3,6-anhydro-α-L-galactose, is capable of forming a homogeneous network. In the presence of the agarose network, the calcium carbonate crystals exhibit a unique star-shaped morphology (Fig. 4.34a).[313]

The efficiency of functional polymeric materials as active substrates for crystal nucleation is extensively reported in the literature.[314] Amphiphilic polymeric materials with the appropriate molecular architecture and functionalities, can serve as templates to control the nucleation, growth and alignment of inorganic particles. In particular, block copolymers bearing -$COCH_3$, COOH, or SO_3H functionalities have been proved capable of nucleating salts such as hydroxyapatite, calcite or CdS.[315] Block copolymers employed in such processes usually consist of one functional block segment capable of interacting with the surfaces of the inorganic mineral and another hydrophilic segment which provides dissolution in the aqueous media without interacting with the inorganic salt. For example, *Antonietti et. al.* have demonstrated that a PEO-*b*-PMAA-C_{12} block copolymer that has been end-functionalized with a dodecylamine group, promoted the controlled growth of calcium phosphate $Ca_3(PO_4)_2$ at various pHs. Hybrid nanofilaments arranged in an unusual neuronlike morphology were obtained.[316] Furthermore, block copolymers possessing a phosphonated block segment have been shown to effectively control the crystallization of $BaCO_3$ resulting in nanofiber morphologies.[317]

In the present work, preliminary investigations on the effect of the $PEGMA_x$-*b*-$AEMA_y$ diblock copolymers on the nucleation behaviour of malachite ($Cu_2(OH)_2CO_3$) have been carried out in aqueous solutions. Malachite is one of the most interesting minerals, commonly used in jewelry and is frequently employed in catalysts, coatings, and pigments. It is also used as a copper source to prepare other copper compounds with special

Petri Papaphilippou

morphologies, such as CuO, which has been widely exploited for diverse applications such as heterogeneous catalysts, gas sensors. These preliminary studies were carried out in the research group of Prof. H. Cölfen, by Dr. R. Song (Max-Planck Institute of Colloids and Interfaces, Germany).

4.2.2. Crystallization of malachite $Cu_2(OH)_2CO_3$ in the presence of the $PEGMA_x$-b-$AEMA_y$ in aqueous media.

Malachite has the tendency to crystalize in a biscuit-like morphology in the absence of any additives, as shown in the TEM images presented in Fig. 4.35.[318]

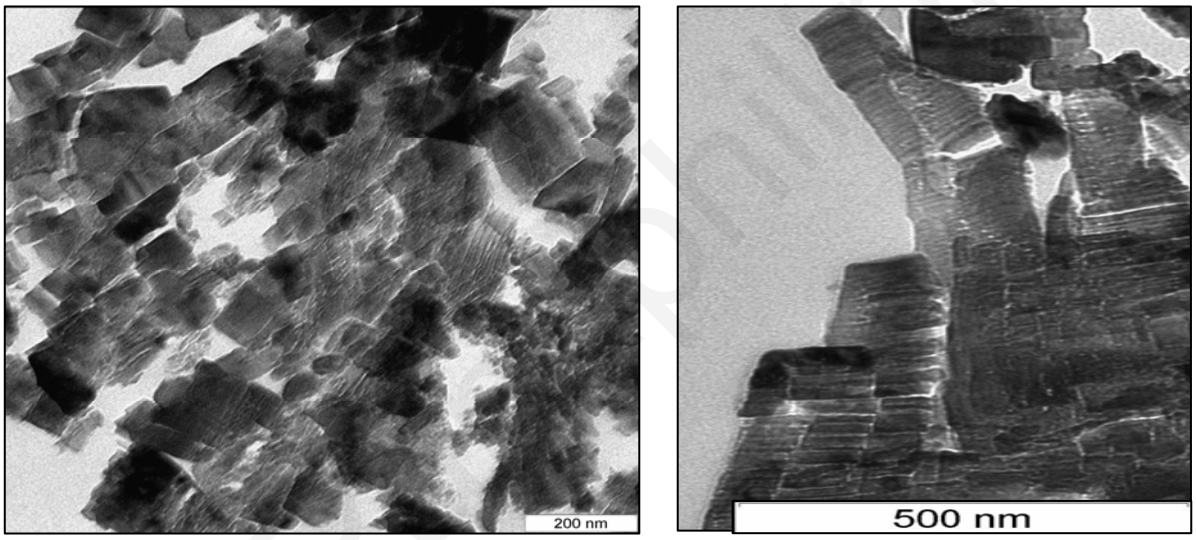

Figure 4.35. *TEM images of malachite nanobiscuits obtained in the absence of additives.*

As previously mentioned, in biomineralization processes functionalized molecules act as templates for the growth of nanocrystals. Specific interactions occurring between these molecules with some crystallographic surfaces of the initial nuclei, are responsible for controlling the size and shape of the final crystal structure of the inorganic product. Control over nucleation of an inorganic material can be also achieved by using supramolecular or colloidal pre-organization that can build-up a structural "cage" for the construction of an inorganic nanostructure (exo-template). For example, *Antonietti et al.* have reported the formation of "*nanonugget*" morphologies of gold colloids, resulting from the reduction of gold salts incorporated in poly(styrene sulfonate) microgels.[319]

Preliminary studies demonstrated that the $PEGMA_x$-*b*-$AEMA_y$ diblock copolymers strongly influence the mineralization process of malachite. TEM revealed the formation of malachite nanofibers which were further grown into unusual net-like superstructures (Figure 4.36.).[321]

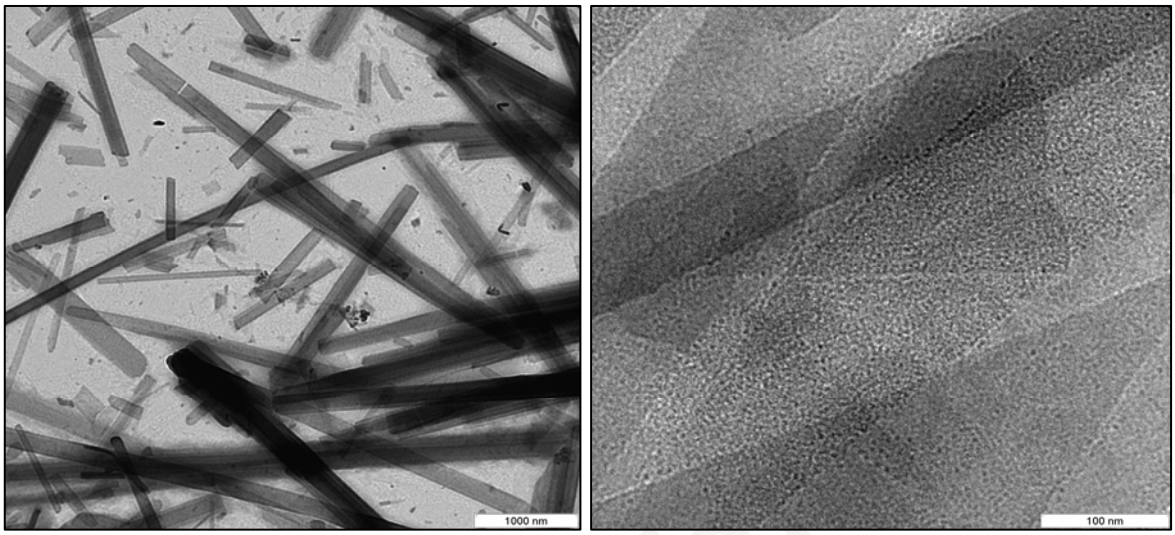

Figure 4.36. *TEM images of malachite "nanofibers" which are further grown into net-like superstructures, generated in the presence of a* $PEGMA_x$*-b-*$AEMA_y$ *diblock copolymer in an aqueous solution.*[318]

It might be possible that nucleation of malachite in the presence of the $PEGMA_x$-*b*-$AEMA_y$ block copolymer micelles generated in aqueous media, involves an "exo-template" route: Micelles of the $PEGMA_x$-*b*-$AEMA_y$ formed in an aqueous solution may act as an exo-template for the nucleation of malachite.

Further experiments are required for determining the mechanism involved in the formation of such morphologies. Future work towards this direction may include the systematic investigation of the effect of various parameters (polymer concentration, micellar shape) on the structural characteristics of malachite as well as the transformation of malachite into copper oxide. The latter material finds important applications in catalysis and in gas sensor technologies.

Petri Papaphilippou

4.3. Stimuli-responsive amphiphilic diblock copolymers containing pH and temperature-responsive functionalities: Synthesis, characterization and evaluation as drug release systems.

4.3.1. Preface.

Cancer or *malignant neoplasm* in medical terms is classified as one of the worst diseases affecting people at all ages. Cancer is usually treated by chemotherapy which is the most widely used cure with the combination of radiotherapy and surgery. In chemo, many therapeutic anticancer drugs are employed which, although they are effective in destroying cancer cells, they present significant toxicity effects. For example, doxorubicin (DOX) is one of the most commonly used chemotherapeutic drugs, which presents an excellent anti-tumor activity. Unfortunately, DOX has strong side effects causing the death of both, cancerous and healthy cells. Thus many attempts have been carried out aiming to decrease the toxicity of doxorubicin to normal tissues and improve its therapeutic efficacy upon encapsulation of the drug into polymer-based micellar drug delivery vehicles.[320]

The present work aimed towards the synthesis and characterization of well-defined hexa(ethylene glycol) methyl ether methacrylate-*block*-(2-diethylamino) ethyl methacrylate ($HEGMA_x$-*b*-$DEAEMA_y$) diblock copolymers and the evaluation of the corresponding micelles as pH-triggered drug delivery systems. HEGMA was chosen to be the repeating unit constituting the hydrophilic block within the block copolymer, due to its biocompatibility and improved blood circulation times as well as its thermoresponsive properties[213] whereas DEAEMA was chosen to be the hydrophobic segment due to its ability to turn from hydrophilic into hydrophobic and *vice versa* upon changing the pH.

4.3.1.1. Synthesis

RAFT polymerization was employed for the synthesis of well-defined diblock copolymers consisting of (2-diethylamino) ethyl methacrylate (DEAEMA) and hexa(ethylene glycol) methyl ether methacrylate (HEGMA). The synthesis of well-defined HEGMA-*b*-DEAEMA diblock copolymers has been already reported in the literature. *Vamvakaki and co-workers* have prepared a symmetric PHEGMA-*b*-PDEAEMA diblock copolymer by employing group

Petri Papaphilippou

transfer polymerization and investigated its solution properties as a function of the degree of ionization of the PDEAEMA block.[321] Moreover, the same group has reported on the use of PHEGMA-*b*-PDEAEMA diblock copolymer micelles and DEAEMA-containing microgels as containers for Pt nanoparticles.[322]

Although these systems are not novel in regards to their chemical structure, to the best of our knowledge this is the first systematic work dealing with the investigation of these polymers towards their controlled drug release ability, upon changing the pH. Furthermore, for the first time, RAFT controlled radical polymerization was employed for the preparation of these systems. The synthetic methodology followed is illustrated in Fig. 4.37.

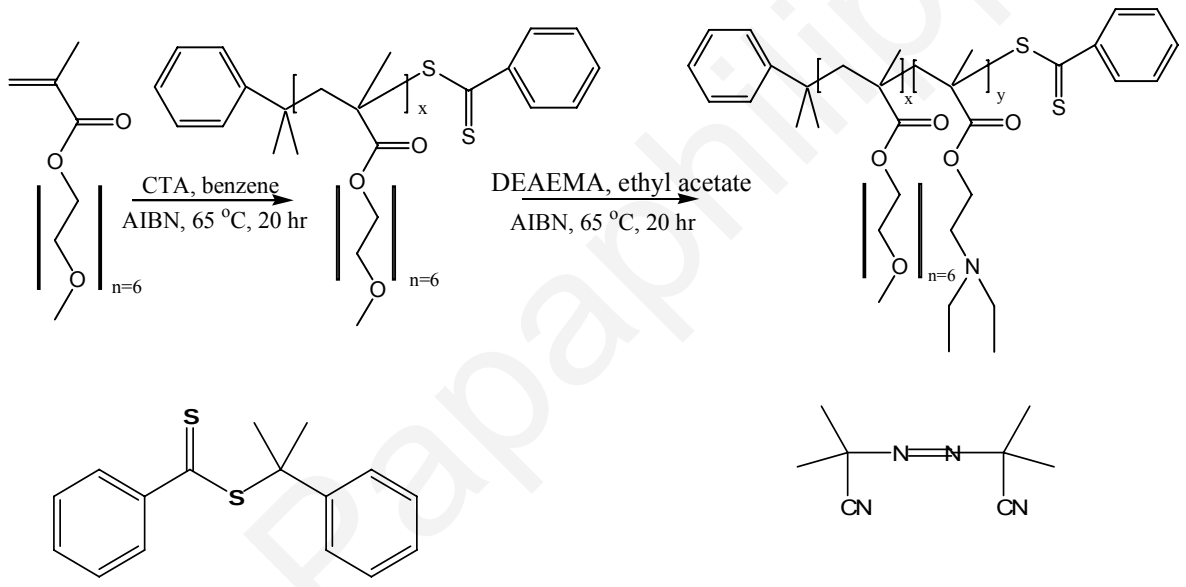

Figure 4.37. *Synthetic methodology followed for the preparation of the HEGMA$_x$-b-DEAEMA$_y$ diblock copolymers by RAFT.*

As shown in Fig. 4.37, the preparation of the HEGMA$_x$-*b*-DEAEMA$_y$ diblock copolymers was accomplished in two steps. HEGMA was polymerized first in benzene in the presence of CDTB and AIBN. The resulting HEGMA$_x$ homopolymer was then used as the macroCTA for the growth of the second block segment DEAEMA$_y$. Moreover, a DEAEMA$_x$-*b*-HEGMA$_y$ diblock copolymer was prepared upon polymerizing first the DEAEMA followed

Petri Papaphilippou

by the polymerization of the HEGMA. However this alternative route presented difficulties in terms of isolation and purification of the $DEAEMA_x$ homopolymer during the first step.

4.3.1.2 Characterization

The MW, MWD and chemical composition of the $HEGMA_x$ and $DEAEMA_x$ homopolymers and the corresponding $HEGMA_x$-*b*-$DEAEMA_y$ diblock copolymers were determined by SEC and ^{1}H NMR, respectively. These results are presented in Table 4.6.

Table 4.6. *Characteristics of the polymers based on HEGMA and DEAEMA obtained by RAFT (MWs, MWDs and Compositions).*

Homopolymers[a]	Sample code	SEC[b] Mn	PDI	^{1}H-NMR MW (g/mol)
$HEGMA_{128}$	PPR18	38700	1.25	-
$DEAEMA_{30}$	PPR34	5548	1.16	-
$HEGMA_{121}$	PPR37	36300	1.21	-
Diblock Copolymers[a]				
$HEGMA_{128}$-*b*-$DEAEMA_{34}$	PPR28	39211	1.16	45000
$HEGMA_{128}$-*b*-$DEAEMA_{18}$	PPR36	39593	1.25	41700
$HEGMA_{121}$-*b*-$DEAEMA_{18}$	PPR39	39331	1.18	41700
$DEAEMA_{30}$-*b*-$HEGMA_{210}$	PPR41	92808	1.48	68600

[a] Determined by SEC and ^{1}H NMR. [b] SEC calibrated with PMMA standards, *M*n number average molecular weight, PDI: polydispersity index. PEGMA: poly(ethylene glycol) methyl ether methacrylate; AEMA: 2-(acetoacetoxy) ethyl methacrylate, n.d.: not determined.

Fig. 4.38 exemplarily shows the SEC traces of the $DEAEMA_{30}$ homopolymer and the corresponding $HEGMA_{121}$-*b*-$DEAEMA_{18}$ diblock copolymer. The SEC eluogram of the diblock copolymer is slightly shifted towards higher MWs compared to that of the $HEGMA_{18}$, demonstrating the block efficiency from homopolymer to block copolymer.

Petri Papaphilippou

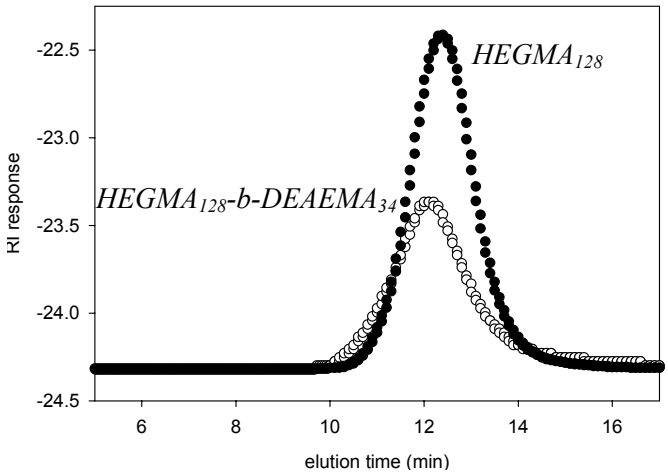

Figure 4.38. *SEC traces of the HEGMA$_{34}$ homopolymer and the corresponding HEGMA$_{128}$-b-DEAEMA$_{34}$ diblock copolymer.*

^{1}H NMR spectroscopy confirmed the expected chemical structure of the diblock copolymers. Figure 4.39 illustrates the ^{1}H NMR spectrum of the DEAEMA$_{30}$-*b*-HEGMA$_{210}$ diblock copolymer. The peak assignments are shown in the spectrum.

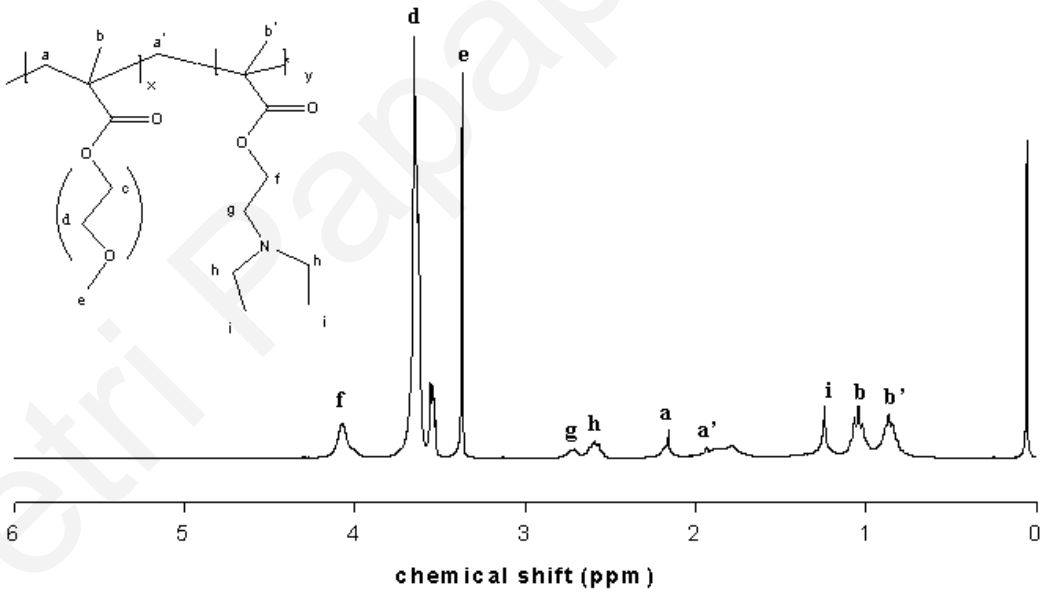

Figure 4.39. *^{1}H NMR spectrum of the DEAEMA$_{30}$-b-HEGMA$_{210}$ diblock copolymer recorded in CDCl$_{3}$.*

Petri Papaphilippou

The molar ratios of the two blocks were calculated by using the relative intensities between the $–CH_2$ signal corresponding to the DEAEMA (g) units and the $-CH_3$ signal corresponding to the HEGMA (e) units, appearing at 2.71 and 3.39 ppm, respectively.

TGA measurements of the $DEAEMA_{30}$ homopolymer and the corresponding $DEAEMA_{30}$-*b*-$HEGMA_{210}$ diblock copolymer were performed to determine the polymer decomposition temperatures.

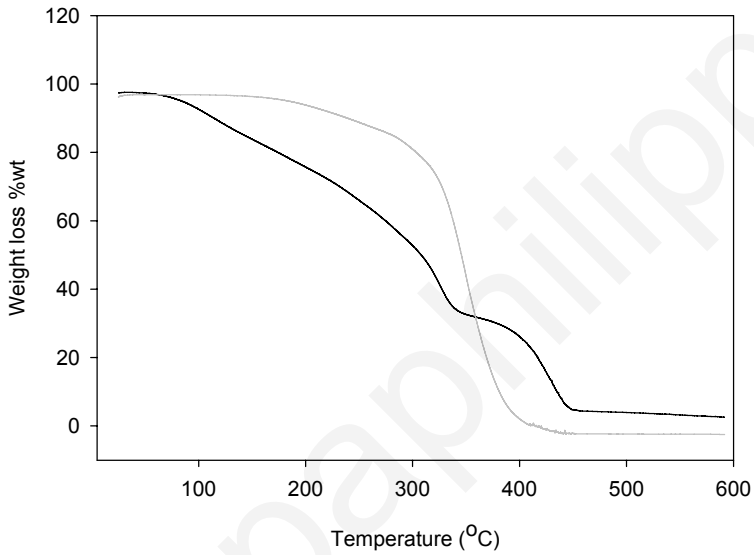

Figure 4.40. *TGA thermograms of $DEAEMA_{30}$ homopolymer (black line) and the $DEAEMA_{30}$-b-$HEGMA_{210}$ diblock copolymer (grey line).*

In Fig. 4.40, the TGA traces of the above-mentioned systems are shown. As seen in the figure, the decomposition of the homopolymer begins at ~ 100 °C and ends at ~ 450 °C *via* a two-step decomposition process. The TGA thermogram of the $DEAEMA_{30}$-*b*-$HEGMA_{210}$ diblock copolymer begins at higher temperatures at about 200 °C and ends at ~ 400 °C.

Petri Papaphilippou

4.3.1.3. Fabrication of DOX-loaded HEGMA$_x$-b-DEAEMA$_y$ micelles.

Synthesis

A general description of the methodology followed to prepare DOX-loaded HEGMA$_x$-*b*-DEAEMA$_y$ micelles is given as follows: The anti-cancer drug doxorubicin (DOX) was loaded into the HEGMA$_x$-*b*-DEAEMA$_y$ diblock copolymer micelles using the oil/water emulsion method. DOX loading was quantified by measuring the absorbance at 490 nm (characteristic absorption wavelength of DOX). The concentration of the DOX that has been loaded into the micelles was then determined by using the absorption *vs* concentration calibration curve constructed by measuring the absorbance of DOX.HCl solutions of known concentrations prepared in DPBS, as shown in Fig. 4.41.

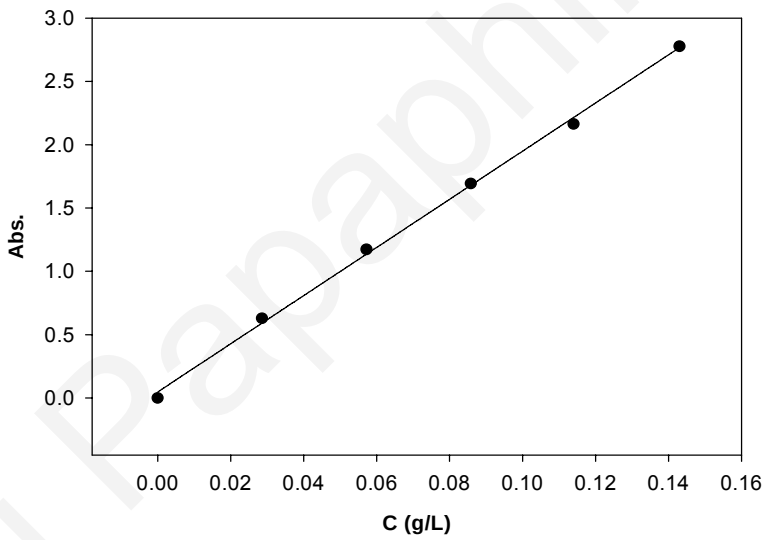

Figure 4.41. *Calibration curve of DOX.HCl in different concentrations in DPBS.*

The drug content within the HEGMA-*b*-DEAEMA micelles was determined by using the following equation: % loaded drug = [mass of the encapsulated drug/total mass of the drug] x 100, and it was found to range between ~ 3 - 6.5% which is similar (1.3-4.4%) to the of DOX loaded inside the micellar core of the MPEG-*b*-PCL diblock copolymer.[320]

Petri Papaphilippou

pH-dependent DOX release from the HEGMA$_x$-b-DEAEMA$_y$ micelles.

The presence of pH-responsive DEAEMA moieties in the HEGMA$_x$-*b*-DEAEMA$_y$ micelles renders these systems capable of responding to pH changes occurring in the surrounding environment. In particular, the DEAEMA units are hydrophobic (non-ionizable) above a certain pH value (the pKa value of the DEAEMA) whereas below this value they become ionizable and hydrophilic (Fig. 4.42a).

Titration experiments were carried out in order to determine the pKa value of the DEAEMA$_y$ block segment within the HEGMA$_x$-b-DEAEMA$_y$. The latter was found to be ~ 6.8 as seen in the titration curve presented in Fig. 4.42 b.

(a)

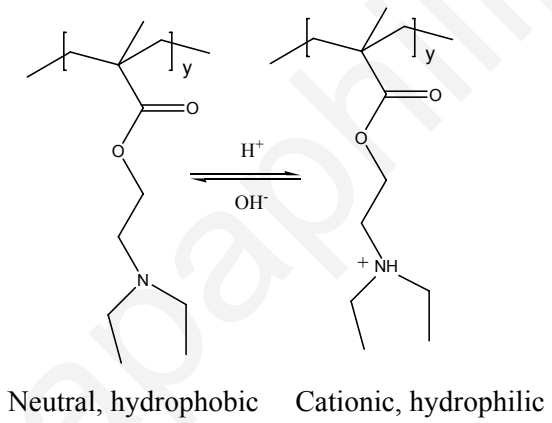

(b)

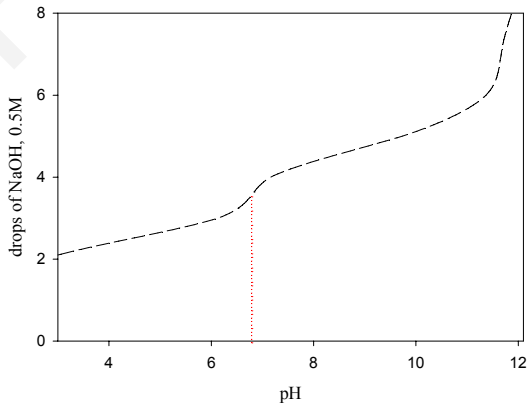

Figure 4.42. *(a) Protonation of the DEAEMA units upon lowering the pH, resulting in a hydrophilic character (b) Titration curve of the HEGMA$_x$-b-DEAEMA$_y$ diblock copolymer.*

In aqueous media at pH values greater than 6.8, micelles are formed by the HEGMA$_x$-*b*-DEAEMA$_y$ diblock copolymers. These micelles consist of a hydrophilic HEGMA corona and

Petri Papaphilippou

a hydrophobic DEAEMA core. Upon protonation of the DEAEMA units at lower pHs rendering them hydrophilic, these micelles are expected to dissociate into unimers. The above-mentioned mechanism may be used for controlled release of pharmaceutical compounds at specific sites in the body characterized by lower pHs (for example in the vicinity of cancerous cells) as schematically illustrated in Fig. 4.43.

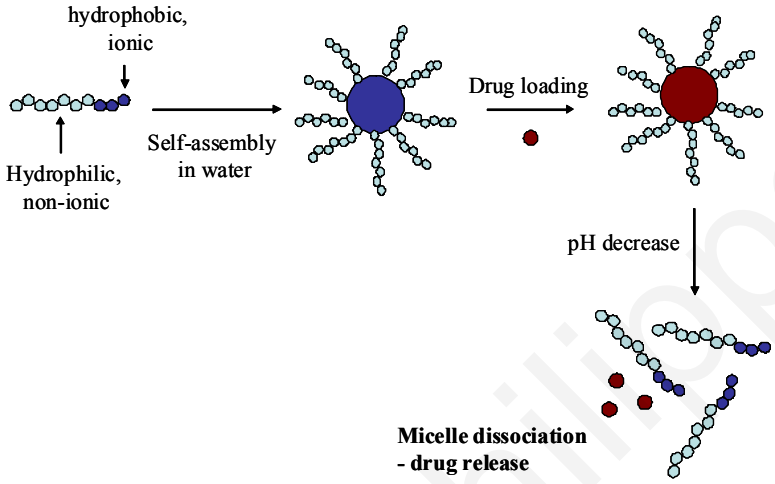

Figure 4.43. *Self-assembly of PEGMA$_x$-b-DEAEMA$_y$ block copolymers in micelle form in aqueous solution at pH > 6.8. Hydrophobic drug such as DOX can be loaded inside the core of the micelles. At acidic pHs, DEAEMA are protonated and become hydrophilic resulting the dissociation of the micelles and eventually the drug is released.*

In DPBS solution where the pH is about 7.2 (above the pKa = 6.8 of the DEAEMA units), the HEGMA$_x$-*b*-DEAEMA$_y$ block copolymers self-assemble into micelles consisting of a HEGMA hydrophilic corona and a DEAEMA hydrophobic core. The latter serves as a nano-container for the encapsulation of hydrophobic pharmaceutical compounds such as DOX *via* the presence of attractive hydrophobic interactions developed between the drug and the hydrophobic (neutral) DEAEMA units. Upon decreasing the pH below the pKa, the DEAEMA units become hydrophilic resulting in the collapsing of the micelles into unimers and the release of the drug. Besides their pH-responsive properties, the HEGMA$_x$-*b*-DEAEMA$_y$ diblock copolymers exhibit also thermoresponsive behavior due to the presence of the HEGMA block segment. Consequently, these systems might be promising candidates for the controlled drug release *via* two different mechanisms, based on either temperature, or pH changes in the surrounding environment.

Petri Papaphilippou

Kinetic drug release measurements were carried out upon immersing a dialysis cassette containing the drug loaded micellar solution prepared in DPBS (pH = 7.2) into: (a) acetate buffer solution (pH = 4.6) and (b) citric acid buffer solution (pH = 6.0). The micellar solution was removed periodically from the dialysis cassette and after its absorbance was measured at ~ 490-500 nm, it was returned back to the cassette. This process was repeated several times until the drug was released from the micelles.

Kinetic studies were performed for two different block copolymer systems as follows:

a. DOX-release from $HEGMA_{128}$-*b*-$DEAEMA_{34}$ micelles at pH = 4.6
b. DOX-release from $HEGMA_{128}$-*b*-$DEAEMA_{34}$ micelles at pH = 6.0
c. DOX-release from $DEAEMA_{30}$-*b*-$HEGMA_{210}$ micelles at pH = 4.6
d. DOX-release from $DEAEMA_{30}$-*b*-$HEGMA_{210}$ micelles at pH = 6.0

Fig. 4.44 exemplarily presents the UV-Vis spectra of the DOX-loaded $HEGMA_{128}$-*b*-$DEAEMA_{34}$, recorded at different time intervals after having the dialysis cassette containing the micellar solution immersed into the acetate buffer solution (pH 6.0). Since the absorption recorded at ~ 500 nm corresponding to the drug that is present within the micelles decreases with time, it is clearly demonstrated that at pH = 6, the micellar aggregates collapse (upon protonation of the DEAEMA units) resulting in the release of the drug.

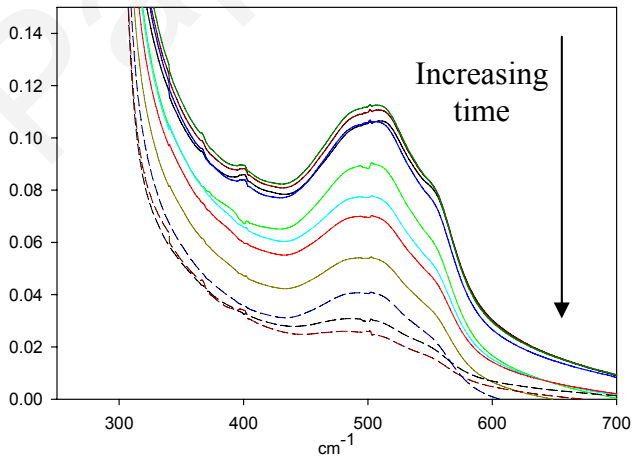

Figure 4.44. *UV-Vis spectra of the DOX-loaded $HEGMA_{128}$-b-$DEAEMA_{34}$ micelles recorded at several time intervals (pH 6.0).*

Petri Papaphilippou

Fig. 4.45 presents the absorption (at ~ 490-500 nm) *versus* time plots corresponding to: (a) the DOX-loaded $HEGMA_{128}$-*b*-$DEAEMA_{34}$ micelles at pH 6.0 and 4.6 and (b) the DOX-loaded $DEAEMA_{30}$-*b*-$HEGMA_{210}$ micelles at pH 6.0 and 4.6.

(a)

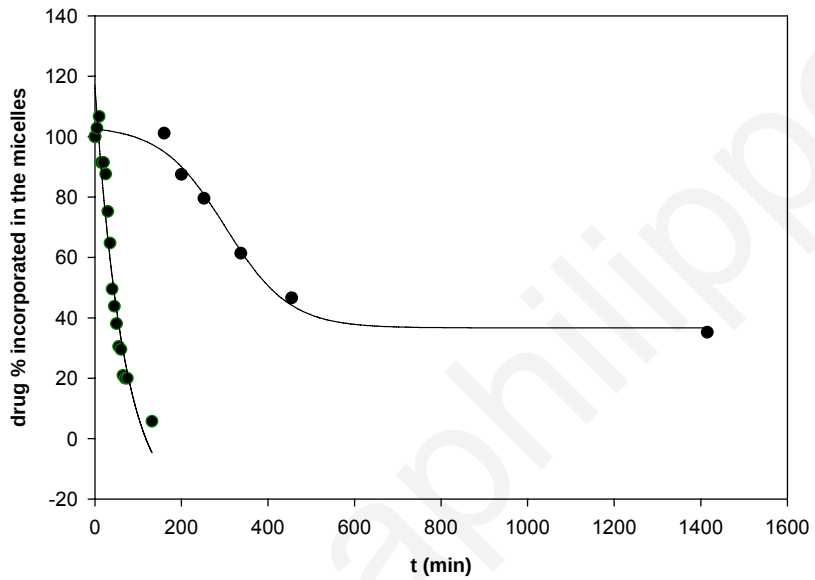

(b)

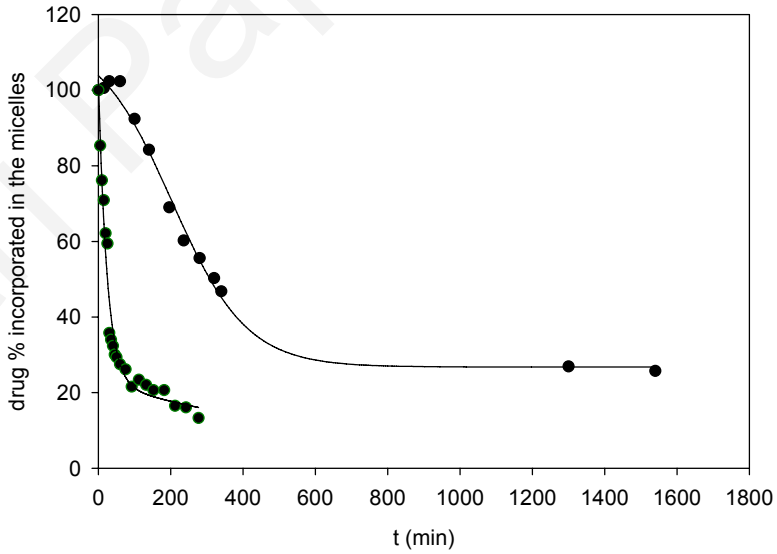

Figure 4.45. *DOX release kinetics from (a) $PEGMA_{128}$-b-$DEAEMA_{34}$ and (b) $DEAEMA_{30}$-b-$PEGMA_{210}$ micelles at different pHs at room temperature: pH 4.6 (green), pH 6.0 (black).*

Petri Papaphilippou

From the plots presented in Fig. 4.45, it can be observed that the DOX release rate from the micelles is accelerated upon decreasing the pH of the outer environment from 6.0 to 4.6. Similar observations (i.e. faster drug release rate from pH-responsive micellar systems at lower pHs) have been reported in the literature.[137, 153, 323]

4.3.1.4. In-vitro assessment of antiproliferative and pro-apoptotic efficacy of DOX-loaded HEGMA-b-DEAEMA micelles.

The potential toxicity of the HEGMA-*b*-DEAEMA micelles (DOX-loaded and unloaded) on MB231 breast cancer cell viability in culture was assessed against DPBS (pH = 7.2) following incubation with various concentrations of the micelles (0.01-0.1 g/L) over 72 h (Fig. 4.46). This work was carried out in collaboration with Dr. A. Odysseos and Dr. Y. Christou, EPOS-Iasis R&D, Biomedical Tissue Engineering/Nanobiotechnology Lab.

Fig. 4.46*a* demonstrates that in the presence of free DOX the viability of MB231 breast cancer cells was dramatically compromised. Compared to free DOX, cell viability was higher with micelles loaded with DOX (MD1).[321] In line with this observation unloaded micelles showed the highest cell viability as expected. However, as seen from the plots the cell viability decreases upon increasing the concentration of the micellar solutions, in both, the loaded and the unloaded systems. This finding is attributed to the presence of organic solvent residues entrapped into the polymeric materials during the polymerization process, which were not effectively removed from the materials upon drying. *Shuai et al.* showed that cell viability decreases extensively in the presence either of free DOX or DOX-loaded (MPEG-b-PCL) in the drug concentration range from 0.01 to 10 μM. [320]

Fig. 4.46*b* shows that the unloaded micelles M1 demonstrated the highest cell viability. The loaded micelles MD1 and MD3 exhibited similar viability effects. This could be due to the similar molecular weight of the hydrophobic block (DEAEMA). Furthermore, viability was decreased upon increasing concentrations of MD1 or MD3, whereas in the case of MD2 cell viability did not differ upon increasing its concentration. In Fig. 4.47 the brightfield microscopy images of MB231 following treatment with the unloaded and loaded micelles and the free DOX are presented. Cell death is occurred when free drug is introduced, whereas cell viability improves significantly when DOX is encapsulated within the micelles.

Petri Papaphilippou

(a)

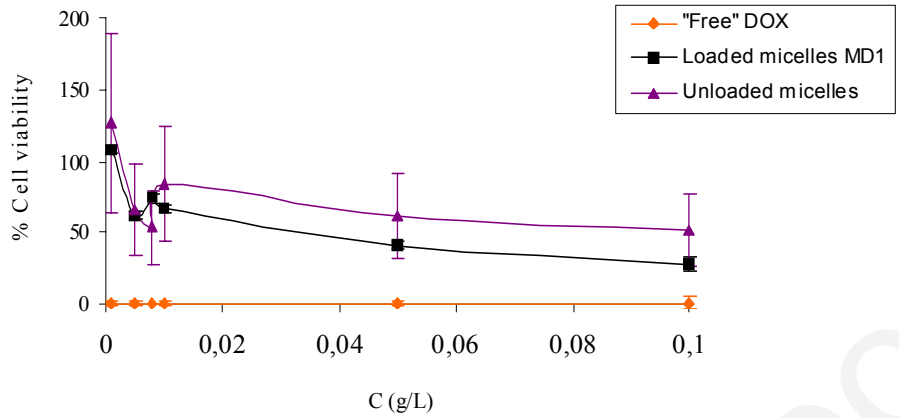

(b)

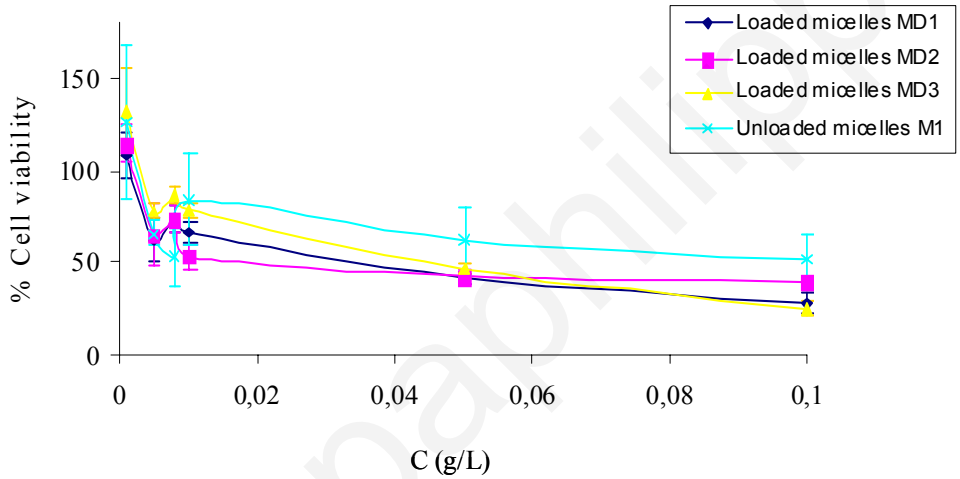

Figure 4.46. *(a)The MTT colorimetric assay was used to assess the cell viability of the loaded and unloaded micelles on MB231 breast cancer cells. For comparison, cell viability was also determined in the presence of free DOX. Untreated cells in the presence of only DPBS (control) were considered to have 100% viability and the results were normalized accordingly. Results are given as the means of six values resulting from triplicate measurements of two representative experiments; ±SD. Variability of the error bars principally corresponds to the experimental uncertainty in each measurement. (b) Cell viability studies carried out of three different systems: HEGMA$_{120}$-b-DEAEMA$_{34}$/DOX (MD1), HEGMA$_{121}$-b-DEAEMA$_{18}$/DOX (MD2), DEAEMA$_{30}$-b-HEGMA$_{210}$ (MD3).*

Petri Papaphilippou

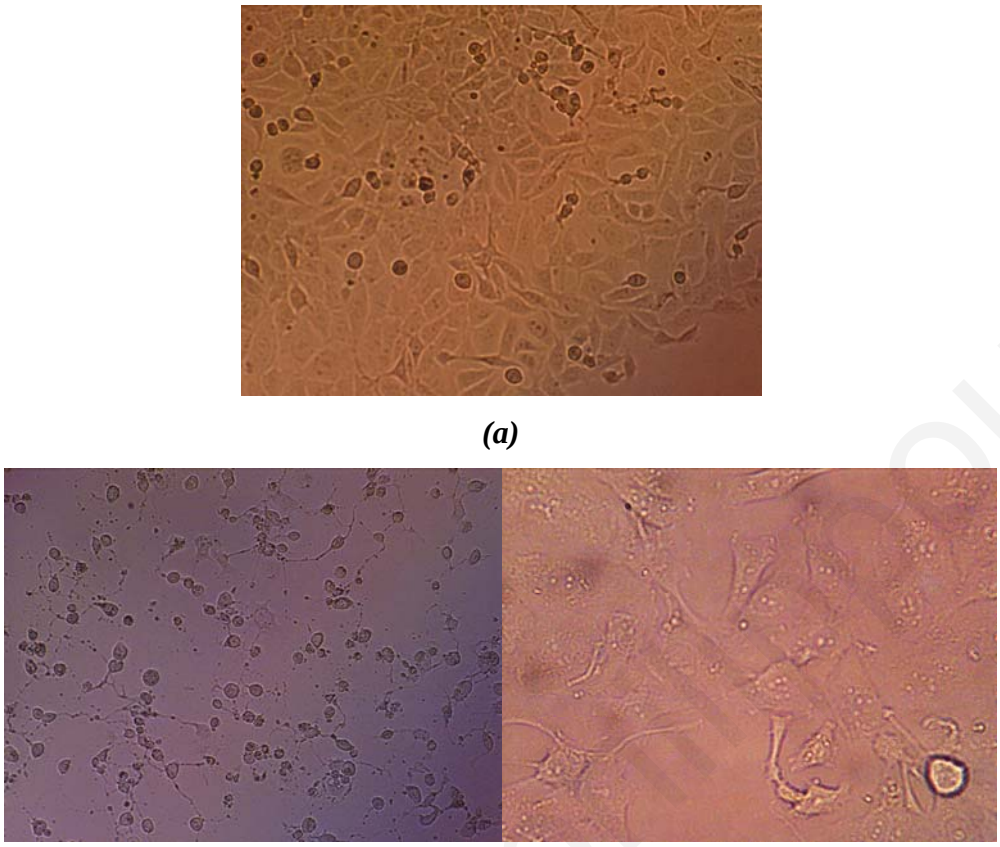

(a)

(b) ***(c)***

Figure 4.47. *Bright-field microscopy images of MB231 cells. (a) Unloaded micelle-treated cells (b) Free DOX treated cells, then are rounded suggestive of necrosis. (c) Loaded DOX-micelle treated cells; they demonstrate condensed nuclei (higher magnification) suggestive of apoptosis.*

Petri Papapanou

[204] P. Papaphilippou, L. Loizou, N. C. Popa, A. Han, L. Vekas, A. Odysseos, T. Krasia-Christoforou, *Biomacromolecules,* 10, **2009**, 2662.

[205] T. Krasia, R. Soula, H. G. Borner, H. Schlaad, *Chem. Commun.,* 4, **2003**, 538.

[206] J-F Lutz, S. Stiller, A. Hoth, L. Kaufner, U. Pison, R. Cartier, *Biomacromolecules*, 7, **2006**, 3132.

[207] J. Chiefari, Y. K. Chong, F. Ercole, J. Krstina, J. Jeffrey, T.P.T. Le, R. Mayadunne, G. F. Meijs, C. L. Moad, G. Moad, E. Rizzardo, S. H. Thang, *Macromolecules*, 31, **1998**, 5559.

[208] G. Moad, E. Rizzardo, S. H. Thang, *Aust. J. Chem.,* 58, **2005**, 379.

[209] G. Moad, E. Rizzardo, S. H. Thang, *Aust. J. Chem.,* 59, **2006**, 669.

[210] G. Dimarco, M. Lanza , M. Pieruccini, *Solid State Ionics,* 89, **1996**, 117.

[211] J. F. Lutz, *J. Polym. Sci., Part A : Polym. Chem.,* 46, **2008**, 3459.

[212] J-F Lutz, O. Akdemir, A. Hoth, *J. Am. Chem. Soc.,* 128, **2006**, 13046.

[213] J-F Lutz, A. Hoth, *Macromolecules,* 39, **2006**, 893.

[214] B. Zhao, D. Li, F. Hua, D. R. Green, *Macromolecules*, 38, **2005**, 9509.

[215] Y. Maeda, T. Kubota, H. Yamauchi, T. Nakaji, H. Kitano, *Langmuir,* 23, **2007**, 11259.

[216] S. Chen, Y. Li, C. Guo, J. Wang, J. Ma, X. Liang, L-R Yang, H-Z Liu, *Langmuir*, 23, **2007**, 12669.

[217] S. R. Wan, J. S. Huang, M. Guo, H. Zhang, Y. Cao, H. Yan, K. J. Liu, *Biomed. Mater. Res.*, 80A, **2007**, 946.

[218] T. Neuberger, B. Schopf, H. Hofmann, M. Hofmann, B. Von Rechenberg, *J. Magn. Magn. Mater.,* 293, **2005**, 483.

[219] C. R. Heald, S. Stolnik, K. S. Kujawinski, C. De Matteis, M. C. Garnett, L. Illum, S. S. Davis, S. C. Purkiss, R. J. Barlow, P. R. Gellert, *Langmuir*, 18, **2002**, 3669.

[220] Y. Liu, L. Wang, C. Pan, *Macromolecules*, 32, **1999**, 8301.

[221] R. Massart, *IEEE Trans. Magn.,* 17(2), **1981**, 1247.

[222] S. Shouheng, H. Zeng, *J. Am. Chem. Soc*., 124, **2002**, 8204.

[223] D. K. Kim, M. Mikhaylova, Y. Zhang, M. Muhammed, *Chem. Mater*., 15, **2003**, 1617.

[224] Y-S. Kang, S. Risbud, J. F. Rabolt, P. Stroeve, *Chem. Mater*., 8, **1996**, 2209.

[225] D. Bica L. Vekas, M. V. Avdeev, O. Marinica, V. Socoliuc, M. Balasoiu, *Journal of Magnetism and Magnetic Materials*, 311, **2007**, 17.

[226] K. Hanabusa, T. Suzuki, T. Koyoama, H. Shirai, *Macromol. Chem.,* 193, **1992**, 2149.

[227] M. M. Dell' Anna, P. Mastrorilli, A. Rizzuti, G. P. Suranna, C. F. Nobile, *Inorg. Chim. Acta.,* 304, **2000**, 21.

Petri Papaphilippou

[228] M. M. Dell' Anna, M. Gagliardi, P. Mastrorilli, G. P. Suranna, C. F. Nobile, *J. Mol. Catal. A,* 304, **2000**, 515.

[229] T. Krasia, H. Schlaad, "*In Metal Containing and Metall-supramolecular Polymers and Materials*" G. R. Newkome, I. Manners, U. S. Schubert, Eds., ACS Symposium Series 928, American Chemical Society: Washington, DC, **2006**, 157.

[230] A. Pich, S. Bhattacharya, Y. Lu, V. Boyko, H-J Adler, *Langmuir*, 20, **2004**, 10706.

[231] F. Suriano, O. Coulembier, P. Degee, P. Dubois, *J. Polym. Sci., Part A : Polym. Chem.,* 46, **2008**, 3662.

[232] L. Jiang, W. Sun, J. Kim, *Materials Chemistry and Physics*, 101, **2007**, 291.

[233] S. Wan, Y. Zheng, Y. Liu, H. Yan, K. Liu, *J. Mater. Chem.,* 15, **2005**, 3424.

[234] L. C. Li, J. Jiang, F. Xu, *Mater. Lett.,* 61, **2007**, 1091.

[235] K. R. Reddy, K-P Lee, A. I. Gopalan, *J. Appl. Polym. Sci.,* 106, **2007**, 1181.

[236] M. Hamoudeh, A. A. Faraj, E. Canet-Soulas, F. Bessueille, D. Leonard, H. Fessi, *International Journal of Pharmaceutics,* 338, **2007**, 248.

[237] G. DiMarco, M. Lanza, M. Pieruccini, *Solid State Ionics,* 89, **1996**, 117.

[238] A. Kaiser, T. Gelbrich, A. M. Schmidt, *J. Phys.:Condens. Matter.,* 18, **2006**, S2563.

[239] T. Gelbrich, M. Feyen, A. M. Schmidt, *Macromolecules,* 39, **2006**, 3469.

[240] H. Lee, E. Lee, K. Do Kim, N. K. Jang, Y. Y. Jeong, S. Jon, *J. Am. Chem. Soc.,* 128, **2006**, 7383.

[241] S. Metz, G. Bonaterra, M. Rudelius, M. Settles, E. J. Rummeny, H. E. Link Daldrup, *Eur. Radiol.,* 14, **2004**, 1851.

[242] S. Iijima, *Nature*, 354, **1991**, 56.

[243] S-R Ji, C. Liu, B. Zhang, F. Yang, J. Xu, J. Long, C. Jin, D-L Fu, Q-X Ni, X-J Yu, *Biochimica et Biophysica Acta*, **2010**.

[244] A. A. Faraj, K. Cieslar, G. Lacroix, S. Gaillard, E. Canet-Soulas, Y. Cremillieux, *Nano Letters,* 9(3), **2009**, 1023.

[245] C. Huiqun., Z. Meifang, L. Yaogang, *Journal of Solid State Chemistry,* 179, **2006**, 1208.

[246] H. Wang, L. Cao, S. Yan, Z. Huang, Z. Xiao, *Materials Science and Engineering B*, 164, **2009**, 191.

[247] L. Zhang, Q-Q Ni, T. Natsuki, Y. Fu, *Applied Surface Science,* 255, **2009**, 8676.

[248] P. Xu, D. Cui, B. Pan, F. Gao, R. He, Q. Li, T. Huang, C. Bao, H. Yang. *Applied Surface Science*, 254, **2008**, 5236.

[249] L. Jiang, L. Gao, *Chem. Mater.,*15, **2003**, 2848.

[250] B. Jia, L. Gao, J. Sun, *Carbon,* 45, **2007**, 1476.

[251] C. Huiqun, Z. Meifang, L. Yaogang, *J. Magn. Mater.,* 305, **2006**, 321.

[252] I.T. Kim, G. A. Nunnery, K. Jacob, J. Schwartz, X. Liu, R. Tannenbaum, *J. Phys. Chem. C*, 114, **2010**, 6944.

[253] A. Hirsch, *Angw. Chem. Int. Ed.,* 40 (11), **2002**, 1853.

[254] C. A. Dyke, J. M. Tour, *J. Phys. Chem. A,* 108, **2004**, 11151.

[255] Y. Zhang, H. He, C. Gao, J. Wu, *Langmuir*, 25(10), **2009**, 5814.

[256] W. Shen, Z. Li, Y. Liu, *Recent Patents on Chemical Engineering*, 1, **2008**, 27.

[257] I. D. Rosca, F. Watari, M. Uo, T. Akasaka, *Carbon*, 43, **2005**, 3124.

[258] (a) Z. Spitalsky, D. Tasis, K. Papagelis, C. Galiotis, *Progress in Polymer Science*, 35(3), **2010**, 35. (b) J. Li, W-D He, L-P Yang, X-L Sun, Q. Hua, *Polymer*, 48(15), **2007**, 4352.

[259] F-M Xu, J-P Xu, J. Ji, J-C Shen, *Colloids and Surfaces B: Biointerfaces*, 67(1), **2008**, 67.

[260] S. Bose, R. A. Khare, P. Moldenaers, *Polymer*, 51, **2010**, 975.

[261] V. N. Bliznyuk, S. Singamaneni, R. L. Sanford, D. Chiappetta, B. Crooker, P. V. Shibaev, *Polymer*, 47, **2006**, 3915.

[262] B. Z. Tang, H. Xu, *Macromolecules*, 32, **1999**, 2569.

[263] L. Kong, X. Lu, W. Zhang, *Journal of Solid State Chemistry*, 181, **2008**, 628.

[264] V. Georgakilas, V. Tzitzios, D. Gournis, D. Petridis, *Chem. Mater.,* 17(7), **2005**, 1613.

[265] T. M. Wu, S. J. Yen, E. C. Chen, R. K. Chiang, *Journal of Polymer Science Part B: Polymer Physics,* 46, **2008**, 727.

[266] C. Qin, J. Shen, Y. Hu, M. Ye, *Composites Science and Technology*, 69, **2009**, 427.

[267] C. Gao, W. Li, H. Morimoto, Y. Nagaoka, T. Maekawa, *Journal of Physical Chemistry B*, 110(14), **2006**, 7213.

[268] Q. Zhang, M. Zhu, Q. Zhang, Y. Li, H. Wang, *Composites Science and Technology*, 69, **2009**, 633.

[269] P. C. Papaphilippou , T. Krasia-Christoforou et al., in Preparation.

[270] C. Y. Hong, Y. Z. You, C. Y. Pan, *Polymer,* 47, **2006**, 4300.

[271] Y. X. Zhao, I. L. Spain, *Phys. Rev. B*, 40, **1989**, 993.

[272] T-M. Wu, S.-J. Yen, E.-C. Chen, R.-K. Chiang, *Journal of Polymer Science Part B: Polymer Physics*, 46, **2008**, 727.

[273] T. Krasia, H. Schlaad, C. Patrickios, *Macromolecules*, 34, **2001**, 7585.

[274] J. Feng, W. Cai, J. Sui, Z. Li, J. Wan, W. Ali, A. N. Chakoli, *Polymer,* 49, **2008**, 4989.

Petri Papaphilippou

[275] C. S. Patrickios, T. K. Georgiou, *Curr. Opin. Colloid Interface Sci.,* 8, **2003**, 76.

[276] N. Badi, J-F Lutz, *Journal of Controlled Release*, 140, **2009**, 224.

[277] S. S. Nitin, J. Z. Hilt, *Journal of Controlled Release*, 130, **2008**, 246.

[278] L. Klouda, A. G. Mikos, *Eur. J. Pharm. Biopharm.,* 68, **2008,** 34.

[279] C. Alvarez-Lorenzo, L. Bromberg, A. Concheiro, *Photochem. Photobiol.,* 85, **2009**, 848.

[280] P. J. Resendiz-Hernandez, O. S. Rodriguez-Fernandez, L. A. Garcia-Cerda, *J. Magn. Magn. Mater*., 320, **2008**, e373.

[281] R. V. Kulkarni, S. Biswanath, *J. Appl. Biomater. Biomech*., 5, **2007**, 125.

[282] R. A. Frimpong,, S. Fraser, J. Z. Hilt, *Journal of Biomedical Materials Research Part A,* 80a, **2007,** 1.

[283] N. Sahiner, *Colloid and Polymer Science,* 285, **2006**, 283.

[284] R. Yoshida, K. Sakai, T. Okano, Y. Sakurai, *Adv. Drug Deliv. Rev.,* 11, **1993**, 85.

[285] L. Dong, H. Jiang, Soft Matter, 3, **2007**, 1757.

[286] T-Y. Liu, S-H. Hu, K-H. Liu, D-M Liu, S-Y Chen, *Journal of Controlled Release*, 126, **2008**, 228.

[287] T. Y. Liu, S.-H. Hu, T-Y. Liu, D-M Liu, S-Y Chen*, Langmuir*, 22, **2006**, 5974.

[288] Y. Y. Liang, L. M. Zhang, W. Jiang, *ChemPhysChem.,* 8, **2007**, 2367.

[289] D. Szabo, G. Szeghy, M. Zrinyi, *Macromolecules*, 31, **1998**, 6541.

[290] P. C. Papaphilippou, A. Pourgouris, O. Marinica, A. Taculescu, G. I. Athanasopoulos, L. Vekas, T. Krasia-Christoforou, *J. Magn.Magn. Mater.,* **2010,** submitted.

[291] J-F Lutz, *J. Polym. Sci. Part A: Polym. Chem*., 46, **2008**, 3459.

[292] J-F Lutz, O. Akdemir, A. Hoth, *J. Am. Chem. Soc.,* 128, **2006**, 1304.

[293] J-F Lutz, A. Hoth, K. Schade, *Designed Monomers and Polymers*, 12, **2009**, 343.

[294] Y. Lee, D. N. Kim, D. Choi, *Polymers for Advanced Technologies*, 19, **2008**, 852.

[295] M. K. Nguyen, C. T. Huynh, D. S. Lee, *Polymer*, 50, **2009**, 5205.

[296] B. V. Slaughter, S. S. Khurshid, O. Z. Fisher, A. Khademhosseini, N. A. Peppas, *Adv. Mater.,* 21, **2009**, 3307.

[297] R. Tadmor, R. E. Roswensweig, J. Frey, J. Klein, *Langmuir*, 16, **2000**, 9117.

[298] M. V. Avdeev, D. Bica, L. Vekas, *J. Coll. and Int. Sci.,* 334, **2009**, 37.

[299] L. Vekas, M. V. Avdeev, D. Bica, "*Magnetic Nanofluids: Synthesis and structure, Chapter 25 in: Nanoscience in Biomedicine*", (Ed. Donglu Shi) *Springer*, **2009**, (USA), 645.

[300] T. C. Krasia, C. S. Patrickios, *Macromolecules*, 39, **2006**, 2467.

[301] Y. Maeda, T. Kubota, H. Yamauchi, T. Nakaji, H. Kitano, *Langmuir*, 23, **2007**, 11259.

Petri Papaphilippou

[302] E. goiti, M. M. Salinas, G. Arias, D. Puglia, J. M. Kenny, C. Mijangos, *Polymer Degradation and Stability*, 92, **2007**, 2198.

[303] S. Wan, Y. Zheng, Y. Liu, H. Han, K. Liu, *J. Mater. Chem.,* 15, **2005**, 3424.

[304] S. G. Starodubtsev, E. V. Saenko, M. E. Dokukin, V. L. Aksenov, V. V. Klechkovskaya, I. S. Zanaveskina, A. R. Khokholov, *J. Phys.: Cond. Matter.,* 17, **2005**, 1471.

[305] M. Yamaura, R. L. Camilo, L. C. Sampaio, M. A. Macedo, M. Nakamura, H. E. Toma, *J. Magn. Magn. Mater.,* 279, **2004**, 210.

[306] K. S. Sivudu, K. Y. Rhee, *Colloids and Surfaces A: Physicochem. Eng. Aspects,* 349, **2009**, 29.

[307] S. J. Mann, *Chem. Soc. Dalton, Trans.* **1993**, 1.

[308] P. Kasparova, PhD Thesis, Universität Potsdam, **2002**

[309] P. K. Ajikumar, B. J. M. Low, S. Valiyaveettil, *Surface & Coatings Technology*, 198, **2005**, 227.

[310] T. Wang, G. Rother, H. Colfen, *Macromol. Chem. Phys.,* 206, **2005**, 1619.

[311] B. R. Heywood, S. Mann, *Adv. Matter.,* 6(1), **1994**, 9.

[312] D. Yang, L. Qi, J. Ma, *Chem. Commun.,* **2003**, 1180.

[313] S. B. Mykkamala, A. K. Powell, *Chem. Commun.,* **2004**, 918.

[314] P. A. Bianconi, J. Lin, A. R. Strzelecki, *Nature* (London), 349, **1991**, 315.

[315] E. Dalas, *J. Mater. Chem,* 1, **1991**, 473.

[316] M. Antonietti, M. Breulmann, C. G. Goltner, H. Colfen, K. K. W. Wong, D. Walsh, S. Mann, *Chem. Eur. J.,* 4(12), **1998**, 2493.

[317] T. Wang, A-W Xu, H. Colfen, *Angew. Chem. Int. Ed.,* 45, **2006**, 4451.

[318] H. Cölfen, R. Song et al., in preparation.

[319] M. Antonietti, F. Grohn, J. Hartmann, L. Bronstein, *Angew. Chem. Int. Engl.,* 36(19), **1997**, 2080.

[320] X. Shuai, H. Ai, N. Nasongkla, S. Kim, J. Gao, *Journal of Controlled Release,* 98*,* **2004**, 415.

[321] M. Vamvakaki, D. Palioura, A. Spyros, S. P. Armes, and S. H. Anastasiadis, *Macromolecules*, 39, **2006**, 5106.

[322] (a) S. H. Anastasiadis, M. Vamvakaki, *International Journal of Nanotechnology*, 6, **2009**, 46, (b) L. M. Bronstein, M. Vamvakaki, M. Kostylev, V. Katsamanis, B. Stein, S. H. Anastasiadis, *Langmuir*, 21, **2005**, 9747.

[323] E. S. Lee, K. Na, Y. H. Bae, *Journal of Controlled Release*, 91, **2003**, 103.

Petri Papaphilippou

Petri Papaphilippou

Summary and Outlook

(i) Magneto-responsive polymer-based materials

Magneto-responsive micelles

In the present work the synthesis of well-defined diblock copolymers based on a ligating block segment possessing *β*-ketoester functionalities and a hydrophilic and thermoresponsive block comprised of hexa(ethylene glycol) side-chains was introduced for the first time *via* RAFT controlled radical polymerization. A series of well-defined PEGMA-*b*-AEMA diblock copolymers (13 in total) of various chemical compositions, was successfully prepared by RAFT and characterized by employing various characterization methods. SEC and ^{1}H NMR were employed for determining their molecular characteristics and TGA and DSC for obtaining information in regards to their thermal properties. Moreover, turbidimetry measurements demonstrated the thermoresponsive character of these materials, exhibiting a phase transition at around 60 ^{o}C, due to the presence of the hexa(ethylene glycol) side-chains within their structures, presenting a LCST in aqueous media.

The amphiphilic character of this novel type of block copolymer systems led to microphase separation in aqueous media. The aggregation behavior of a series of PEGMA$_x$-*b*-AEMA$_y$ was investigated in water by DLS. These systems are capable of forming micellar nanomorphologies in water. By varying the block lengths of the two segments within the block copolymer, micelles of tunable diameters were obtained (ranging from 11-70 nm).
The micellar nanomorphologies of the above-mentioned diblock copolymers have been employed for the first time as nanocontainers for the encapsulation and stabilization of magnetic nanoparticles in aqueous media, leading to the generation of novel magneto-responsive micelles.

The presence of strong *β*-ketoester ligands inside the core of the PEGMA$_x$-*b*-AEMA$_y$ micelles generated in aqueous media, facilitated coordination of the Fe^{3+}/Fe^{2+} salts. The subsequent addition of a weak base, led to the formation of magneto-responsive micelles containing iron oxide nanoparticles. XRD spectroscopy was employed to determine the nanocrystalline phase adopted by the iron oxide nanoparticles embedded inside the polymer matrix. The obtained data indicated the presence of magnetite.

Petri Papaphilippou

The $PEGMA_x$-*b*-$AEMA_y$/iron oxide nanohybrids, exhibited great stability for several months, even under physiological conditions, i.e. in the presence of NaCl. Systematic coagulation kinetics measurements were carried out by DLS, demonstrating the salt tolerance of these systems.

Magnetic measurement studies showed that these systems present a superparamagnetic behavior, indicated by the symmetrical sigmoidal shape of the magnetization curves exhibiting no hysteresis. The latter is a very important parameter for the applicability of these materials as contrast enhancement agents in magnetic resonance imaging. Furthermore, the saturation magnetization (Ms) increased upon increasing the magnetic content within the micelles.

Cell growth assays on prostate cancer cells treated with the superparamagnetic $PEGMA_x$-*b*-$AEMA_y$/Fe_3O_4 micelles did not yield statistically significant compromise on cell viability when compared to either H_2O or Resovist®, a clinically approved SPION of comparable size. *In vitro* uptake by macrophages was pronouncedly lower than Resovist®, further suggesting that these agents are expected to have enhanced *in vivo* efficacy.

Magneto-responsive SWCNTs

Magneto-responsive nanohybrids, consisting of single-wall carbon nanotubes decorated with iron oxide nanoparticles (Fe_xO_y) and stabilized by the $PEGMA_x$-*b*-$AEMA_y$ diblock copolymers in aqueous media were also prepared following a three-step synthetic methodology: (i) Mixing of the SWCNTs (carboxylated) with the copolymer in water, (ii) Addition of a Fe^{3+}/Fe^{2+} salts, (iii) Addition of a weak base resulting to the formation of iron oxide nanoparticles.

The resulting systems presented good stability in water for several months. It was noted that the presence of the $PEGMA_x$-*b*-$AEMA_y$ diblock copolymers, the molar ratio between the AEMA groups of the polymer and the iron salts as well as the purity and functionalization of CNTs played a significant role in the stabilization of these systems in aqueous media.

Information regarding the morphological characteristics of these systems was obtained by TEM, which revealed the presence of spherical, iron oxide nanoparticles onto the CNT

Petri Papaphilippou

surfaces. Moreover, VSM measurements performed at 300K, demonstrated the superparamagnetic behavior of these materials.

Magneto-responsive random co-networks

A new approach for the fabrication of composite amphiphilic random co-networks presented in this work involved the random copolymerization of hexa(ethylene glycol) methyl ether methacrylate (HEGMA, hydrophilic, thermoresponsive) and 2-(acetoacetoxy)ethyl methacrylate (AEMA, hydrophobic, metal-chelating) in the presence of either preformed oleic-acid coated magnetite nanoparticles (OA.Fe_3O_4) or non-coated magnetic iron oxide (nano)particles (Fe_xO_y). In total, three series of composite co-netoworks have been prepared. The first two series (Series A and B) were synthesized in the presence of OA.Fe_3O_4 in two different solvent systems, whereas in the 3rd series (Series C), Fe_xO_y nanoparticles (non-coated) have been incorporated into the co-networks during the polymerization process.

The degrees of swelling (DSs) of all co-networks were determined in organic and in aqueous media. The nanocrystalline phase adopted by the embedded oleic acid-coated nanoparticles was investigated by XRD spectroscopy. The obtained diffraction patterns indicated the presence of magnetite (Fe_3O_4).

Deswelling kinetic studies that were carried out at ~ 60 ^oC in water, demonstrated the thermoresponsive properties of these systems, attributed to the presence of the hexa(ethylene glycol) side chains within the co-networks. Moreover, thermal gravimetric analysis (TGA) measurements showed that these materials exhibited superior thermal stability compared to the pristine polymer co-networks.

Further to the characterization of compositional and thermal properties, assessment of magnetic characteristics by VSM at 300K, disclosed superparamagnetic behavior for the OA.Fe_3O_4-containing systems. Moreover, these materials presented tunable superparamagnetic behaviour, depending on the amount of magnetic nanoparticles incorporated within the co-networks.

Petri Papaphilippou

In contrast, the co-networks containing the non-coated Fe_xO_y (nano)particles presented a ferrimagnetic behavior at both, 5K and 300K, indicated by the presence of a hysteresis loop in the M = f(H) magnetization curves.

(ii) Stimuli-responsive polymer-based drug nanocarriers

Besides the synthesis and characterization of novel, magneto-responsive, polymer-based materials, this PhD thesis aimed towards the synthesis and characterization of stimuli-responsive diblock copolymers and their evaluation as pH-triggered drug delivery systems. A series of well-defined $HEGMA_x$-*b*-$DEAEMA_y$ diblock copolymers has been prepared by RAFT. The HEGMA units provided hydrophilicity, biocompatibility as well as thermoresponsive properties to the diblock copolymer, whereas the DEAEMA presented the capability to turn from hydrophilic into hydrophobic and *vice versa* upon changing the pH. In particular, the DEAEMA units are hydrophobic (non-ionizable) above the pKa value (~6.8) whereas below this value they become ionizable and hydrophilic.

The molecular characteristics of the $HEGMA_x$-*b*-$DEAEMA_y$ diblock copolymers (i.e. molecular weights, molecular weight distributions and chemical compositions) were determined by SEC and ^{1}H NMR respectively. In aqueous media and at pH values greater than 6.8, the $HEGMA_x$-b-$DEAEMA_y$ formed micelles, consisting of a hydrophilic HEGMA corona and a hydrophobic DEAEMA core. Protonation of the DEAEMA units at lower pHs, resulted to the transformation of the DEAEMA block segment from hydrophobic into hydrophilic, which in turn led to the dissociation of the micelles into unimers. The above-mentioned mechanism was employed for the controlled release of the anti-cancer pharmaceutical compound Doxorubicin (DOX) at low pHs.

DOX was initially loaded into the micelles by using an oil-in-water emulsion method. The loading efficiency was found to range between ~ 3 - 6.5%. Kinetic drug release measurements were carried out at pH 4.6 and 6.0 for two different DOX-loaded micellar systems, employing UV-vis spectroscopy. The decrease in the absorption signal appearing at $\lambda \sim 500$ nm - which corresponds to the encapsulated drug - with time, clearly demonstrated that at acidic pHs the micellar aggregates collapse, resulting in the release of the drug. Furthermore, it was found that the DOX release rate is accelerated upon decreasing the pH of the outer environment from 6.0 to 4.6.

Petri Papaphilippou

Finally, the potential toxicity of the $HEGMA_x$-*b*-$DEAEMA_y$ micelles (DOX-loaded and unloaded) on MB231 breast cancer cell viability in culture was assessed against DPBS (pH = 7.2). The cell viability of the DOX-loaded micelles was found to be higher compared to free DOX. Unloaded micelles showed the highest cell viability as expected. However, the cell viability decreased upon increasing the concentration of the micellar solutions, in both, the loaded and the unloaded systems.

(iii) Biomineralization

Besides the main objectives of this PhD Thesis described in (i) and (ii), the effect of the water-soluble $PEGMA_x$-*b*-$AEMA_y$ diblock copolymers on the crystallization behavior of malachite was investigated in aqueous solution. Preliminary studies demonstrated that the $PEGMA_x$-*b*-$AEMA_y$ diblock copolymers strongly influence the mineralization process of malachite. TEM revealed the formation of malachite nanofibers which were further grown into unusual net-like superstructures. A possible mechanism for the formation of these structures may involve an "exo-template" route, i.e. the micelles of the $PEGMA_x$-*b*-$AEMA_y$ generated in aqueous solution may build-up a structural "cage" for the construction of an inorganic nanostructure, hence acting as exo-template for the nucleation of malachite.

Nowadays, the fabrication of nanoparticulate systems (NPs) destined for use in both, therapeutic and diagnostic applications attracts considerable scientific and societal attention. The applicability of nanotechnology in the medical field involves the development of novel nanomaterials with potential use as therapeutic and diagnostic (theranostic) applications.
Future work towards this direction, may involve the design and synthesis of well-defined block copolymers capable of acting as effective stabilizers for magnetic nanoparticles and at the same time demonstrating a pH- or temperature-triggered drug-release capability, aiming to develop novel nanotheranostic polymer-based vehicles. Moreover, the introduction of biological targeting moieties onto the surfaces of such multifunctional nanoparticles may be another objective towards targeted delivery and controllable potent therapeutic effect.

Multimodal imaging is another research area of future exploitation, since multimodal nanoparticulate systems bearing complementary imaging moieties, allow for the investigation of the particle localization across a number of platforms, such as magnetic, optical or nuclear

Petri Papaphilippou

imaging. Using a variety of nanomaterials for multiplex diagnostics and imaging applications may offer sensitive, rapid and cost-effective solutions for the modern clinical laboratory.

During the last few years, CNTs combined with imaging probes for *in vitro* and *in vivo* detection and monitoring attract considerable scientific attention. Future work towards this direction may involve the optimization of the synthetic methodology followed for the preparation of the $PEGMA_x$-*b*-$AEMA_y$/SWCNTs/Fe_xO_y systems, in order to increase the magnetization by introducing a higher magnetic content onto the CNTs surfaces, retaining at the same time the superparamagnetic behavior as well as the colloidal stability in aqueous media. Another future goal is the investigation and understanding of the interactions taking place between these materials and biological systems and their interconnection to the question of nanosafety.

As far as the magneto-responsive HEGMA-*co*-AEMA/iron oxide composite co-networks is concerned, ongoing experiments involve the incorporation of an oligo-(ethylene glycol) methyl ether methacrylate possessing a lower number of PEG side chains within the co-networks, aiming to decrease the LCST from 60 ^{o}C down to 42-45 °C. This property in combination with the heating of SPIONs by applying an alternating magnetic field causing an elevation in temperature within this range, may lead to novel magnetothermally-trigerred drug delivery systems.

Finally, preliminary studies presented in this work suggest that water-soluble polymers bearing *β*-ketoester functionalities may act as potential candidates in biomineralization applications. Future work, besides the in-depth examination of the mechanism involved in the biomineralization process of malachite in the presence of the $PEGMA_x$-*b*-$AEMA_y$ diblock copolymers, may involve the investigation of the effect of water-soluble copolymers having *β*-ketoester functionalities on the mineralization behavior of other well-known minerals including $CaCO_3$ and $BaSO_4$.

Petri Papaphilippou

Bibliography

[1] F. W. Billmeyer, "*Textbook of Polymer Science*", Wiley-Interscience Publications, 3rd edition, **1984**, Wiley.

[2] H. R. Allcock, F. W. Lampe, J. E. Mark, "*Contemporary Polymer Chemistry*", 3rd edition, **2004**, Prentice Hall.

[3] N. Kumar, N. V. Majeti, Ravikumar, A. J. Domb, *Advanced Drug Delivery Reviews*, 53, **2001**, 23.

[4] J. R. Fried,"*Polymer Science and technology*", **1995**, Prentice Hall.

[5] R. Savic, Aa. Eisenberg, D. Maysinger, *Journal of Drug Targeting*, 14, **2006**, 343.

[6] V. Lima, X. Jiang, J. Broken-Sijp, P. J. Schoenmakers, B. Klumperman, R. V. Der Linde, *Journal of Polymer Science: Part A: Polymer Chemistry*, 43, **2005**, 959.

[7] M. F. Cunningham, *Prog. Polym. Sci*., 27(6), **2002**, 1039.

[8] C. E. Lipscomb, M. K. Mahanthappa, *Macromolecules*, 42, **2009**, 4571.

[9] Y. S. Jo, A. J. Van der Vlies, J. Gantz, S. Antonijevic, D. Demurtas, D. Velluto, J. A. Hubbell, *Macromolecules*, 41, **2008**, 1140.

[10] L. A. Connal, Q. Li, J. F. Quinn, E. Tjipto, F. Caruso, G. G. Qiao, *Macromolecules*, 41, **2008**, 2620.

[11] H. Mori, H. Ookuma, T. Endo, *Macromolecules*, 41, **2008**, 6925.

[12] Y. Zhang, Z. Shen, D. Yang, C. Feng, J. Hu, G. Lu, X. Huang, , *Macromolecules*, 43, **2010,** 117.

[13] M. Achilleos, T. Krasia-Christoforou, C. S. Patrickios, *Macromolecules*, 40, **2007**, 5575.

[14] J. B. Mcleary, M. P. Tonge, D. de Wet Roos, R. D. Sanderson and B. Klumperman, *Journal of Polymer Science: Part A: Polymer Chemistry*, 42, **2004**, 960.

[15] J. Chiefari, Y. K. Chong, F. Ercole, J. Krstina, J. Jeffery, T. P. T. Le, R. T. A. Mayadunne, G. F. Meijs, C. L. Moad, G. Moad, E. Rizzardo, S. H. Thang, *Macromolecules*, 31, **1998**, 5559.

[16] Z. Zhang, J. Zhu, Z. Cheng, X. Zhu, *Polymer*, 48, **2007**, 4393.

[17] G. Moad, Y. K. Chong, A. Postma, E. Rizzardo, S. H. Thang, *Polymer*, 46, **2005**, 8458.

[18] B. Y. K. Chong, J. Krstina, T. P. T. Le, G. Moad, A. Postma, E. Rizzardo, S. H. Thang, *Macromolecules*, 36, **2003**, 2256.

Petri Papaphilippou

[19] G. Moad, R. T.A. Mayadunne, E. Rizzardo, M. Skidmore, S. H. Thang, *Macromol. Symp*. 192, **2003**, 1.

[20] V. Coessens, T. Pintaeur, K. Matyjaszewski, *Prog. Polym. Sci.*, 26, **2001**, 337.

[21] P. V. R. Mesa, J. Belincanta, L. M. F. Lona, *European Symposium on Computer Aided Process Engineering*, **2005**.

[22] M. D. Nur Alam, P. B. Zetterlund, M. Okubo, *Journal of Polymer Science: Part A: Polymer Chemistry*, 45, **2007**, 2007.

[23] P. B. Zetterlund, Y. Saka, R. Mchale, T. Nakamura, F. Aldabbagh. M. Okubo, *Polymer*, 47, **2007**, 7900.

[24] P. M. Kazmaier, K. Daimon, M. K. Georges, G. K. Hamer, R. P. N. Veregin, *Macromolecules*, 30, **1997**, 2228.

[25] C. K. Hong, H. S. Jang, S. H. Hong, S. E. Shim, *Macromolecular Research*, 17(1), 2009, 14.

[26] G. Riess, *Prog. Polym. Sci*., 28, **2003**, 1107.

[27] H. Otsuka, Y. Nagasaki, K. Kataoka, *Current Opinion in Colloid & Interface Science*, 6, **2001**, 3.

[28] J. Leroux, *Eur. J. Pharm. Biopharm*., 48, **1999**, 101.

[29] V. P. Torchilin, *Journal of Controlled Release*, 73, **2001**, 137.

[30] L. Zhang, A. Eisenberg, *Science*, 268, **1995**, 1728.

[31] S. Svenson, *"Carrier-Based Drug Delivery"*, Chapter 1, ACS Symposium Series, Washington, DC, **2004**.

[32] M. Oba, K. Aoyagi, K. Miyata, Y. Matsumoto, K. Itaka, N. Nishiyama, Y. Yamasaki, H. Koyama, K. Kataoka, *Molecular Pharmaceutics*, 5, **2008**, 1080.

[33] X. Zhao, F. Pan, Z. Zhang, C. Grant, Y. Ma, S. P. Armes, Y. Tang, A. L. Lewis, T. Waigh, J. R. Lu, *Biomacromolecules*, 8, **2008**, 3493.

[34] C. Allen, D. Maysinger, A. Eisenberg, *Colloids and Surfaces B: Biointerfaces*, 16, **1999**, 3.

[35] A. Harada, K. Kataoka, *Prog. Polym. Sci*., 31, **2006**, 949.

[36] B. Hamdoun, *European Polymer Journal*, 40, **2004**, 1559.

[37] R. C. Hayward, D. J. Pochan, *Macromolecules*, 43, **2010**, 3577.

Petri Papaphilippou

[38] (a) M. Wilson, K. Kannangara, G. Smith, M. Simmons, B. Raguse, *"Nanotechnology: Basic Science and Emerging Technologies"*, **2002**, Chapman and Hall. (b) MME 461, Postgraduate course, *"Mechanics and thermodynamics in nanoscale"*, Dr. Andreas Kyprianou, **2007**.

[39] K. J. Kurzydlowski, *Materials Science*., 42, **2006**, 85.

[40] S. Ven, R. V. Kulkami, K. S. Saxena, *Appl. Phys. Lett*., 89, **2006**, 261901.

[41] L. Levy, Y. Sahoo, K. S. Kim, E. J. Bergey, P. N. Prasad, *Chem Mater*., 14, **2002**, 3715.

[42] H. T. Song, J. S. Choi, Y. M. Huh, S. Kim, Y. Jun, J. S. Suh, J. Cheon, *J. Am. Chem. Soc*., 127, **2005**, 12387.

[43] J-H Kim, K. Park, H. Y. Nam, S. Lee, K. Kim, C. Kwon, *Prog. Polym. Sci.*, 32, **2007**, 1031.

[44] G-P Yan, L. Robinson, P. Hogg, *Radiography*, 13, **2007**, e5.

[45] D. Pan, G. M. Lanza, S. A. Wickline, S. D. Caruthers, *European Journal of Radiology*, 70, **2009**, 274.

[46] A. H. Faraji, P. Wipf, *Bioorg. Med. Chem*., 17, **2009**, 2950.

[47] S. J. Rota, *J. Magn. Magn. Mater*., 122, **1993**, 329.

[48] (a) K. Raj, B. Moskowitz, R. Casciari, *Magn. Magn. Mater*., 149, **1995**, 174, (b) S. A. Rovers, R. Hoogenboom, M. F. Kemmere, J. T. F. Keurentjes, *J. Phys. Chem. C*, 112, **2008**, 15463.

[49] V. T. Peikov, K. S. Jeon, A. M. Lane, J. *Magn. Magn. Mater*., 193, **1999**, 307.

[50] J. M. Perez, F. J. Simeone, Y. Saeki, L. Josephson, R. Weissleder, *J. Am. Chem. Soc*., 125(34), **2003**, 10192.

[51] A. A. Atia, A. M. Donia, A. M. Yousif, *Separation and Purification Technology*, 61, **2008**, 348.

[52] P. I. Girginova, A. L. Daniel-da-Silva, C. B. Lopes, P. Figueira, M. Otero, V. S. Amaral, E. Pereira, T. Trindade, *Journal of Colloid and Interface Science*, 345, **2010**, 234.

[53] W. Shourong, H. Junsheng, G. Miao, Z. Hongkai, C. Youjia, Y. Husheng, L. Keliang, *Journal of Biomedical Materials Research Part A*, **2006**, 946.

[54] H. Daniel, S. Nataliya, L. Frastisek, *Journal of Polymer Science: Part A*, 41, **2003**, 1848.

[55] H. Daniel, B. Nataliya, *Journal of Polymer Science Part A*, 42, **2004**, 5827.

[56] S. Shouheng, H. Zeng, *J. Am. Chem. Soc*., 124, **2002**, 8204.

Petri Papaphilippou

[57] K. D. Kim, M. Mikhaylova, Y. Zhang, M. Muhammed, *Chem. Mater*., 15, **2003**, 1617.

[58] K. A. Boal, L. B. Frankamp, O. Uzun, T. M. Tuominem, M. V. Rotello, *Chem. Mater.*, 16, **2004**, 3252.

[59] A. Ditsch, E. P. Laibinis, C. L. Wang, A. Hatton, *Langmuir*, 21, **2005**, 6006.

[60] J. K. Bacri, R. Perzynski, D. Salin, V. Cabuil, R. Massart, *J. Magn. Magn. Mater.*, 85, **1990**, 27.

[61] L. Shen, A. Stachowiak, K. Fateen, E. P. Laibinis, A. Alan Hatton, *Langmuir*, 17, **2001**, 288.

[62] M. Aslam, A. E. Schultz, T. Sun, T. Meade, P. V. Dravid, *Crystal Growth & Design*, 7, **2007**, 471.

[63] H. Khalil, D. Majan, M. Rafailovich, M. Gelfer, K. Pandya, *Langmuir*, 20, **2004**, 6896.

[64] J-F Berret, N. Schonbeck, F. Gazeau, E. D. Kharrat, O. Sandre, A. Vacher, M. Airiau, *J. Am. Chem. Soc*., 128, **2006**, 1755.

[65] G. Li, J. Fan, R. Jiang, Y. Gao, *Chem. Mater*., 16, **2004**, 1835.

[66] A. Zhu, L. Yuan, W. Jin, S. Dai, Q. Wang, Z. Xue, A. Qin, *Acta Biomaterialia*, 5, **2009**, 1489.

[67] D. L. Leslie-Pelecky, V. Labhasetwar, R. H. Kraus,"*Nanobiomagnetics"* in *Advanced Magnetic Nanostructures*, Springer, **2006**, 461.

[68] E. Tombacz, D. Bica, A. Hadju, E. Illes, A. Majsik and L. Vekas, *J. Phys.: Condens. Matter.*, 20, **2008**, 204103.

[69] M. Arruebo, R. Fernandez-Pacheco, M. R. Ibarra and J. Santamaria, *Nanotoday*, 2(3), **2007**, 22.

[70] C. Sun, J. S. H. Lee, M. Zhang, *Advanced Drug Delivery Reviews*, 60, **2008**, 1252.

[71] L. Vekas, D. Bica and M. V. Avdeev, *China Particuology*, 5, **2007**, 43.

[72] T. Gong, D. Yang, J. Hu, W. Yang, C. Wang and J. Q. Lu, *Colloids and Surfaces A: Physicochem. Eng. Aspects*, 339, **2009**, 232.

[73] C. Giacomelli, G. Lafitte and R. Borsali, *Makromol. Symp.*,229, **2005**, 107.

[74] Y. S. Kim, G. I. Shin, M. Y. Lee, G. C. Cho and K. Y. Sung, *Journal of Controlled Release*, 51, **1998**, 13.

[75] C. Lemarchand, R. Gref, P. Couvreur, *Europeran Journal of Pharmaceutics and Biopharmaceutics*, 58, **2004**, 327.

Petri Papaphilippou

[76] Q. Yuan, R. Venkatasubramanian, S. Hein, R. D. K. Misra, *Acta Biomaterialia*, 4, **2008**, 1024.

[77] J. Leroux, *Eur. J. Pharm. Biopharm.*, 48, **1999**, 101.

[78] K. D. Kim, M. Mikhaylova, Y. Zhang, M. Muhammed, *Chem. Mater*., 15, **2003**, 1617.

[79] M. Aslam, A. E. Schultz, T. Sun, T. Meade, P. V. Dravid, *Crystal Growth & Design*, 7, **2007**, 471.

[80] B. Tural, N. Ozkan, M. Volkan, *Journal of Physics and Chemistry of Solids*, 70, **2009**, 860.

[81] E. Marutani, S. Yamamoto, T. Ninjbadgar, Y. Tsujii, T. Fukuda, M. Takano, *Polymer*, 45, **2004**, 2231.

[82] J-F Lutz, S. Stiller, A. Hon, L. Kaufner, U. Pison, R. Cartier, *Biomacromolecules*, 7, **2006**, 3132.

[83] B-S Kim, J-M Qiu, J-P Wang, T. A. Taton, *Nano Lett.*, 5, **2005**, 1987.

[84] A. Aqil, S. Vasseur, E. Duguet, C. Passirani, J.P. Benoit, A. Roch, R. Muller, R. Jerome, C. Jerome, *Europeran Polymer Journal*, 44, **2008**, 3191.

[85] Y. Bai, B. Teng, S. Chen, Y. Chang, Z. Li, *Macromol. Rapid. Commun.*, 27, **2006**, 2107.

[86] M. Rutnakornpituk, S. Meerod, B. Boontha, U. Wichai, *Polymer*, 50, **2009**, 3508.

[87] S. Meerod, G. Tumcharern, U. Wichai, M. Rutnakornpituk, *Polymer*, 49, **2008**, 3950.

[88] A. D. Burke, D. H. Stover, P. F. Dawson, *Chem. Mater*., 14, **2002**, 4752.

[89] H. Lee, E. Lee, Do K. Kim, N. K. Jang, Y. Y. Jeong and S. Jon, *J. Am. Chem. Soc*., 128, **2006**, 7383.

[90] M. Kim, J. Jung, J. Lee, K. Na, S. Park, J. Hyun, *Colloids and Surfaces B: Biointerfaces*, 76, **2010**, 236.

[91] H. Wakamatsu, K. Yamamoto, A. Nakao, T. Aoyagi, *Journal of Magnetism and Magnetic Materials*, 302, **2006**, 327.

[92] S. Wan, Y. Zheng, Y. Liu, H. Yan, K. Liu, *J. Mater. Chem.*, 15, **2005**, 3430.

[93] S. Wan, J. Huang, H. Yan, K. Liu, *J. Mater. Chem.*, 16, **2006**, 298.

[94] Q. Zhang, S. M. Thompson, Y. A. Garmichael-Baranauskas, L. B. Caba, A. M. Zalich, Y-N Lin, T. O. Mefford, M. R. Davis, S. J. Riffle, *Langmuir*, 23, **2007**, 6927.

[95] N. Guan, J. Xu, L. Wang, D. Sun, *Colloids snd Surfaces A: Physicochem. Eng. Aspects*, 346, **2009**, 221.

Petri Papaphilippou

[96] Y. Sahoo, M. Cheon, S. Wang, H. Luo, P. E. Furlani, N. P. Prasad, *J. Phys. Chem B*, 108, **2004**, 3380.

[97] K. A. Boal, L. B. Frankamp, O. Uzun, T. M. Tuominem, M. V. Rotello, *Chem. Mater*., 16, **2004**, 3252.

[98] Y. Koseoglu, H. Kavas, B. Aktas, *Phys. Stat. Sol*., 203(7), **2006**, 1595.

[99] R. S. Ahmed, B. S. Ogale, C. G. Papaefthymiou, R. Ramesh, P. Kofinas, *J. Appl. Phys. Lett*., 80, **2002**, 1616.

[100] Y. Hou, S. Gao, T. Ohtra, H. Kondoh, *Eur. J. Inorg. Chem*., **2004**, 1169.

[101] M. Yamagata, M. Abe, H. Handa, H. Kawaguchi, *Macromol. Symp*, 245, **2006**, 363.

[102] Z. Ma, Y. Guan, H. Liu, *Journal of Polymer Science: Part A, 43*, **2005**, 3433.

[103] P. V. Torchilin, *Advanced Drug Delivery Reviews*, 57, **2005**, 95.

[104] P. V. Torchilin, *Journal of Controlled Release*, 73, **2001**, 137.

[105] T. Inoue, G. Chen, K. Nakamae, A. S. Hoffman, *Journal of Controlled Release*, 51, **1998**, 221.

[106] K. Kataoka, A. Harada, Y. Nagasaki, *Advanced Drug Delivery Reviews*, 47, **2001**, 113.

[107] N. Nishiyama, K. Kataoka, *Pharmacology & Therapeutics*, 112, **2006**, 630.

[108] G. Gaucher, M-H. Dufrense, V. P. Ant, N. Kang, D. Maysinger, J-C Leroux, *Journal of Controlled Release*, 109, **2005**, 169.

[109] V. P. Torchilin, *Cell. Mol. Life Sci.*, 61, **2004**, 2549.

[110] H. Maeda, J. Wu, T. Sawa, Y. Matsumura, K. Hori, *Journal of Controlled Release*, 65, **2000**, 271.

[111] K. Greish, *Journal of Drug Targeting*, 15(7), **2007**, 457.

[112] *"Polymer properties and polymers in medical applications"*, Postgraduate course, www.eng.ucy.ac.cy/krasia, MME 555, Dr. Theodora Krasia-Christoforou, **2008**.

[113] H. Lee, E. Lee, K. D. Kim, N. K. Jang, Y. Y. Jeong, S. Jon, *J. Am. Chem. Soc*., 128, **2006**, 7383.

[114] A. Rosler, G. W. M. Vandermeulen, H-A Klok, *Advanced Drug Delivery Reviews*, 53, **2001**, 95.

[115] K. Kataoka, G. S. Kwon, M. Yokoyama, T. Okano, Y. Sakurai, *Journal of Controlled Release*, 24, **1993**, 119.

[116] C. H. Wang, G. H. Hsiue, *Biomacromolecules*, 4, **2003**, 1487.

Petri Papaphilippou

[117] A. N. Lukyanov, V. P. Torchilin, *Adv. Drug Deliv. Rev.*, 56, **2004**, 1273.

[118] G. Zuccari, R. Carosio, A. Fini, PG. Montaldo, I. Orienti, *J. Control Release*, 103, **2005**, 369.

[119] M. Nakayama, T. Okano, T. Miyazaki, F. Kohori, K. Sakai, M. Yokoyama, *Journal of Controlled Release* 115, **2006**, 46.

[120] T. Riley, T. Govender, S. Stolnik, C. D. Xiong, M. C. Garnett, L. Illum, S. S Davis, *Colloids and Surfaces B: Biointerfaces*, 16, **1999**, 147.

[121] D. Cohn, H. Younes, *Journal of Biomedical Materials Research*, 22, **1988**, 993.

[122] S. Ben-Shabat, N. Kumar, A. J. Domb, *Macromol. Biosci.*, 6, **2006**, 1019.

[123] Y. S. Kim, G. I. Shin, M. Y. Lee, G. C. Cho, K. Y. Sung, *Journal of Controlled Release*, 51, **1998**, 13.

[124] C. Giacomelli, G. Lafitte, R. Borsali, *Makromol. Symp.*,229, **2005**, 107.

[125] K. Letchford, R. Liggins, H. Burt, *Journal of Pharmaceuticals Sciences*, 97, **2007**, 1179.

[126] S. B. La, T. Okano, K. Kataoka, *Journal of Pharmaceuticals Sciences*, 85, **1996**, 85.

[127] G. Kwon, M. Naito, M. Yokohama, T. Okano, Y. Sakurai, K. Kataoka, *Journal of Controlled Release*, 48, **1997**, 195.

[128] Y. I. Jeong, J. B. Cheon, S. H. Kim, J. W. Nah, Y. M. Lee, Y. K. Sung, T. Akaike, C. S. Cho, *Journal of Controlled Release*, 51, **1998**, 169.

[129] S. A. Hagan, A. G. A. Coombes, M. C. Garnett, S. E. Duna, M. C. Davies, L. Illum, S. S. Davis, *Langmuir*, 12, **1996**, 2153.

[130] M. Ramaswamy, X. Zhang, H. M. Burt, K. M.-Wasan, *Journal of Pharmaceuticals Sciences*, 86, **1997**, 460.

[131] K. Yasugi, Y. Nagasaki, M. Kato, K. Kataoka, *Journal of Controlled Release*, 62, **1999**, 89.

[132] C. Donini, D. N. Robinson, P. Colombo, F. Giordano, N. A. Peppas, *International Journal of Pharmaceutics*, 245, **2002**, 83.

[133] M. Yokohama, M. Miyauchi, N. Yamada, T. Okano, Y. Sakurai, K. Kataoka, S. Inoue, *Cancer Res.*, 50, **1990**, 1693.

[134] A. Harada, K. Kataoka, *Macromolecules*, 31, **1998**, 288.

Betti Papaphilippou

[135] S. V. Trubetskoy, S. G. Gazelle, L. G. Wolf, P. V. Torchilin, *Journal of Drug Targeting*, 4, **1997**, 381.

[136] S. Katayose, K. Kataoka, *Journal of Pharmaceuticals Sciences*, 87, **1998**, 160.

[137] Eun S. Lee, K. Na, You H. Bae, *Journal of Controlled Release*, 91, **2003**, 103.

[138] A. V. Kabanov, V. A. Kabanov, *Advanced Drug Delivery Reviews*, 30, **1990**, 49.

[139] Yan Wu, Fu-Bin Che, Jiang-Han Chen, *Journal of Applied Polymer Science*, 110, **2008**, 1118.

[140] D. W. Miller, E. V. Batrakova, O. T. Waltner, V. Y. Alakhov, A. V. Kabanov, *Bioconj. Chem.*, 8, **1997**, 649.

[141] A. Kabanov, E. V. Batrakova, V. Y. Alakhov, *Journal of Controlled Release*, 82, **2002**, 189.

[142] K. T. Oh, H. Yin, Eun S. Lee, You H. Bae, *J. Mater. Chem.*, 17, **2007**, 3987.

[143] J. E. Chung, M. Yokoyama, M. Yamato, T. Aoyagi, Y. Sakurai, T. Okano, *Journal of Controlled Release*, 62, **1999**, 115.

[144] D. R. Friend, S. Pangburn, *Medicinal Research Reviews*, 7, **1987**, 53.

[145] Y. Bae, N. Nishiyama, K. Kataoka, *Bioconj. Chem.*, 18, **2007**, 1131.

[146] Y. Bae, W-D Jang, N. Nishiyama, S. Fukushima, K. Kataoka, *Mol. Biosyst.*, 1, **2005**, 242.

[147] Z. Sezgin, N. Yuksel, T. Baykara, *European Journal of Pharmaceutics and Biopharmaceutics*, 64, **2006**, 261.

[148] M. Yokoyama, S. Fukushima, R. Uehara, K. Okamoto, K. Kataoka, Y. Sakurai, T. Okano, *Journal of Controlled Release*, 50, **1998**, 79.

[149] P. Opanasopit, M. Yokoyama, M. Watanabe, K. Kawano, Y. Maitani, T. Okano, *Pharmaceutical Research*, 21, **2004**, 2001.

[150] N. Nishiyama, M. Yokoyama, T. Aoyyagi, T. Okano, Y. Sakurai, K. Kataoka, *Langmuir*, 15, **1999**, 377.

[151] N. Nishiyama, K. Kataoka, *Journal of Controlled Release*, 74, **2001**, 83.

[152] M. Watanabe, K. Kawano, M. Yokoyama, P. Opanasopit, T. Okano, Y. Maitani, *International Journal of Pharmaceutics*, 308, **2006**, 183.

[153] K. Kataoka, T. Matsumoto, M. Yokoyama, T. Okano, Y. Sakurai, S. Fukushima, K. Okamoto, G. S. Kwon, *Journal of Controlled Release*, 64, **2000**, 143.

Petri Papaphilippou

[154] O. Soga, C. F. van Nostrum, M. Fens, C. J.F. Rijcken, R. M. Schiffelers, G. Storm, W. H. Hennink, *Journal of Controlled Release*, 103, **2005**, 341.

[155] T. O. Kyung, E. S. Lee, D. Kim, Y. H. Bae, *International Journal of Pharmaceutics*, 358, **2008**, 177.

[156] N. Babazadeh, *Journal of Applied Polymer Science*, 104, **2007**, 2403.

[157] N. Nishiyanna, S. Okazaki, H. Cabral, M. Miyamoto, Y. Kato, Y. Sugiyama, *Cancer Res.*, 63, **2003**, 8977.

[158] V. Y. Alakhov, E. Y. Moskaleva, E. V. Batrakova, A. V. Kabanov, *Bioconj. Chem.*, 7, **1996**, 209.

[159] Y-C Chang, I-M Chu, *European Polymer Journal*, 44, **2008**, 3922.

[160] Y. Li, S. Pan, W. Zhang, Z. Du, *Nanotechnology*, 20, **2005**, 1.

[161] J. Heung, K. Emoto, M. Iigima, Y. Nagasaki, T. Aoyagi, T. Okano, Y. Sakurai, K. Kataoka, *Polym. Adv. Tecnhol.*, 10, **1999**, 647.

[162] V. A. Sethuraman, M. C. Lee, Y. H. Bae, *Pharmaceutical Research*, 25, **2008**, 657.

[163] S-H Hua, Y-Y Li, Y. Liu, W. Xiao, C. Li, F-W Huang, X-Z Zhang, R-X Zhuo, *Macromol. Rapid Commun.*, 31, **2010**, 81.

[164] Y. Tian, L. Bromberg, S. N. Lin, T. A. Hatton, K. C. Tam, *Journal of Controlled Release*, 121, **2007**, 137.

[165] H. S. Na, Y. K. Lim, Y-I Jeong, H. S. Lee, Y. J. Lim, M. S. Kang, C-S Cho, H. C. Lee, *International Journal of Pharmaceutics*, 383, **2010**, 192.

[166] http://biotech.icmb.utexas.edu/botany/tax.html

[167] Y. Bae, N. Nishiyama, S. Fukushima, H. Koyama, M. Yasuhiro, K. Kataoka, *Bioconj. Chem.*, 16, **2005**, 122.

[168] M. Stubbs, P. M. J. McSheehy, J. R. Griffiths, C. L.Bashford, *Molecular Medicine Today*, 6, **2000**, 15.

[169] K. Newel, A. Franchi, J. Pouyessegur, I. Tannok, *Proc. Natl. Acad. Sci.*, 90, **1993**, 1127.

[170] I. F. Tannock, D. Rotin, *Cancer Res.*, 49, **1989**, 4373.

[171] S. Kwon, T. Okano, K. Kataoka, *Advanced Drug Delivery Reviews*, 21, **1996**, 107.

[172] P. Chytil, T. Etrych, C. Konak, M. Sirova, T. Mrkvan, B. Rihova, K. Ulbrich, *Journal of Controlled Release*, 115, **2006**, 26.

Petri Papaphilippou

[173] *"Hyperthermia in Cancer Treatment: Questions and Answers"*, *National Cancer Institute FactSheet*, http://www.cancer.gov/publications

[174] C. R. Blanchard, "*Atomic Force Microscopy"*, Springer, **1996**.

[175] E. Meyer, H. J. Hug, R. Bennewitz, "*Scanning Probe Microscopy: The lab on a Tip*", **2003**, Springer.

[176] History of AFM, Pacific Nanotechnology (Nanotechnological advances), LOT.

[177] B. Ruozi, G. Tosi, E. Leo, M.A. Vandelli, *Talanta*, 73, **2007**, 12.

[178] H. N. Pishkenari, N. Jalili, A. Meghdari, *Mechatronics*, 16, **2006**, 655.

[179] www.nanoscience.com/education/AFM.html.

[180] K. Oikawa, H. Kimb, N. Watanabe, M.Shigeno,Y. Shirakawabe, K. Yasuda, *Ultramicroscopy*, 107, **2007**, 1061.

[181] *"Characterization techniques of materials"*, www.eng.ucy.ac.cy/kyratsi, MME 554, Postgraduate course, Dr. Theodora Kyratsi, **2008**.

[182] "*Characterization methods of polymers and colloids*", www.eng.ucy.ac.cy/krasia, MME 551, Postgraduate course, Dr. Theodora Krasia-Christoforou, **2008**.

[183] B. Fultz, J. M. Howe, "*Transmission Electron Microscopy and Diffractometry of Materials*", **2007**, Springer.

[184] H. K. D. H. Bhadeshia, *"Differential Scanning Calorimetry"*, Materials Science and Metallurgy.

[185] J. McMurry, *«Organic Chemistry»*, Volume 1, University of Crete publishing.

[186] www.teaching.shu.ac.uk/hwb/chemistry/tutorials/molspec/nmr 1.html

[187] www.cem.msu.edu/reusch/VirtualText/Spectrpy/nmr/nmr 1.html

[188] C. Hammond, "*The basics of Crystallography and Diffraction"*, **1977,** Oxford Science Publications.

[189] B. TH. De Keijser, E. J. Mittemeijer, H. C. F. Rozendaal, *J. Appl. Cryst*. 16, **1983**, 309.

[190] R. L. Pecsok, L. Shields, T. Cairns, I. McWilliam, *«Modern Methods of Chemical Analysis»*, **1980**, John Wiley & Sons.

[191] M. Sartor, *"Dynamic Light Scattering"*, University of California.

[192] Charles S. Johnson and Don A. Gabriel, *"Laser Light Scattering: Basic Principles Practise"*, **1991,** Academic Press,.

Betti Papaphilippou

[193] H. R. Allcock, F. W. Lampe, J. E. Mark, "*Contemporary Polymer Chemistry*", 3rd edition, **2004**, Prentice Hall.

[194] L. H. Sperling,"*Introduction to Physical Polymer Science*", **2006,** John Wiley & Sons.

[195] C. Sun, J. S. H. Lee, M. Zhang, *Advanced Drug Delivery*, 60, **2008**, 1252.

[196] Albert Figuerola, Riccardo Di Corato, Liberato Manna and Teresa Pellegrino, *Pharmacological Research*,**2010**.

[197] J. S. Miller, M. Drillon,"*Magnetism: Molecules to Materials III*", *Nanosized Magnetic Materials*, **2002**, Wiley-VCH.

[198] DMS Vibrating Sample Magnetometer, AD Tecnhologies.

[199] H. Pasch, B. Trathnig, *HPLC of Polymers*, **1997,** Springer: Berlin.

[200] M. McElfresh,"*Fundamentals of Magnetism and Magnetic measurements featuring quantum design's Magnetic Property Measurement System*", Purdue University.

[201] (a) D. Bica, *Rom.Rep.Phys*., 47, **1995**, 265. (b) L. Vekas, D. Bica, M.V. Avdeev, *China Particuology*, 5, **2007**, 43. (c) L. Vékás, M.V. Avdeev, Doina Bica, *Magnetic Nanofluids: Synthesis and Structure, Chapter 25 in: NanoScience in Biomedicine* (Ed. Donglu Shi) Springer, **2009**, (USA) 645.

[202] T. P. T. Le, G. Moad, E. Rizzardo, S. H. Thang, *PCT. Int. Appl. WO* 9801478 Al 980115.

[203] E. R. Gillies, J. M. Frechet, *Bioconjugate. Chem.*, 16, **2005**, 361.

[204] P. Papaphilippou, L. Loizou, N. C. Popa, A. Han, L. Vekas, A. Odysseos, T. Krasia-Christoforou, *Biomacromolecules*, 10, **2009**, 2662.

[205] T. Krasia, R. Soula, H. G. Borner, H. Schlaad, *Chem. Commun.*, 4, **2003**, 538.

[206] J-F Lutz, S. Stiller, A. Hoth, L. Kaufner, U. Pison, R. Cartier, *Biomacromolecules*, 7, **2006**, 3132.

[207] J. Chiefari, Y. K. Chong, F. Ercole, J. Krstina, J. Jeffrey, T.P.T. Le, R. Mayadunne, G. F. Meijs, C. L. Moad, G. Moad, E. Rizzardo, S. H. Thang, *Macromolecules*, 31, **1998**, 5559.

[208] G. Moad, E. Rizzardo, S. H. Thang, *Aust. J. Chem.*, 58, **2005**, 379.

[209] G. Moad, E. Rizzardo, S. H. Thang, *Aust. J. Chem.*, 59, **2006**, 669.

[210] G. Dimarco, M. Lanza , M. Pieruccini, *Solid State Ionics*, 89, **1996**, 117.

[211] J. F. Lutz, *J. Polym. Sci., Part A : Polym. Chem.*, 46, **2008**, 3459.

Petri Papaphilippou

[212] J-F Lutz, O. Akdemir, A. Hoth, *J. Am. Chem. Soc.*, 128, **2006**, 13046.

[213] J-F Lutz, A. Hoth, *Macromolecules*, 39, **2006**, 893.

[214] B. Zhao, D. Li, F. Hua, D. R. Green, *Macromolecules*, 38, **2005**, 9509.

[215] Y. Maeda, T. Kubota, H. Yamauchi, T. Nakaji, H. Kitano, *Langmuir*, 23, **2007**, 11259.

[216] S. Chen, Y. Li, C. Guo, J. Wang, J. Ma, X. Liang, L-R Yang, H-Z Liu, *Langmuir*, 23, **2007**, 12669.

[217] S. R. Wan, J. S. Huang, M. Guo, H. Zhang, Y. Cao, H. Yan, K. J. Liu, *Biomed. Mater. Res.*, 80A, **2007**, 946.

[218] T. Neuberger, B. Schopf, H. Hofmann, M. Hofmann, B. Von Rechenberg, *J. Magn. Magn. Mater.*, 293, **2005**, 483.

[219] C. R. Heald, S. Stolnik, K. S. Kujawinski, C. De Matteis, M. C. Garnett, L. Illum, S. S. Davis, S. C. Purkiss, R. J. Barlow, P. R. Gellert, *Langmuir*, 18, **2002**, 3669.

[220] Y. Liu, L. Wang, C. Pan, *Macromolecules*, 32, **1999**, 8301.

[221] R. Massart, *IEEE Trans. Magn.*, 17(2), **1981**, 1247.

[222] S. Shouheng, H. Zeng, *J. Am. Chem. Soc*., 124, **2002**, 8204.

[223] D. K. Kim, M. Mikhaylova, Y. Zhang, M. Muhammed, *Chem. Mater*., 15, **2003**, 1617.

[224] Y-S. Kang, S. Risbud, J. F. Rabolt, P. Stroeve, *Chem. Mater*., 8, **1996**, 2209.

[225] D. Bica L. Vekas, M. V. Avdeev, O. Marinica, V. Socoliuc, M. Balasoiu, *Journal of Magnetism and Magnetic Materials*, 311, **2007**, 17.

[226] K. Hanabusa, T. Suzuki, T. Koyoama, H. Shirai, *Macromol. Chem.*, 193, **1992**, 2149.

[227] M. M. Dell' Anna, P. Mastrorilli, A. Rizzuti, G. P. Suranna, C. F. Nobile, *Inorg. Chim. Acta.*, 304, **2000**, 21.

[228] M. M. Dell' Anna, M. Gagliardi, P. Mastrorilli, G. P. Suranna, C. F. Nobile, *J. Mol. Catal. A*, 304, **2000**, 515.

[229] T. Krasia, H. Schlaad, "*In Metal Containing and Metall-supramolecular Polymers and Materials*" G. R. Newkome, I. Manners, U. S. Schubert, Eds., ACS Symposium Series 928, American Chemical Society: Washington, DC, **2006**, 157.

[230] A. Pich, S. Bhattacharya, Y. Lu, V. Boyko, H-J Adler, *Langmuir*, 20, **2004**, 10706.

[231] F. Suriano, O. Coulembier, P. Degee, P. Dubois, *J. Polym. Sci., Part A : Polym. Chem.*, 46, **2008**, 3662.

[232] L. Jiang, W. Sun, J. Kim, *Materials Chemistry and Physics*, 101, **2007**, 291.

Petri Papaphilippou

[233] S. Wan, Y. Zheng, Y. Liu, H. Yan, K. Liu, *J. Mater. Chem.*, 15, **2005**, 3424.

[234] L. C. Li, J. Jiang, F. Xu, *Mater. Lett.*, 61, **2007**, 1091.

[235] K. R. Reddy, K-P Lee, A. I. Gopalan, *J. Appl. Polym. Sci.*, 106, **2007**, 1181.

[236] M. Hamoudeh, A. A. Faraj, E. Canet-Soulas, F. Bessueille, D. Leonard, H. Fessi, *International Journal of Pharmaceutics*, 338, **2007**, 248.

[237] G. DiMarco, M. Lanza, M. Pieruccini, *Solid State Ionics*, 89, **1996**, 117.

[238] A. Kaiser, T. Gelbrich, A. M. Schmidt, *J. Phys.:Condens. Matter.*, 18, **2006**, S2563.

[239] T. Gelbrich, M. Feyen, A. M. Schmidt, *Macromolecules*, 39, **2006**, 3469.

[240] H. Lee, E. Lee, K. Do Kim, N. K. Jang, Y. Y. Jeong, S. Jon, *J. Am. Chem. Soc.*, 128, **2006**, 7383.

[241] S. Metz, G. Bonaterra, M. Rudelius, M. Settles, E. J. Rummeny, H. E. Link Daldrup, *Eur. Radiol.*, 14, **2004**, 1851.

[242] S. Iijima, *Nature*, 354, **1991**, 56.

[243] S-R Ji, C. Liu, B. Zhang, F. Yang, J. Xu, J. Long, C. Jin, D-L Fu, Q-X Ni, X-J Yu, *Biochimica et Biophysica Acta*, **2010**.

[244] A. A. Faraj, K. Cieslar, G. Lacroix, S. Gaillard, E. Canet-Soulas, Y. Cremillieux, *Nano Letters*, 9(3), **2009**, 1023.

[245] C. Huiqun., Z. Meifang, L. Yaogang, *Journal of Solid State Chemistry*, 179, **2006**, 1208.

[246] H. Wang, L. Cao, S. Yan, Z. Huang, Z. Xiao, *Materials Science and Engineering B*, 164, **2009**, 191.

[247] L. Zhang, Q-Q Ni, T. Natsuki, Y. Fu, *Applied Surface Science*, 255, **2009**, 8676.

[248] P. Xu, D. Cui, B. Pan, F. Gao, R. He, Q. Li, T. Huang, C. Bao, H. Yang. *Applied Surface Science*, 254, **2008**, 5236.

[249] L. Jiang, L. Gao, *Chem. Mater.*,15, **2003**, 2848.

[250] B. Jia, L. Gao, J. Sun, *Carbon*, 45, **2007**, 1476.

[251] C. Huiqun, Z. Meifang, L. Yaogang, *J. Magn. Mater.*, 305, **2006**, 321.

[252] I.T. Kim, G. A. Nunnery, K. Jacob, J. Schwartz, X. Liu, R. Tannenbaum, *J. Phys. Chem. C*, 114, **2010**, 6944.

[253] A. Hirsch, *Angw. Chem. Int. Ed.*, 40 (11), **2002**, 1853.

[254] C. A. Dyke, J. M. Tour, *J. Phys. Chem. A*, 108, **2004**, 11151.

Petri Papaphilippou

[255] Y. Zhang, H. He, C. Gao, J. Wu, *Langmuir*, 25**(**10), **2009**, 5814.

[256] W. Shen, Z. Li, Y. Liu, *Recent Patents on Chemical Engineering*, 1, **2008**, 27.

[257] I. D. Rosca, F. Watari, M. Uo, T. Akasaka, *Carbon*, 43, **2005**, 3124.

[258] (a) Z. Spitalsky, D. Tasis, K. Papagelis, C. Galiotis, *Progress in Polymer Science*, 35(3), **2010**, 35. (b) J. Li, W-D He, L-P Yang, X-L Sun, Q. Hua, *Polymer*, 48(15), **2007**, 4352.

[259] F-M Xu, J-P Xu, J. Ji, J-C Shen, *Colloids and Surfaces B: Biointerfaces*, 67(1), **2008**, 67.

[260] S. Bose, R. A. Khare, P. Moldenaers, *Polymer*, 51, **2010**, 975.

[261] V. N. Bliznyuk, S. Singamaneni, R. L. Sanford, D. Chiappetta, B. Crooker, P. V. Shibaev, *Polymer*, 47, **2006**, 3915.

[262] B. Z. Tang, H. Xu, *Macromolecules*, 32, **1999**, 2569.

[263] L. Kong, X. Lu, W. Zhang, *Journal of Solid State Chemistry*, 181, **2008**, 628.

[264] V. Georgakilas, V. Tzitzios, D. Gournis, D. Petridis, *Chem. Mater.*, 17(7), **2005**, 1613.

[265] T. M. Wu, S. J. Yen, E. C. Chen, R. K. Chiang, *Journal of Polymer Science Part B: Polymer Physics*, 46, **2008**, 727.

[266] C. Qin, J. Shen, Y. Hu, M. Ye, *Composites Science and Technology*, 69, **2009**, 427.

[267] C. Gao, W. Li, H. Morimoto, Y. Nagaoka, T. Maekawa, *Journal of Physical Chemistry B*, 110(14), **2006**, 7213.

[268] Q. Zhang, M. Zhu, Q. Zhang, Y. Li, H. Wang, *Composites Science and Technology*, 69, **2009**, 633.

[269] P. C. Papaphilippou , R. Turcu, T. Krasia-Christoforou, in preparation.

[270] C. Y. Hong, Y. Z. You, C. Y. Pan, *Polymer*, 47, **2006**, 4300.

[271] Y. X. Zhao, I. L. Spain, *Phys. Rev. B*, 40, **1989**, 993.

[272] T-M. Wu, S.-J. Yen, E.-C. Chen, R.-K. Chiang, *Journal of Polymer Science Part B: Polymer Physics*, 46, **2008**, 727.

[273] T. Krasia, H. Schlaad, C. Patrickios, *Macromolecules*, 34, **2001**, 7585.

[274] J. Feng, W. Cai, J. Sui, Z. Li, J. Wan, W. Ali, A. N. Chakoli, *Polymer*, 49, **2008**, 4989.

[275] C. S. Patrickios, T. K. Georgiou, *Curr. Opin. Colloid Interface Sci.*, 8, **2003**, 76.

[276] N. Badi, J-F Lutz, *Journal of Controlled Release*, 140, **2009**, 224.

[277] S. S. Nitin, J. Z. Hilt, *Journal of Controlled Release*, 130, **2008**, 246.

Petri Papaphilippou

[278] L. Klouda, A. G. Mikos, *Eur. J. Pharm. Biopharm.*, 68, **2008,** 34.

[279] C. Alvarez-Lorenzo, L. Bromberg, A. Concheiro, *Photochem. Photobiol.*, 85, **2009**, 848.

[280] P. J. Resendiz-Hernandez, O. S. Rodriguez-Fernandez, L. A. Garcia-Cerda, *J. Magn. Magn. Mater*., 320, **2008**, e373.

[281] R. V. Kulkarni, S. Biswanath, *J. Appl. Biomater. Biomech*., 5, **2007**, 125.

[282] R. A. Frimpong,, S. Fraser, J. Z. Hilt, *Journal of Biomedical Materials Research Part A*, 80a, **2007,** 1.

[283] N. Sahiner, *Colloid and Polymer Science*, 285, **2006**, 283.

[284] R. Yoshida, K. Sakai, T. Okano, Y. Sakurai, *Adv. Drug Deliv. Rev.*, 11, **1993**, 85.

[285] L. Dong, H. Jiang, Soft Matter, 3, **2007**, 1757.

[286] T-Y. Liu, S-H. Hu, K-H. Liu, D-M Liu, S-Y Chen, *Journal of Controlled Release*, 126, **2008**, 228.

[287] T. Y. Liu, S.-H. Hu, T-Y. Liu, D-M Liu, S-Y Chen, *Langmuir*, 22, **2006**, 5974.

[288] Y. Y. Liang, L. M. Zhang, W. Jiang, *ChemPhysChem.*, 8, **2007**, 2367.

[289] D. Szabo, G. Szeghy, M. Zrinyi, *Macromolecules*, 31, **1998**, 6541.

[290] P. C. Papaphilippou, A. Pourgouris, O. Marinica, A. Taculescu, G. I. Athanasopoulos, L. Vekas, T. Krasia-Christoforou, *J. Magn.Magn. Mater.*, in press.

[291] J-F Lutz, *J. Polym. Sci. Part A: Polym. Chem.*, 46, **2008**, 3459.

[292] J-F Lutz, O. Akdemir, A. Hoth, *J. Am. Chem. Soc.*, 128, **2006**, 1304.

[293] J-F Lutz, A. Hoth, K. Schade, *Designed Monomers and Polymers*, 12, **2009**, 343.

[294] Y. Lee, D. N. Kim, D. Choi, *Polymers for Advanced Technologies*, 19, **2008**, 852.

[295] M. K. Nguyen, C. T. Huynh, D. S. Lee, *Polymer*, 50, **2009**, 5205.

[296] B. V. Slaughter, S. S. Khurshid, O. Z. Fisher, A. Khademhosseini, N. A. Peppas, *Adv. Mater.*, 21, **2009**, 3307.

[297] R. Tadmor, R. E. Roswensweig, J. Frey, J. Klein, *Langmuir*, 16, **2000**, 9117.

[298] M. V. Avdeev, D. Bica, L. Vekas, *J. Coll. and Int. Sci.*, 334, **2009**, 37.

[299] L. Vekas, M. V. Avdeev, D. Bica, "*Magnetic Nanofluids: Synthesis and structure, Chapter 25 in: Nanoscience in Biomedicine*", (Ed. Donglu Shi) *Springer*, **2009**, (USA), 645.

[300] T. C. Krasia, C. S. Patrickios, *Macromolecules*, 39, **2006**, 2467.

Petri Papaphilippou

[301] Y. Maeda, T. Kubota, H. Yamauchi, T. Nakaji, H. Kitano, *Langmuir*, 23, **2007**, 11259.

[302] E. goiti, M. M. Salinas, G. Arias, D. Puglia, J. M. Kenny, C. Mijangos, *Polymer Degradation and Stability*, 92, **2007**, 2198.

[303] S. Wan, Y. Zheng, Y. Liu, H. Han, K. Liu, *J. Mater. Chem.*, 15, **2005**, 3424.

[304] S. G. Starodubtsev, E. V. Saenko, M. E. Dokukin, V. L. Aksenov, V. V. Klechkovskaya, I. S. Zanaveskina, A. R. Khokholov, *J. Phys.: Cond. Matter.*, 17, **2005**, 1471.

[305] M. Yamaura, R. L. Camilo, L. C. Sampaio, M. A. Macedo, M. Nakamura, H. E. Toma, *J. Magn. Magn. Mater.*, 279, **2004**, 210.

[306] K. S. Sivudu, K. Y. Rhee, *Colloids and Surfaces A: Physicochem. Eng. Aspects*, 349, **2009**, 29.

[307] S. J. Mann, *Chem. Soc. Dalton, Trans.* **1993**, 1.

[308] P. Kasparova, PhD Thesis, Universität Potsdam, **2002**

[309] P. K. Ajikumar, B. J. M. Low, S. Valiyaveettil, *Surface & Coatings Technology*, 198, **2005**, 227.

[310] T. Wang, G. Rother, H. Colfen, *Macromol. Chem. Phys.*, 206, **2005**, 1619.

[311] B. R. Heywood, S. Mann, *Adv. Matter.*, 6(1), **1994**, 9.

[312] D. Yang, L. Qi, J. Ma, *Chem. Commun.*, **2003**, 1180.

[313] S. B. Mykkamala, A. K. Powell, *Chem. Commun.*, **2004**, 918.

[314] P. A. Bianconi, J. Lin, A. R. Strzelecki, *Nature* (London), 349, **1991**, 315.

[315] E. Dalas, *J. Mater. Chem*, 1, **1991**, 473.

[316] M. Antonietti, M. Breulmann, C. G. Goltner, H. Colfen, K. K. W. Wong, D. Walsh, S. Mann, *Chem. Eur. J.*, 4(12), **1998**, 2493.

[317] T. Wang, A-W Xu, H. Colfen, *Angew. Chem. Int. Ed.*, 45, **2006**, 4451.

[318] H. Cölfen, R. Song et al., in preparation.

[319] M. Antonietti, F. Grohn, J. Hartmann, L. Bronstein, *Angew. Chem. Int. Engl.*, 36(19), **1997**, 2080.

[320] H. Cölfen, R. Song et al., in preparation

[321] X. Shuai, H. Ai, N. Nasongkla, S. Kim, J. Gao, *Journal of Controlled Release*, 98, **2004**, 415.

Petri Papaphilippou

[322] M. Vamvakaki, D. Palioura, A. Spyros, S. P. Armes, and S. H. Anastasiadis, *Macromolecules*, 39, **2006**, 5106.

[323] (a) S. H. Anastasiadis, M. Vamvakaki, *International Journal of Nanotechnology*, 6, **2009**, 46, (b) L. M. Bronstein, M. Vamvakaki, M. Kostylev, V. Katsamanis, B. Stein, S. H. Anastasiadis, *Langmuir*, 21, **2005**, 9747.

[324] E. S. Lee, K. Na, Y. H. Bae, *Journal of Controlled Release*, 91, **2003**, 103.

Petri Papaphilippou